Aspects of Low Scale Leptogenesis and Connection to Dark Matter

Devabrat Mahanta

A thesis submitted for the degree of

Doctor of Philosophy

Supervisor

Dr. Debasish Borah

Department of Physics
Indian Institute of Technology Guwahati
Guwahati - 781039, Assam, India

To my Parents

Declaration

Devabrat Mahanta,
Roll No. 176121007
Department of Physics
Indian Institute of Technology Guwahati
Guwahati, India
email: devab176121007@iitg.ac.in

I hereby declare that works presented in the thesis entitled "**Aspects of Low Scale Leptogenesis and Connection to Dark Matter**" have been carried out by me under the supervision of **Dr. Debasish Borah** at the Department of Physics, Indian Institute of Technology Guwahati, India. The thesis has not been submitted anywhere else for any degree. Works presented in the thesis are all my own unless referenced to the contrary in the thesis.

Date: March 6, 2023

Signature

Certificate

Dr. Debasish Borah,
Associate Professor
Department of Physics
Indian Institute of Technology Guwahati
Guwahati, India
email: dborah@iitg.ac.in

It is certified that the work contained in the thesis entitled **"Aspects of Low Scale Leptogenesis and Connection to Dark Matter"** by Mr. Devabrat Mahanta (Roll No 176121007), a Ph.D. student in the Department of Physics, Indian Institute of Technology Guwahati is carried out under my supervision and has not been submitted elsewhere for the award of any other degree.

Date: March 6, 2023

Signature

Thesis consists of :

1. **"Fermion dark matter with N_2 leptogenesis in minimal scotogenic model"**
   Devabrat Mahanta, Debasish Borah.
   *e*print: arXiv: 1906.03577 (hep-ph)
   Published in **JCAP 11 (2019) 021**

2. **"Dark sector assisted low scale leptogenesis from three-body decay "**
   Debasish Borah, Arnab Dasgupta, **Devabrat Mahanta**,
   *e*print: arXiv: 2008.10627 (hep-ph)
   Published in **Phys.Rev.D 105, 015015 (2022)**

3. **"Low scale Dirac leptogenesis and dark matter with observable $\Delta N_{\rm eff}$ "**
   Devabrat Mahanta, Debasish Borah
   *e*print: arXiv: 2101.02092 (hep-ph)
   Published in **Eur.Phys.J.C 82 (2022) 5, 495**

4. **"TeV scale leptogenesis with dark matter in non-standard cosmology "**
   Devabrat Mahanta, Debasish Borah
   *e*print: arXiv: 1912.09726
   Published in **JCAP 04 (2020) 032**

5. **"WIMPy leptogenesis in non-standard cosmologies "**
   Debasish Borah, **Devabrat Mahanta**
   *e*print: arXiv: 2208.11295 (hep-ph)
   Published in **JCAP 03 (2023) 049**

Other publications :

1. **"Observable gravitational waves in minimal scotogenic model "**
   Debasish Borah, Arnab Dasgupta, Kohei Fujikura, Sin Kyu Kang, **Devabrat Mahanta**
   *e*print: arXiv: 2003.02276 (hep-ph)
   Published in **JCAP 08 (2020) 046**

2. **"Low scale leptogenesis and dark matter in the presence of primordial black holes "**
   Suruj Jyoti Das, **Devabrat Mahanta**, Debasish Borah
   *e*print: arXiv: 2104.14496 (hep-ph)
   Published in **JCAP 11 (2021) 019**

3. **"TeV Scale resonant leptogenesis with $L_\mu - L_\tau$ gauge symmetry in the light of muon $(g-2)$"**
   Debasish Borah, Arnab Dasgupta, **Devabrat Mahanta**
   *e*print: arXiv: 2106.14410 (hep-ph)
   Published in **Phys.Rev.D 104, 075006 (2021)**

भारतीय प्रौद्योगिकी संस्थान गुवाहाटी
Indian Institute of Technology Guwahati

Acknowledgements

It is indeed difficult to mention all the people who have helped me directly or indirectly during the completion of this thesis. Therefore, let me apologise in advance if I forget to mention someone. I express my gratitude to my parents for showing continuous support in every decision I made in my career.

I want to thank my PhD supervisor Dr. Debasish Borah who has guided me in every possible way in the completion of this thesis. He introduced me to this amazing research field and to the excellent ideas he had. His constant guidance, valuable advice, and encouragement to work hard have taught me some important lessons in life. During the PhD period, I learnt a lot about work ethics, sincerity and discipline from him.

I would like to thank my doctoral committee members Prof. Arunansu Sil, Dr. Subhaditya Bhattacharya, and Dr. Sovan Chakraborty, for their valuable comments and suggestions during my thesis. I also want to thank Dr. Debaprasad Maity, Dr. Meduri C Kumar and Prof. Poulose Poulose for encouraging me in different ways during the PhD period. I wish to thank the Department of Physics, IIT Guwahati, for providing me with a rich and informal environment where I could complete the thesis.

I would like to thank my collaborators and co-authors Dr. Arnab Dasgupta, Dr. Kohei Fujikura, Prof. Sin Kyu Kang and Suruj Jyoti Das. Because of them, I got the opportunity to work on different problems relevant to current trends in high-energy physics. I can not express my gratitude in words for Dr. Arnab Dasgupta who has helped me in clearing my doubts on many occasions. I owe a lot to Dr. Rishav Roshan, with whom I had many fruitful discussions on related topics of this thesis. I am also grateful to my senior Dr. Dibyendu Nanda who helped me in learning different computational skills important for my thesis. The evening discussions with him about physics and life have taught me a lot. I would like to take this opportunity to thank my teachers Prof. Madhurjya Prashad Bora, Dr. Sanjeev Kalita, Dr. Bimal Sarma and Surajit Sarma who encouraged me in many ways to pursue physics as my career. I also express my sincere gratitude to Prof. Jiten Kalita for sharing his valuable suggestions during an important phase of my PhD period. I am extremely thankful to my sister Dr. Upasana Mahanta who has always shown me the right path in my career.

I feel lucky to have our group members Dr. Pritam Das, Suruj Jyoti Das, Indrajit Saha, Nayan Das and Disha Bandopadhyay in our group. While discussing physics and non-physics topics I have learnt a lot with them. I am extremely grateful to meet some of the nicest human beings as my friends during this PhD period. The list includes Devender, Subrata, Ipsita, Madhurima, Lopamudra, Kajal, Prantik, Arghyajit, Sahabub, and Suresh.

भारतीय प्रौद्योगिकी संस्थान गुवाहाटी
Indian Institute of Technology Guwahati

Abstract

After the discovery of the Higgs boson at the Large Hadron Collider (LHC), the Standard Model (SM) of particle physics has been established as the most successful theory explaining the fundamental particles and their interaction except gravity. However, there are several observed phenomena and theoretical questions, that the SM fails to explain. Among the observed phenomena, the existence of matter-antimatter asymmetry or baryon asymmetry of the universe (BAU), as suggested by the observed light nuclei abundance as well as cosmic microwave background (CMB) anisotropies, has been a longstanding puzzle. While this demands a dynamical origin, the necessary criteria for the same as laid out by Andrei Sakharov, can not be realised in required amount in the SM. Therefore, new physics beyond the SM is required to successfully generate the observed baryon asymmetry. While there have been several such proposals in the literature, in this thesis we study the framework of leptogenesis where a non-zero lepton asymmetry is generated initially and gets converted later into baryon asymmetry by electroweak sphaleron transitions. It is also motivating from the fact that typical leptogenesis models can also explain the origin of light neutrino masses, another observed fact which the SM fails to address. Apart from the BAU, the origin of non-luminous, non-baryonic matter, popularly known as dark matter (DM) giving rise to almost 26% of present universe's energy density has been another mystery. Although the first indication of DM appeared in 1930s, it was the observations made by V. C. Rubin and her collaborators in the 1980s after which it became an accepted fact that most of the mass holding the galaxies is non-luminous. Similar conclusions can be reached for galaxy clusters as well. Despite multiple astrophysical and cosmological evidences for the presence of DM, there has not been any observation of DM particle in particle physics experiments. The nature of DM particles and their non-gravitational interactions with the SM particles or among themselves are unknown to us. Similar to the BAU, the SM also fails to explain the origin of DM, leading to several interesting proposals for particle DM candidates. Depending upon DM interactions with the SM, the DM particles can be either thermally or non-thermally produced in the early universe. This has also led to two broad class of particle DM scenarios, known as weakly interacting massive particle (WIMP) and Feebly interacting massive particle (FIMP).

In this thesis, we aim to study a few leptogenesis scenarios which can also shed light on dark matter. A common framework for explaining both the BAU and DM is motivating due to its minimal and predictive nature. We consider a few realistic particle physics models where there exist new particles and symmetries beyond those in the SM. While canonical neutrino mass models, also known as seesaw models, predict high scale leptogenesis ($M \geq \mathcal{O}(10^9\text{GeV})$), we focus on leptogenesis and DM scenarios where scale of leptogenesis can

be brought down to TeV corner such that these scenarios can be tested at near future experiments. Accordingly, the thesis is divided into five different chapters. In chapter 1, we first introduce the observational evidences for the baryon asymmetry of the universe as well as dark matter followed by discussion of the popular production mechanisms for both. In chapter 2, we propose a fermion singlet dark matter scenario within the minimal scotogenic model where neutrinos get mass at one-loop level with dark sector particles going inside the loop. The lepton asymmetry is generated due to the decay of next to lightest singlet fermion. We then discuss the interplay of light neutrino mass hierarchy on leptogenesis as well as production mechanism of fermion singlet DM. In chapter 3 we propose a concrete model for three-body decay leptogenesis together with DM. In this first of its kind proposal, leptogenesis can occur from the interference of multiple $1 \longrightarrow 3$ diagrams with some of the final state particles playing the role of dark matter at the same time. A two-component dark matter scenario naturally appears in the model due to the chosen charge assignments of different particles under the chosen symmetries. Due to phase space suppression and presence of additional free parameters not affecting light neutrino masses directly, the scale of leptogenesis can be much lower in this setup compared to the minimal scotogenic model discussed earlier. In chapter 4, we consider a different scenario where light neutrinos are of Dirac nature unlike in the models discussed earlier. While canonical seesaw models including the minimal scotogenic model predict Majorana nature of light neutrinos due to in-built lepton number violation by two units, there have not been any lepton number violating signatures at experiments. The model we propose is based on a $B - L$ gauge extension of the standard model where the particle content is chosen in such a way that light neutrinos remain Dirac fermions. Leptogenesis occurs from the decay of additional Majorana fermions which do not induce Majorana masses to light neutrinos. The right chiral neutrinos being light and charged under the $B-L$ gauge symmetry also contribute to the effective number of relativistic degrees of freedom in the universe ($N_{\rm eff}$), offering a complementary cosmological probe at CMB experiments. Also, the anomaly cancellation demands the addition of new chiral fermions states, which play the role of DM. A TeV scale $B - L$ model of this type not only provides a solution to the BAU and DM, but also remain verifiable at collider, cosmology as well as DM direct search experiments. In chapter 5, we study the impact of some non-standard cosmological histories on leptogenesis and dark matter. We mainly consider two modified cosmological histories; firstly when the universe expands faster than the radiation and another one when the universe is dominated by a matter field prior to the Big Bang Nucleosynthesis (BBN) era. To study the effect of such modified cosmologies we consider two kinds of leptogenesis scenarios. First, we consider the leptogenesis from decay of heavy fermions in the minimal scotogenic model and then a WIMPy leptogenesis scenario where the lepton asymmetry is generated from the annihilation of WIMP type dark matter. We show the non-trivial effects of modified cosmological stories in shifting the scale of leptogenesis as well as DM towards either side. Finally, we summarise our key results in chapter 6.

भारतीय प्रौद्योगिकी संस्थान गुवाहाटी
Indian Institute of Technology Guwahati

Permissions and Attributions

- The content of Chapter 2 is based on the following work,
  (a) **"Fermion dark matter with N_2 leptogenesis in minimal scotogenic model"**, **JCAP 11 (2019) 021** in collaboration with Debasish Borah.
- The content of Chapter 3 is based on the following work,
  (a) **"Dark sector assisted low scale leptogenesis from three-body decay"**, **Phys.Rev.D 105, 015015** in collaboration with Debasish Borah, Arnab Dasgupta.
- The content of chapter 4 is based on the following work,
  (a) **"Low scale Dirac leptogenesis and dark matter with observable $\Delta N_{\rm eff}$"**, **Eur.Phys.J. C 82 (2022) 5, 495** in collaboration with Debasish Borah.
- The content of chapter 5 is based on the following works,
  (a) **"TeV scale leptogenesis with dark matter in non-standard cosmology"**, **JCAP 04 (2020) 04, 032** in collaboration with Debasish Borah.
  (b) **"WIMPy leptogenesis in non-standard cosmologies"**, **JCAP 03 (2023) 049** in collaboration with Debasish Borah.

भारतीय प्रौद्योगिकी संस्थान गुवाहाटी
Indian Institute of Technology Guwahati

Contents

List of Figures

List of Tables

CHAPTER 1

Introduction

It is observed that the present universe is populated with only matter. Outside of particle accelerators, antimatter has hardly been seen on earth. While the survival of planetary probes indicate the solar system to be dominated by matter only, composition of cosmic rays observed on earth provides another evidence suggesting the dominance of matter at galactic and extra-galactic levels. The amount of antiprotons in cosmic rays stands at approximately 10^{-4} of the same for protons. Such a tiny amount of antiprotons in cosmic rays seems to validate hypothesis that the antiprotons are secondary products of cosmic ray collisions with the interstellar medium, and not necessarily a signature of antimatter in the galaxy. The abundance of anti- ^{4}He is about 10^{-5} compared to the abundance of ^{4}He. Thus, cosmic rays provide a very good evidence for matter-antimatter asymmetry at galactic scales. The evidence of asymmetry on larger scales is weaker. X-ray emissions from the clusters of galaxies indicate the existence of some intercluster gas within them. If, galaxies made out of matter and antimatter would have existed in the same cluster there would have been strong γ-ray emission from the annihilation of nucleons and antinucleons. The non-observation of such γ-ray flux is the evidence that the nearby clusters of galaxies (like Virgo) are fully composed of either baryons or of antibaryons. This asymmetry between matter and antimatter is commonly known as the matter-antimatter asymmetry or baryon asymmetry of the universe (BAU).

The asymmetry is often quantified in two ways [1–3],

$$\eta_{\rm B} = \left.\frac{n_{\rm B}-n_{\bar{\rm B}}}{n_\gamma}\right|_0 = (6.21\pm0.16)\times10^{-10}, \tag{1.1}$$

$$Y_{\rm B} = \left.\frac{n_{\rm B}-n_{\bar{\rm B}}}{s}\right|_0 = (8.75\pm0.23)\times10^{-11}. \tag{1.2}$$

Here $n_{\rm B}$, and $n_{\bar{\rm B}}$ are the number densities of baryons and antibaryons while n_γ and s represent the number density of photons and entropy density of the universe respectively. The subscript 0 implies that the quantities are evaluated at the present epoch. The quantity $\eta_{\rm B}$ is known as the baryon to photon ratio and the Y_B is known as the comoving number density of baryons. The two ratios are related by $Y_{\rm B} = (n_{\gamma_0}/s_0)\eta_{\rm B} \simeq \eta_{\rm B}/7.04$. Another way of representing the BAU is in terms of the ratio of baryon energy density to the critical energy density of the universe $\Omega_{\rm B} \equiv \rho_{\rm B}/\rho_{\rm crit}$. The baryon to photon ratio can be expressed in terms of

Ω_B as $\eta_B = 2.74 \times 10^{-8}\Omega_B h^2$. Here h is the reduced Hubble parameter given by $h = \mathbf{H}/100\,\mathrm{kms}^{-1}\mathrm{Mpc}^{-1}$ with $\mathbf{H} = 67.4 \pm 0.5\,\mathrm{kms}^{-1}\mathrm{Mpc}^{-1}$ being the Hubble parameter at present epoch [3]. The critical energy density of the present universe is given by $\rho_{\mathrm{crit}} = 3\mathbf{H}^2/8\pi G$ where G is the constant of gravitation. The recently measured value of $\Omega_B h^2$ by the Planck satellite [3] is $\Omega_B h^2 = 0.0224 \pm 0.0001$. While the asymmetry in the visible matter has been an unsolved puzzle to particle physicists for a long time, another feature of the overall matter component of the present universe adds more to it. It is found that only approximately 20% of the total matter density of the present universe consists of visible matter while the rest is composed of some non-luminous, non-baryonic form of matter, popularly known as dark matter (DM). Both astrophysical and cosmological observations have shown strong evidence for the existence of DM [3–6]. Like the baryon asymmetry, DM abundance is also expressed by the DM fraction of total critical energy density $\Omega_{\mathrm{DM}} = \rho_{\mathrm{DM}}/\rho_{\mathrm{Crit}}$. The recently measured value of it is $\Omega_{\mathrm{DM}} h^2 = 0.120 \pm 0.001$ at a 68% confidence level (CL) [3].

While no particle from the standard model (SM) particle content can be a viable DM candidate, the SM also fails to explain the origin of BAU. This has led to several beyond the standard model (BSM) proposals in the literature. Interestingly, it is also important to note that $\Omega_{\mathrm{DM}} \simeq 5\Omega_B$. Though this could be a mere coincidence, it is interesting to look for solutions where the origin of BAU and DM could be explained simultaneously. In this thesis, we look for some minimal and well-motivated BSM frameworks where the origin of both BAU and DM can be connected. As we will see, these frameworks can also solve another longstanding problem in particle physics namely, the origin of light neutrino mass, as confirmed by the discovery of neutrino oscillations [2]. Below we discuss the details related to the observational evidence of BAU and DM along with some widely studied production mechanisms.

1.1 Evidences of baryon asymmetry

There have been different sources of evidence which establish the fact that the present universe is dominated by matter over antimatter. However, the quantitative evidence of the BAU is inferred primarily from two different observations, as we summarise below.

1.1.1 Light element abundance predicted by BBN

The first quantitative evidence of the BAU comes from the observation of the light element abundance in the universe [7–9]. A successful Big Bang Nucleosynthesis (BBN) predicts the abundance of the light elements D, ^{3}He, ^{4}He, and ^{7}Li in the universe. The abundances of these elements are sensitive to η_B. Particularly, D and ^{3}He abundances are very sensitive to η_B. The abundances of D and ^{3}He are crucial in the synthesis of ^{4}He via the two-body reactions $\mathrm{p} + \mathrm{D} \longrightarrow {}^3\mathrm{He} + \gamma$ and $\mathrm{D} + {}^3\mathrm{He} \longrightarrow {}^4\mathrm{He} + p$. The rate of these processes increases with the increase in number densities of the incoming nuclei. The number densities of D and ^{3}He depend on η_B as $n(\mathrm{D}) \propto \eta_B$ and $n({}^3\mathrm{He}) \propto \eta_B^2$ as D and ^{3}He are produced by the reactions $p + n \longrightarrow \mathrm{D} + \gamma$ and $p + \mathrm{D} \longrightarrow {}^3\mathrm{He} + \gamma$ respectively. Therefore for larger η_B, the reaction rates of these processes will be large and the ^{4}He producing reactions will stop (the reaction rate become smaller than the expansion rate of the universe) later. This results in smaller

freeze-out abundances for D and ^{3}He. A larger value of $\eta_{\rm B}$ means that the relative number of photons, especially photons which have energies higher than the binding energies of nuclei is smaller. Hence the abundances of D, ^{3}H and ^{3}He build up earlier. As a consequence, the synthesis of ^{4}He also starts earlier which results in a larger abundance of ^{4}He. On the other hand, the dependence of ^{7}Li abundance on η_B is much more complicated, as Li^7 can be produced in two ways which have opposite dependencies with $\eta_{\rm B}$. In Fig.1.1 the variation in abundances of these light elements with the baryon to photon ratio is shown. The different coloured bands show the abundances of different elements as predicted by successful BBN (at 95 % confidence level). The yellow patches represent the observed light element abundances. The range of $\eta_{\rm B}$, consistent with the abundances of ^{4}He + D provide strong support for the hot big bang cosmology model. At 95% CL the range is given by [2],

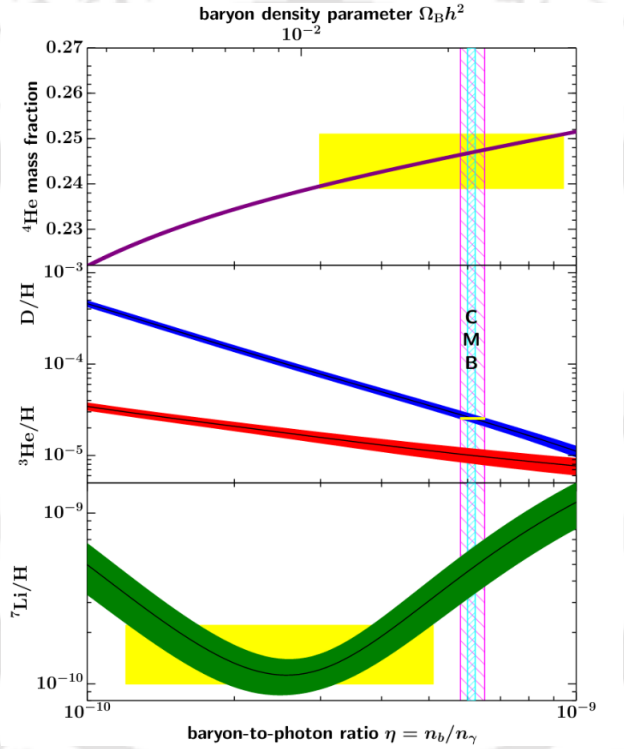

Figure 1.1: The primordial abundances of the light elements ^{4}He, D, ^{3}He, and ^{7}Li against η_B predicted by successful Big-Bang nucleosynthesis. The bands for each element show the 95% CL range [10]. The yellow patches represent the light element abundances which are being observed. The narrow vertical indicated by the blue colour band indicates the estimate of η_B based on cosmic microwave background (CMB) measurements, while the magenta coloured wider band indicates BBN prediction for η_B. The figure is taken from [2].

$$5.8 \times 10^{-10} \leq \eta_B \leq 6.5 \times 10^{-10} \qquad 0.021 \leq \Omega_{\rm B} h^2 \leq 0.024 \tag{1.3}$$

1.1.2 CMB anisotropies

The other measurement of $\Omega_{\rm B}$ comes from the observation of the anisotropies in the cosmic microwave background (CMB) radiation [11, 12]. The CMB spectrum matches a perfect blackbody spectrum with nearly a constant temperature up to an excellent approximation. However, there are small fluctuations in the CMB temperature as discovered by WMAP and Planck satellites. The basic observable in the CMB spectrum is the fluctuation of temperature defined as $\Theta(\hat{n}) = \Delta T/T$, where $\hat{n}$ specifies the direction in the sky. The crucial epoch for the CMB in the history of the universe is that of recombination. At the epoch of recombination, the temperature of the universe becomes low enough such that protons and electrons could combine to form neutral hydrogen atoms. The recombination happened at a redshift $z \simeq 1000$. Prior to this, the cosmological plasma can be assumed to be a fluid of photons and baryons. Therefore the CMB temperature fluctuation should follow the dynamical equations in fluid mechanics. Neglecting the dynamical effect of gravity and the baryons, the equation of motion for the temperature fluctuation is given by

$$\ddot{\Theta}^2 + c_{\rm S}^2 k^2 \Theta \;\; = \;\; 0, \tag{1.4}$$

where $c_{\rm S} = \sqrt{\dot{p}/\dot{\rho}} = \sqrt{1/3}$ is the speed of sound in the baryon-free fluid (ρ and p are the energy density and pressure of the photons). The modification due to gravity and the baryonic interactions can be explained by adding their effects to the right-hand side of Eq.(1.4)

$$\ddot{\Theta}^2 + c_{\rm S}^2 k^2 \Theta = F \;\; . \tag{1.5}$$

Here F represents the force term due to gravity. In presence of baryons, $c_{\rm S}$ gets modified as $c_{\rm S} = 1/\sqrt{3(1+3\rho_{\rm B}/\rho_\gamma)}$, where $\rho_{\rm B}$ and ρ_γ are the energy densities of the baryons and photons respectively. The presence of the baryons provides additional gravity enhancing the compression into the potential wells. This enhances the compressional phases which translate into an increase in the heights of the odd peaks in the CMB power spectrum. Therefore, the measurement of the difference between the heights of odd and even peaks put a constraint on the baryon energy density. The temperature fluctuation is conveniently analyzed by decomposing it into spherical harmonics

$$\frac{\Delta T}{T} = \sum_{l,m} a_{\rm lm} Y_{\rm lm}\left(\theta, \phi\right), \tag{1.6}$$

where θ and ϕ are the polar angles. Here, $a_{\rm lm}$ are the expansion coefficients for different spherical harmonics. The CMB power spectrum is defined as

$$C_l = \left\langle \mid a_{\rm lm} \mid^2 \right\rangle . \tag{1.7}$$

It is conventional to plot $C_l l(l+1)$ against l. From Fig.1.2 the change of the peaks can be seen with the change in baryon density $\Omega_{\rm B}$. The fit with the most recent observation of the CMB spectrum by the Planck satellite [3] predicts (at 68%CL)

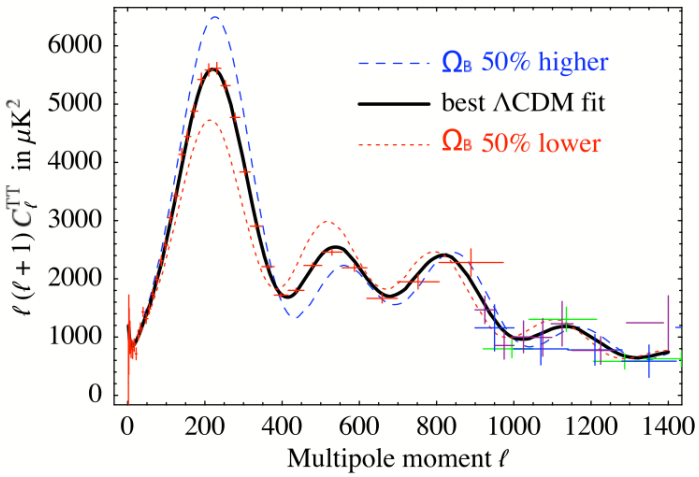

Figure 1.2: CMB power spectrum against the multiple moments, l. The figure is taken from [13] .

$$0.0223 \leq \Omega_{\rm B} h^2 \leq 0.0225. \tag{1.8}$$

In Fig.1.1 the blue coloured narrow vertical band indicates the CMB estimate of η_B and the wider band indicates the estimate by BBN predictions for D $+^4$ He agreement range. It can be observed that these two predictions based on different experimental observations are in excellent agreement with each other. Therefore any framework which can explain the origin of BAU dynamically, known as the mechanism of baryogenesis, should reproduce this number for the $\Omega_{\rm B} h^2$. However, from Fig.1.1 it can be seen that the observed abundance of ^{7}Li is significantly less than the standard BBN prediction for the preferred range of $\eta_{\rm B}$ also singled out by CMB data. This inconsistency is commonly known as the cosmic Li problem, review of which may be found in [2, 7, 9].

1.2 Necessary criteria for baryogenesis

In principle, the universe may start with a baryon asymmetric condition. However, any such initial asymmetry is expected to be diluted away by the exponential expansion of the universe during the inflationary phase [14]. Hence the asymmetry has to be dynamically generated after the inflationary phase ends. The necessary conditions to dynamically generate such an asymmetry were first realized by Sakharov several decades ago [15]. They are as follows.

1. Violation of baryon number: Some baryon number (B) violating interactions are necessary to generate a baryon asymmetry from a baryon symmetric state of the universe.

2. Violation of C and CP: Violation of baryon number alone is not sufficient to generate a baryon asymmetry. If such baryon number-violating interactions conserve C and CP

then the process involving antibaryons would occur exactly at the same rate as the process involving baryons. This will not lead to any net asymmetry generation.

3. Departure from equilibrium: In chemical equilibrium, the chemical potentials associated with all the non-conserved quantum numbers vanish. Therefore in chemical equilibrium, no baryon asymmetry can be generated. Besides CPT invariance guarantees that the masses of baryons and antibaryons are the same. On the other hand, in thermal equilibrium, the phase space density of baryons and antibaryons ($[1+\exp((p^2+m^2)/T)]^{-1}$) would be the same which implies $n_{\rm B} = n_{\bar{\rm B}}$.

We elaborate on the necessity of each of these requirements below.

1.2.1 Violation of baryon number

To get baryon asymmetric phase of the universe starting with a baryon symmetric phase, one must have some baryon number violating interactions. These interactions can be decay or scattering. The conservation of the baryon number is an accidental symmetry within the standard model. In some other theories such as the grand unified theories (GUT), the quarks and the leptons appear as members of the same isospin multiplets and therefore provide a generic explanation for baryon number violation. The gauge bosons mediated interactions can transform quarks into leptons or antiquarks, thereby violating B. In GUT, simple dimensional analysis results for the lifetime of the proton to be $\tau_p \sim \alpha_{\rm GUT}^{-2} M^4 m_{\rm p}^{-5}$, M being the mass of the gauge boson in the GUT. The non-observation of the proton decay demands $\tau_p \gtrsim 10^{31} - 10^{33}$ years. This signifies that such additional gauge boson has to be very heavy $M \gtrsim 10^{14}$ GeV or so. In addition to that, there is the possibility of the existence of Higgs bosons with baryon number-violating interaction. The typically weaker coupling of Higgs boson allows them to have mass somewhat less than the gauge boson, perhaps as low as 10^{10} GeV. In both cases, the large mass of the intermediate bosons is responsible for the non-observation of baryon number-violating interaction today. Apart from GUT there are other ways of baryon number violation. We discuss some of these possibilities in the section 1.3 some of which (like low scale leptogenesis) may be testable directly at ongoing or near future experiments.

1.2.2 Violation of C and CP

To explain why C and CP violations are necessary to generate a net baryon asymmetry, let us consider a particle P, having baryon number violating interactions. Let the particle decays to quark/lepton final state qq(B = 2/3) and $\bar{q}\bar{l}$ (B=-1/3). Since the two final states have different baryon numbers, the decay of P and $\bar{P}$ violates the baryon number. Considering C and CP to be violated, the branching ratio (BR) for $P \longrightarrow qq$ will not be the same with $\bar{P} \longrightarrow \bar{q}\bar{q}$. Let the BR for $P \longrightarrow qq$ be x and that of $\bar{P} \longrightarrow \bar{q}\bar{q}$ be $\bar{x}$ such that $x \neq \bar{x}$. Since CPT invariance demands that the decay rates for P and $\bar{P}$ be the same the BRs and final state baryon numbers for all the decay channels of P and $\bar{P}$ can be determined as shown in table 1.1.

decay channel	branching ratio	final state B number
$P \longrightarrow qq$	x	2/3
$P \longrightarrow \bar{q}\bar{l}$	$1-x$	-1/3
$\bar{P} \longrightarrow \bar{q}\bar{q}$	$\bar{x}$	-2/3
$\bar{P} \longrightarrow ql$	$1-\bar{x}$	1/3

Table 1.1: Final states and branching ratios of P and $\bar{P}$.

Let us imagine the universe to start with a symmetric initial condition, i.e., an equal number of P and $\bar{P}$ particles. Following the details given in table 1.1, the mean net baryon number produced by the decay of P is $B_{\rm P} = x(2/3) + (1-x)(-1/3)$ and that produced from the decay of $\bar{P}$ is $B_{\bar{\rm P}} = \bar{x}(-2/3) + (1-\bar{x})(1/3)$. Therefore the mean net baryon number generated from the decay of a pair of P, $\bar{P}$ particle is $\epsilon = B_{\rm P} + B_{\bar{\rm P}} = x - \bar{x}$. The net baryon number will be zero if there is no C and CP violation ($x = \bar{x}$). On the other hand, if C and CP are violated, in absence of other baryon number-violating reactions, a net baryon number will survive after the decay of all the P and $\bar{P}$ particles. To explicitly see how the C and CP violations enter, let us consider two superheavy bosons P and Q with baryon number violating decays. The generalization of CP asymmetry parameter defined above is

$$\epsilon_{\rm P} = \sum_{\rm f} b_f \frac{\Gamma_{\rm P\longrightarrow f} - \Gamma_{\bar{\rm P}\longrightarrow \bar{\rm f}}}{\Gamma_P}, \tag{1.9}$$

$$\epsilon_{\rm Q} = \sum_{\rm f} b_f \frac{\Gamma_{\rm Q\longrightarrow f} - \Gamma_{\bar{\rm Q}\longrightarrow \bar{\rm f}}}{\Gamma_Q}, \tag{1.10}$$

where the sum runs over all possible final states fermions. $b_{\rm f}$ is the baryon number of the fermion f and $\Gamma_{\rm P}(\Gamma_{\rm Q})$ is the decay width of $P(Q)$. Following the notations of [14], we briefly outline the basics of CP asymmetry calculation starting with a generic Lagrangian. For simplicity, we assume two final states for the P and Q boson decay, and the relevant part of the Lagrangian is given by

$$-\mathcal{L} \supset g_1 P f_2^\dagger f_1 + g_2 P f_4^\dagger f_3 + g_3 Q f_1^\dagger f_3 + g_4 Q f_2^\dagger f_4 + \text{h.c.} \tag{1.11}$$

Here f_1, f_2, f_3 and f_4 are the final state fermions (quarks and leptons) and g_is are the coupling strengths which can be complex in general. The Lagrangian leads to the following decay processes: $P \longrightarrow \bar{f}_1 + f_2, \bar{f}_3 + f_4$ and $Q \longrightarrow f_1 + \bar{f}_3, f_2 + \bar{f}_4$. The tree level decays can not contribute to the CP asymmetry, as $\Gamma_{\rm P\longrightarrow \bar{f}_1 f_2} = |g_1|^2 \mathcal{I}_{\rm P} = \Gamma_{\bar{\rm P}\longrightarrow \bar{\rm i}_1 \bar{\rm i}_2} = |g_1^*|^2 \mathcal{I}_{\bar{\rm P}}$, where the kinematic factor $\mathcal{I}_{\rm P} = \mathcal{I}_{\bar{\rm P}}$ arises from the phase space integrals. The non-zero CP asymmetry arises from the interference of tree level and one-loop diagrams shown in Fig.1.3 and Fig.1.4 respectively. These interference terms are given by

$$\Gamma_{\rm P\longrightarrow \bar{f}_1 f_2} = g_1 g_2^* g_3 g_4^* \mathcal{I}_{\rm PQ} + (g_1 g_2^* g_3 g_4^* \mathcal{I}_{\rm PQ})^*, \tag{1.12}$$

$$\Gamma_{\bar{\rm P}\longrightarrow \bar{\rm i}_1 \bar{\rm i}_2} = g_1^* g_2 g_3^* g_4 \mathcal{I}_{\rm PQ} + (g_1^* g_2 g_3^* g_4 \mathcal{I}_{\rm PQ})^*, \tag{1.13}$$

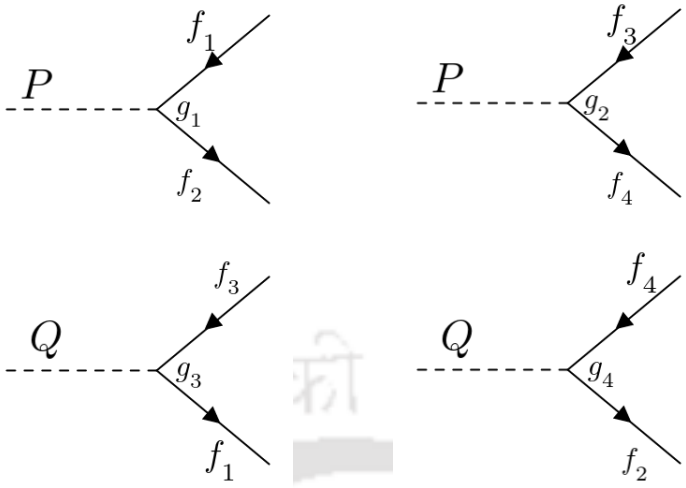

Figure 1.3: Lowest-order Feynman graphs for the P and Q decay.

where the phase space factors $\mathcal{I}_{\rm IJ}$ $(I, J = P, Q)$ also include the kinematic factors appearing from the loop integration. If the intermediate particles (f_1, f_2, f_3, f_4) in the loops can be on-shell, then $\mathcal{I}_{IJ}$ will be complex. The difference between the decay widths of $P \longrightarrow \bar{f}_1 f_2$ and $\bar{P} \longrightarrow f_1 \bar{f}_2$ is

$$\begin{aligned}\Gamma_{\rm P\longrightarrow \bar{f}_1 f_2} - \Gamma_{\rm \bar{P}\longrightarrow f_1 \bar{f}_2} &= 2i\mathcal{I}_{\rm PQ}{\rm Im}[g_1 g_2^* g_3 g_4^*] + 2i\mathcal{I}^*_{\rm PQ}{\rm Im}[g_1^* g_2 g_3^* g_4], \\ &= 4{\rm Im}[\mathcal{I}_{\rm PQ}]{\rm Im}[g_1^* g_2 g_3^* g_4]. \end{aligned} \tag{1.14}$$

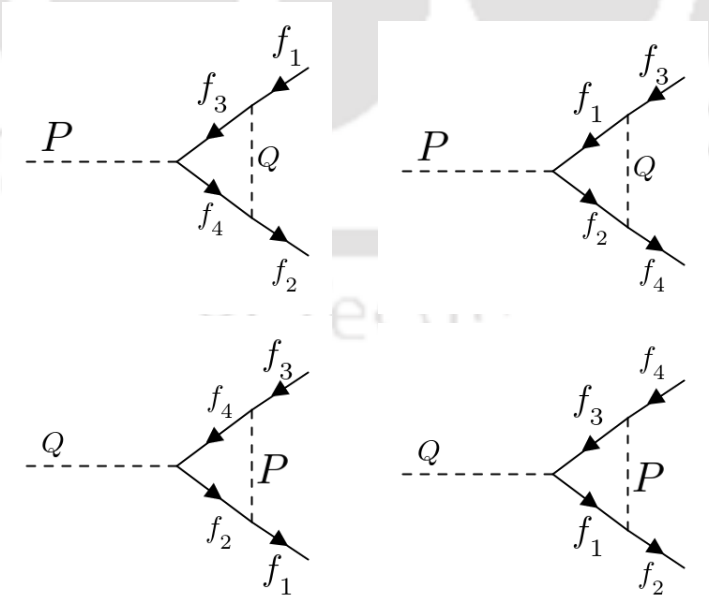

Figure 1.4: Vertex correction diagrams in P and Q decay up to one-loop.

Similar calculation for the other decay mode leads to

$$\epsilon_{\rm P} = \frac{4}{\Gamma_{\rm P}}{\rm Im}\mathcal{I}_{\rm PQ}{\rm Im}[g_1^* g_2 g_3^* g_4]\left[(b_{\rm f_4}-b_{\rm f_3})-(b_{\rm f_2}-b_{\rm f_1})\right]. \tag{1.15}$$

Repeating the same calculation for Q decay one can show that

$$\epsilon_{\rm Q} = \frac{4}{\Gamma_{\rm Q}}{\rm Im}\mathcal{I}'_{\rm PQ}{\rm Im}\left[g_1^* g_2 g_3^* g_4\right]\left[(b_{\rm f_2}-b_{\rm f_4})-(b_{\rm f_1}-b_{\rm f_3})\right]. \tag{1.16}$$

From Eqs.(1.15) and (1.16) it can be understood that to have the net asymmetry $\epsilon = \epsilon_{\rm P}+\epsilon_{\rm Q}$ non-zero, we must have the following conditions satisfied

- There must be two particles having baryon numbers violating decays. The mass of each of them needs to be heavier than the total mass of the fermions in the internal loops.
- At least one of the couplings has to be complex.
- The decaying particles P and Q must have different masses. Otherwise $\epsilon_P = -\epsilon_Q$ leading to vanishing net asymmetry.

1.2.3 Departure from equilibrium

The departure from the equilibrium condition can be realised if the expansion rate of the universe is faster than the interaction rates of the relevant particles. In an expanding universe, initially, the particles P and $\bar{P}$ can be in thermal equilibrium with the SM plasma. In fact, for $T \gg m_{\rm P}$, their number densities follow $n_{\rm P} = n_{\bar{\rm P}} = n_\gamma$. When the temperature falls $T \lesssim m_{\rm P}$ then $n_{\rm P} = n_{\bar{\rm P}} = (m_{\rm P}T)^{3/2}\exp\left(-m_{\rm P}/T\right) \ll n_\gamma$. The P, $\bar{P}$ bosons will be in equilibrium if the interactions creating or destroying P, $\bar{P}$ are occurring rapidly enough such that the rate of interactions satisfy $\Gamma \gtrsim \mathbf{H}$. The scattering processes are self-quenching since $\Gamma_{\rm P} \propto n_{\rm P}$. The decay processes are the most important for maintaining the equilibrium number for the P, $\bar{P}$ bosons.

The necessary condition for the departure from equilibrium can be quantified in terms of the reaction rates for the P and $\bar{P}$ bosons. The decay rate of P ($\Gamma_{\rm D}$), the inverse decay rate of P ($\Gamma_{\rm ID}$) and the $2 \longleftrightarrow 2$ B violating scattering processes mediated by the P, $\bar{P}$ boson exchange ($\Gamma_{\rm S}$), and the expansion rate of the universe ($\mathbf{H}$) are given by

$$\Gamma_{\rm D} \simeq \alpha m_{\rm P}\begin{cases} m_{\rm P}/T & T \gtrsim m_{\rm P} \\ 1, & T \lesssim m_{\rm P}\end{cases}, \tag{1.17}$$

$$\Gamma_{\rm ID} \simeq \Gamma_{\rm D}\begin{cases} 1 & T \gtrsim m_{\rm P} \\ (m_{\rm P}/T)^{3/2}\exp(-m_{\rm P}/T) & T \lesssim m_{\rm P}\end{cases}, \tag{1.18}$$

$$\Gamma_{\rm S} \simeq T^3\alpha^2\frac{T^2}{(T^2+m_{\rm P}^2)^2}, \tag{1.19}$$

$$\mathbf{H} \simeq g_*^{1/2}T^2/M_{\rm Pl}. \tag{1.20}$$

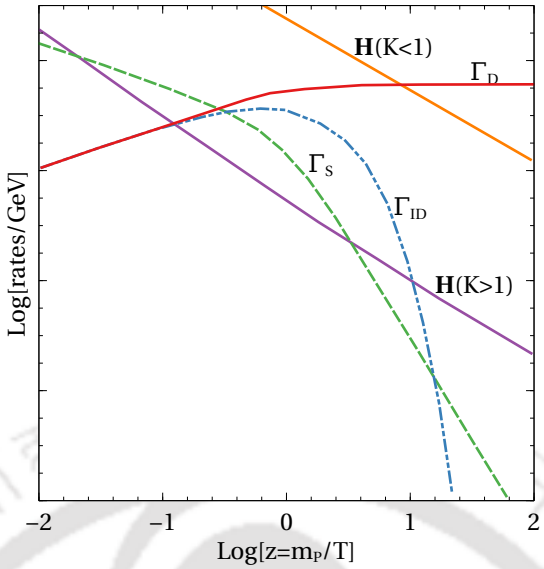

Figure 1.5: Interaction rates for P, $\bar{P}$ along with the expansion rate $\mathbf{H}$ (schematic diagram redrawn from [14]).

Here α represents the coupling strength of the P and $M_{\rm Pl}$ is the Planck mass. The decay rate of P is small at high temperatures due to the time dilation factor, and the Boltzmann suppression factor at low temperatures keep the inverse decays inefficient. The scattering cross-section at high temperature is $\sigma \simeq \alpha^2/T^2$ and at low temperatures $\sigma \simeq \alpha^2 T^2/m_{\rm P}^4$. A schematic comparison of the relevant rates is shown in Fig.1.5. It is important to note that all the reaction rates are dependent on $m_{\rm P}$ while $\mathbf{H}$ is independent of $m_{\rm P}$.

As the decay and inverse decay mainly regulate the number density of P, the decay and inverse decay rates become the most important rates for baryogenesis. Let us define an important parameter known as the decay parameter,

$$K = \frac{\Gamma_D}{2\mathbf{H}}\bigg|_{T=m_{\rm P}} = \frac{\alpha M_{\rm Pl}}{3.3 g_*^{1/2} m_{\rm P}}. \tag{1.21}$$

The decay parameter K determines the effectiveness of decays when P starts becoming non-relativistic ($T \sim m_{\rm P}$). For $T \lesssim m_{\rm P}$, K determines the effectiveness of inverse decays and $2-2$ scatterings. When the decaying particle become non-relativistic, the inverse decay rate is $\Gamma_{\rm ID}/\mathbf{H} \sim (m_{\rm P}/T)^{3/2}\exp(-m_{\rm P}/T)K$ and the scattering rate is given by $\Gamma_{\rm S}/\mathbf{H} \sim \alpha(T/m_{\rm P})^5 K$. If $K \ll 1$, then at $T \sim m_{\rm P}$ the decay rate $\Gamma_{\rm D}$ is less than the expansion rate of the universe $\mathbf{H}$. As a result, P, $\bar{P}$ do not decrease in number. Equilibrium will not be maintained and the P, $\bar{P}$ boson will be overabundant near $T \sim m_{\rm P}$. In this case, the P, $\bar{P}$ drift away from their thermal equilibrium abundance and eventually decay at later times. In the limit of pure drift, it is easy to calculate the baryon asymmetry. When the P, $\bar{P}$ finally decay, they are very much overabundant $n_{\rm P} = n_{\bar{\rm P}} \sim n_\gamma$ i.e. no suppression to their number densities. Since a net baryon number ϵ is produced from each decay, the final baryon asymmetry produced will be $n_{\rm B} \sim \epsilon n_{\rm P} \sim \epsilon n_\gamma$. For $K \ll 1$, both the inverse decays and the B violating $2-2$ scatterings are of negligible rates when the decays finally occur and therefore can be safely

ignored. On the other hand, when $K \gg 1$ the abundances of P, $\bar{P}$ bosons track equilibrium abundance as $\Gamma_{\rm D} \gg \mathbf{H}$ for $T \sim m_{\rm P}$. If the equilibrium abundance is tracked precisely enough, no departure from equilibrium can occur. As a result, a net baryon asymmetry can not be generated. When K is in the intermediate regime, i.e K is not too large from 1, the scenario becomes more interesting. In such scenario, the asymmetry generation from decay and the washouts from inverse decay as well as the scattering play significant roles.

1.3 Popular mechanisms for baryogenesis

All the necessary ingredients mentioned in the last section can, in principle, be realised in a gauge theory like the SM with an expanding universe. While B number conservation is an accidental symmetry in the SM, Gerard t'Hooft first realised that it is possible to violate $(B + L)$ with L being the lepton number, while conserving $(B - L)$ within the SM by non-perturbative instanton effects [16]. In such a case, the necessary out-of-equilibrium condition is provided by the first order phase transition (FOPT) [17] of the Higgs potential. In SM, for the electroweak phase transition to be first first order, the required Higgs mass should be $m_{\rm H} \lesssim 72$ GeV [18, 19]. After the discovery of Higgs Boson at the LHC with a mass of around 125 GeV [20,21], this possibility is now ruled out. Coming to the C and CP violation, C is maximally violated in the electroweak interactions. Weak interaction also violates CP via the Kobayashi-Maskawa mechanism [22]. The CP violation is usually parametrized in terms of the Jarlskog invariant [23]. The Jarlskog invariant, upon appropriate normalization is of order 10^{-20} in the SM. With such a small CP violation and in absence of any dynamic enhancement it is not possible to generate the observed baryon asymmetry ($\eta_B \sim 10^{-10}$), even if the electroweak phase transition were of first order. Therefore, new sources of CP violation are required beyond the Kobayashi-Maskawa phase of the SM. This demands the need for BSM physics. There have been different BSM proposals for baryogenesis out of which we briefly comment upon the most widely studied ones below.

GUT baryogenesis: In GUT scenarios, baryon number is naturally violated as the quarks and leptons appear as components of the same isospin multiplets. In such theories a net baryon asymmetry is generated from the out-of-equilibrium decay of heavy gauge bosons [24–31]. The authors of [32] have discussed the details of relevant Boltzmann equations in such theories. Although GUT theories provide an elegant explanation for the cosmic baryon asymmetry they face difficulties from the non-observation of the proton decay. It puts a lower limit on the mass of the new gauge bosons in GUT theories. This also demands a very high reheat temperature after the end of inflation. Simple inflationary scenarios do not lead to such high reheat temperatures. Furthermore, typical GUT models violate $B + L$ but not $B - L$. Consequently, the $B + L$ violating SM sphaleron, which is in equilibrium at a temperature $T \lesssim 10^{12}$GeV, will destroy this asymmetry.

Electroweak baryogenesis: In this class of baryogenesis scenarios, known as electroweak baryogenesis [33–35], the departure from equilibrium is provided by a first order electroweak phase transition (EWPT). However, as mentioned before, the electroweak phase transition is not strongly first order [18, 19, 36] in SM. Besides, the CP violation within the SM is too small [37, 38] to generate the observed asymmetry. Thus, any new model of elec-

troweak baryogenesis modifies the scalar potential such that the phase transition becomes strongly first order with new sources of CP violations. One such simple extension is the two Higgs doublet model (2HDM) [39]. Here, due to the presence of another Higgs doublet, the Higgs potential has more parameters. Therefore achieving the FOPT is possible by tuning the parameters appropriately. Also, unlike the SM Higgs potential it can violate CP provided due to the presence of complex couplings. Another popular example is the minimal supersymmetric SM (MSSM) [40, 41] where FOPT can be achieved. While it is possible in principle, to realise electroweak baryogenesis in such simple BSM frameworks, they also face tight experimental constraints from colliders as well as neutron electric dipole moment, which we do not elaborate further.

The Affleck-Dine mechanism: In this scenario, [42,43] the asymmetry first arises in a classical scalar field. Such a scalar field carries a net B number and the scalar potential breaks B explicitly. The cosmological evolution of the scalar field then lead to a net generation of B asymmetry. The scalar field later decays to particles converting the asymmetry. This mechanism is capable of generating asymmetry in any combination of B and L.

Leptogenesis: The idea of leptogeneis was proposed by Fukugita and Yanagida in [44]. It provides an elegant explanation of the cosmic baryon asymmetry with potential connection with the lepton sector physics including theo origin of light neutrino masses. In the simplest models of leptogenesis, new gauge singlet fermions are introduced which are of Majorana type. After the electroweak symmetry breaking, light neutrinos acquire sub-eV masses via the type-I seesaw mechanism [45–48]. The Yukawa couplings of the singlet neutrinos can be complex and hence they provide the necessary sources of CP violation as well. Therefore, when these Majorana singlet fermions decay they can generate an asymmetry in the lepton sector. The Yukawa couplings of the singlet fermions can be chosen appropriately such that their interaction rate remains slow enough ($\Gamma \lesssim \mathbf{H}$) to result in the required departure from thermal equilibrium. The non-perturbative sphaleron processes then convert this lepton asymmetry into a baryon asymmetry [35].

1.4 The basics of vanilla leptogenesis

The existence of non-zero neutrino mass, suggested by different neutrino oscillation experiments has shown strong evidence for physics beyond SM. Leptogenesis can be a common solution for the existence of neutrino mass as well as the BAU. In the most minimal leptogenesis model, new gauge singlet right handed neutrinos are incorporated which also generate light neutrino masses via the type-I seesaw mechanism [45–50] mentioned earlier. The Majorana nature of the neutrinos provides the necessary condition of lepton number violation. To summarise the basic idea of leptogenesis, we consider the type-I seesaw model with heavy singlet right handed neutrinos. The Lagrangian is given by,

$$\mathcal{L} \;=\; \mathcal{L}_{\rm SM} + \bar{N}_i i\partial\!\!\!/ N_i - y_{\alpha j}\bar{L}_\alpha H l_{R_j} - h_{\alpha j}\bar{L}_\alpha \tilde{H}\nu_{R_j} - \frac{1}{2}\overline{\nu^C_{R_i}}(M_R)_{ij}\nu_{R_j} + \text{h.c.} \qquad (1.22)$$

where $L_\alpha = (\nu_{L_\alpha}, l_{L_\alpha})^T$ is the left-handed lepton doublet and $\tilde{H} = i\sigma_2 H^*$, $H = (H^+, H^0)^T$ being the SM Higgs doublet and σ_2 is the Pauli matrix. $y_{\alpha j}$ and $h_{\alpha j}$ are the Yukawa couplings

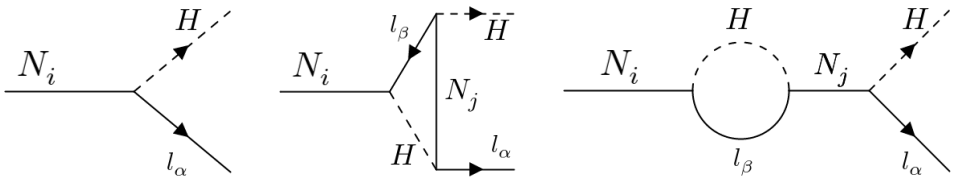

Figure 1.6: Tree level and one-loop corrected Feynman diagrams contributing to a net CP asymmetry from decays of heavy Majorana neutrinos.

of the charged leptons and the neutrinos respectively. As the right handed neutrinos (RHN) are singlet under the SM gauge group, the Majorana mass term for the right handed neutrinos is allowed breaking lepton number by two units. Without the loss of any generality the Majorana mass matrix $(M_R)_{ij}$ can be chosen to real and diagonal. When the electroweak symmetry gets broken, the SM Higgs doublet gets a vacuum expectation value (VEV) $\langle H \rangle = v/\sqrt{2}$ and both the charged leptons and neutrinos acquire masses. The Dirac masses for the charged leptons and the neutrinos are given, respectively, by

$$m_l = \frac{yv}{\sqrt{2}}, \qquad m_{\rm D} = \frac{hv}{\sqrt{2}}. \tag{1.23}$$

The neutrino mass matrix is therefore given by

$$M_\nu = \begin{pmatrix} 0 & m_{\rm D} \\ m_{\rm D}^T & M_{\rm R} \end{pmatrix}.$$

Now, the block diagonalisation of the above mass matrix in the limit $m_D \ll M_R$ leads to the light neutrino mass matrix

$$m_\nu \simeq -m_{\rm D} \frac{1}{M_{\rm R}} m_{\rm D}^T \tag{1.24}$$

which can be diagonalised by the Pontecorvo-Maki-Nakagawa-Sakata (PMNS) mixing matrix U, in the diagonal charged lepton basis. The decays of the right handed neutrino, $N_i \longrightarrow l_\alpha H$ and $N_i \longrightarrow \bar{l_\alpha} \bar{H}$, can produce a lepton asymmetry. The necessary CP violation arises from the interference of the tree level and one-loop diagrams shown in Fig.1.6.

1.4.1 CP asymmetry in heavy neutrino decay

In vanilla leptogenesis, the required CP asymmetry arises from the decay of the right handed neutrinos ($N_i \longrightarrow lH$). As discussed earlier, at the tree level there can not be any net CP violation. In Fig.1.6 the tree level and one-loop corrected diagrams are shown from the interference of which a net CP asymmetry is generated. To have a non-zero CP asymmetry, the conditions mentioned in section 1.2.2 have to be satisfied. The neutrino Yukawa couplings can be complex to introduce new sources of CP violation. The CP asymmetry considering the interference of only the tree and vertex diagram leads to [44, 51]

$$\epsilon^{v}_{i\alpha} = \frac{\Gamma_{N_i\longrightarrow lH} - \Gamma_{N_i\longrightarrow \bar{l}H^\dagger}}{\Gamma_{N_i\longrightarrow lH} + \Gamma_{N_i\longrightarrow \bar{l}H^\dagger}} \tag{1.25}$$

$$= \frac{1}{8\pi(h^\dagger h)_{ii}} \sum_{j\neq i} \mathrm{Im}\left[(h^*)_{\alpha i}(h)_{\alpha j}(h^\dagger h)_{ij}\right] f(M_j^2/M_i^2), \tag{1.26}$$

where the function $f(M_j^2/M_i^2)$ is given by

$$f(z) = \sqrt{z}\left(1 - (1+z)\ln\left(\frac{1+z}{z}\right)\right). \tag{1.27}$$

The contribution coming from the self-energy diagram is calculated in [52, 53]. Later, it is shown that this contribution can be dominant in cases when the right handed neutrinos become degenerate in mass [54]. This contribution is given by

$$\epsilon^{s}_{i\alpha} = \frac{1}{8\pi(h^\dagger h)_{ii}} \sum_{j\neq i} \frac{M_i}{M_j^2 - M_i^2} \mathrm{Im}\{(h^*)_{\alpha i}(h)_{\alpha j}\left[(h^\dagger h)_{ji}M_i + (h^\dagger h)_{ij}M_j\right]\}. \tag{1.28}$$

It can be seen that $\epsilon^{s}_{i\alpha}$ diverges in the limit $M_i = M_j$. In such a case, one needs to take the finite decay widths of the right handed neutrinos in their propagators. This regulates $\epsilon^{s}_{i\alpha}$ in the limit $M_i = M_j$. In the limit, $|M_i - M_j| \sim \Gamma_{i,j}$ the CP asymmetry $\epsilon^{s}_{i\alpha}$ gets resonantly enhanced. In this thesis, we have not studied such a resonant leptogenesis scenario which demands a fine-tuning condition between the right handed neutrino masses. Coming back to the CP asymmetry, in a leading order calculation, the total CP asymmetry parameter is then given by

$$\epsilon_{i\alpha} = \epsilon^{v}_{i\alpha} + \epsilon^{s}_{i\alpha}$$

$$= \frac{1}{8\pi(h^\dagger h)_{ii}} \sum_{j\neq i} \{\mathrm{Im}\left[(h^*)_{\alpha i}(h)_{\alpha j}(h^\dagger h)_{ij}\right] \mathcal{F}(M_j^2/M_i^2)$$

$$+\mathrm{Im}\left[(h^*)_{\alpha i}(h)_{\alpha j}(h^\dagger h)^*_{ij}\right] \mathcal{G}(M_j^2/M_i^2)\}, \tag{1.29}$$

where the loop functions are given by

$$\mathcal{F}(z) = \sqrt{z}\left[1 + \frac{1}{1-z} + (1+z)\ln\left(\frac{z}{1+z}\right)\right], \tag{1.30}$$

$$\mathcal{G}(z) = \frac{1}{1-z}. \tag{1.31}$$

When lepton flavours are summed up, the unflavoured CP asymmetry simply becomes

$$\epsilon_i = \sum_\alpha \epsilon_{i\alpha}$$

$$= \frac{1}{8\pi(h^\dagger h)_{ii}} \sum_j \mathrm{Im}\left[(h^\dagger h)^2_{ij}\right] \mathcal{F}(M_j^2/M_i^2). \tag{1.32}$$

In principle, the asymmetry in each lepton flavour should be tracked independently as each lepton flavour has different interaction rates with the bath [55–58]. In type-I seesaw leptogenesis, such lepton flavour effects are important when the scale of leptogenesis is $M \lesssim 10^{12}$ GeV. In the regime of such flavoured leptogenesis, the CP asymmetry formula given in Eq.(1.29) is used for individual lepton flavours instead of summing them up.

1.5 Boltzmann equations for leptogenesis

Here, we show the derivation of the Boltzmann equations to track the $B-L$ asymmetry in the case of simple "vanilla" leptogenesis. We assume the right handed neutrinos to be hierarchical, which implies that the asymmetry generated from the lightest right handed neutrino (N_1) is only relevant. Any asymmetry generated from the decay of heavier right handed neutrinos ($N_{2,3}$) will be washed out by the inverse decays of N_1. Furthermore, we will consider only one flavour of lepton since the Boltzmann equations for other lepton flavours are expected to take similar forms. The most general Boltzmann equation for any species can be written as

$$\hat{L}[f] = C[f], \tag{1.33}$$

where $\hat{L}$ is the Liouville operator, C is the total collision operator and f is the distribution function for the species. In a homogeneous and isotropic universe, the Liouville operator is given by

$$\hat{L} = E\frac{\partial}{\partial t} - \mathbf{H}|\mathbf{p}|^2\frac{\partial}{\partial E}. \tag{1.34}$$

Here, E and $\mathbf{p}$ are the energy and three momenta of the species respectively and $\mathbf{H}$ is the Hubble parameter. Replacing the Liouville operator in Eq.(1.33) the Boltzmann equation for N_1 can be written as

$$\frac{\partial f_{\mathrm{N}_1}}{\partial t} - |\mathbf{p}_{\mathrm{N}_1}|\mathbf{H}\frac{\partial f_{\mathrm{N}_1}}{\partial |\mathbf{p}_{N_1}|} = C_{\mathrm{D}}\left[f_{\mathrm{N}_1}\right] + C_{\mathrm{S}}\left[f_{\mathrm{N}_1}\right], \tag{1.35}$$

where f_{N_1} is the phase space distribution function of N_1 and $\mathbf{p}_{\mathrm{N}_1}$ is the N_1 momentum. The right hand side of the Eq.(1.35) consists of the collision terms. $C_{\mathrm{D}}\left[f_{\mathrm{N}_1}\right]$ represents the N_1 decays to lepton and Higgs while the term $C_{\mathrm{S}}\left[f_{\mathrm{N}_1}\right]$ represent the scattering processes which can change the number of N_1. These collision operators are related to the one in Eq.(1.33) as $C = EC_{\mathrm{D}} + EC_{\mathrm{S}}$.

The Boltzmann equations of leptons and antileptons with phase space distribution f_l and $f_{\bar{l}}$ have a similar form to Eq.(1.35). Since we wish to track the evolution of the difference between lepton and antilepton number densities, it is useful to define

$$f_{\Delta \mathrm{L}} \equiv f_l - f_{\bar{l}}. \tag{1.36}$$

Then the Boltzmann equation for $f_{\Delta L}$ becomes

$$\frac{\partial f_{\Delta \mathrm{L}}}{\partial t} - |\mathbf{p}_l|\mathbf{H}\frac{\partial f_{\Delta \mathrm{L}}}{\partial |\mathbf{p}_l|} = C_{\mathrm{D}}[f_{\Delta \mathrm{L}}] + C_{\mathrm{S}}[f_{\Delta \mathrm{L}}], \tag{1.37}$$

where the collision terms are $C_{\mathrm{D,S}}\left[f_{\Delta \mathrm{L}}\right] \equiv C_{\mathrm{D,S}}\left[f_l\right] - C_{\mathrm{D,S}}\left[f_{\bar{l}}\right]$. The number density of lepton asymmetry can be found out by doing the phase space integration of $f_{\Delta \mathrm{L}}$,

$$n_{\Delta \mathrm{L}} \equiv \frac{g_l}{(2\pi)^3}\int d^3 p_l f_{\Delta \mathrm{L}}. \tag{1.38}$$

The lepton asymmetry per comoving photon is defined as

$$n_{\Delta \mathrm{L}} \equiv \frac{n_{\Delta \mathrm{L}}}{n_\gamma^{\mathrm{eq}}}, \tag{1.39}$$

where $n_\gamma^{\mathrm{eq}} = (\zeta(3)/\pi^2) g_\gamma T^3$ is the equilibrium number density of photon with $g_\gamma = 2$ being the internal degrees of freedom of photon.

It is convenient to write the Eqs.(1.35) and (1.37) in terms of the dimensionless variables $z = M_1/T$ and $x = |\mathbf{p}_{\mathrm{N}_1}|/T$, where M_1 is the mass of N_1. Using the relation $dT/dt = -\mathbf{H}T$, the differential operator $\partial_t - |\mathbf{p}_{\mathrm{N}_1}|\mathbf{H}\partial|\mathbf{p}_{\mathrm{N}_1}|$ becomes $z\mathbf{H}\partial_z$. Therefore Eqs.(1.35) and (1.37) become

$$\frac{\partial f_{\mathrm{N}_1}(z,x)}{\partial z} = \frac{z}{\mathbf{H}(M_1)}\left(C_{\mathrm{D}}\left[f_{\mathrm{N}_1}(z,x)\right] + C_{\mathrm{S}}\left[f_{\mathrm{N}_1}(z,x)\right]\right), \tag{1.40}$$

$$\frac{\partial f_{\Delta \mathrm{L}}(z,x)}{\partial z} = \frac{z}{\mathbf{H}(M_1)}\left(C_{\mathrm{D}}\left[f_{\Delta \mathrm{L}}(z,x)\right] + C_{\mathrm{S}}\left[f_{\Delta \mathrm{L}}(z,x)\right]\right). \tag{1.41}$$

Here $\mathbf{H}(M_1)$ is the Hubble expansion rate evaluated at $T = M_1$ and M_{Pl} is the Planck mass. Given the particle physics interactions of N_1 and the leptons Eqs.(1.40) and (1.41) track the evolution of N_1 and the lepton asymmetry.

To calculate the collision terms we first consider the simplest case where N_1 does not have any number-changing interaction except the decay and inverse decay. For this simplest case $C_{\mathrm{S}} = 0$. In such case, the collision integral takes the following form

$$\begin{aligned} C_{\mathrm{D}}\left[f_{\mathrm{N}_1}\right] &= \frac{1}{2E_{\mathrm{N}_1}}\int \frac{d^3 p_l}{2E_l(2\pi)^3}\frac{d^3 p_{\mathrm{H}}}{2E_{\mathrm{H}}(2\pi)^3}(2\pi)^4\delta^4(p_{\mathrm{N}_1} - p_l - p_{\mathrm{H}}) \\ &\times \left[f_{\mathrm{H}} f_l(1 - f_{\mathrm{N}_1})\left(|\mathcal{M}_{Hl\longrightarrow N_1}|^2\right) + \left(|\mathcal{M}_{H^\dagger \bar{l}\longrightarrow N_1}|^2\right)\right. \\ &- \left. f_{\mathrm{N}_1}(1 - f_l)(1 + f_{\mathrm{H}})\left(|\mathcal{M}_{N_1\longrightarrow Hl}|^2 + |\mathcal{M}_{N_1\longrightarrow H^\dagger \bar{l}}|^2\right)\right], \end{aligned} \tag{1.42}$$

where E_i and p_i are the energy and 4−momenta of the species i. Here the matrix element for any process A is represented by $\mathcal{M}_{\mathrm{A}}$. At the tree level, the matrix element squared for the decay of N_1 is given by

$$|\mathcal{M}_{N_1\longrightarrow Hl}| = 2\frac{(m_{\mathrm{D}}^\dagger m_{\mathrm{D}})_{11}}{v^2} p_l p_{\mathrm{N}_1}, \tag{1.43}$$

where v is the VEV of SM Higgs boson, and $m_{\rm D}$ is the Dirac mass matrix for the neutrinos. The Eq.(1.42) is reducible to a one dimensional form [59],

$$C_{\rm D}\left[f_{\rm N_1}\right] = \frac{M_1\Gamma_{\rm N_1}}{E_{\rm N_1}p_{\rm N_1}}\int_{(E_{\rm N_1}-p_{\rm N_1})/2}^{(E_{\rm N_1}+p_{\rm N_1})/2} dp_{\rm H}\left[f_{\rm H}f_l(1-f_{\rm N_1}) - f_{\rm N_1}(1-f_l)(1+f_{\rm H})\right]. \tag{1.44}$$

Here

$$\Gamma_{\rm N_1} = \frac{\tilde{m}_1 M_1^2}{8\pi v^2}, \tag{1.45}$$

is the total decay width of N_1, with $\tilde{m}_1 = (m_{\rm D}^\dagger m_{\rm D})_{11}/M_1$ being the effective neutrino mass [60]. For the leptons, the corresponding collision integral is given by

$$\begin{aligned} C_{\rm D}\left[f_l\right] &= \frac{1}{2E_l}\int \frac{d^3p_{N_1}}{2E_l(2\pi)^3}\frac{d^3p_{\rm H}}{2E_{\rm H}(2\pi)^3}(2\pi)^4\delta^4(p_{\rm N_1}-p_l-p_{\rm H}) \\ &\times \left[f_{\rm N_1}(1-f_l)(1+f_{\rm H})\mid \mathcal{M}_{N_1\longrightarrow Hl}\mid^2 - \right. \\ &\left. f_{\rm H}f_l(1-f_{\rm N_1})\mid \mathcal{M}_{Hl\longrightarrow N_1}\mid^2\right]. \end{aligned} \tag{1.46}$$

A similar expression for the antileptons can be derived by replacing $f_l \longrightarrow f_{\bar{l}}$, $\mathcal{M}_{N_1\longrightarrow Hl} \longrightarrow \mathcal{M}_{N_1\longrightarrow H^\dagger\bar{l}}$ and $\mathcal{M}_{Hl\longrightarrow N_1} \longrightarrow \mathcal{M}_{H^\dagger\bar{l}\longrightarrow N_1}$. From CPT-invariance we can write some important relations between these matrix elements

$$|\mathcal{M}_{N_1\longrightarrow Hl}|^2 = |\mathcal{M}_{H^\dagger\bar{l}\longrightarrow N_1}|^2 = |\mathcal{M}_0|^2(1+\epsilon_1), \tag{1.47}$$

$$|\mathcal{M}_{N_1\longrightarrow H^\dagger\bar{l}}|^2 = |\mathcal{M}_{Hl\longrightarrow N_1}|^2 = |\mathcal{M}_0|^2(1-\epsilon_1). \tag{1.48}$$

Where $|\mathcal{M}_0|^2$ is the tree level matrix elements given in Eq.(1.43). CPT-invariance guarantees that if N_1 decays prefer the production of L then its inverse decays prefer the destruction of $\bar{L}$. Therefore a net lepton asymmetry can be generated even if N_1 is in thermal equilibrium. It seems to contradict Sakharov's condition. This trouble can be corrected by subtracting the real intermediate state (RIS) contribution from the scattering process $lH \longrightarrow \bar{l}H^\dagger$ [32,61]. To explicitly break the scattering process into RIS and the remainder one needs to calculate the process including the one-loop and vertex corrections in the resonance region. Implementing this procedure proposed in [62], we add the following term in the collision integral of Eq.(1.39)

$$f_{\rm H}f_{\bar{l}}(1-f_{\rm N_1})|\mathcal{M}_{H^\dagger\bar{l}\longrightarrow N_1}|^2_{\rm sub} - f_{\rm H}f_l(1-f_{\rm N_1})|\mathcal{M}_{Hl\longrightarrow N_1}|^2_{\rm sub}. \tag{1.49}$$

Where $|\mathcal{M}_{Hl\longrightarrow N_1}|^2_{\rm sub}$ and $|\mathcal{M}_{H^\dagger\bar{l}\longrightarrow N_1}|^2_{\rm sub}$ are the RIS contribution subtracted matrix elements and are given by

$$|\mathcal{M}_{H\bar{l}\longrightarrow N_1}|^2_{\rm sub} = |\mathcal{M}|^2_{\Delta \rm L=2} - \epsilon_1|\mathcal{M}_0|^2, \tag{1.50}$$

$$|\mathcal{M}_{Hl\longrightarrow N_1}|^2_{\rm sub} = |\mathcal{M}|^2_{\Delta \rm L=2} + \epsilon_1|\mathcal{M}_0|^2. \tag{1.51}$$

We now derive the conventional integrated Boltzmann equations by integrating the Boltzmann Eqs.(1.40) and (1.41) over momentum. Finding a closed form of the integrated Boltzmann equations is not possible if certain approximations are not considered. First, the effects of quantum statistics are neglected. Maxwell-Boltzmann distribution function is considered for each particle. Besides, it is assumed that all the SM particles are in thermal equilibrium sharing the same temperature due to their strong gauge interactions. Also, kinetic equilibrium is considered among the RHNs. With these simplifying assumptions and using the conservation of energy, we get

$$f_{\rm H} f_l = e^{-(E_{\rm H}+E_l)/T} = e^{-E_{\rm N_1}/T} = f^{\rm eq}_{\rm N_1}. \tag{1.52}$$

Then the collision integral in Eq.(1.44) becomes

$$C_{\rm D}\left[f_{\rm N_1}\right] = \frac{M_1\Gamma_{\rm N_1}}{E_{\rm N_1}p_{\rm N_1}}\int_{(E_{\rm N_1}-p_{\rm N_1})/2}^{(E_{\rm N_1}+p_{\rm N_1})/2} dp_{\rm H}\left[f^{\rm eq}_{\rm N_1} - f_{\rm N_1}\right]. \tag{1.53}$$

Completing the integration over $p_{\rm H}$ and replacing $C_{\rm D}\left[f_{\rm N_1}\right]$ in Eq.(1.40) yields

$$\frac{\partial f_{\rm N_1}}{\partial z} = \frac{z\Gamma_{\rm N_1}}{\mathbf{H}(M_1)}\frac{M_1}{E_{\rm N_1}}\left(f^{\rm eq}_{\rm N_1} - f_{\rm N_1}\right). \tag{1.54}$$

The kinetic equilibrium for the RHNs allows us to write $f_{\rm N_1}/f^{\rm eq}_{\rm N_1} \approx n_{\rm N_1}/n^{\rm eq}_{N_1}$, where $n_{\rm N_1}$ is the number density of N_1. Now, integrating Eq.(1.54) over the RHN phase space it is easy to obtain

$$\frac{\partial n_{\rm N_1}}{\partial z} = -zK_1\left\langle\frac{M_1}{E_{\rm N_1}}\right\rangle(n_{\rm N_1} - n^{\rm eq}_{\rm N_1}), \tag{1.55}$$

where $K_1 = \Gamma_{\rm N_1}/\mathbf{H}(M_1)$, and $\langle\Gamma_{\rm N_1}\rangle \equiv \Gamma_{\rm N_1}\langle M_1/E_{\rm N_1}\rangle = (\Gamma_{\rm N_1}/n^{\rm eq}_{\rm N_1})\int d^3p_{\rm N_1}/(2\pi)^3 f^{\rm eq}_{\rm N_1}(M_1/E_{\rm N_1})$ is the thermal average decay rate [32]. The dilation factor coming due to the thermal average is given by the ratio of the modified Bessel functions of the second kind and second order, $\langle M_1/E_{\rm N_1}\rangle = \kappa_1(z)/\kappa_2(z)$. Dividing Eq.(1.55) by equilibrium photon density, the usual Boltzmann equation can be obtained for the comoving number density $Y_{\rm N_1} = n_{\rm N_1}/n_\gamma$,

$$\frac{\partial Y_{\rm N_1}}{\partial z} = -D_1\left(Y_{\rm N_1} - Y^{\rm eq}_{\rm N_1}\right), \tag{1.56}$$

where

$$D_1 = zK_1\langle M_1/E_{\rm N_1}\rangle \tag{1.57}$$

$$= \frac{\langle\Gamma_{\rm N_1}\rangle}{\mathbf{H}z}. \tag{1.58}$$

The equilibrium comoving number density for N_1 is given by

$$Y^{\rm eq}_{\rm N_1} = \frac{3}{8}z^2\kappa_2(z). \tag{1.59}$$

In order to get the most realistic results, Fermi-Dirac distribution is considered for the right handed neutrinos while calculating $Y^{\rm eq}_{\rm N_1}$, which results in $n^{\rm eq}_{\rm N_1} = [3\xi(3)g_{\rm N_1}TM_1^2/(8\pi^2)]\,\kappa_2(z)$.

Here the internal degrees of freedom of the RHN $g_{\rm N_1} = 2$ and $\xi(3) \approx 1.202$. This consideration leads to an extra prefactor $(3/4)\xi(3)$ in the definition of $Y^{\rm eq}_{\rm N_1}$ compared to the strictly Maxwell-Boltzmann case.

Similarly from Eqs.(1.40), (1.46) and (1.48) the BE for the $f_{\Delta \rm L}$ is given by,

$$\frac{\partial f_{\Delta \rm L}}{\partial z} = -\frac{z^2 K_1}{2x_l^2} \int_{x^0_{\rm N_1}}^{\infty} dx_{\rm N_1} \frac{x_{\rm N_1}}{(E_{\rm N_1}/T)} \left[f_{\rm H} f_{\Delta \rm L} - 2\epsilon_1 (f_{\rm N_1} - f^{\rm eq}_{\rm N_1}) \right], \tag{1.60}$$

Here we define $x^0_{\rm N_1} = \frac{z^2 - 4x_l^2}{4x_l}$. Using energy conservation and the kinetic equilibrium condition for the right handed neutrinos, the Eq.(1.60) can be integrated out to be,

$$\frac{\partial f_{\Delta \rm L}}{\partial z} = -\frac{z^2 K_1}{2x_l^2} e^{-\frac{z^2 + 4x_l^2}{4x_l}} \left[e^{x_l} - 2\epsilon_1 \left(\frac{n_{\rm N_1} - n^{\rm eq}_{\rm N_1}}{n^{\rm eq}_{\rm N_1}} \right) \right]. \tag{1.61}$$

Further, considering both chemical and kinetic equilibrium for the SM leptons we can write,

$$\begin{aligned} f^{\rm eq}_{\Delta \rm L} &= e^{-(E_l - \mu)/T} - e^{-(E_l + \mu)/T} \simeq 2(\mu/T) e^{-E_l/T}, \\ n^{\rm eq}_{\Delta \rm L} &\simeq 2(\mu/T) n^{\rm eq}_l, \\ f_{\Delta \rm L} &\simeq \frac{n_{\Delta \rm L}}{n^{\rm eq}_l} e^{-x_l}, \end{aligned} \tag{1.62}$$

where $\mu \ll 1$ is the chemical potential of the leptons and $n^{\rm eq}_l$ is the equilibrium number density of the leptons. Finally, integrating the Eq.(1.61) over the lepton phase space the BE for the lepton asymmetry becomes

$$\frac{\partial n_{\Delta \rm L}}{\partial z} = -\frac{z^3 K_1 T^3}{2\pi^2} \kappa_1(z) \left[\frac{n^{\rm eq}_{\Delta \rm L}}{n^{\rm eq}_l} - 2\epsilon_1 \left(\frac{n_{\rm N_1} - n^{\rm eq}_{\rm N_1}}{n^{\rm eq}_{\rm N_1}} \right) \right], \tag{1.63}$$

Now, dividing the Eq.(1.63) by n_γ it is straight forward to show that

$$\frac{\partial Y_{\Delta \rm L}}{\partial z} = \epsilon_1 D_1 (Y_{\rm N_1} - Y^{\rm eq}_{\rm N_1}) - W_{\rm ID} Y_{\Delta \rm L}, \tag{1.64}$$

where

$$W_{\rm ID} = \frac{1}{4} K_1 z^3 \kappa_1(z). \tag{1.65}$$

The first term on the right-hand side of Eq.(1.64) signifies the asymmetry generated by the CP violating out of equilibrium decay of RHN and the second term represents the washout of the lepton asymmetry due to the inverse decay. In addition to the inverse decay, there can be scattering processes which can contribute to the washout of the asymmetry. Some of the main washout scattering processes in minimal type-I seesaw-based models are

1. $\Delta L = 1$ process: $N_1 l \longrightarrow t\bar{q}$,
2. $\Delta L = 2$ process: $lH \longrightarrow \bar{l} H^\dagger$, $ll \longrightarrow H^\dagger H^\dagger$, $\bar{l}\bar{l} \longrightarrow HH$.

Such scattering processes will add to the Boltzmann equation for the lepton asymmetry as washout leading to

$$\frac{\partial Y_{\Delta \mathrm{L}}}{\partial z} = \epsilon_1 D_1 (Y_{\mathrm{N}_1} - Y^{\mathrm{eq}}_{\mathrm{N}_1}) - (W_{\mathrm{ID}} + \Delta W) Y_{\Delta L}, \tag{1.66}$$

where $\Delta W = \langle \Gamma_{\mathrm{S}} \rangle / \mathbf{H} z$ corresponds to the washout due to all such scattering processes. Here $\langle \Gamma_{\mathrm{S}} \rangle$ is the thermal average rate of the scattering processes.

1.5.1 Converting L asymmetry into B asymmetry

Finally, the lepton asymmetry needs to be converted into baryon asymmetry. This is done by the electroweak sphaleron processes [17]. The electroweak $B + L$ anomaly implies the processes which create a $u_L d_L d_L \nu_L$ state out of the vacuum. These vacuum transitions are referred to as the sphaleron processes. The amount of lepton asymmetry which gets converted into baryon asymmetry is known as the sphaleron conversion factor which can be derived following the standard approach outlined in [63].

Any particle asymmetry is often conveniently expressed in terms of its chemical potential. The important relation between the particle anti-particle asymmetry and the chemical potentials is given below,

$$n_+ - n_- = \frac{gT^3}{3}\left[\frac{\mu}{T}\right] \quad \text{(for Bosons)}, \tag{1.67}$$

$$n_+ - n_- = \frac{gT^3}{6}\left[\frac{\mu}{T}\right] \quad \text{(for Fermions)}, \tag{1.68}$$

$$\tag{1.69}$$

where n_+ and n_- are the equilibrium number densities of particles and antiparticles respectively. g is the internal degrees of freedom of the species. The quantum numbers, for instance, the lepton (L) number is defined as $L = (n_l - n_{\bar{l}})/s$, where s is the entropy density of the universe. Therefore to find the sphaleron conversion factor we have to consider different constraints appearing among the chemical potentials of different particles due to various processes.

To calculate the sphaleron conversion factor, consider a particle physics model model with N_f generations of quarks, leptons and m Higgs doublets in addition to the SM gauge fields. The N_f generations of fermions imply N_f generations of left-handed quark doublets $(u_{iL}, d_{iL})^T$, N_f generations of left-handed lepton doublets $(\nu_{iL}, e_{iL})^T$, N_f generations of right-handed up type quark singlets (u_{iR}), N_f generations of right-handed down type quark singlets (d_{iR}) and N_f generations of right-handed charged lepton singlets (e_{iR}). The gluons as well as other neutral gauge fields have zero chemical potentials. We now assign the chemical potentials to different fields having non-zero chemical potentials as follows: μ_W for W^-, μ_0 or all m neutral components of the doublets H^0, μ_- for all the charged components of the doublets H^-, μ_{uL} for all the left-handed up type quark, μ_{dL} for all the left-handed down type quark, μ_{uR} for all right-handed up type quarks, μ_{dR} for all right-handed down type quarks, μ_i for all left-handed neutrinos, μ_{iL} for all left-handed charged leptons and μ_{iR} for right-handed charged leptons. Here we assume that the mixing coming from the Cabibbo angles

should be able to maintain the equality of different up and down quark states and the mixing between multiple Higgs doublet should maintain the equality among themselves. Some rapid electroweak processes enforcing the equilibrium relations among different chemical potentials are given below

$$\begin{aligned}
\mu_W &= \mu_- + \mu_0 \quad (W^- \longrightarrow H^- + H^0), && (1.70)\\
\mu_{dL} &= \mu_{uL} + \mu_W \quad (W^- \longrightarrow \bar{u}_L + d_L), && (1.71)\\
\mu_{iL} &= \mu_i + \mu_W \quad (W^- \longrightarrow \bar{\nu}_{iL} + e_{iL}), && (1.72)\\
\mu_{uR} &= \mu_0 + \mu_{uL} \quad (H^0 \longrightarrow \bar{u}_L + u_R), && (1.73)\\
\mu_0 &= \mu_{dL} - \mu_{dR} \quad (H^0 \longrightarrow d_L + \bar{d}_R),\\
\Rightarrow \mu_{dR} &= -\mu_0 + \mu_{uL} + \mu_W, && (1.74)\\
\mu_0 &= \mu_{iL} - \mu_{iR} \quad (H^0 \longrightarrow e_{iL} + \bar{e}_{iR}),\\
\Rightarrow \mu_{iR} &= \mu_i + \mu_W - \mu_0. && (1.75)
\end{aligned}$$

By applying these relations one can write all the chemical potentials in terms of μ_W, μ_0, μ_{uL}, and μ_i. In addition, the electroweak sphaleron process imposes the following condition

$$\begin{aligned}
N_f(\mu_{uL} + 2\mu_{dL}) + \sum_i \mu_i &= 0,\\
3N_f\mu_{uL} + 2N_f\mu_W + \mu &= 0. && (1.76)
\end{aligned}$$

Here we have written $\sum_i \mu_i = \mu$ for convenience. The B, L, charge, and the third component of weak isospin number densities can be expressed in terms of our chosen $3 + N_f$ chemical potential as follows

$$\begin{aligned}
B &= N_f(\mu_{uL} + \mu_{uR}) + N_f(\mu_{dL} + \mu_{dR})\\
&= 4N_f\mu_{uL} + 2N_f\mu_W, && (1.77)\\
L &= \sum_i (\mu_i + \mu_{iL} + \mu_{iR}),\\
&= 3\mu + 2N_f\mu_W - N_f\mu_0, && (1.78)\\
Q &= 2N_f(\mu_{uL} + \mu_{uR}) - N_f(\mu_{dL} + \mu_{dR}) - \sum_i (\mu_{iL} + \mu_{iR})\\
&\quad -\mu_W - 2m\mu_-,\\
&= 2N_f\mu_{uL} - 2\mu - (4N_f + 2m + 4)\mu_W + (4N_f + 2m)\mu_0, && (1.79)\\
& && (1.80)
\end{aligned}$$

$$\begin{aligned}
Q_3 &= \frac{3N_f}{2}(\mu_{uL} - \mu_{dL}) + \frac{1}{2}\sum_i (\mu_i - \mu_{iL}) - 4\mu_W - m(\mu_0 + \mu_-),\\
&= -(2N_f + m + 4)\mu_W. && (1.81)
\end{aligned}$$

Above the critical temperature T_C (the temperature at which the electroweak symmetry gets broken) both Q and Q_3 must vanish. Therefore, from Eq.(1.81), $\mu_W = 0$. Also from the Eq.(1.79), we get $\mu_0 = (\mu - N_f\mu_{uL})/2N_f + m$. Putting these values in the Eqs.(1.81) and (1.78) one can arrive at the following relations,

$$B = 4N_f\mu_{uL}, \tag{1.82}$$

$$L = -\frac{14N_f^2 + 9N_f m}{2N_f + m}\mu_{uL}. \tag{1.83}$$

A straightforward calculation leads to the following important relations between the B and L numbers,

$$B = \frac{8N_f + 4m}{22N_f + 13m}(B - L), \tag{1.84}$$

$$L = -\frac{14N_f + 9m}{22N_f + 13m}(B - L), \tag{1.85}$$

$$B + L = -\frac{14N_f + 9m}{22N_f + 13m}(B - L). \tag{1.86}$$

For the SM (N_f=3, $m = 1$), the sphaleron conversion factor from $B - L$ asymmetry to B asymmetry is the well-known result

$$B = \frac{28}{79}(B - L). \tag{1.87}$$

1.5.2 Lower bound on leptogenesis scale

As discussed earlier, leptogenesis provides an elegant explanation for the BAU in connection with the neutrino masses and mixing. The Yukawa couplings involved in the lepton number violating decay also generate the Dirac masses for the light neutrinos. Therefore, the results of leptogenesis are strictly constrained by neutrino masses as well as mixings. In the context of type-I seesaw models, there is a strict lower bound on the mass of the decaying right handed neutrino required for successful leptogenesis. This bound was first pointed out in [64]. To see how the lower bound on the right handed neutrino mass appears, let us start with the CP asymmetry generated from the decay of right handed neutrino N_i given in Eq.(1.32). Assuming the right handed neutrinos are hierarchical in mass the lepton asymmetry is essentially generated from the decay of the lightest right handed neutrino and the relevant CP asymmetry becomes

$$\epsilon_1 = -\frac{3}{8\pi}\frac{1}{(h^\dagger h)_{11}}\sum_{j\neq 1}\mathrm{Im}\left\{\left(h^\dagger h\right)^2_{1j}\right\}\left(\frac{M_1}{M_j}\right) = -\frac{3}{8\pi}\frac{M_1}{v^2}\frac{1}{(h^\dagger h)_{11}}\mathrm{Im}\{\left(hm_\nu^\dagger h^T\right)_{11}\}. \tag{1.88}$$

The Dirac Yukawa coupling h can be parameterised by the Casas-Ibarra (CI) parametrisation introduced in [65]. Following the CI parametrisation we can write

$$h = \frac{1}{v} D_{\sqrt{M}} R D_{\sqrt{m}} U^{\dagger}. \tag{1.89}$$

Here $D_{\sqrt{A}} = \sqrt{D_A}$ is for any matrix A. $D_M = \text{diag}\{M_1, M_2, M_3\}$ is the diagonal mass matrix for the right handed neutrinos and $D_m = \text{diag}\{m_1, m_2, m_3\}$ is the diagonal light neutrino mass matrix and R is any complex orthogonal matrix. Substituting Eq.(1.89) in Eq.(1.88),

$$\epsilon_1 \simeq -\frac{3}{8\pi} \frac{M_1}{v^2} \frac{\sum_j m_j^2 \text{Im}(R_{1j}^2)}{\sum_j m_j |R_{1j}|^2}. \tag{1.90}$$

Now, using the orthogonality condition for the R matrix $\sum_j R_{1j}^2 = 1$, it is easy to show that

$$|\epsilon_1| \lesssim \frac{3}{8\pi} \frac{M_1}{v^2} (m_3 - m_1). \tag{1.91}$$

It is important to note that the CP asymmetry goes to zero if the light neutrinos degenerate in mass. For hierarchical right handed neutrino masses, the left-handed neutrinos are also hierarchical. Therefore one can assume $m_3 \gg m_1$, hence

$$|\epsilon_1| \lesssim \frac{3}{8\pi} \frac{M_1 m_3}{v^2}. \tag{1.92}$$

From Eqs.(1.91) and (1.92) it can be seen that the CP asymmetry crucially depends on the right handed neutrino mass and also on the light neutrino masses. In thermal leptogenesis the CP asymmetry required to generate the observed baryon to photon ratio is $\epsilon_1 > 10^{-6}$. To generate this amount of CP asymmetry for the experimentally measured values of light neutrino mass, one needs a right handed neutrino mass to be $M_1 > 4 \times 10^9$ GeV, known as the Davidson-Ibarra bound [64]. While we have discussed this lower bound for the type-I seesaw model, similar bounds exist for leptogenesis in other canonical seesaw models like type-II [48, 50, 66–69] and type-III [70]. This bound can however, be relaxed in resonant leptogenesis regime [71] where even for TeV scale M_1, one can generate correct light neutrino mass and required lepton asymmetry via resonantly enhanced CP asymmetry.

1.6 Observational evidence of dark matter

1.6.1 Dark matter evidence in galaxies and galaxy clusters

The strongest and most well-known evidence for the existence of DM comes from the observation of spiral galaxies. The arms of a spiral galaxy consist of stars, intergalactic gas, and dust. These objects move around the centre of the galaxy due to the gravitational interaction with the galactic centre. By using Newtonian gravity, the circular velocity v_C for these objects is found to be

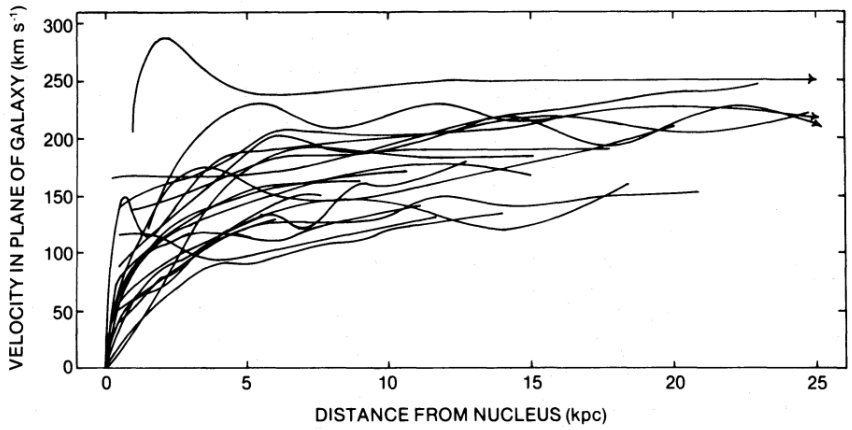

Figure 1.7: Circular velocity plotted against radial distance from the centre of galaxies, observed by Rubin *et al* [4]. Figure is taken from [14].

$$v_C(r) = \left(\frac{GM(r)}{r}\right)^{1/2}, \tag{1.93}$$

where G is the gravitational constant and $M(r)$ is the total mass within a galactic disk of radius r. Using Gauss' law in Eq.(1.93), it can be seen clearly that the v_C should increase with the increase in radius at least up to some radius $r_{\max}$ (order of few kpcs) within which most of the visible matter is contained. Beyond this radius, one would expect the v_C to fall as $1/\sqrt{r}$. However, it is observed that after rising r beyond $r_{\max}$, v_C remains constant, implying that $M(r) \propto r$. This indicates that apart from the visible matter, there exists an additional kind of matter whose mass linearly increases with radial distance r. Fig.1.7 shows the rotation curves of 21 Sc spiral galaxies observed by Rubin *et al* [4]. It shows that the circular velocity becomes almost flat at a large radial distance from the galactic centre. After this discovery, there have been multiple studies and shreds of evidence supporting the same conclusion [72–75].

There is similar evidence of the existence of DM on the galaxy cluster scales. General relativity tells us that, the gravitational field of any massive object bends the path of light passing near it. This phenomenon is known as gravitational lensing. This lensing completely relies on gravitational interaction and includes both luminous as well as non-luminous matter. Due to this gravitational lensing, we could in principle, observe multiple images, arcs, or even rings, known as Einstein rings. This type of gravitational lensing is known as strong gravitational lensing. Unfortunately, in many practical cases, the lensing is much weaker. In these cases, instead of observing multiple images and arcs, one can still get to observe a weakly distorted image of the source, appearing more elliptical. By observing a large ensemble of such sources, this noise can be averaged out to obtain information on the intermediate matter distribution. By using this weak lensing method people have impressively mapped the distribution of masses in a collision of two galaxy clusters, "Bullet Cluster (1E0657-558)" [76, 77]. It is one of the most convincing signatures supporting the existence of DM within galaxy clusters. It is a collision of two giant galaxies which occurred at about 4 billion

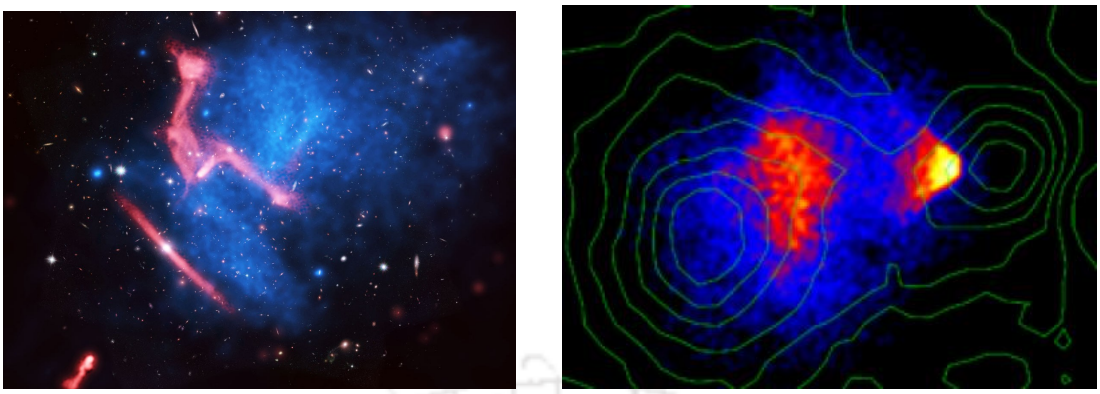

Figure 1.8: Representation of two galaxy clusters collision. The red patches are visible matter observed by Chandra X-ray observatory. The Blue patches are the DM region mapped by the gravitational lensing. The left panel figure is taken from [80] and the right panel figure is taken from [6].

light years from our solar system. The visible matter from the collision is mapped by the Chandra X-ray observatory. In Fig.1.8 the representation of the collision is shown. The red patches are visible matter observed by the Chandra X-ray observatory while the blue patches represent the region where the non-luminous matter is situated mapped by the weak lensing. It can be seen that due to strong electromagnetic interaction, the visible matter is held up near the centre whereas the non-luminous part has passed straight through. This event not only provides support for the existence of DM but also suggests the weakly interacting nature of DM. Observations of galaxy clusters like MACS J0025.4-1222 [78], and Abel cluster [79] have also reported similar results.

1.6.2 Dark matter in ΛCDM cosmology

The ΛCDM model of cosmology is the most successful cosmological model so far. There are six independent parameters in the ΛCDM cosmology, which are baryon density ($\Omega_{\rm B}h^2$), the DM density ($\Omega_{\rm DM}h^2$), scalar spectrum index (n_s), age of the universe (t_0), curvature fluctuation amplitude (Δ_r^2) and the reionization optical depth (τ). Other parameters are derivable from these six parameters. The CMB anisotropy measurements [3] are in excellent agreement with the ΛCDM model. The universe is observed to be spatially isotropic and homogeneous. Such a universe is described by the Friedmann-Lemaitre-Robertson-Walker (FLRW) metric which is given by

$$ds^2 = dt^2 - a^2(t)\left(\frac{dr^2}{1-kr^2} + r^2\left(d\theta^2 + \sin^2\theta d\phi^2\right)\right), \tag{1.94}$$

where, r, θ, ϕ, t are comoving coordinates, $a(t)$ is the cosmic scale factor. Here, k determines the spatial curvature of the universe. It takes values $+1, -1, 0$ representing positive, negative and flat spatial curvature of the universe respectively.

The dynamical equation of motion known as the Friedmann equation is derived by using the FLRW metric in the Einstein field equation

$$\mathcal{R}_{\mu\nu} - \frac{1}{2}Rg_{\mu\nu} = 8\pi G T_{\mu\nu} + \Lambda g_{\mu\nu}. \tag{1.95}$$

Here $\mathcal{R}_{\mu\nu}$, R and $T_{\mu\nu}$ are the Ricci tensor, Ricci scalar and stress-energy tensor respectively and Λ is the cosmological constant. For a universe composed of a perfect fluid, the energy momentum is given by

$$T_{\mu\nu} = -pg_{\mu\nu} + (p+\rho)u_\mu u_\nu, \tag{1.96}$$

where p and ρ are the pressure and energy density of the perfect fluid respectively. $u_{\mu,\nu}$ are the velocity vector in comoving coordinates. The pressure and the energy density is related by the equation of state $p = \omega\rho$. The equation of state parameter ω takes different values depending on the dominant component of the universe's energy density. Finally, the dynamic Friedmann equations for the scale factor can be derived to be

$$\mathbf{H}^2 = \frac{\dot{a}^2}{a^2} = \frac{8\pi G\rho}{3} - \frac{k}{a^2} + \frac{\Lambda}{3}, \tag{1.97}$$

$$\frac{\ddot{a}}{a} = \frac{\Lambda}{3} - \frac{4\pi G}{3}(p+3\rho), \tag{1.98}$$

where $\mathbf{H}$ is the Hubble expansion rate. From the above two equations, one can find an important equation indicating the evolution of the energy density of the universe,

$$\dot{\rho} = -3\mathbf{H}\left(p+\rho\right). \tag{1.99}$$

We now define the energy densities for each component of the universe. For radiation $\Omega_{\rm rad} = \rho_{\rm rad}/\rho_{\rm crit}$, matter $\Omega_{\rm m} = \rho_{\rm m}/\rho_{\rm crit}$ and dark energies as $\Omega_\Lambda = \Lambda/\rho_{\rm crit}$, where $\rho_{\rm crit}$ is critical density of the universe. In terms of these energy densities, Eq.(1.97) can be written as

$$\frac{k}{a^2\mathbf{H}^2} = \Omega_{\rm rad} + \Omega_{\rm m} + \Omega_\Lambda - 1. \tag{1.100}$$

The Planck satellite has precisely measured all the above-mentioned parameters. These estimates are also supported by estimates from large-scale structure (LSS), supernovae and BBN measurements. Fig.1.9 shows an excellent agreement between these observations.

1.7 Properties of dark matter particle

The multiple pieces of evidence discussed above establish the existence of DM in the universe. However, the particle nature of DM is yet to be understood. For a new particle to be a DM candidate, must have certain properties. Firstly, DM candidates should be stable, at least they should be stable over the cosmological time scale to be present in sizeable abundance at present time. Also, the particle should be electrically neutral since DM do not have electromagnetic interaction. The Bullet Cluster observation indicates that if DM has any interaction except gravity it must be very weak, at least it should be weaker than that of baryonic matter. Also, the cosmic N-body simulations on the large-scale structures of the

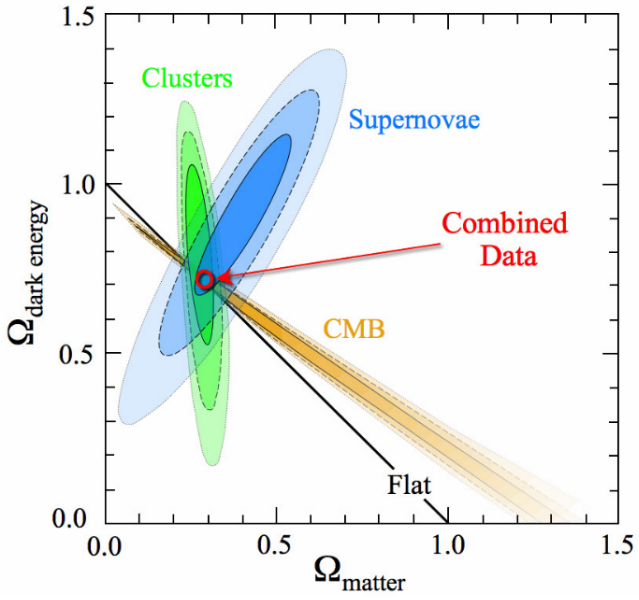

Figure 1.9: Figure showing incredible agreement between the measurements from LSS, supernova, BBN, and CMB. It also suggests that our universe is almost spatially flat. The figure is taken from [81].

universe suggest that the DM must be cold to form such structures. Interestingly, none of the SM particles can satisfy all the above-mentioned properties. None of the SM particles satisfies the properties of a DM particle. The SM neutrinos satisfy some of the properties as they are electrically neutral, weakly interacting and also stable. However, the neutrinos are extremely light and therefore have extremely high free-streaming lengths. The formation of cosmic structure would not have been possible with such light DM particles. In addition to that the neutrinos can only contribute to a very small fraction of the total observed DM abundance.

The absence of a DM candidate in the SM is one of the most compelling pieces of evidence for the existence of new physics beyond the SM. In the next chapter, we discuss the production mechanism in two widely studied classes of particle DM.

1.7.1 Thermal production of dark matter

In literature, thermal DM is the most widely studied particle DM candidate. Thermal DM can be a new elementary particle having sizable interactions with the SM bath such that it can be produced thermally in the early universe. The well known freeze-out mechanism [82, 83] determines the relic abundance of such thermal DM. Interestingly, to satisfy the observed DM relic, such DM particles should have interaction strength of the order of weak interaction for DM masses around the electroweak scale. This co-incidence is commonly known as WIMP (weakly interacting massive particle) miracle. A recent review of such WIMP type models

can be found in [84]. The typical masses of WIMPs can range between a few GeV to hundreds of TeV. Therefore they could become non-relativistic in the very early epochs of the universe and thereby they satisfy the cold DM behaviour.

The time evolution of DM number density can be obtained by operating the DM distribution function by the Liouville operator along with the collision terms. Like in the case of leptogenesis, we can start by writing the most general Boltzmann equation for DM as

$$\hat{L}[f] = C_{\rm DM}[f], \tag{1.101}$$

where $\hat{L}$ is the Liouville operator and $C_{\rm DM}$ is the collision operator. For a homogeneous and isotropic universe $f(x^\mu, p^\mu) \equiv f(t, E)$ and the Liouville operator takes the form given in Eq.(1.34). Integrating Eq.(1.101) over the phase space we have,

$$\frac{g_{\rm DM}}{(2\pi)^3}\int \frac{\hat{L}[f]}{E} d^3\mathbf{p} = \frac{g_{\rm DM}}{(2\pi)^3}\int \frac{C_{\rm DM}[f]}{E} d^3\mathbf{p}. \tag{1.102}$$

It can be shown that

$$\frac{g_{\rm DM}}{(2\pi)^3}\int \frac{\hat{L}[f]}{E} d^3\mathbf{p} = \frac{dn_{\rm DM}}{dt} + 3\mathbf{H}n_{\rm DM}. \tag{1.103}$$

The collision term encodes all the microphysical descriptions of particle interaction for the DM particles. In principle, it incorporates all the number-changing processes for the DM. Here, we consider the simplest case where a pair of SM particles (X, Y) annihilate into a pair of DM particles (labelled as 1,2) or vice versa.

In such case of annihilation the right hand side of Eq.(1.102) becomes

$$\begin{aligned}
\frac{g_{\rm DM}}{(2\pi)^3}\int \frac{C_{\rm DM}[f]}{E} d^3\mathbf{p} &= -\int d\Pi_{\rm X} d\Pi_{\rm Y} d\Pi_1 d\Pi_2 (2\pi)^4 \delta(p_{\rm X} + p_{\rm Y} - p_1 - p_2) \\
&\quad \left[\mid \mathcal{M}_{12\longrightarrow {\rm XY}} \mid^2 f_1 f_2 (1 \pm f_{\rm X})(1 \pm f_{\rm Y}) - \mid \mathcal{M}_{{\rm XY}\longrightarrow 12} \mid^2 f_{\rm X} f_{\rm Y} (1 \pm f_1)(1 \pm f_2) \right] \\
&= -\int d\Pi_{\rm X} d\Pi_{\rm Y} d\Pi_1 d\Pi_2 (2\pi)^4 \delta(p_{\rm X} + p_{\rm Y} - p_1 - p_2) \\
&\quad \left[\mid \mathcal{M}_{12\longrightarrow {\rm XY}} \mid^2 f_1 f_2 - \mid \mathcal{M}_{{\rm XY}\longrightarrow 12} \mid^2 f_{\rm X} f_{\rm Y} \right].
\end{aligned} \tag{1.104}$$

Where $d\Pi_i$ is the space space corresponding to each particle defined as

$$d\Pi_i = \frac{g_i}{(2\pi)^3}\frac{d^3\mathbf{p}_i}{2E_i}. \tag{1.105}$$

The terms $(1 \pm f_j)$ account for the viable phase space of the produced particles, taking into account of the fact that whether they are fermions $(-)$ or bosons $(+)$. Assuming no CP violation in the annihilation, one can write $\mid \mathcal{M}_{12\longrightarrow XY} \mid^2 = \mid \mathcal{M}_{XY\longrightarrow 12} \mid^2 \equiv \mid \mathcal{M} \mid^2$. From the conservation of energy we can write $E_{\rm X} + E_{\rm Y} = E_1 + E_2$. Therefore we can write

$$f_{\rm X} f_{\rm Y} = f_{\rm X}^{\rm eq} f_{\rm Y}^{\rm eq} = e^{-\frac{E_{\rm X} + E_{\rm Y}}{T}} = e^{-\frac{E_1 + E_2}{T}} = f_1^{\rm eq} f_2^{\rm eq}. \tag{1.106}$$

Here, in the first equality it is assumed that the SM particles are in thermal equilibrium. Therefore the Eq.(1.104) becomes

$$\frac{g_{\rm DM}}{(2\pi)^3}\int\frac{C_{\rm DM}[f]}{E}d^3\mathbf{p} = -\langle\sigma v\rangle(n_{\rm DM}^2 - (n_{\rm DM}^{\rm eq})^2), \tag{1.107}$$

here $\langle\sigma v\rangle$ is the thermally averaged annihilation cross-section defined as

$$\langle\sigma v\rangle = \frac{1}{(n_{\rm DM}^{eq})^2}\int d\Pi_X d\Pi_Y d\Pi_1 d\Pi_2 (2\pi)^4\delta(p_X+p_Y-p_1-p_2)\mid\mathcal{M}\mid^2 f_1^{\rm eq}f_2^{\rm eq}. \tag{1.108}$$

The thermally averaged annihilation cross-section is similar to a cross-section, but one needs to consider the fact that all the initial particles do not have fixed definite energies. Therefore one has to integrate all possible energies that the particles can have in a thermal bath. This explains why the extra integrals over the phase space of initial particles with a distribution function $f_1^{\rm eq}f_2^{\rm eq}$ are appearing. Finally, we are left with the following form of the Boltzmann equation,

$$\frac{dn_{\rm DM}}{dt} + 3\mathbf{H}n_{\rm DM} = -\langle\sigma v\rangle(n_{\rm DM}^2 - (n_{\rm DM}^{\rm eq})^2). \tag{1.109}$$

Again, for convenience, the Boltzmann equation is written in terms of the comoving number density $Y_{\rm DM} = n_{\rm DM}/s$ (s being the entropy density of the universe) instead of the number density $n_{\rm DM}$, as it nullifies the decrease of DM number density due to the expansion of the universe. Also, it is convenient to express the Boltzmann equation in terms of the dimensionless variable $z = m_{\rm DM}/T$ instead of time (t).

From the definition of comoving number density $Y_{\rm DM} = n_{\rm DM}/s$

$$\frac{dY_{\rm DM}}{dt} = \frac{d}{dt}\left(\frac{n_{\rm DM}}{s}\right) = \frac{d}{dt}\left(\frac{a^3n}{a^3s}\right) = \frac{1}{a^3s}\left(3a^2\dot{a}n + a^3\frac{dn_{\rm DM}}{dt}\right) = \frac{1}{s}\left(3\mathbf{H}n_{\rm DM} + \frac{dn_{\rm DM}}{dt}\right). \tag{1.110}$$

Here it is assumed that during the expansion of the universe, the entropy remains constant $a^3s =$ constant. This allows us to re-write Eq.(1.109) as follows

$$\frac{dY_{\rm DM}}{dt} = -s\langle\sigma v\rangle\left(Y_{\rm DM}^2 - (Y_{\rm DM})^2\right). \tag{1.111}$$

Since the scale factor and entropy density follow the relation $a \propto T^{-1}$ and $s \propto T^3$ it is easy to show that

$$\frac{dz}{dt} = \mathbf{H}z. \tag{1.112}$$

This allows us to write,

$$\frac{dY_{\rm DM}}{dt} = \frac{dY_{\rm DM}}{dz}\frac{dz}{dt} = \frac{dY_{\rm DM}}{dz}\mathbf{H}z. \tag{1.113}$$

Using the Eq.(1.113) in Eq.(1.111) we get

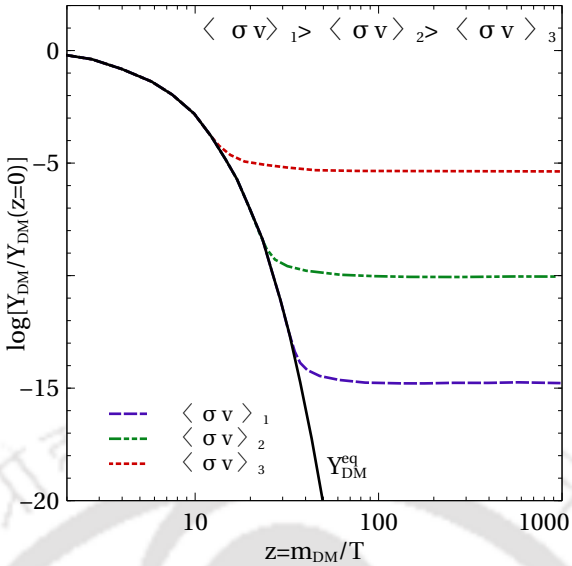

Figure 1.10: The comoving number density of DM ($Y_{\rm DM}$) is shown against $z = m_{\rm DM}/T$ for three different interaction strengths of DM. The black solid line represents the comoving equilibrium number density of DM.

$$\frac{dY_{\rm DM}}{dz} = -\frac{s}{\mathbf{H}z}\langle\sigma v\rangle\left(Y_{\rm DM}^2 - (Y_{\rm DM}^{\rm eq})^2\right). \tag{1.114}$$

Eq.(1.114) is the guiding equation to track the number density of DM given its annihilation cross-section. The typical evolution of a WIMP DM is shown in Fig.1.10. It can be seen that with the increase in interaction strength WIMP abundance freezes out at low temperatures leading to a decrease in final abundance. Once we know the frozen number density of DM, it is straightforward to calculate its relic density as

$$\Omega_{\rm DM}h^2 = 2.755\times10^8\left(\frac{m_{\rm DM}}{\rm GeV}\right)Y_{\rm DM}(z=\infty). \tag{1.115}$$

Direct search for thermal dark matter

After discussing the production mechanism of thermal dark matter and the calculation of its relic abundance in the previous section, we discuss the detection mechanism of such thermal dark matter in this section. The detection of an unknown fundamental particle is not an easy task. However, the WIMP paradigm for thermal DM provides some elegant ways for the possible detection of thermal DM particles. If we are really surrounded by DM halos and the DM particles have interaction of the order of weak interaction with the DM particles then the DM particles should show some collisions with the nucleons in the laboratories. If somehow the recoil energies of the nucleus can be measured due to such collisions, one could possibly reveal the properties of DM particles. The idea of measuring the nucleon recoil due to such collision was first discussed by Goodman and Witten in 1985 [85]. There can be two different types of DM-nucleus interaction. First, DM can interact coherently with the nucleus. In such cases, the DM-nucleus cross-section can be given as

$$\sigma_{\rm XN} \approx \sigma_{Xn} A^2.$$

Here A is the mass number of the nucleus and σ_{Xn} is the DM-nucleon cross-section. This type of coherent DM-nucleus scattering cross-section is known as the spin-independent direct detection cross-section. On the other hand, if the DM particle couples to the spin of the nucleon and as spin add incoherently inside a nucleus, the DM-nucleus cross-section become

$$\sigma_{\rm XN} \approx \sigma_{\rm Xn}.$$

This type of DM-nucleus scattering cross-section is known as spin-dependent direct detection cross-section. It is important to have an estimate of the recoil energy generated by such DM-nucleus collision to see whether the WIMP DM are at all detectable or not. This can be done by using some simple kinematics. The expression for the recoil energy is given by

$$E_{\rm R} = \frac{\mu_{X_T}^2}{m_T} v_X^2 (1 - cos\theta), \tag{1.116}$$

where m_T and μ_{X_T} are the mass of the target nucleus and the reduced mass of the DM-target nucleus system respectively. θ is the scattering angle in the centre of the mass frame, and v_X is the velocity of the DM particles. Now, the rate of any such process depends on the number of target nuclei (N_T), the average flux of the incident particles (ϕ_X) as well as on the differential cross-section of the process. Therefore for the rate of such a process, we can write

$$\frac{dR}{dE_{\rm R}} = N_T \phi_X \frac{d\sigma_{XN}}{dE_{\rm R}}. \tag{1.117}$$

From Eqs.(1.116) and (1.117) we can write

$$\frac{dR}{dE_{\rm R}} = N_T \frac{\rho_{\rm X} m_T}{m_X \mu_{X_T}^2} \int_{v_{\rm min}}^{v_{\rm esc}} \frac{f(v)}{v} \frac{d\sigma_{XN}}{d\cos\theta} d^3v. \tag{1.118}$$

Here the DM flux ϕ_X is replaced in terms of the velocity distribution function $f(v)$ of DM particles inside the DM halo [86]. The particle physics details of DM have appeared only through the differential cross-section $d\sigma_{XN}/d\cos\theta$. The recoil rate can be roughly estimated by considering some realistic value of the differential cross-section. If the mass of the DM particles is in GeV range and the detector has a threshold energy of a few keV the event rate per day per kg of detector mass is calculated to be [86],

$$R = \frac{0.06}{\text{kg day}} \left(\frac{100}{A}\right) \left(\frac{\sigma_{XN}}{10^{-38}\text{cm}^2}\right) \left(\frac{\rho_{\rm X}}{0.3\text{GeV/cm}^3}\right) \left(\frac{v}{200\text{km/s}}\right). \tag{1.119}$$

If the cross-section has a value of the type of weak interaction i.e $\sigma_{XN} \sim 10^{-38}\text{cm}^2$, then the rate become sizable enough to be detected. Few dedicated experiments like LUX [87], XENON100 [88], XENON1T [89, 90], PANDA [91, 92] are looking for events triggered by such thermal DM. Since none of these experiments has found any positive signal for such DM, the negative results from these experiments have put upper bounds on the DM-nucleus scattering cross-section. Recently, the LZ experiment has given the most stringent upper limit on spin-independent DM-nucleon scattering cross-section [93].

Indirect searches for dark matter

Apart from the direct search method discussed above, there exists another type of DM search known as the indirect search for DM. In this type of DM search, instead of detecting the DM itself, one searches for particles that could be products of the annihilation of a pair of DM or decay of DM. Although the probability of DM particles annihilating themselves is very less after its thermal freeze-out, it can still be observable in highly DM-dense regions inside the galaxies. Depending on DM models, it can directly annihilate into a pair of photons or by some other intermediate SM particles, which can further give rise to photons as secondary products. Apart from photons, the indirect search experiments are also looking for other particles as possible products of DM annihilations. These products can be charged particles such as protons, anti-protons, and electrons. Satellite-borne experiments like PAMELA [94], AMS [95] are looking for such signals. On the other hand, they can also be neutrinos. Experiments like ICECUBE [96], and ANTARES [97] have the potential to detect such neutrinos. DM can also produce diffuse or monochromatic photon lines which ground-based experiments like H.E.S.S [98], VARITUS [99] as well as space-based experiments like FERMI-LAT [100] could in principle be able to detect. Similar to direct detection experiments, there have been no convincing signatures of DM annihilation or decay at these experiments so far.

Dark matter at particle colliders

Apart from the direct and indirect signatures of DM discussed above, one can also have the possibility of detecting it in particle colliders. Here, it is important to ask whether it is possible for a WIMP-like DM particle to be detected in the same way we detect the SM particles. With the current luminosity of the LHC it is impossible to produce a large number of DM particles to detect them directly. Even if we detect some signal at a collider, it will be unclear whether it is a galactic DM or not. Also, it would be difficult to know whether it is stable over the age of the universe with the right cosmic abundance. With the weak strength of DM interaction (if they interact at all except gravity) with the SM particles, it is difficult to get some visible signatures. Therefore, the transverse momentum conservation is the only way by which production of DM particles at colliders could be inferred. There have been dedicated DM searches at the LHC based on simplified particle physics models [101–105] as well as effective field theory (EFT) based setups. Since we do not study collider prospects of DM in this thesis, we do not elaborate upon these collider aspects further.

1.7.2 Non-thermal production of dark matter

As discussed in the previous sections, many experiments have been looking for thermal or WIMP kind of DM for a few decades. However, the null results from such experiments motivate people to look for other possibilities to produce DM beyond the WIMP paradigm. If the DM particles have a much weaker interaction with the SM bath, such DM particles could never be produced thermally in the early universe. Rather, they can be non-thermally produced from the decay or annihilation of other particles. Due to the very feeble coupling with the SM bath, these types of DM particles are commonly known as Feebly Interacting Massive Particles (FIMP) [106, 107]. Unlike WIMPs, FIMPs have vanishing or almost

vanishing abundance in the very early universe. Later they slowly freeze in as the universe evolves. One particular behaviour of the thermal freeze-out mechanism is that the decoupling temperature is usually a factor of $20-30$ below the mass of DM. This is independent of any thermal history of the early universe and possible new interactions at higher scales. However, the final DM abundance is highly sensitive to its interaction strength as shown in Fig.1.10. For a freeze-in DM case, the exact opposite of that happens.

Let us now consider a bunch of particles in equilibrium sharing the same temperature among themselves and suppose we have a feebly interacting particle χ. If the particle χ has very feeble interaction with the bath particles then their interaction rate (Γ_χ) will always be smaller than the expansion rate of the universe ($\mathbf{H}$),

$$\frac{\Gamma_\chi(T)}{\mathbf{H}(T)} \ll 1 \quad \forall\, T. \tag{1.120}$$

Then the χ particle can only get produced from the decay or collision of bath particles. First, let us consider that χ is produced from the decay of a heavier particle A ($A \longrightarrow \chi\chi$) present in the bath. Here, it is important to point out that if both decay and annihilation can produce χ involving the same couplings, then decay will always dominate over annihilation. However, in case the decaying particle is itself not in equilibrium then the calculation will be more involved [108] as one has to calculate the distribution function of both the mother particle as well as DM. Following the [106,107], the Boltzmann equation for χ produced from a decaying particle A in bath can be written as

$$\frac{dn_\chi}{dt} + 3\mathbf{H}n_\chi = 2\frac{\kappa_1(m_{\rm A}/T)}{\kappa_2(m_{\rm A}/T)}\Gamma_{\rm A} n_{\rm A}^{\rm eq}, \tag{1.121}$$

where $m_{\rm A}$, and $n_{\rm A}^{\rm eq}$ are the mass and the equilibrium number density of the decaying particle A. $\Gamma_{\rm A}$ is the decay width for $A \longrightarrow \chi\chi$. Similar to Eq.(1.114) for freeze-out, it is convenient to write the equation in terms of comoving number density $Y_i = n_i/s(T)$ ($s(T)$ being the entropy density of the universe) and dimensionless variable $z = m_{\rm A}/T$. After some algebraic simplifications, the Boltzmann equation takes the form

$$\frac{dY_\chi}{dz} = 2\frac{\kappa_1(m_{\rm A}/T)}{\kappa_2(m_{\rm A}/T)}\frac{\Gamma_{\rm A}}{\mathbf{H}z}Y_{\rm A}^{\rm eq}. \tag{1.122}$$

A typical solution of this equation is shown in Fig.1.11. Here, one can notice the opposite behaviour of DM abundance with increasing interaction strength of DM. Final abundance of DM increases for larger decay width of A and hence larger interaction strength of DM with bath particles. If the bath particles are assumed to follow the Maxwell-Boltzmann distribution, one can find an approximate analytical solution to Eq.(1.122) such that the final relic abundance of FIMP DM candidate χ is given as

$$\Omega_\chi h^2 = 4.48\times10^8 \frac{g_{\rm A}}{g_{*s}\sqrt{g_*}}\left(\frac{m_\chi}{\rm GeV}\right)\frac{M_{\rm Pl}\Gamma_{\rm A}}{m_{\rm A}^2}. \tag{1.123}$$

Here $g_{\rm A}$ is the internal degrees of freedom of the decaying particle A, m_χ is the mass of the FIMP χ. The relativistic degrees of freedom in energy and entropy densities are denoted by g_*, g_{*s} respectively. It can be seen that the final DM relic is proportional to the decay width

of the decaying particle, and thus the final relic increases with the increase in interaction strength of DM. This is quite opposite compared to WIMP whose final relic decreases with increase in interaction rate with the SM bath. However, the interaction strength of FIMP can not be increased arbitrarily as, beyond a particular point these interactions would thermalise the FIMP changing their nature to WIMP.

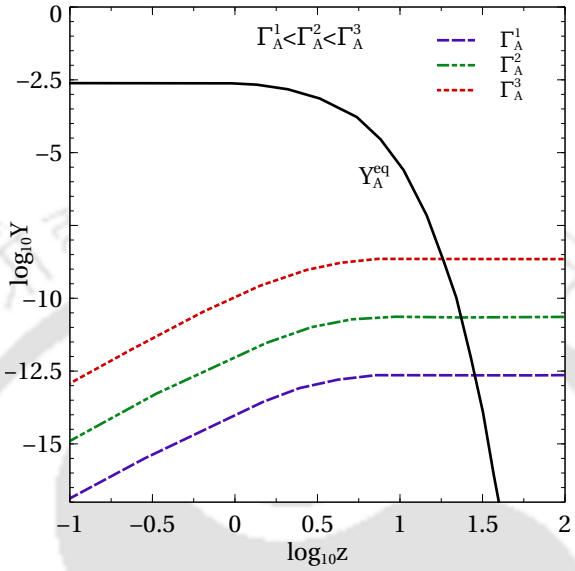

Figure 1.11: Evolution plot for the co-moving number density of FIMP χ and the equilibrium density of the decaying particle A. The black solid line represents the equilibrium comoving number density of the decaying particle while the dashed lines represent the comoving number density of the FIMP χ for three different values of Γ_A.

While FIMP provides an alternative to WIMP paradigm which is facing stringent direct detection constraints, it is difficult to probe it directly. Depending upon the specific model implementation, some indirect FIMP signatures can be obtained, as discussed in some recent works [109–111]. Since we do not study detection prospects of FIMP in this thesis, we do not discuss it further here.

Although the origin of BAU and DM can be unrelated to each other, there are scenarios where their origin can be addressed within a common framework. In this thesis, we study a few minimal extensions of the SM, which can explain the observed baryon asymmetry through leptogenesis and also generate the observed amount of DM relic simultaneously. The vanilla leptogenesis scenario widely studied in the context of canonical seesaw mechanisms of neutrino mass requires the scale of leptogenesis to be very high, set by the Davidson-Ibarra (DI) bound [64], out of any direct experimental reach. In this thesis, within the context of a common framework of leptogenesis and dark matter, we explore the possibility of lowering the scale of leptogenesis either by (a) going beyond the canonical seesaw framework e.g., radiative seesaw model, (b) decoupling the origin of light neutrino mass from the origin of lepton asymmetry and (c) incorporating non-standard cosmological histories. We show that some of these possibilities or a combination of them can indeed lower the scale of leptogenesis to as low as a TeV with interesting implications for neutrino mass hierarchy as well as dark matter. Apart from providing a minimal and combined framework to explain multiple

observed phenomena in the universe like baryon asymmetry, dark matter and neutrino mass, the possibility of new physics at a low scale significantly enhances the detection prospects of these scenarios in near future experiments compared to vanilla leptogenesis scenarios widely studied in the literature.

CHAPTER 2

Fermion dark matter with N_2 leptogenesis in minimal scotogenic model

In this chapter, we study the possibility of singlet fermion DM and successful leptogenesis in the minimal scotogenic model [112] which also provides a radiative origin of light neutrino masses. In the minimal scotogenic model, the SM is extended by three gauge singlet fermions and one additional scalar doublet, all odd under an in-built Z_2 symmetry. In a few earlier works like [113], the possibility of creating lepton asymmetry from the decay of the lightest Z_2-odd singlet fermion (N_1) was studied. It was shown that the scale of leptogenesis can be as low as $M_1 \sim 10$ TeV even with hierarchical Z_2 odd singlet fermion masses. To allow the decay of the lightest singlet fermion, the neutral component of the Z_2-odd scalar doublet had to be the DM candidate in these scenarios. Here we consider another possibility where the lightest singlet fermion is also the lightest Z_2 odd particle, and hence the DM candidate. In this case, the heavier singlet fermion N_2 decay is primarily responsible for generating the required lepton asymmetry. The relevant Yukawa couplings for the RHNs are found out by the usual Casas-Ibarra (CI) parametrisation [65, 114]. The CI parametrisation links the new Yukawa couplings to the lightest active neutrino mass m_{lightest} and λ_5, an important quartic coupling of the scotogenic model affecting light neutrino masses. We solve the relevant Boltzmann equations to get the final lepton asymmetry from N_2 decay. We also point out the importance of new washout terms, which are sub-dominant in the usual N_1 dominated leptogenesis while highlighting the difference in results for normal and inverted ordering of light neutrino masses. We also study the possibility of both thermal as well as non-thermal fermion singlet DM and discuss the consequences for leptogenesis.

2.1 Scotogenic Model

As pointed out earlier, we consider the minimal model belonging to the scotogenic framework in our study. It is an extension of the SM by three copies of SM-singlet fermions N_i (with $i = 1, 2, 3$) and one $SU(2)_L$-doublet scalar field η (also called inert doublet), all being odd under an in-built and unbroken Z_2 symmetry, while the SM fields remain Z_2-even, i.e. under the Z_2-symmetry, we have

$$N_i \to -N_i, \quad \eta \to -\eta, \quad \Phi_1 \to \Phi_1, \quad \Psi_{\text{SM}} \to \Psi_{\text{SM}}\,, \tag{2.1}$$

where Φ_1 is the SM Higgs doublet and $\Psi_{\rm SM}$'s stand for the SM fermions. This Z_2 symmetry, though *ad hoc* in this minimal setup, could be realised naturally as a subgroup of a continuous gauge symmetry like $U(1)_{B-L}$ with non-minimal field content [115, 116].

The relevant Yukawa Lagrangian involving the lepton sector is

$$-\mathcal{L} \supset \frac{1}{2}(M_N)_{ij} N_i N_j + \left(Y_{ij}\, \overline{L}_i \tilde{\eta} N_j + \text{h.c.}\right) . \tag{2.2}$$

The Z_2 symmetry also prevents the usual Dirac Yukawa term $\overline{L}\tilde{\Phi}_1 N$ involving the SM Higgs, and hence, the Dirac mass term in the seesaw mechanism. This eventually forbids the generation of light neutrino masses at tree level through the conventional type-I seesaw mechanism [45–47, 49, 50, 117].

The scalar sector of the model is the same as the inert Higgs doublet model (IHDM) [118], a minimal extension of the SM by a Z_2 odd scalar doublet in order to accommodate a DM candidate [112, 115, 119–131]. The scalar potential of the model involving the SM Higgs doublet Φ_1 and the inert doublet η can be written as

$$\begin{aligned} V(\Phi_1, \eta) \;=\; & \mu_1^2 |\Phi_1|^2 + \mu_2^2 |\eta|^2 + \frac{\lambda_1}{2}|\Phi_1|^4 + \frac{\lambda_2}{2}|\eta|^4 + \lambda_3 |\Phi_1|^2 |\eta|^2 \\ & + \lambda_4 |\Phi_1^\dagger \eta|^2 + \left[\frac{\lambda_5}{2}(\Phi_1^\dagger \eta)^2 + \text{h.c.}\right] . \end{aligned} \tag{2.3}$$

As mentioned earlier, in order to ensure that none of the neutral components of the inert Higgs doublet η acquire a nonzero VEV, $\mu_2^2 > 0$ is assumed.

After the EWSB, these two scalar doublets can be written in the following form in the unitary gauge:

$$\Phi_1 \;=\; \begin{pmatrix} 0 \\ \frac{v+h}{\sqrt{2}} \end{pmatrix}, \qquad \eta \;=\; \begin{pmatrix} H^\pm \\ \frac{H^0 + i A^0}{\sqrt{2}} \end{pmatrix} , \tag{2.4}$$

where h is the SM-like Higgs boson, H^0 and A^0 are the CP-even and CP-odd scalars, and $H^\pm$ are the charged scalars from the inert doublet. The masses of the physical scalars at tree level can be written as

$$\begin{aligned} m_h^2 &= \lambda_1 v^2, \\ m_{H^\pm}^2 &= \mu_2^2 + \frac{1}{2}\lambda_3 v^2, \\ m_{H^0}^2 &= \mu_2^2 + \frac{1}{2}(\lambda_3 + \lambda_4 + \lambda_5) v^2 \;=\; m_{H^\pm}^2 + \frac{1}{2}\left(\lambda_4 + \lambda_5\right) v^2, \\ m_{A^0}^2 &= \mu_2^2 + \frac{1}{2}(\lambda_3 + \lambda_4 - \lambda_5) v^2 \;=\; m_{H^\pm}^2 + \frac{1}{2}\left(\lambda_4 - \lambda_5\right) v^2 . \end{aligned} \tag{2.5}$$

Without any loss of generality, we consider $\lambda_5 > 0$ so that the CP-odd scalar is lighter than the CP-even one. Since the lightest component of the inert doublet is not the DM candidate in our scenario, we can have any mass ordering among its components. This will not change the analysis we are going to do in upcoming sections, however, these possibilities can be distinguished by their signatures at collider experiments like the large hadron collider (LHC).

Light neutrino masses which arise at one-loop level can be evaluated as [112, 132]

$$(M_\nu)_{ij} = \sum_k \frac{Y_{ik}Y_{jk}M_k}{32\pi^2}\left(\frac{m^2_{H^0}}{m^2_{H^0}-M^2_k}\ln\frac{m^2_{H^0}}{M^2_k} - \frac{m^2_{A^0}}{m^2_{A^0}-M^2_k}\ln\frac{m^2_{A^0}}{M^2_k}\right)$$
$$\equiv \sum_k \frac{Y_{ik}Y_{jk}M_k}{32\pi^2}\left[L_k(m^2_{H^0}) - L_k(m^2_{A^0})\right], \tag{2.6}$$

where M_k is the mass eigenvalue of the mass eigenstate N_k in the internal line and the indices $i, j = 1, 2, 3$ run over the three neutrino generations as well as three copies of N_i. The function $L_k(m^2)$ is defined as

$$L_k(m^2) = \frac{m^2}{m^2 - M^2_k}\ln\frac{m^2}{M^2_k}. \tag{2.7}$$

From the expressions for physical scalar masses given in Eq.(2.5), we can write $m^2_{H^0} - m^2_{A^0} = \lambda_5 v^2$. Therefore, in the limit $\lambda_5 \to 0$, the neutral components of inert doublet η become mass degenerate. Also, a vanishing λ_5 implies vanishing light neutrino masses which is expected as the λ_5-term in the scalar potential (2.3) breaks lepton number by two units, when considered together with the SM-singlet fermions Lagrangian (2.2). Since setting $\lambda_5 \to 0$ allows us to recover the lepton number global symmetry, the smallness of λ_5 is technically natural in the 't Hooft sense [133]. We will see later that such small λ_5 is indeed required for certain scenarios in order to achieve the desired phenomenology.

As we will see in the upcoming sections, the requirement of correct DM phenomenology for N_1 DM significantly constrains the Yukawa couplings. In particular, the requirement of FIMP DM tightly constrains the Yukawa couplings involving N_1 very small $\leq 10^{-8}$ while for WIMP DM the same Yukawa couplings should be of order one $\mathcal{O}(1)$. Accordingly, the parameter λ_5 has to be tuned in order to generate the correct light neutrino masses. It is important to ensure that the choice of Yukawa couplings as well as other parameters involved in light neutrino mass are consistent with the cosmological upper bound on the sum of neutrino masses, $\sum_i m_i \leq 0.11$ eV [3], as well as the neutrino oscillation data [134, 135]. In order to incorporate these constraints on model parameters, it is often useful to rewrite the neutrino mass formula given in Eq.(2.6) in a form resembling the type-I seesaw formula:

$$M_\nu = Y\Lambda^{-1}Y^T, \tag{2.8}$$

where we have introduced the diagonal matrix Λ with elements

$$\Lambda_i = \frac{2\pi^2}{\lambda_5}\zeta_i\frac{2M_i}{v^2}, \tag{2.9}$$

$$\text{and} \quad \zeta_i = \left(\frac{M_i^2}{8(m^2_{H^0} - m^2_{A^0})}\left[L_i(m^2_{H^0}) - L_i(m^2_{A^0})\right]\right)^{-1}. \tag{2.10}$$

The light neutrino mass matrix (2.8) which is complex symmetric, can be diagonalised by the usual Pontecorvo-Maki-Nakagawa-Sakata (PMNS) mixing matrix U [1], written in terms

[1] Usually, the leptonic mixing matrix is given in terms of the charged lepton diagonalising matrix (U_l) and light neutrino diagonalising matrix U_ν as $U = U_l^\dagger U_\nu$. In the simple case where the charged lepton mass matrix is diagonal which is true in our model, we can have $U_l = \mathbb{1}$. Therefore we can write $U = U_\nu$.

of neutrino oscillation data (up to the Majorana phases) as

$$U = \begin{pmatrix} c_{12}c_{13} & s_{12}c_{13} & s_{13}e^{-i\delta} \\ -s_{12}c_{23} - c_{12}s_{23}s_{13}e^{i\delta} & c_{12}c_{23} - s_{12}s_{23}s_{13}e^{i\delta} & s_{23}c_{13} \\ s_{12}s_{23} - c_{12}c_{23}s_{13}e^{i\delta} & -c_{12}s_{23} - s_{12}c_{23}s_{13}e^{i\delta} & c_{23}c_{13} \end{pmatrix} U_{\rm Maj} \tag{2.11}$$

where $c_{ij} = \cos\theta_{ij}$, $s_{ij} = \sin\theta_{ij}$ and δ is the leptonic Dirac CP phase. The diagonal matrix $U_{\rm Maj} = {\rm diag}(1, e^{i\alpha}, e^{i(\zeta+\delta)})$ contains the undetermined Majorana CP phases α, ζ. The diagonal light neutrino mass matrix is, therefore,

$$D_\nu \;=\; U^\dagger M_\nu U^* \;=\; {\rm diag}(m_1, m_2, m_3)\,, \tag{2.12}$$

where the light neutrino masses can follow either normal ordering (NO) or inverted ordering (IO). Since the inputs from neutrino data are only in terms of the mass-squared differences and mixing angles, it would be useful for our purpose to express the Yukawa couplings in terms of light neutrino parameters. This is possible through the Casas-Ibarra parametrisation [65] extended to radiative seesaw model [114] which allows us to write the Yukawa coupling matrix satisfying the neutrino data as

$$Y \;=\; U D_\nu^{1/2} R^\dagger \Lambda^{1/2}\,, \tag{2.13}$$

where R is an arbitrary complex orthogonal matrix satisfying $RR^T = \mathbb{1}$.

2.2 Fermion Dark matter in Scotogenic Model

As pointed out earlier, the DM candidate in our model is the lightest Z_2 odd singlet fermion N_1. Being gauge singlet, the production mechanism of N_1 DM crucially depends upon its Yukawa couplings with the SM leptons and inert doublet η. Depending upon the size of these Yukawa couplings, one can either realise WIMP or FIMP-type DM in our model.

For WIMP type DM which is produced thermally in the early universe, its thermal relic abundance can be obtained by solving the Boltzmann equation for the evolution of the DM number density n:

$$\frac{dn}{dt} + 3Hn \;=\; -\langle\sigma v\rangle \left[n^2 - (n^{\rm eq})^2\right], \tag{2.14}$$

where $n^{\rm eq}_{\rm DM}$ is the equilibrium number density of DM and $\langle\sigma v\rangle$ is the thermally averaged annihilation cross section, given by [136]

$$\langle\sigma v\rangle \;=\; \frac{1}{8m_{\rm DM}^4 T\kappa_2^2\left(\frac{m_{\rm DM}}{T}\right)} \int_{4m_{\rm DM}^2}^{\infty} \sigma(s - 4m_{\rm DM}^2)\sqrt{s}\,\kappa_1\left(\frac{\sqrt{s}}{T}\right) ds\,, \tag{2.15}$$

where $\kappa_i(x)$'s are modified Bessel functions of order i. In the presence of coannihilation, one follows the recipe given by [137] to calculate the relic abundance. For a recent study on such coannihilation effects on fermion DM in this model, please see [138]. As we will show later, the requirement of successful N_2 leptogenesis pushes the masses of $N_{2,3}$ to higher values,

making their coannihilations with N_1 highly inefficient. However, the mass of η can remain very close to that of N_1 enhancing the coannihilation effects.

On the other hand, if the Yukawa couplings of N_1 with SM leptons are very small, the FIMP possibility will arise. In such a case, as mentioned earlier, N_1 never reaches thermal equilibrium with the standard bath and has to be generated from the decay or scattering of particles in the thermal bath. If the same couplings are involved in both scattering and decay, then decay contributions dominate [106]. In our model, the most dominant decay-producing N_1 is the two-body decay of $\eta \to lN_1$ given by

$$\Gamma_{\eta\to N_1 l} \cong \frac{m_\eta Y^2}{8\pi}\left(1-\frac{M_1^2}{m_\eta^2}\right)^2 \tag{2.16}$$

where Y is the effective Yukawa coupling (up to the flavour indices), M_1 is the mass of FIMP type DM particle N_1 and m_η is the mass of the mother particle. By virtue of its gauge interactions, η can be thermally produced in the early universe. Therefore, the coupled Boltzmann equations for comoving number densities of N_1 and η can be written as

$$\frac{dY_\eta}{dz} = -\frac{4\pi^2}{45}\frac{M_{\rm Pl} m_\eta}{1.66}\frac{\sqrt{g_*(z)}}{z^2}\left[\sum_{p\equiv \text{SM particles}} \langle\sigma v\rangle_{\eta\eta\to pp}\left(Y_\eta^2 - (Y_\eta^{\rm eq})^2\right)\right] \tag{2.17}$$

$$-\frac{M_{\rm Pl}}{1.66}\frac{z}{m_\eta^2}\frac{\sqrt{g_*(z)}}{g_s(z)}\Gamma_{\eta\to N_1 l} Y_\eta, \tag{2.18}$$

$$\frac{dY_{N_1}}{dz} = \frac{M_{\rm Pl}}{1.66}\frac{z}{m_\eta^2}\frac{\sqrt{g_*(z)}}{g_s(z)}\Gamma_{\eta\to N_1 l} Y_\eta, \tag{2.19}$$

where $z = \dfrac{m_\eta}{T}$ is a dimensionless variable and $M_{\rm Pl}$ is the Planck mass. $g_s(z)$ is the number of effective relativistic degrees of freedom associated with the entropy density of the universe at some z, and the $g_*(z)$ is defined by

$$\sqrt{g_\star(z)} = \frac{g_{\rm s}(z)}{\sqrt{g_\rho(z)}}\left(1-\frac{1}{3}\frac{{\rm d}\ln g_{\rm s}(z)}{{\rm d}\ln z}\right). \tag{2.20}$$

Here, $g_\rho(x)$ denotes the effective number of degrees of freedom related to the energy density of the universe at z.

2.3 N_2 Leptogenesis in Scotogenic Model

As mentioned earlier, a net lepton asymmetry can be generated in this model via out-of-equilibrium decay of the N_i [113, 121, 139–143]. Similar to the Davidson-Ibarra bound in type-I seesaw leptogenesis mentioned earlier, here also one can derive a comparable lower bound with only two Z_2 odd singlet fermions in the strong washout regime. With three singlet fermions in the scotogenic model, this bound can be lowered down to around 10 TeV [113, 143] without any need of resonance enhancement [54, 144]. Here we consider the

heavier singlet fermion N_2 decay to be responsible for leptogenesis. It should be noted that N_2 decay dominating leptogenesis in usual type-I seesaw mechanism was discussed in several earlier works [145–157]. In these scenarios, the right handed neutrino spectrum is hierarchical and N_1 is too light to generate a sizeable asymmetry (lighter than the Davidson-Ibarra upper bound [64]). The next to lightest right handed neutrino N_2 can be heavy enough and can produce the correct asymmetry for some parameter space of the models. This vanilla N_2 leptogenesis scenario is however, different from ours as in our case N_1 is perfectly stable and can not decay. Since we consider the leptogenesis to be generated from N_2 decay effectively, by considering N_1 to be the lightest Z_2 odd particle which can not decay, our scenario is more constrained compared to the ones discussed in [113, 143]. Although N_3 decay can also generate lepton asymmetry, in principle, we consider the asymmetry generated by N_3 decay or any pre-existing asymmetry to be negligible due to strong washout effects mediated either by N_2 or N_3 themselves. We also neglect $\Delta L = 1$ scattering processes and flavour effects.

The CP asymmetry parameter is defined as

$$\epsilon_i = \frac{\sum_\alpha \Gamma(N_i \to l_\alpha \eta) - \Gamma(N_i \to \bar{l_\alpha}\bar{\eta})}{\sum_\alpha \Gamma(N_i \to l_\alpha \eta) + \Gamma(N_i \to \bar{l_\alpha}\bar{\eta})}. \tag{2.21}$$

The CP asymmetry parameter for $N_i \to l_\alpha \eta, \bar{l_\alpha}\bar{\eta}$ is given by

$$\epsilon_{i\alpha} = \frac{1}{8\pi (Y^\dagger Y)_{ii}} \sum_{j\neq i} \left[f\left(\frac{M_j^2}{M_i^2}, \frac{m_\eta^2}{M_i^2}\right) \mathrm{Im}[Y^*_{\alpha i} Y_{\alpha j} (Y^\dagger Y)_{ij}] - \frac{M_i^2}{M_j^2 - M_i^2} \left(1 - \frac{m_\eta^2}{M_i^2}\right)^2 \mathrm{Im}[Y^*_{\alpha i} Y_{\alpha j} H_{ij}] \right] \tag{2.22}$$

where, the function $f(r_{ji}, \eta_i)$ is coming from the interference of the tree-level and one-loop diagrams and has the form

$$f(r_{ji}, \eta_i) = \sqrt{r_{ji}} \left[1 + \frac{(1 - 2\eta_i + r_{ji})}{(1 - \eta_i^2)^2} \ln\left(\frac{r_{ji} - \eta_i^2}{1 - 2\eta_i + r_{ji}}\right) \right] \tag{2.23}$$

with $r_{ji} = M_j^2/M_i^2$ and $\eta_i = m_\eta^2/M_i^2$. The self energy contribution H_{ij} is given by

$$H_{ij} = (Y^\dagger Y)_{ij} \frac{M_j}{M_i} + (Y^\dagger Y)^*_{ij}. \tag{2.24}$$

Now, the CP asymmetry parameter, neglecting the flavour effects (summing over final state flavours α) is

$$\epsilon_i = \frac{1}{8\pi (Y^\dagger Y)_{ii}} \sum_{j\neq i} \mathrm{Im}[((Y^\dagger Y)_{ij})^2] \frac{1}{\sqrt{r_{ji}}} F(r_{ji}, \eta_i) \tag{2.25}$$

where the function $F(r_{ji}, \eta)$ is defined as

$$F(r_{ji}, \eta_i) = \sqrt{r_{ji}} \left[f(r_{ji}, \eta_i) - \frac{\sqrt{r_{ji}}}{r_{ji} - 1} (1 - \eta_i)^2 \right]. \tag{2.26}$$

Let us define the decay parameter as

$$K_{N_2} = \frac{\Gamma_2}{\mathbf{H}(z = 1)} \tag{2.27}$$

where Γ_2 is the N_2 decay width, $\mathbf{H}$ is the Hubble parameter and $z = M_2/T$ with T being the temperature of the thermal bath. Leptogenesis occurs far above the electroweak scale where the universe was radiation dominated. In this era the Hubble parameter can be expressed in terms of the temperature T as follows

$$\mathbf{H} = \sqrt{\frac{8\pi^3 g_*}{90}}\frac{T^2}{M_{Pl}} = \mathbf{H}(z=1)\frac{1}{z^2} \tag{2.28}$$

where g_* is the effective number of relativistic degrees of freedom and $M_{\rm Pl} \simeq 1.22 \times 10^{19}$ GeV is the Planck mass. The decay width Γ_2 can be calculated as

$$\Gamma_2 = \frac{M_2}{8\pi}(Y^\dagger Y)_{22}(1-\eta_2)^2. \tag{2.29}$$

The frequently appearing $Y^\dagger Y$ is calculated using Casas-Ibarra parametrisation and it is given as

$$(Y^\dagger Y)_{ij} = \sqrt{\Lambda_i \Lambda_j}(R D_\nu R^\dagger)_{ij}. \tag{2.30}$$

$D_\nu = \text{diag}(m_1, m_2, m_3)$ is the diagonal active neutrino mass matrix. One important point here is to note down that the important quantity $Y^\dagger Y$ for leptogenesis is independent of the lepton mixing PMNS matrix, whereas it is dependent on the complex angles of the CI parametrisation. Thus the CP violating phases relevant for leptogenesis are independent of the CP violating phases in the PMNS matrix. The dependence of the CP asymmetry on M_i and λ_5 is evident through Λ_i.

The basic equations to track the dynamics of leptogenesis are the Boltzmann equations given by [62]

$$\frac{dn_{N_2}}{dz} = -D_2(n_{N_2} - n_{N_2}^{\rm eq}), \tag{2.31}$$

$$\frac{dn_{\rm B-L}}{dz} = -\epsilon_2 D_2(n_{N_2} - n_{N_2}^{\rm eq}) - W^{\rm Total} n_{\rm B-L}, \tag{2.32}$$

where n_{N_2}, $n_{\rm B-L}$ are the comoving number density of N_2 and $B-L$ asymmetry respectively. $n_{N_2}^{\rm eq} = \frac{z^2}{2}\kappa_2(z)$ is the equilibrium comoving number density of N_2 (with $\kappa_i(z)$ being the modified Bessel function of i-th kind). The quantity on the right hand side of the above equations

$$D_2 \equiv \frac{\Gamma_2}{\mathbf{H}z} = K_{N_2} z \frac{\kappa_1(z)}{\kappa_2(z)} \tag{2.33}$$

measures the total decay rate of N_2 with respect to the Hubble expansion rate, and similarly, $W^{\rm Total} \equiv \frac{\Gamma_W}{\mathbf{H}z}$ measures the total washout rate. The washout term is the sum of two contributions, i.e. $W^{\rm Total} = W_1 + W_{\Delta L}$, where the washout due to the inverse decays $\ell\eta$, $\bar{\ell}\eta^* \to N_2$ is given by

$$W_1 = W_{\rm ID} = \frac{1}{4}K_{N_2} z^3 \kappa_1(z). \tag{2.34}$$

The other contribution to washout $W_{\Delta L}$ originates from scatterings which violate lepton number by $\Delta L = 1, 2$. The contribution from $\Delta L = 2$ scatterings $\ell\eta \leftrightarrow \bar{\ell}\eta^*$, $\ell\ell \leftrightarrow \eta^*\eta^*$ is given by [113]

$$W_{\Delta L=2} \simeq \frac{18\sqrt{10}\, M_{\rm Pl}}{\pi^4 g_\ell \sqrt{g_*} z^2 v^4} \left(\frac{2\pi^2}{\lambda_5}\right)^2 M_2 \bar{m}_\zeta^2 \,, \tag{2.35}$$

where we have assumed $\eta_2 \ll 1$ for simplicity, g_ℓ stands for the internal degrees of freedom for the SM leptons, and $\bar{m}_\zeta$ is the effective neutrino mass parameter, defined as

$$\bar{m}_\zeta^2 \simeq 4\zeta_1^2 m_l^2 + \zeta_2 m_{h_1}^2 + \zeta_3^2 m_{h_2}^2 \,, \tag{2.36}$$

with m_l, m_{h_1,h_2} are being the lightest and heavier neutrino mass eigenvalues, ζ_i defined in Eq. (2.10) and $L_i(m^2)$ defined in Eq. (2.7). It should be noted that Eq. (2.35) is similar to the $\Delta L = 2$ washout term in vanilla leptogenesis, except for the $\left(\frac{2\pi^2}{\lambda_5}\right)^2$ factor. In N_2 leptogenesis, which we discuss here, there can be other scattering diagrams which can significantly contribute to the washout processes. We include all of them in our work. One possible $\Delta L = 2$ washout relevant at $T = M_2$ is from the processes $\ell\ell \longrightarrow N_1 N_1$ which can be written as

$$W^{(1)}_{\Delta L=2} = \frac{zs}{\mathbf{H}(z=1)} n_\ell^{\rm eq} \langle\sigma v\rangle_{\ell\ell \longrightarrow N_1 N_1} \tag{2.37}$$

where s is the entropy density in radiation dominated universe. The other two relevant $\Delta L = 2$ washout contributions can be written as

$$W^{(2)}_{\Delta L=2} = \frac{zs}{\mathbf{H}(z=1)} (n_\eta^{\rm eq} \langle\sigma v\rangle_{\eta l \longleftrightarrow \eta^* \bar{\ell}} + n_{N_1}^{\rm eq} \langle\sigma v\rangle_{N_1 \ell \longleftrightarrow N_1 \bar{\ell}}) \tag{2.38}$$

where $r_j = \dfrac{n_j^{\rm eq}}{n_l^{\rm eq}}$. The contribution from $\Delta L = 1$ washout processes can be estimated as

$$W_{\Delta L=1} = \frac{zs}{\mathbf{H}(z=1)} n_\ell^{\rm eq} (r_{W^\pm} \langle\sigma v\rangle_{\ell W^\pm \longleftrightarrow N_1 \eta^\pm} + r_Z \langle\sigma v\rangle_{\ell Z \longleftrightarrow N_1 \eta^0}) \tag{2.39}$$

After obtaining the numerical solutions of the above Boltzmann Eqs.(2.31) and (2.32), we convert the final $B-L$ asymmetry $n^f_{\rm B-L}$ just before electroweak sphaleron freeze-out into the observed baryon to photon ratio by the standard formula

$$\eta_B = \frac{3}{4}\frac{g_*^0}{g_*} a_{\rm sph} n^f_{\rm B-L} \simeq 9.2 \times 10^{-3}\, n^f_{\rm B-L} \,, \tag{2.40}$$

where $a_{\rm sph} = \frac{8}{23}$ is the sphaleron conversion factor (taking into account two Higgs doublets). We take the effective relativistic degrees of freedom to be $g_* = 110.75$, slightly higher than that of the SM at such temperatures as we are including the contribution of the inert doublet too. In the WIMP DM scenario it will be enhanced by approximately 1 as N_1 remains in thermal equilibrium. The heavier singlet fermions $N_{2,3}$ do not contribute as they have already decoupled from the bath by this epoch. In the above expression $g_*^0 = \frac{43}{11}$ is the effective relativistic degrees of freedom at the recombination epoch.

2.4 Results and discussion

We first consider normal ordering of light neutrino masses and solve the Boltzmann equations for lepton asymmetry mentioned in the previous section. In order to achieve FIMP type DM so that the Yukawa coupling of N_1 comes out to be tiny, we consider the complex matrix R to have the following form

$$\mathbf{R}= \begin{pmatrix} 1 & 0 & 0 \\ 0 & \cos(z_R + iz_I) & \sin(z_R + iz_I) \\ 0 & -\sin(z_R + iz_I) & \cos(z_R + iz_I) \end{pmatrix}$$

with $z_R = 0.42$ and $z_I = -0.4232$. The justification behind such choice of R and other possibilities of R matrix are mentioned in Appendix A.1. We further choose the relevant parameters as $m_\eta = 201$ GeV, $M_1 = 200$ GeV, $m_1 = 10^{-3}$ eV, $\lambda_5 = 0.5$, $M_2 = 10^{10}$ GeV and $M_3/M_2 = 10^2$ and plot the evolution of comoving number densities of N_2 and $n_{\rm B-L}$ as a function of z in Fig.2.1. As the temperature cools or z increases, the number density of N_2 decreases due to its decay while lepton asymmetry increases. For the chosen benchmark parameters, the washout effects are significant, giving rise to a dilution of the asymmetry before saturation.

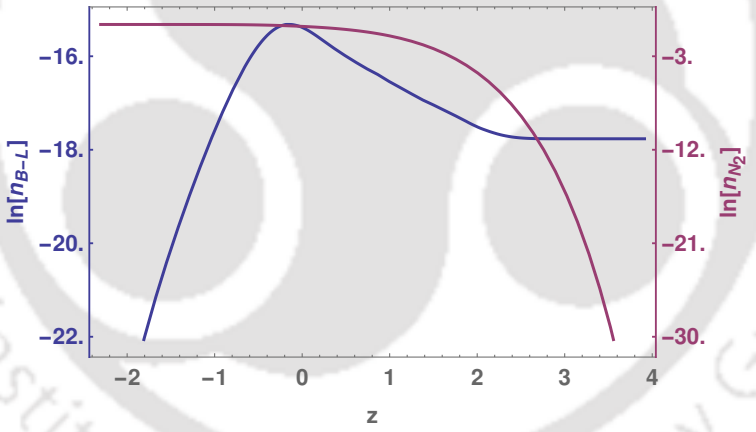

Figure 2.1: Evolution of $n_{N_2}, n_{\rm B-L}$ (Comoving number densities of N_2, $B-L$) with z for NO. The set of parameters used are $M_2 = 10^{10}$ GeV, $M_3/M_2 = 10^2$, $M_1 = 200$ GeV, $m_\eta = 201$ GeV, $\lambda_5 = 0.5, m_1 = 10^{-3}$ eV.

We then show the significance of different parameters on the evolution of $n_{\rm B-L}$ in Fig.2.2. In the upper left panel plot, it can be seen that the washout effects are stronger for larger values of the m_1. However, the variation of the $n_{\rm B-L}$ is small with m_1, because, this variation is due to $\Delta L = 1$ scatterings $lW^{\pm}(Z) \longrightarrow N_1\eta$. As we increase m_1 the Yukawa couplings for N_1 increase leading to an increase in the washout. On the other hand on the upper right panel plot of Fig.2.2 it can be seen that with the increase in λ_5 the final $n_{\rm B-L}$ increases. In N_2 leptogenesis scenario, we are necessarily in a strong washout region with NO of light neutrino mass. This can be understood from the structure of the Yukawa matrix in Eq.(2.41). It can

be easily seen that one does not have much freedom on the Yukawa couplings of N_2 from the light neutrino sector in the case of NO. The Yukawa couplings are large enough for the inverse decays to have strong washout effects. On the other hand following the Casas-Ibarra parametrisation one can see that the Yukawa couplings can be decreased by increasing λ_5. Therefore with the increase in λ_5 the inverse decay decreases leading to an increase in the final asymmetry. In the lower left panel plot of Fig.2.2, it can be seen that there is a small variation of $n_{\rm B-L}$ with the change in M_1. Although this variation is very small, it can be understood from the fact that with the increase in M_1 the Yukawa couplings corresponding to N_1 also increase leading to an increase in washout coming from the scattering processes. In the lower right panel plot of Fig.2.2 one can see that with the increase in M_2, $n_{\rm B-L}$ also increases. This can be understood as follows, with the increase in M_2 the decay rate for N_2 increases while the inverse decays get suppressed. This results in an increase in asymmetry generation and a decrease in washouts and thereby an increase in $B-L$ asymmetry.

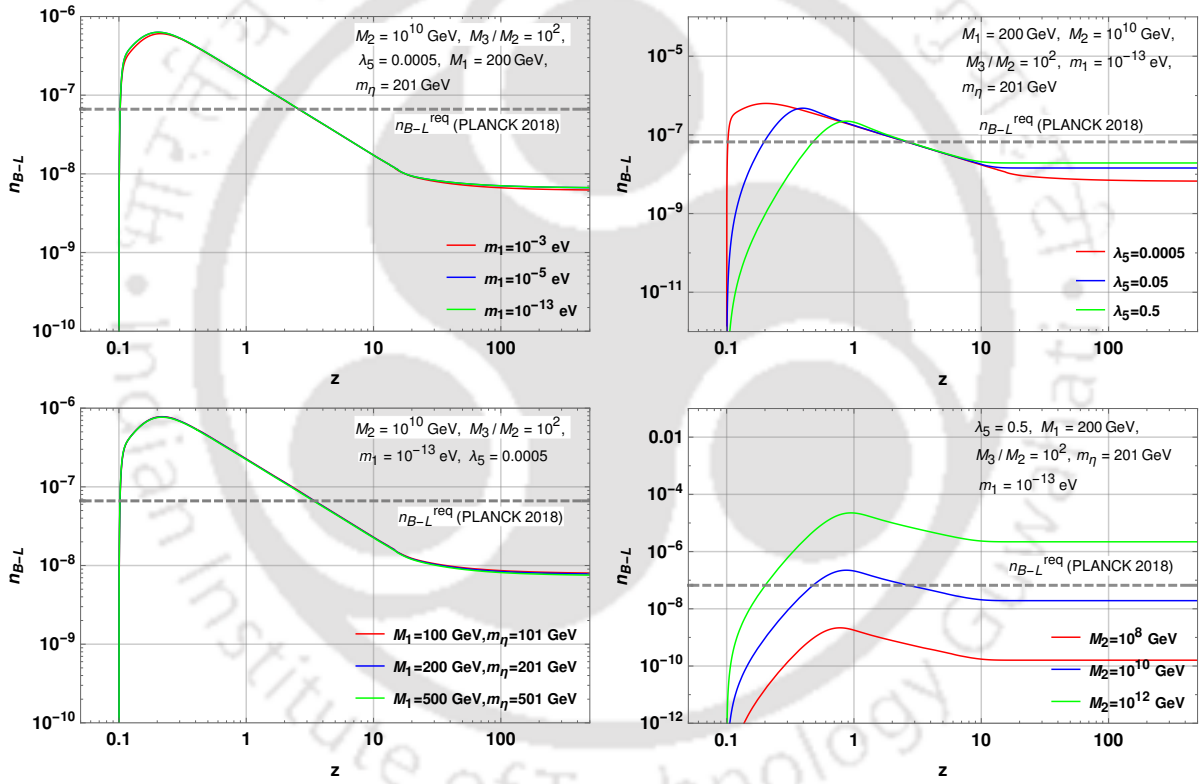

Figure 2.2: Evolution of $n_{\rm B-L}$ (Comoving number density of $B-L$) with z for NO with different benchmark values of m_1 (upper left panel), λ_5 (upper right panel), M_1 (lower left panel) and M_2 (lower right panel). The horizontal black dashed line in all the plots indicate the required value of $B-L$ asymmetry to produce the observed baryon asymmetry after sphaleron transitions.

We then evaluate baryon to photon ratio η_B from the lepton asymmetry using the formula given in Eq.(2.40). We show the variation of η_B with M_2 for different benchmark values of relevant parameters like λ_5 and M_1 in Fig.2.3 keeping the other parameters fixed. In all these plots, we can see that the correct baryon asymmetry (shown as the horizontal dashed

black line) can be obtained for different values of these model parameters.

We finally scan the parameter space in $M_2 - \lambda_5$ plane by fixing $M_3/M_2 = 10^2$ and choosing different combinations of m_η, M_1, m_1. The resulting parameter spaces that satisfies the correct baryon asymmetry are shown in Fig.2.4 and Fig.2.5 for $m_1 = 10^{-3}$ eV and $m_1 = 10^{-13}$ eV respectively. Different coloured bands correspond to different combinations of m_η, M_1 as indicated. As can be seen from these plots, the scale of leptogenesis M_2 gets pushed up as we decrease λ_5. Smaller values of λ_5 result in larger Yukawa couplings from the requirements of light neutrino masses through Casas-Ibarra parametrisation. However, for a fixed lightest neutrino mass and m_η, M_1, such increase in Yukawa couplings will not only enhance the production of asymmetry but also increase the strength of washout scatterings, of which the latter dominates. For smaller m_1, due to the smallness of Yukawa couplings responsible for washout scatterings, the scale of leptogenesis can be slightly lower, as seen by comparing Fig.2.4 with Fig.2.5. In both the cases, we notice that the scale of leptogenesis is around 10^{10} GeV, below which successful leptogenesis is not possible.

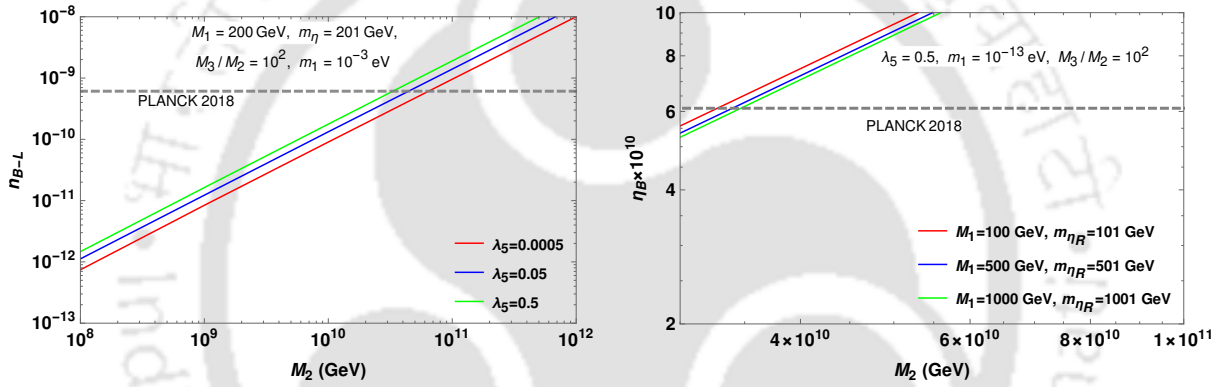

Figure 2.3: Variation of baryon to photon ratio with M_2 for different benchmark values of λ_5 (Upper panel plots) and M_1 (Lower panel plots) in case of NO. The horizontal dashed line represents the observed η_B in all the plots.

We then study the possibility of N_1 dark matter in the normal ordering scenario of light neutrino masses. To study the FIMP possibility we first choose a benchmark of model parameters which show the possibility of realising tiny Yukawa couplings of N_1 required for their non-thermal nature. We fix $M_1 = 200$ GeV, $M_2 = 10^{10}$ GeV, $M_3 = 10^2 M_2, m_\eta = 201$ GeV, and $\lambda_5 = 0.1$ and vanishingly small lightest neutrino mass m_1. The Dirac Yukawa structure for this choice of benchmark is given, according to Casas-Ibarra parametrisation, by

$$Y = \begin{pmatrix} 3.856 \times 10^{-10} + 0.i & -0.0008 - 0.0058i & -0.03210 + 0.0204i \\ -1.3328 \times 10^{-10} + 2.5186 \times 10^{-11} i & 0.0159 + 0.0076i & -0.1599 - 0.0566i \\ 2.2980 \times 10^{-10} + 2.1432 \times 10^{-11} i & 0.0016 + 0.0086i & 0.1822 - 0.0068i \end{pmatrix}.$$

In general, the analytical form of Yukawa matrix, followed from the Casas-Ibarra parametrisation discussed before and for the choice of R matrix mentioned before, can be written

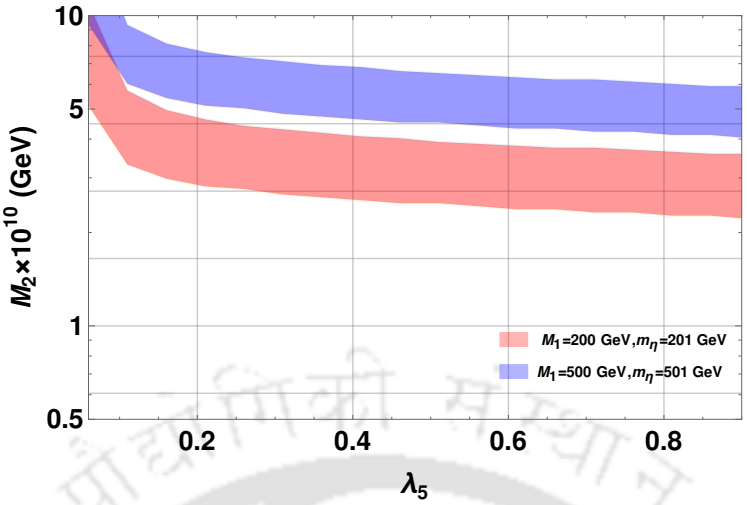

Figure 2.4: Scan plot for M_2 vs λ_5 for $m_1 = 10^{-3}$ eV, and $M_3/M_2 = 10^2$ for which the observed baryon asymmetry is generated in case of NO of the light neutrinos.

as

$$Y = \begin{pmatrix} \sqrt{m_1}\sqrt{\Lambda_1}U_{11} & \sqrt{m_2}C^*(z)\sqrt{\Lambda_2}U_{12} - \sqrt{m_3}S^*(z)\sqrt{\Lambda_2}U_{13} & \sqrt{m_2}S^*(z)\sqrt{\Lambda_3}U_{12} + \sqrt{m_3}C^*(z)\sqrt{\Lambda_3}U_{13} \\ \sqrt{m_1}\sqrt{\Lambda_1}U_{21} & \sqrt{m_2}C^*(z)\sqrt{\Lambda_2}U_{22} - \sqrt{m_3}S^*(z)\sqrt{\Lambda_2}U_{23} & \sqrt{m_2}S^*(z)\sqrt{\Lambda_3}U_{22} + \sqrt{m_3}C^*(z)\sqrt{\Lambda_3}U_{23} \\ \sqrt{m_1}\sqrt{\Lambda_1}U_{31} & \sqrt{m_2}C^*(z)\sqrt{\Lambda_2}U_{32} - \sqrt{m_3}S^*(z)\sqrt{\Lambda_2}U_{33} & \sqrt{m_2}S^*(z)\sqrt{\Lambda_3}U_{32} + \sqrt{m_3}C^*(z)\sqrt{\Lambda_3}U_{33} \end{pmatrix}, \tag{2.41}$$

where $C(z) = \cos z$, $S(z) = \sin z$ and U_{ij} are the elements of PMNS mixing matrix. Clearly, the Yukawa couplings of N_1 to SM leptons and η are decided by m_1, which is the lightest active neutrino mass in NO. So in case of NO, we can have arbitrarily small Yukawa couplings of N_1 required for FIMP dark matter by taking m_1 very small. We can also make the Yukawa couplings sizeable by taking m_1 similar to the scale of mass squared differences or in the quasi-degenerate light neutrino mass regime, if we want to realise the WIMP scenario for N_1. On the contrary, we can not choose m_1 to be arbitrarily low for IO of active neutrino mass, thereby restricting our Yukawa couplings to be higher than certain values. However, as we comment in Appendix A.1, choosing a different or more general R matrix can make it possible to have FIMP type Yukawa for N_1 in IO which however does not affect the results related to leptogenesis significantly. We will discuss about it later when we go to the discussion of IO part.

To show the FIMP abundance, we choose benchmark values of Yukawa couplings $Y = Y_{11} = Y_{21} = Y_{31} = 10^{-10}, 10^{-9}$ for simplicity and show N_1 abundance as a function of $z = m_\eta/T$ in Fig.2.6 for different benchmark values of parameters. As can be seen from these plots, the initial abundance of FIMP is negligible followed by its rise at two distinct epochs: first when the mother particle is in equilibrium and later when the mother particle freezes-out and then decays. Depending upon the Yukawa couplings the equilibrium contribution varies, for example, when the Yukawa coupling is larger the equilibrium contribution to FIMP abundance is also larger. For larger Yukawa, the final abundance of FIMP remains higher, as can be seen by comparing the left and right panel plots of Fig.2.6.

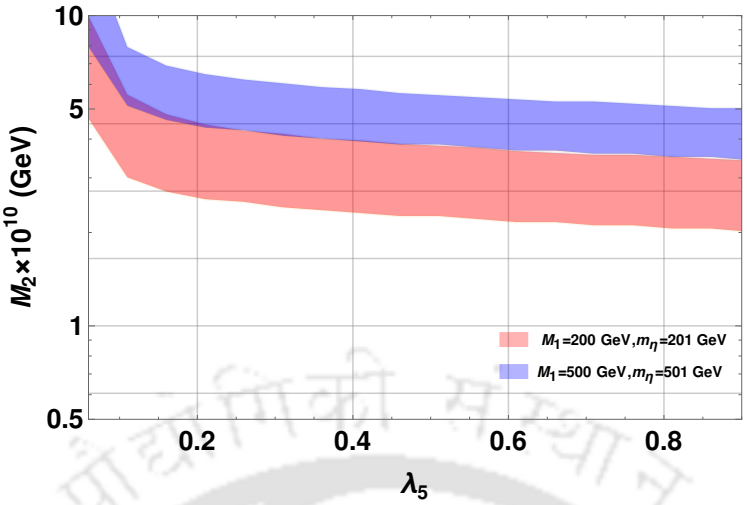

Figure 2.5: Scan plot showing the viable parameter space in M_2 vs λ_5 for $m_1 = 10^{-13}$ eV, and $M_3/M_2 = 10^2$ in case of NO of the light neutrinos.

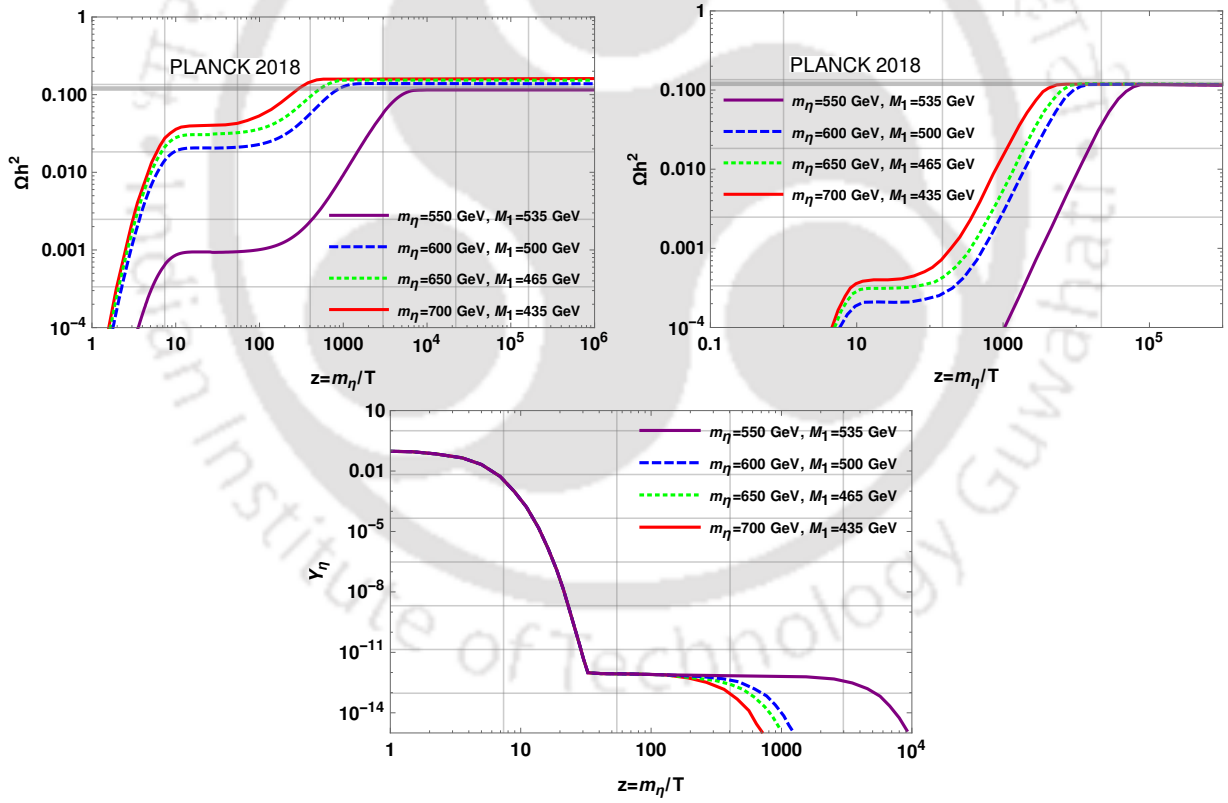

Figure 2.6: Dark Matter (N_1) relic versus $z = m_\eta/T$ (upper panel) taking both equilibrium and out-of-equlibrium contribution and the comoving number density of the mother particle η as a function of $z = m_\eta/T$ (Lower panel). The set of parameters used are $\lambda_3+\lambda_4+\lambda_5 = 0.001$, $\lambda_5 = 0.1$ and $Y_{i1} = 10^{-9}$ (Upper left panel), $Y_{i1} = 10^{-10}$ (Upper right panel). The set of parameters used for the lower panel plot are $\lambda_3 + \lambda_4 + \lambda_5 = 0.001$, $\lambda_5 = 0.1, Y_{i1} = 10^{-9}$.

The difference due to the choices of $(m_\eta, m_{\rm DM})$ is coming as these parameters affect the decay width of η into N_1. As FIMP mass becomes closer to the mother particle's mass, the decay width decreases and hence the yield of DM also decreases slightly. In order to compare the evolution of FIMP abundance with that of the mother particle's abundance we also show the variation of η abundance as a function of z in the lower panel plot of Fig.2.6. As can be seen there, the mother particle was in thermal equilibrium in early epochs followed by its thermal freeze-out and then subsequent fall in its abundance at lower temperatures (or higher z) due to its decay into FIMP. We have used `micrOMEGAs` package [158] to calculate the freeze-out details of η in our work.

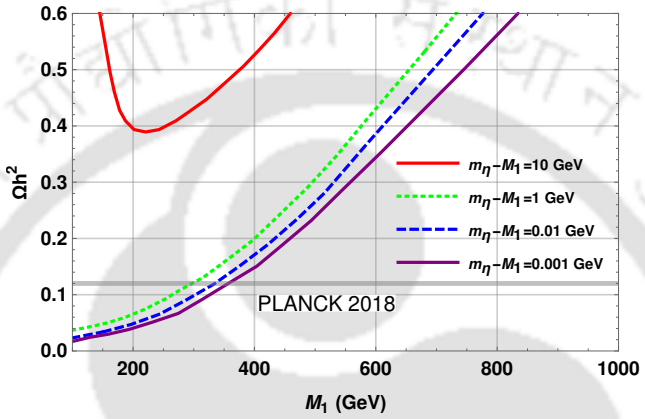

Figure 2.7: WIMP Dark matter relic vs Dark matter mass for different benchmark parameters in case of NO. The chosen benchmark is $\lambda_5 = 5 \times 10^{-4}$ and $m_1 = 10^{-3}$ eV.

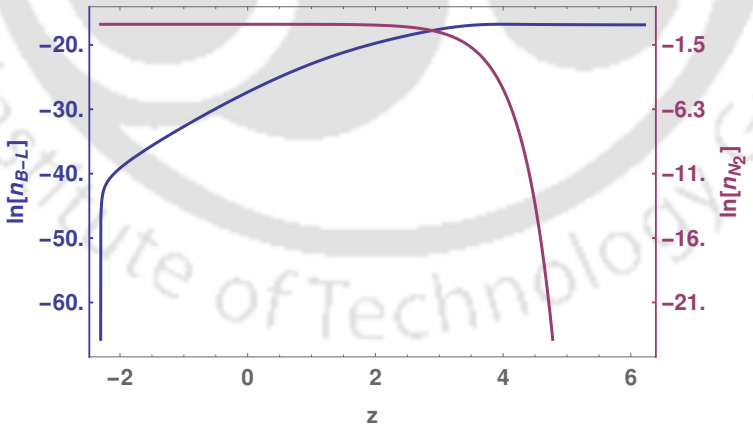

Figure 2.8: Evolution of $n_{N_2}, n_{\rm B-L}$ with z for IO. The set of parameters used are $M_2 = 10^5$ GeV, $M_3/M_2 = 10^2$, $M_1 = 200$ GeV, $m_\eta = 201$ GeV, $\lambda_5 = 5 \times 10^{-4}, m_3 = 10^{-13}$ eV.

We also check the possibility of N_1 being WIMP DM with NO of neutrino mass. However, for WIMP DM we need much larger Yukawa couplings than the ones mentioned above for FIMP. Such larger couplings are required in order to produce N_1 thermally in the early

universe which later undergoes thermal freeze-out leaving the right relic abundance. We generate such large Yukawa couplings by increasing the lightest active neutrino mass to $m_1 = 10^{-3}$ eV from $m_1 = 10^{-13}$ eV before. Such increase in lightest active neutrino mass does not affect the leptogenesis results significantly for NO. The relic abundance for WIMP DM as a function of its mass is shown in Fig.2.7 for different benchmark parameters. As can be seen from this plot, the mass splitting between η and N_1 plays a crucial role in generating the correct abundance. For smaller mass splittings the coannihilation between η and N_1 gets enhanced, bringing down the relic abundance within the observed limits. Here also we have implemented the model in `micrOMEGAs` to calculate the relic abundance of N_1.

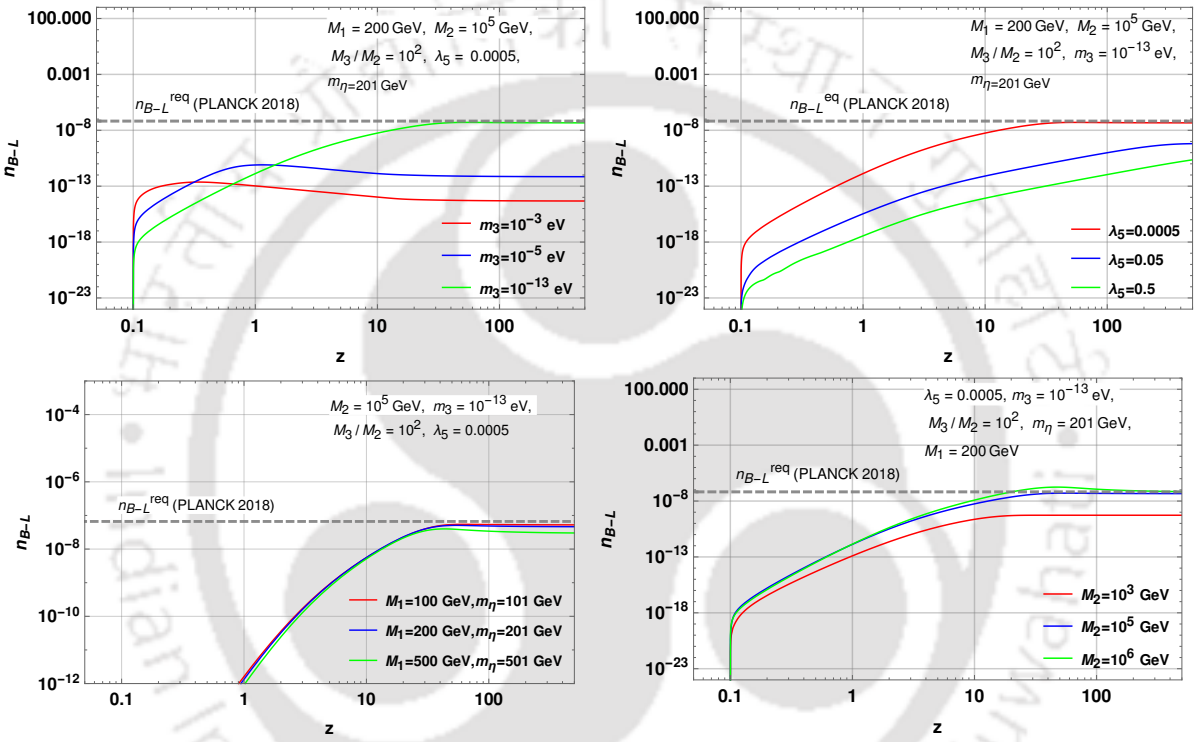

Figure 2.9: Evolution $n_{\mathrm{B-L}}$ with z for IO with different benchmark values of m_3 (Upper left panel), λ_5 (Upper right panel), M_1 (Lower left panel) and M_2 (Lower right panel). The horizontal black dashed line in all the plots indicates the required value of $B-L$ asymmetry to produce the observed baryon asymmetry after sphaleron transitions.

We now move on to discussing the results for IO of light neutrino masses. We choose the following R matrix in order to generate the desired Yukawa structure:

$$\mathbf{R}= \begin{pmatrix} 1 & 0 & 0 \\ 0 & \cos(z_R + iz_I) & \sin(z_R + iz_I) \\ 0 & -\sin(z_R + iz_I) & \cos(z_R + iz_I) \end{pmatrix}$$

with $z_R = 1.5707$ and $z_I = -0.0008$. Once again, the justification behind such choice of R and other possibilities of R matrix are mentioned in Appendix A.1. The following Yukawa structure is obtained for N_2 leptogenesis with the benchmark parameter as $M_1 = 200$ GeV,

$M_2 = 10^5$ GeV, $M_3/M_2 = 10^2$, $m_\eta = 201$ GeV, $\lambda_5 = 5 \times 10^{-4}$ and vanishingly small lightest neutrino mass m_3.

$$\mathbf{Y}= \begin{pmatrix} 0.0003 + 0.i & 2.9995 \times 10^{-8} - 2.4960 \times 10^{-8} i & -0.0023 - 1.7669 \times 10^{-11} i \\ -0.0001 + 0.2459 \times 10^{-5} i & 1.3062 \times 10^{-7} - 9.4011 \times 10^{-8} i & -0.0094 - 0.0005 i \\ 0.0002 + 0.2093 \times 10^{-5} i & -1.1472 \times 10^{-7} + 1.0759 \times 10^{-7} i & 0.0094 - 0.0004 i \end{pmatrix}$$

Clearly, the Yukawa coupling of the lightest right handed neutrino do not become arbitrarily small, unlike in NO case mentioned earlier.

In Fig.2.8, we show the evolution of comoving number densities for N_2 and $B - L$ asymmetry for chosen benchmark parameters $M_2 = 10^5$ GeV, $M_3/M_2 = 10^2$, $M_1 = 200$ GeV, $m_\eta = 201$ GeV, $\lambda_5 = 5 \times 10^{-4}, m_3 = 10^{-13}$ eV. Clearly, the number density of N_2 decreases due to its decay while the $B - L$ asymmetry increases as N_2 abundance decreases. Once again, the final value of $n_{\rm B-L}$ satisfies the criteria of producing correct baryon asymmetry after sphaleron transitions and the washout effects are minimal for the chosen parameters. We then show the evolution of $n_{\rm B-L}$ with z for different benchmark model parameters in Fig.2.9 for IO of light neutrino mass. In the upper left panel plot of Fig.2.9, it is seen that with the increase in m_3 the $n_{\rm B-L}$ decreases. This is because with the increase in m_3 the Yukawa couplings for N_2 increase for IO. Therefore, with the increase of m_3 we start falling into strong washout region. This effect is clearly visible in the plot. In the upper right panel plot of Fig.2.9, it is seen that with the increase in λ_5 the asymmetry decreases. This is because we have chosen $m_3 = 10^{-13}$ eV for the upper right panel plot and for such small values of m_3 the N_2 Yukawas are very small and we are in a weak washout region. With the increase in λ_5 the N_2 Yukawas become further small giving rise to smaller values of CP asymmetry parameter resulting in a decrease of $n_{\rm B-L}$. This behaviour is opposite to what is observed for NO. In the lower left panel plot of Fig.2.9 it can be seen that with the increase in M_1 the $n_{\rm B-L}$ decreases. This is similar to what is observed in the case of NO. With the increase in M_1 the N_1 Yukawa couplings increase leading to an enhancement in the washout coming from the scattering processes. On the bottom right panel plot the variation of $n_{\rm B-L}$ with the change of M_2 is shown. One can see the expected behaviour of $n_{\rm B-L}$ with the increase of M_2, as explained in the case of NO.

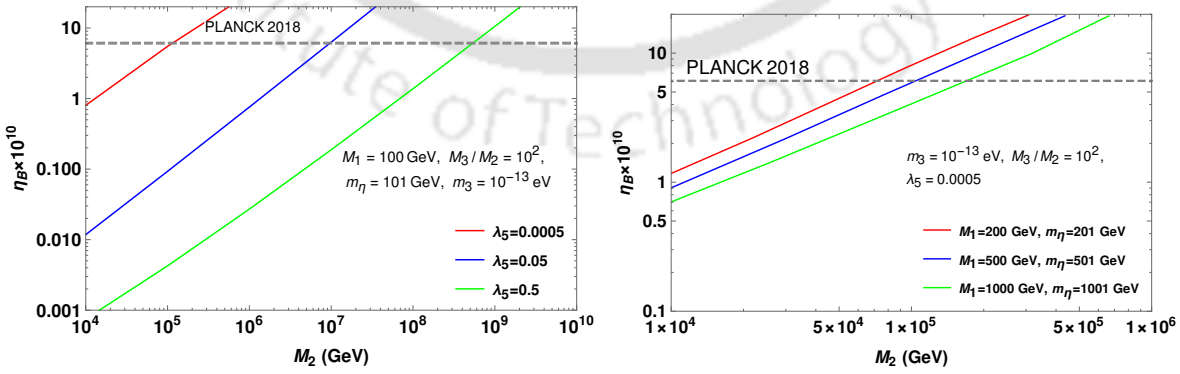

Figure 2.10: Variation of η_B with M_2 for different benchmark values of λ_5 (left panel plot) and for different benchmark combination of M_1 and m_η (right panel plot) in case of IO. The horizontal gray dashed line represents the observed η_B from Planck 2018 data [3].

We then show the variation of baryon to photon ratio (η_B) with mass of N_2 for different benchmark parameters in Fig.2.10 and compare it with the observed baryon asymmetry. Clearly, the observed baryon asymmetry can be produced by appropriate choices of benchmark parameters. Interestingly, the scale of leptogenesis can be as low as few tens of TeV, unlike in case of NO where the scale of leptogenesis was several order of magnitudes above TeV scale. This is particularly possible when both λ_5 and lightest neutrino mass m_3 are chosen small and we are in a weak washout regime. We finally show the parameter space in terms of M_2 and λ_5 which leads to the observed baryon asymmetry for different choices of m_η, M_1, m_3 and show them in Fig.2.11 and Fig.2.12 for $m_3 = 10^{-3}$ eV and $m_3 = 10^{-13}$ eV respectively. It can be seen that for $m_3 = 10^{-3}$ eV the scale of leptogenesis is pushed to higher values, while for $m_3 = 10^{-13}$ eV the scale of leptogenesis can be few TeV. Sharp contrast can be noticed for the scale of leptogenesis with λ_5 between both the plots. In Fig.2.11 it is seen that the scale of leptogenesis is pushed to higher values as we decrease λ_5. This is due to the similar reason we mentioned in the discussion of NO results, for $m_3 = 10^{-3}$ eV, the washout effects start dominating over the production processes as we lower λ_5 further leading to corresponding rise in Yukawa couplings. On the other hand, in Fig.2.12, it can be seen that the scale of leptogenesis decreases as we decrease λ_5. For very small value of the lightest neutrino mass $m_3 = 10^{-13}$ eV, we are in weak washout region and therefore the asymmetry can be increased by decreasing λ_5. It is also observed that beyond a certain small value of λ_5 the M_2 required to satisfy the correct asymmetry increases for IO with $m_3 = 10^{-13}$ eV. It is due to the increase in the washout with the decrease in λ_5. Even though decreasing λ_5 helps in increasing the asymmetry for IO with vanishingly small m_3 Beyond a certain small value of λ_5 the washouts become very dominant. From Fig.2.12 it can be seen that the scale of leptogenesis can be as low as $\mathcal{O}(50\text{TeV})$ for $M_1 = 200$ GeV and $m_\eta = 201$ GeV.

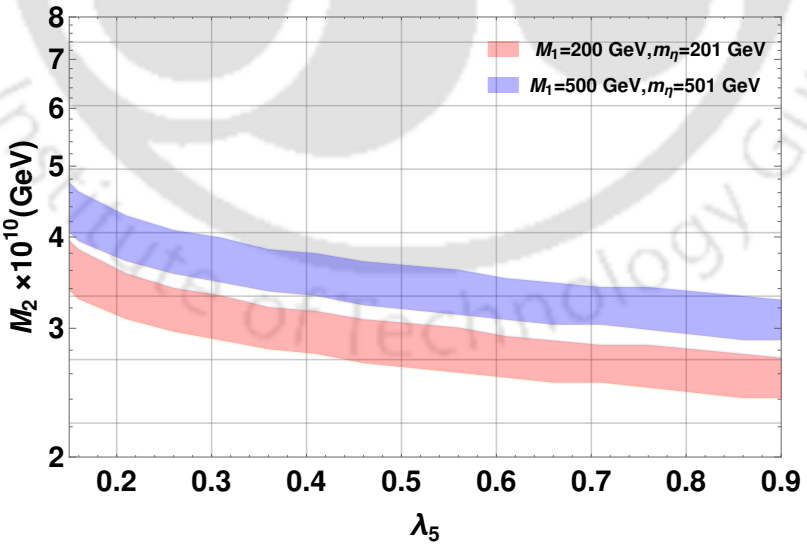

Figure 2.11: Parameter space in M_2 vs λ_5 plane for $m_3 = 10^{-3}$ eV with the parameter choice $M_3/M_2 = 10^2$ for which the observed baryon asymmetry is generated for IO.

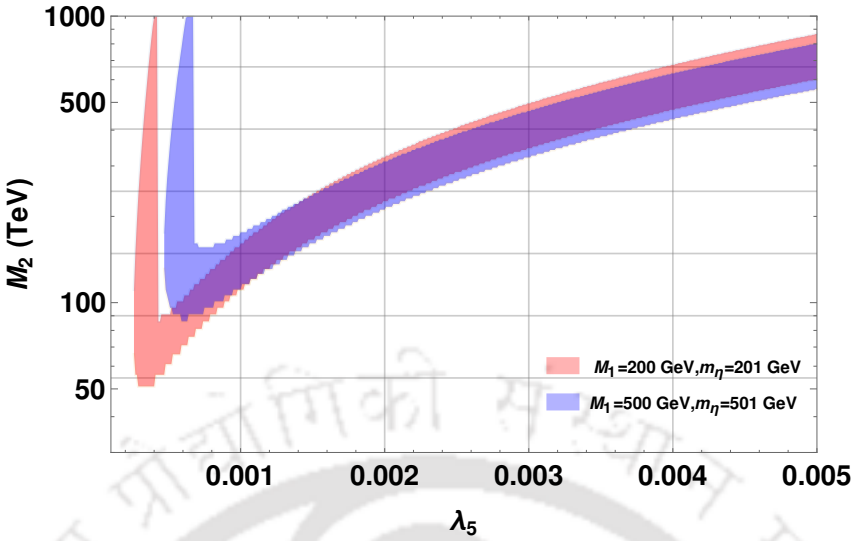

Figure 2.12: Parameter space in M_2 vs λ_5 plane for $m_3 = 10^{-13}$ eV with the parameter choice $M_3/M_2 = 10^2$ for which the observed baryon asymmetry is generated for IO.

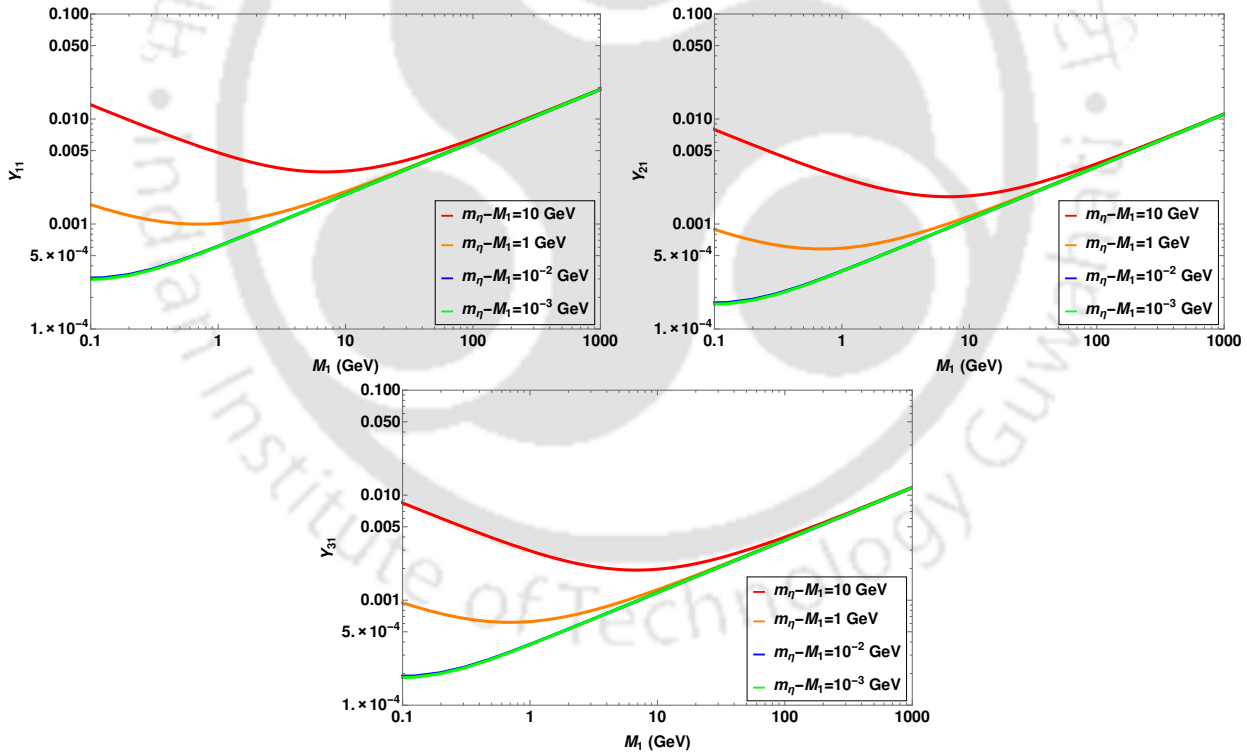

Figure 2.13: Variation of Yukawa coupling with respect to DM mass for IO. The chosen benchmark is $\lambda_5 = 10^{-6}$.

As mentioned earlier, we can not have FIMP type Yukawa coupling of DM in IO case due to the structure of Yukawa matrix in terms of light neutrino parameters, for the particular R matrix chosen. We first show the variation of Yukawa couplings of N_1 with its mass in

Fig.2.13. It can be seen that the couplings can not be made as small as the ones for FIMP dark matter, even though we use the lightest active neutrino mass very small $m_3 = 10^{-13}$ eV. We therefore, pursue the WIMP possibility here and show that for small mass splitting between N_1 and η it is possible to produce the observed relic abundance. The relic abundance of WIMP DM in IO scenario is very similar to the WIMP results obtained in case of NO and hence we do not show the corresponding plot here.

2.5 Results of N_2 Leptogenesis with Flavour Effects

Finally, we check the role of lepton flavour effects on our results of leptogenesis. In our earlier discussion, we ignored such flavour effects and hence summed over all flavours leading to the CP asymmetry parameter given in Eq.(2.25). As pointed out in several earlier works [55–58], flavour effects can significantly alter the leptogenesis predictions. For a recent review on flavour effects in leptogenesis, please see [159]. Here, we adopt the prescription given in [58] and calculate the final baryon asymmetry considering a three flavour regime.

The Boltzmann equations for such three flavoured leptogenesis can be written as

$$\frac{dn_{N_2}}{dz} = -D_2(n_{N_2} - n_{N_2}^{eq}) \tag{2.42}$$

$$\frac{dn_{\Delta_\alpha}}{dz} = -\epsilon_{2\alpha} D_2(n_{N_2} - n_{N_2}^{eq}) - P_{2\alpha} W_2^{ID} n_{\Delta_\alpha} - P_{2\alpha} \Delta W_{\Delta L=1} n_{\Delta\alpha} - P_{2\alpha} n_{\Delta\alpha} \sum_{\beta=e,\mu,\tau} P_{2\beta} (\Delta W_{\Delta L=2})_{\alpha\beta}. \tag{2.43}$$

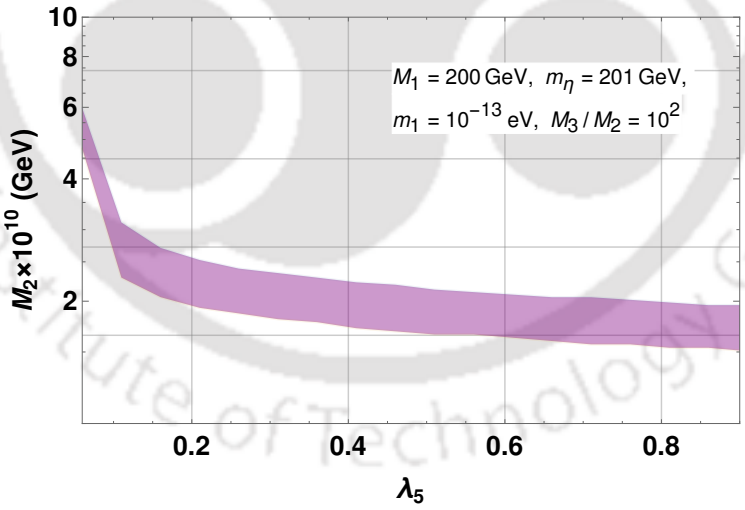

Figure 2.14: Scan plot for flavoured leptogenesis with NO of neutrino mass in $M_2 - \lambda_5$ plane. The benchmark parameters taken for this scan are $m_1 = 10^{-13}$ eV and $M_3/M_2 = 10^2$.

Here, there are three equations corresponding to $\alpha = e, \mu, \tau$. n_{N_2} and $n_{\Delta\alpha}$ are the comoving number densities of N_2 and the $B/3 - L_\alpha$ (for each flavor of leptons). $P_{2\alpha}$ are the projectors defined by

$$P_{2\alpha} = \frac{\Gamma_{2\alpha}}{\Gamma_2}. \tag{2.44}$$

Where Γ_2 is the total decay width of N_2 while $\Gamma_{2\alpha}$ is the corresponding partial decay width to a particular lepton flavour denoted by α. The washout terms $\Delta W_{\Delta L=1}, \Delta W_{\Delta L=2}$ are same as the ones discussed earlier. The flavoured CP asymmetry parameter $\epsilon_{2\alpha}$ is given in Eq.(2.22). We choose the same R matrix as before and find the parameter space for flavoured leptogenesis that can give rise to the correct final baryon asymmetry. The resulting parameter space for NO and IO are shown in Figs. 2.14 and 2.15 respectively. As can be seen from these plot, the scale of leptogenesis can be lower compared to the unflavoured leptogenesis. To be more specific, in case of IO, the leptogenesis scale can be lower significantly with successful leptogenesis occurring at M_2 as low as 30 TeV. On the other hand even after taking the flavour effects the scale of leptogenesis can not be less than $\mathcal{O}(10^{10})$ GeV in the case of NO.

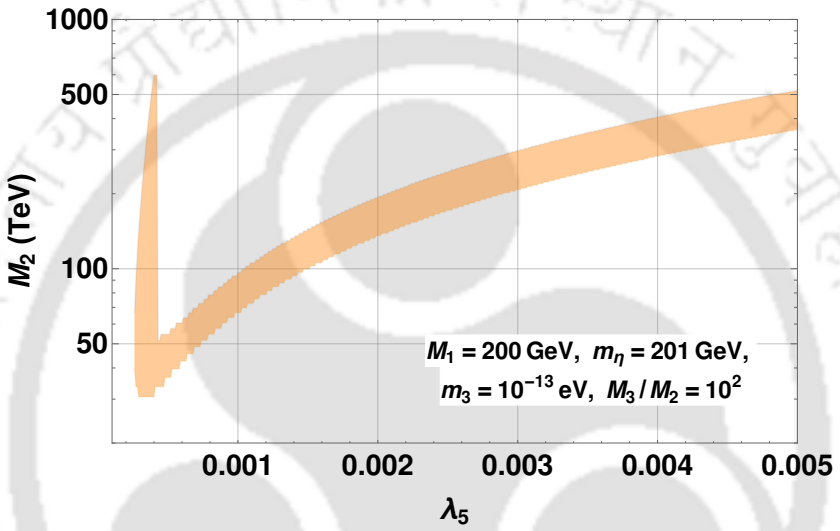

Figure 2.15: Scan plot for flavoured leptogenesis with IO of neutrino mass in $M_2 - \lambda_5$ plane. The benchmark parameters taken for this scan are $m_3 = 10^{-13}$ eV and $M_3/M_2 = 10^2$.

CHAPTER 3

Dark Sector Assisted Low Scale Leptogenesis from Three-Body Decay

In this chapter, we study the possibility of realising leptogenesis from three-body decay along with dark matter and neutrino mass in a minimal framework. We propose a first of its kind model to implement the idea of leptogenesis from three-body decay where CP asymmetry arises from interference of multiple $1 \longrightarrow 3$ diagrams with some of the final state particles playing the role of DM simultaneously. While leptogenesis from three-body decay was covered in earlier works [160–163], a different way of achieving the same was also discussed in different contexts by the authors of [164–168]. These works either considered soft leptogenesis in a supersymmetric framework or leptogenesis due to CP asymmetry arising from interference of from multiple $2 \to 2$ or $1 \to n(n \geq 3)$ diagrams with resummed propagators. While a concrete model to realise leptogenesis from such $2 \to 2$ processes along with dark matter was proposed in [164], there has been no concrete model yet, to realise leptogenesis from three-body decay where non-zero CP asymmetry arises due to interference of multiple $1 \to 3$ decay diagrams with resummed propagators together with dark matter. Here we try to implement this idea in a minimal extension of the scotogenic model discussed in chapter 2. Such an extension is required as in the minimal scotogenic model we can not have non-zero CP asymmetry from three-body decay of right handed neutrinos. We show that successful leptogenesis can be achieved at a scale as low as 2 TeV in this scenario, which gets lowered to even below 1 TeV after including the lepton flavour effects. While, the usual two-body decay of right handed neutrinos in scotogenic model can also contribute to lepton asymmetry, we show that the contribution from three-body decay dominates in the low mass regime. While building such a setup, we also find that the model naturally predicts a two component dark matter scenario. We discuss interplay of different couplings involved in leptogenesis as well dark matter and show the consistency between the possibility of low scale leptogenesis and correct DM relic density in agreement with all experimental constraints including light neutrino masses and mixing.

3.1 The Model

We briefly discuss our model in this section. We stick to a minimal setup required to obtain the desired phenomenology. The SM particle content is extended by three singlet

Particles	$SU(3)_c \times SU(2)_L \times U(1)_Y$	Z_2	Z_2'
Q_L	$(3, 2, \frac{1}{6})$	1	1
u_R	$(3, 1, \frac{2}{3})$	1	1
d_R	$(3, 1, -\frac{1}{3})$	1	1
ℓ_L	$(1, 2, -\frac{1}{2})$	1	1
ℓ_R	(1, 1, -1)	1	1
$N_{1,2}$	(1, 1, 0)	-1	1
ψ	(1, 1, 0)	-1	-1
H	$(1, 2, \frac{1}{2})$	1	1
η	$(1, 2, \frac{1}{2})$	-1	1
S	(1,1,0)	1	-1

Table 3.1: Particle content of the model.

chiral fermions $N_{1,2}, \psi$ and two scalar fields η, S which transform non-trivially under the additional $Z_2 \times Z_2'$ symmetry of the model. This additional discrete symmetry is chosen to remove the unwanted terms so that the desired leptogenesis and dark matter phenomenology can be ensured. UV completion of our model can explain the origin of such discrete gauge symmetries from spontaneous breaking of gauge symmetries at high energy scale, for example see [169–174] and references therein. As we discuss in details below, with the addition of one extra field compared to the minimal scotogenic model [112], we can achieve much richer phenomenology with a new way of generating lepton asymmetry at a scale, lower compared to the one obtained in minimal scotogenic model [113, 143, 175–177].

The particle content of the model is shown in Table 3.1 along with their transformations under the symmetries of the model. The Yukawa Lagrangian can be written as

$$\mathcal{L} = -Y_u \overline{Q_L} \tilde{H} u_R - Y_d \overline{Q_L} H d_R - Y_e \overline{\ell_L} H \ell_R - h_{i\alpha} (\overline{\ell_L})_i \tilde{\eta} N_\alpha - \frac{1}{2} M_\alpha \overline{N_\alpha^c} N_\alpha - y_\alpha \psi N_\alpha S - \frac{1}{2} m_\psi \overline{\psi^c} \psi \tag{3.1}$$

The scalar potential is given by

$$\begin{aligned} V = {} & \mu_H^2 H^\dagger H + \mu_\eta^2 \eta^\dagger \eta + \frac{1}{2} m^2 S^2 + \frac{\lambda_1}{2} (H^\dagger H)^2 + \frac{\lambda_2}{2} (\eta^\dagger \eta)^2 + \frac{1}{2} \lambda_S S^4 + \lambda_3 (H^\dagger H)(\eta^\dagger \eta) \\ & + \lambda_4 (H^\dagger \eta)(\eta^\dagger H) + \frac{\lambda_5}{2} [(H^\dagger \eta)(H^\dagger \eta) + (\eta^\dagger H)(\eta^\dagger H)] + \frac{\lambda_6}{2} (H^\dagger H) S^2 + \lambda_7 (\eta^\dagger \eta) S^2. \end{aligned} \tag{3.2}$$

After the electroweak symmetry breaking (EWSB), the two scalar doublets of the model can be written in the following form in the unitary gauge:

$$H = \begin{pmatrix} 0 \\ \frac{v+h}{\sqrt{2}} \end{pmatrix}, \qquad \eta = \begin{pmatrix} \eta^\pm \\ \frac{\eta_R + i\eta_I}{\sqrt{2}} \end{pmatrix}, \tag{3.3}$$

where h is the SM-like Higgs boson, η_R, η_I are the CP-even and CP-odd neutral scalars respectively, while $\eta^\pm$ are the charged scalars from the additional scalar doublet η. The vacuum expectation value (VEV) of the SM Higgs is denoted by v while the other two scalars do not acquire any VEVs so that the $Z_2 \times Z_2'$ symmetry of the model remains unbroken.

The masses of the physical scalars at tree level can be written as

$$\begin{aligned} m_h^2 &= \lambda_1 v^2,\ m_S^2 = m^2 + \lambda_6 \frac{v^2}{2},\ m_{\eta^\pm}^2 = \mu_\eta^2 + \frac{1}{2}\lambda_3 v^2 \\ m_{\eta_R}^2 &= \mu_\eta^2 + \frac{1}{2}(\lambda_3+\lambda_4+\lambda_5)v^2 \ = \ m_{\eta^\pm}^2 + \frac{1}{2}\left(\lambda_4+\lambda_5\right)v^2, \\ m_{\eta_I}^2 &= \mu_\eta^2 + \frac{1}{2}(\lambda_3+\lambda_4-\lambda_5)v^2 \ = \ m_{\eta^\pm}^2 + \frac{1}{2}\left(\lambda_4-\lambda_5\right)v^2 . \end{aligned} \tag{3.4}$$

Without any loss of generality, we consider $\lambda_5 < 0$ so that the CP-even scalar is lighter than the CP-odd one. Thus η_R is the lightest component of the scalar doublet η and also lighter than the singlet fermions $N_{1,2}$. Similarly the singlet scalar S is chosen to be lighter than ψ. This ensures η_R, S to be the lightest Z_2-odd and Z_2'-odd particles respectively and hence viable dark matter candidates of the model.

As can be seen from the Yukawa Lagrangian in Eq.(3.1), there is no tree level contribution to light neutrino masses, simply because they couple to the heavy neutrinos N_i only via the second scalar doublet η which does not acquire any VEV. However, light neutrino masses can arise at radiative level as originally proposed in the context of minimal scotogenic model [112]. In our setup, the additional scalar doublet η and the singlet fermions $N_{1,2}$ will go inside the loop which generates the light neutrino masses, the expression for which can be evaluated as [112, 132]

$$\begin{aligned} (M_\nu)_{ij} &= \sum_k \frac{h_{ik}h_{jk}M_k}{32\pi^2}\left(\frac{m_{\eta_R}^2}{m_{\eta_R}^2 - M_\alpha^2}\ln\frac{m_{\eta_R}^2}{M_k^2} - \frac{m_{\eta_I}^2}{m_{\eta_I}^2 - M_k^2}\ln\frac{m_{\eta_I}^2}{M_k^2}\right) \\ &\equiv \sum_k \frac{h_{ik}h_{jk}M_k}{32\pi^2}\left[L_k(m_{\eta_R}^2) - L_k(m_{\eta_I}^2)\right] , \end{aligned} \tag{3.5}$$

where M_k is the mass eigenvalue of the mass eigenstate N_k in the internal line and the indices $i, j = 1, 2, 3$ run over the three neutrino generations and $k = 1, 2$ takes into account of two N_α. The loop function $L_k(m^2)$ is defined as

$$L_k(m^2) \ = \ \frac{m^2}{m^2 - M_k^2}\ln\frac{m^2}{M_k^2} . \tag{3.6}$$

From the expressions for physical scalar masses given in Eqs.(C.6), we can write $m_{\eta_R}^2 - m_{\eta_I}^2 = \lambda_5 v^2$. Therefore, in the limit $\lambda_5 \to 0$, the neutral components of inert doublet η become mass degenerate. Also, a vanishing λ_5 implies vanishing light neutrino masses which is expected as the λ_5-term in the scalar potential (3.2) breaks lepton number by two units, when considered together with the fermion Yukawa Lagrangian (3.1). As we will see later, this parameter also plays crucial role in both leptogenesis and DM phenomenology. It should also be noted that the Yukawa coupling h_{ik} is a 3×2 matrix in flavour basis due to the existence of only two right handed neutrinos appearing in light neutrino mass. This predicts a vanishing lightest neutrino mass.

In order to ensure that the choice of Yukawa couplings as well as other parameters involved in light neutrino mass formula discussed above are consistent with the cosmological upper bound on the sum of neutrino masses, $\sum_i m_i \leq 0.11$ eV [3], as well as the neutrino

oscillation data [134, 135], it is often useful to rewrite the neutrino mass formula given in Eq.(3.5) in a form similar to the well known the type-I seesaw formula:

$$M_\nu \;=\; h\Lambda^{-1}h^T\,, \tag{3.7}$$

where we have introduced the diagonal matrix Λ with elements

$$\Lambda_\alpha \;=\; \frac{2\pi^2}{\lambda_5}\zeta_\alpha\frac{2M_\alpha}{v^2}\,, \tag{3.8}$$

$$\text{and}\quad \zeta_\alpha \;=\; \left(\frac{M_\alpha^2}{8(m_{\eta_R}^2-m_{\eta_I}^2)}\left[L_\alpha(m_{\eta_R}^2)-L_\alpha(m_{\eta_I}^2)\right]\right)^{-1}\,. \tag{3.9}$$

The light neutrino mass matrix (3.7) which is complex symmetric by virtue of Majorana nature, can be diagonalised by the usual Pontecorvo-Maki-Nakagawa-Sakata (PMNS) mixing matrix U (in the diagonal charged lepton basis), written in terms of neutrino oscillation data (up to the Majorana phases) as

$$U=\begin{pmatrix} c_{12}c_{13} & s_{12}c_{13} & s_{13}e^{-i\delta} \\ -s_{12}c_{23}-c_{12}s_{23}s_{13}e^{i\delta} & c_{12}c_{23}-s_{12}s_{23}s_{13}e^{i\delta} & s_{23}c_{13} \\ s_{12}s_{23}-c_{12}c_{23}s_{13}e^{i\delta} & -c_{12}s_{23}-s_{12}c_{23}s_{13}e^{i\delta} & c_{23}c_{13}\end{pmatrix}U_{\rm Maj} \tag{3.10}$$

where $c_{ij}=\cos\theta_{ij}$, $s_{ij}=\sin\theta_{ij}$ and δ is the leptonic Dirac CP phase. The diagonal matrix $U_{\rm Maj}={\rm diag}(1,e^{i\alpha},e^{i(\zeta+\delta)})$ contains the undetermined Majorana CP phases α,ζ. The diagonal light neutrino mass matrix is therefore,

$$D_\nu \;=\; U^\dagger M_\nu U^* \;=\; {\rm diag}(m_1,m_2,m_3)\,. \tag{3.11}$$

where the light neutrino masses can follow either normal ordering (NO) or inverted ordering (IO). As mentioned earlier, the model predicts a vanishing lightest neutrino mass implying $m_1=0$ (NO) and $m_3=0$ (IO). Since the inputs from neutrino oscillation data are only in terms of the two mass squared differences and three mixing angles, it would be useful for our purpose to express the Yukawa couplings (h) in terms of light neutrino parameters. This is possible through the Casas-Ibarra (CI) parametrisation [65] extended to radiative seesaw model [114] which allows us to write the Yukawa coupling matrix satisfying the neutrino data as

$$h_{i\alpha} \;=\; \left(UD_\nu^{1/2}R^\dagger\Lambda^{1/2}\right)_{i\alpha}\,, \tag{3.12}$$

where R is an arbitrary complex orthogonal matrix satisfying $RR^T=\mathbb{1}$. It is worth mentioning that, since we have only two right handed neutrinos $N_{1,2}$ taking part in generating radiative light neutrino masses, the lightest neutrino mass is vanishing. Also, in case of only two right handed neutrinos, the R matrix is a function of only one complex rotation parameter $z=z_R+iz_I, z_R\in[0,2\pi], z_I\in\mathbb{R}$ [178] which can affect the results of leptogenesis as we discuss below.

3.1.1 Constraints on Model Parameters

Precision measurements at LEP experiment forbids additional decay channels of the SM gauge bosons. For example, it strongly constrains the decay channel $Z \to \eta_R \eta_I$ requiring $m_{\eta_R} + m_{\eta_I} > m_Z$. Additionally, LEP precision data also rule out the region $m_{\eta_R} < 80$ GeV, $m_{\eta_I} < 100$ GeV, $m_{\eta_I} - m_{\eta_R} > 8$GeV [179]. We take the lower bound on charged scalar mass $m_{\eta^\pm} > 90$ GeV. If $m_{\eta_R,\eta_I} < m_h/2$, the large hadron collider (LHC) bound on invisible Higgs decay comes into play. The constraint on the Higgs invisible decay branching fraction from the ATLAS experiment at LHC is [180]

$$\mathcal{B}(h \to \text{Invisible}) = \frac{\Gamma(h \to \text{Invisible})}{\Gamma(h \to SM) + \Gamma(h \to \text{Invisible})} \leq 26\% \tag{3.13}$$

while the recent ATLAS announcement [181] puts a more stringent constraint at 13%. This can constrain the SM Higgs coupling with η_R, η_I, S namely $\lambda_3 + \lambda_4 \pm \lambda_5, \lambda_6$ respectively to be smaller than around 10^{-3} in the regime $m_{\eta_R}, m_{\eta_I}, m_S < m_h/2$ which however remains weaker than DM direct detection bounds in this mass regime (see for example, [182]).

Additionally, the LHC experiment can also put bounds on the scalar masses in the model, specially the components of scalar doublet η as they can be pair produced copiously in proton proton collisions leading to different final states which are being searched for. Depending upon the mass spectrum of its components, the heavier ones can decay into the lighter ones and a gauge boson, which finally decays into a pair of leptons or quarks. Therefore, we can have either pure leptonic final states plus missing transverse energy (MET), hadronic final states plus MET or a mixture of both. The MET corresponds to DM or light neutrinos. In several earlier works [127, 183, 184], the possibility of opposite sign dileptons plus MET was discussed. In [185], the possibility of dijet plus MET was investigated with the finding that inert scalar masses up to 400 GeV can be probed at high luminosity LHC. In another work [186], tri-lepton plus MET final states was also discussed whereas mono-jet signatures have been studied by the authors of [187, 188]. The enhancement in dilepton plus MET signal in the presence of additional vector like singlet charged leptons was also discussed in [189]. Exotic signatures like displaced vertex and disappearing or long-lived charged track for compressed mass spectrum of inert scalars and singlet fermion DM was studied recently by the authors of [138].

In addition to the collider or direct search constraints, there exists theoretical constraints also. For instance, the scalar potential of the model should be bounded from below in any field direction. This criteria leads to the following co-positivity conditions [190–192]:

$$\begin{aligned}
&\lambda_{1,2,S} \geq 0,\ \ \lambda_3 + \sqrt{\lambda_1 \lambda_2} \geq 0, \\
&\lambda_3 + \lambda_4 - |\lambda_3| + \sqrt{\lambda_1 \lambda_2} \geq 0,\ \ \lambda_6 + 2\sqrt{\lambda_1 \lambda_S} \geq 0, \\
&\sqrt{\lambda_1 \lambda_2 \lambda_S} + 2(\lambda_3 \sqrt{\lambda_S} + \lambda_7 \sqrt{\lambda_1} + \frac{\lambda_6}{2}\sqrt{\lambda_2}) \\
&+ 4\sqrt{\frac{1}{2}(\lambda_3 + \frac{1}{2}\sqrt{\lambda_1 \lambda_2})(\lambda_6 + \sqrt{\lambda_1 \lambda_S})(\lambda_7 + \frac{1}{2}\sqrt{\lambda_2 \lambda_6})} \geq 0.
\end{aligned} \tag{3.14}$$

The coupling constants appeared in above expressions are evaluated at the electroweak scale, v. Also, in order to avoid perturbative breakdown, all dimensionless couplings like quartic

couplings (λ_i, λ_S), Yukawa couplings $(Y_{ij}, h_{i\alpha}, y_i)$, gauge couplings (g_i) should obey the perturbativity conditions:

$$|\lambda_{1,2,3,4,5,6,7}| < 4\pi,\ |\lambda_S| < 4\pi,\ |Y_{u,d,e}, h_{ij}, y_{1,2}| < \sqrt{4\pi},\ |g_s, g, g'| < \sqrt{4\pi} \tag{3.15}$$

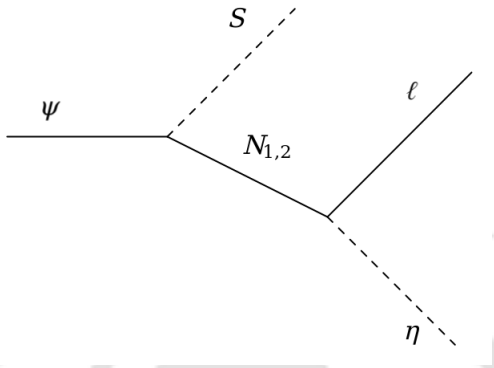

Figure 3.1: Three-body decay of singlet fermion ψ.

3.2 Leptogenesis

In this section, we discuss the details of a new way of generating lepton asymmetry at low scale in our model. Note that, similar to the minimal scotogenic model, here also there are two different ways of generating lepton asymmetry: out of equilibrium decay of the N_i [113, 123, 139–143, 175–177] or annihilation/scattering of dark sector particles [193, 194]. In [123, 141], the authors considered a hierarchical right handed neutrino spectrum to show that successful leptogenesis from two-body decay can occur at a scale as low as a few tens of TeV. Leptogenesis with quasi-degenerate right handed neutrinos in scotogenic model was discussed in [139, 140]. In more recent works [113, 143], successful leptogenesis was shown to be possible at a scale as low as 10 TeV even with hierarchical right handed neutrinos while requiring to be in a weak washout regime predicting a vanishingly small lightest neutrino mass. If leptogenesis occurs only from two heavy neutrinos, then the scale of leptogenesis is pushed above the TeV scale by a few order of magnitudes [175]. This will correspond to our scenario if we do not have ψ, S in our model. To summarise, it has been shown in the above mentioned works that the scale of leptogenesis in scotogenic model can be as low as a few TeV without requiring any resonance enhancement arising due to tiny mass splitting of right handed neutrinos. This significant improvement over the usual Davidson-Ibarra bound on the scale of leptogenesis $M_N > 10^9$ GeV for vanilla leptogenesis in type-I seesaw framework [64] makes the scotogenic model a very attractive and testable framework for leptogenesis. We also note that high scale leptogenesis in scotogenic model was also studied recently by the authors of [195].

In addition to the usual $1 \to 2$ decay or $2 \to 2$ annihilations as sources of lepton asymmetry, we can also have $1 \to 3$ decay in our model. Such three-body decay as a source of lepton asymmetry was discussed earlier by several authors [160–163] in the different contexts like radiative seesaw models, R parity violating supersymmetry and so on. Our present

work is motivated two features namely, (i) dark matter particles assist in such three-body decay processes and (ii) non-zero lepton asymmetry can be generated due to interference of three-body decay diagrams with two different resummed propagators. We show that for our chosen regime of parameter space, such three-body decay leptogenesis can be dominant over other possible sources of leptogenesis and the scale of leptogenesis can be lower than what was found by considering two-body decay or annihilation processes discussed in earlier works.

In our model, we consider the three-body decay of singlet fermion ψ as the origin of CP asymmetry through the process shown in Fig.3.1[1]. To prevent the two-body decay of ψ into N_i, S we impose the kinematical constraint $m_\psi < M_\alpha + m_S$. The relevant decay processes that can generate Lepton asymmetry are $\psi \longrightarrow Sl\eta$ and $N_1 \longrightarrow \eta l$. Although N_2 decay can also generate lepton asymmetry in principle, we consider the asymmetry generated by N_2 decay or any pre-existing asymmetry to be negligible due to strong washout effects mediated either by N_1 or N_2 themselves, to be discussed below. The corresponding CP asymmetry parameters are defined as

$$\epsilon_\psi = \frac{\Gamma_{\psi\longrightarrow Sl_i\eta} - \Gamma_{\psi\longrightarrow S\bar{l}_i\eta^*}}{\Gamma_{\psi\longrightarrow Sl_i\eta} + \Gamma_{\psi\longrightarrow S\bar{l}_i\eta^*}},\ \epsilon_{(N_1)_i} = \frac{\Gamma_{N_1\longrightarrow l_i\eta} - \Gamma_{N_1\longrightarrow \bar{l}_i\eta^*}}{\Gamma_{N_1\longrightarrow l_i\eta} + \Gamma_{N_1\longrightarrow \bar{l}_i\eta^*}} \tag{3.16}$$

The details of these CP asymmetry parameters are given in appendix B.1 and B.2 respectively. Appendix B.1.1 contains the details of one-loop calculation for resummed propagator in such three-body decay, together with the usual tree plus one-loop level interference, giving rise to the same results. In the unflavoured regime, we sum over lepton flavours i to obtain the net CP symmetries $\epsilon_\psi, \epsilon_{N_1}$ which will be used in the Boltzmann equations. Since we are considering sum over all lepton flavours, we are not going to show the flavour index explicitly in the following discussions.

Along with these two decay processes contributing to the creation of lepton asymmetry, there are washout processes too which tend to destroy the asymmetry created. The relevant washout processes in our model can be categorised as

- Inverse decays: $\ell\eta \longrightarrow N_1, \ell\eta S \longrightarrow \psi$
- $\Delta L = 1$ scatterings: $S\ell \longrightarrow \psi\eta$, $\ell\eta \longrightarrow \psi S$, $\psi\ell \longrightarrow S\eta$, $\ell\eta \longrightarrow N_1(W^\pm, Z)$.
- $\Delta L = 2$ scatterings: $\ell\ell \longrightarrow N_1N_1$, $ll \longrightarrow \eta\eta$, $\eta\ell \longrightarrow \eta^*\bar{\ell}$.

The Boltzmann equations relevant for leptogenesis in this model can be summarised as

$$\begin{aligned}\frac{dn_\psi}{dz} &= -D_\psi(n_\psi - n_\psi^{\rm eq}) + D_{N_1\longrightarrow\psi S}(n_{\rm N_1} - n_{\rm N_1}^{\rm eq}) - W_{ID_{N_1\longrightarrow\psi S}} n_\psi \\ &\quad - \frac{s}{\mathbf{H}(z)z}[(n_\psi n_\eta - n_\psi^{\rm eq} n_\eta^{\rm eq})\langle\sigma v\rangle_{\psi\eta\longrightarrow Sl} + [n_\psi n_S - n_\psi^{\rm eq} n_S^{\rm eq}]\langle\sigma v\rangle_{\psi S\longrightarrow l\eta}],\end{aligned} \tag{3.17}$$

[1]In the absence of this process, the source of leptogenesis will be from decay of $N_{1,2}$ only and it was shown earlier that in such two right handed neutrino limit of scotogenic model, the scale of leptogenesis is pushed towards higher side [175].

$$\frac{dn_{\rm N_1}}{dz} = -D_{N_1}(n_{\rm N_1} - n_{\rm N_1}^{\rm eq}) - D_{N_1\longrightarrow\psi S}(n_{\rm N_1} - n_{\rm N_1}^{\rm eq}) - \frac{s}{\mathbf{H}(z)z}[(n_{\rm N_1}^2 - (n_{\rm N_1}^{\rm eq})^2)\langle\sigma v\rangle_{N_1N_1\longrightarrow ll} + [n_{\rm N_1}n_{SM} - n_{\rm N_1}^{\rm eq}n_{SM}^{\rm eq}]\langle\sigma v\rangle_{\eta l\longrightarrow N_1(W^\pm,Z)}], \tag{3.18}$$

$$\frac{dn_{\rm B-L}}{dz} = -\epsilon_\psi D_\psi(n_\psi - n_\psi^{\rm eq}) - \epsilon_{\rm N_1}D_{N_1}(n_{\rm N_1} - n_{\rm N_1}^{\rm eq}) - (W_{N_1} + W_\psi)n_{\rm B-L} - \frac{s}{\mathbf{H}(z)z}[\Gamma_{Sl\longrightarrow\psi\eta} + \Gamma_{l\eta\longrightarrow\psi S} + \Gamma_{ll\longrightarrow\eta\eta} + \Gamma_{ll\longrightarrow N_1N_1} + \Gamma_{l\eta\longrightarrow(N_1W^\pm,Z)} + \Gamma_{\eta l\longrightarrow\eta^*\bar{l}}]n_{\rm B-L}. \tag{3.19}$$

In the above equations $z = \dfrac{m_\psi}{T}$ and $n_f^{\rm eq} = \frac{z^2}{2}\kappa_2(z)$ is the equilibrium number density of $f \equiv N_1, \psi$ (with $\kappa_i(z)$ being the modified Bessel function of i-th kind). n_{N_1}, n_ψ and $n_{\rm B-L}$ are the comoving number density of N_1, n_ψ and $B-L$ asymmetry respectively. The quantity D_f on the right hand side of above equations is

$$D_{N_1} = K_{N_1}z\left(\frac{M_1}{m_\psi}\right)\frac{\kappa_1\left[z\left(\frac{M_1}{m_\psi}\right)\right]}{\kappa_2\left[z\left(\frac{M_1}{m_\psi}\right)\right]},$$

$$D_\psi = K_\psi z\frac{\kappa_1(z)}{\kappa_2(z)},\ D_{N_1\longrightarrow\psi S} = K_{N_1\longrightarrow\psi S}z\left(\frac{M_1}{m_\psi}\right)\frac{\kappa_1\left[z\left(\frac{M_1}{m_\psi}\right)\right]}{\kappa_2\left[z\left(\frac{M_1}{m_\psi}\right)\right]}. \tag{3.20}$$

Here, the decay parameters are defined as

$$K_{N_1} = \frac{\Gamma_{N_1\longrightarrow l\eta}}{\mathbf{H}(m_\psi)},\ K_\psi = \frac{\Gamma_{\psi\longrightarrow Sl\eta}}{\mathbf{H}(m_\psi)},\ K_{N_1\longrightarrow\psi S} = \frac{\Gamma_{N_1\longrightarrow\psi S}}{\mathbf{H}(m_\psi)} \tag{3.21}$$

with Γ_f is the partial decay width of particle f for the specified decay process, $\mathbf{H}$ is the Hubble parameter. Since leptogenesis is a high scale phenomena and occurs in the radiation dominated phase of the universe, the Hubble parameter can be expressed in terms of the temperature T as follows

$$\mathbf{H} = \sqrt{\frac{8\pi^3 g_*}{90}}\frac{T^2}{M_{\rm Pl}} = \mathbf{H}(z=1)\frac{1}{z^2} \tag{3.22}$$

where g_* is the effective number of relativistic degrees of freedom and $M_{\rm Pl} \simeq 1.22\times10^{19}$ GeV is the Planck mass. The washout terms are given as

$$\begin{aligned} W_{N_1} &= \frac{1}{4}z^3\left(\frac{M_1}{m_\psi}\right)^2 K_{N_1}\kappa_1\left[z\frac{M_1}{m_\psi}\right],\ W_\psi = \frac{1}{4}z^3K_\psi\kappa_1(z), \\ W_{N_1\longrightarrow\psi S} &= \frac{1}{4}z\frac{\kappa_1\left[z\frac{M_1}{m_\psi}\right]}{\kappa_2\left[z\frac{M_1}{m_\psi}\right]}K_{N_1\longrightarrow\psi S}\frac{n_{\rm N_1}^{\rm eq}}{n_\psi^{\rm eq}}, \end{aligned} \tag{3.23}$$

The decay process $N_1 \longrightarrow \psi S$ does not contribute to the CP asymmetry but can affect the abundance of ψ, N_1 as can be seen from the Boltzmann equations written above. The decay width for the decay $N_1 \longrightarrow \psi S$ is given by

$$\Gamma_{N_1 \longrightarrow \psi S} = \frac{1}{16\pi M_1^3}\sqrt{M_1^4 + m_\psi^4 + m_S^4 - 2M_1^2 m_\psi^2 - 2m_\psi^2 m_S^2}\{(M_1^2 + m_\psi^2 - m_S^2)|y_1|^2 - 2\mathrm{Re}[y_1^2] m_\psi M_1\}. \tag{3.24}$$

As mentioned earlier, we use the Casas-Ibarra parametrisation to rewrite the Yukawa coupling h_{ij} in terms of light neutrino parameters. Also, in the case of two right handed neutrinos taking part in generating light neutrino masses in our model, the complex orthogonal matrix R is a function of only one rotation parameter $z = z_R + iz_I, z_R \in [0, 2\pi], z_I \in \mathbb{R}$ [65, 178]. Our choice of R matrix is

$$R = \begin{pmatrix} 0 & \cos(z_R + iz_I) & \sin(z_R + iz_I) \\ 0 & -\sin(z_R + iz_I) & \cos(z_R + iz_I) \end{pmatrix} \tag{3.25}$$

Then the Yukawa matrix for normal ordering of light neutrino masses can then be explicitly written as

$$h = \begin{pmatrix} \sqrt{m_2}\sqrt{\Lambda_1}\cos(z)U_{12} + \sqrt{m_3}\sqrt{\Lambda_1}\sin(z)U_{13} & -\sqrt{m_2}\sqrt{\Lambda_2}\sin(z)U_{12} + \sqrt{m_3}\sqrt{\Lambda_2}\cos(z)U_{13} \\ \sqrt{m_2}\sqrt{\Lambda_1}\cos(z)U_{22} + \sqrt{m_3}\sqrt{\Lambda_1}\sin(z)U_{23} & -\sqrt{m_2}\sqrt{\Lambda_2}\sin(z)U_{22} + \sqrt{m_3}\sqrt{\Lambda_2}\cos(z)U_{23} \\ \sqrt{m_2}\sqrt{\Lambda_1}\cos(z)U_{32} + \sqrt{m_3}\sqrt{\Lambda_1}\sin(z)U_{33} & -\sqrt{m_2}\sqrt{\Lambda_2}\sin(z)U_{32} + \sqrt{m_3}\sqrt{\Lambda_2}\cos(z)U_{33}. \end{pmatrix} \tag{3.26}$$

with U_{ij} being the elements of the PMNS mixing matrix mentioned earlier. The other Yukawa coupling which affects lepton asymmetry namely, y_i is not related to the origin of light neutrino mass and hence we keep it as a free parameter. The choice of this Yukawa coupling affect both leptogenesis and dark matter as we discuss in upcoming sections.

After obtaining the numerical solutions of the above Boltzmann Eqs.(3.17), (3.18) and (3.19), we convert the final $B-L$ asymmetry $n^f_{\mathrm{B-L}}$ just before electroweak sphaleron freeze-out into the observed baryon to photon ratio by the standard formula

$$\eta_B \;=\; \frac{3}{4}\frac{g^0_*}{g_*} a_{\mathrm{sph}} n^f_{\mathrm{B-L}} \;\simeq\; 9.2 \times 10^{-3}\, n^f_{\mathrm{B-L}}\,, \tag{3.27}$$

where $a_{\mathrm{sph}} = \frac{8}{23}$ is the sphaleron conversion factor (taking into account two Higgs doublets). We take the effective relativistic degrees of freedom to be $g_* = 111.75$, slightly higher than that of the SM at such temperatures as we are including the contribution of the inert doublet as well as the scalar singlet too. The heavy singlet fermions $N_{1,2}, \psi$ do not contribute as they have already decoupled from the bath by this epoch. In the above expression $g^0_* = \frac{43}{11}$ is the effective relativistic degrees of freedom at the recombination epoch.

3.3 Dark Matter

As mentioned earlier, our model has two DM candidates both of which are stable due to the unbroken $Z_2 \times Z_2'$ symmetry. Although a two component DM was not part of the original

motivation, it emerged naturally due to the chosen charge assignments of different particles namely, η, S, ψ, N_i under $Z_2 \times Z_2'$ symmetry. In fact, the introduction of the second Z_2 symmetry, necessary to forbid direct coupling of ψ with SM leptons, has given rise to the second DM component in the model. A very recent study on such two component DM with scalar doublet and scalar singlet can be found in [196]. For some earlier works on multi-component dark matter, please refer to [173, 174, 182, 194, 197–213, 213–228] and references therein.

Relic abundance of two component DM in our model η_R, S can be found by numerically solving the corresponding Boltzmann equations. Let $n_1 = n_{\eta_R}$ and $n_2 = n_S$ are the total number densities of two dark matter candidates respectively. The two coupled Boltzmann equations in terms of n_2 and n_1 are given below [173],

$$\frac{dn_1}{dt} + 3n_1\mathbf{H} = -\langle\sigma \mathrm{v}_{\eta_R\eta_R\to X\bar{X}}\rangle\left(n_1^2 - (n_1^{\mathrm{eq}})^2\right) - \langle\sigma \mathrm{v}_{\eta_R\eta_R\to SS}\rangle\left(n_1^2 - \frac{(n_1^{\mathrm{eq}})^2}{(n_2^{\mathrm{eq}})^2}n_2^2\right), \quad (3.28)$$

$$\frac{dn_2}{dt} + 3n_2\mathbf{H} = -\langle\sigma \mathrm{v}_{SS\to X\bar{X}}\rangle\left(n_2^2 - (n_2^{\mathrm{eq}})^2\right) + \langle\sigma \mathrm{v}_{\eta_R\eta_R\to SS}\rangle\left(n_1^2 - \frac{(n_1^{\mathrm{eq}})^2}{(n_2^{\mathrm{eq}})^2}n_2^2\right), \quad (3.29)$$

where, n_i^{eq} is the equilibrium number density of dark matter species i and $\mathbf{H}$ denotes the Hubble parameter, defined earlier. In the annihilation processes, X denotes all particles where DM can annihilate into. In the above equations, $\langle\sigma v\rangle$ is the thermally averaged annihilation cross section, given by [136]

$$\langle\sigma v\rangle_{\mathrm{DMDM}\to\mathrm{X\bar{X}}} = \frac{1}{8m_{\mathrm{DM}}^4 T\kappa_2^2\left(\frac{m_{\mathrm{DM}}}{T}\right)}\int_{4m_{\mathrm{DM}}^2}^{\infty}\sigma(s-4m_{\mathrm{DM}}^2)\sqrt{s}\,\kappa_1\left(\frac{\sqrt{s}}{T}\right)ds\,, \quad (3.30)$$

where $\kappa_i(x)$'s are modified Bessel functions of order i mentioned before. The annihilation processes of scalar singlet scalar doublet are shown in Fig.3.2 and 3.3 respectively. While for scalar singlet DM alone, there is no coannihilation processes, scalar doublet dark matter in scotogenic model can have several coannihilation processes, either with the heavier components of the doublet or fermions as shown in Fig.3.3. Such coannihilation effects within the framework of inert doublet model as well as scotogenic model have already been studied in details by several authors [115, 118–131, 229]. In the presence of coannihilations, one follows the recipe given by [137] to calculate the relic abundance. Since scalar singlet DM has just one component, there is no such coannihilations present. Similar to the inert doublet dark matter model, scalar singlet dark matter has also been studied extensively by several authors [230–234].

The second terms on the right hand side of the above Boltzmann equations specifically consider the conversions between two DM candidates η_R, S while assuming the former to be the heavier DM component. Such a conversion can occur either directly due to the λ_6 coupling of the scalar potential given in Eq.(3.2) or via SM Higgs portal interactions. These conversion processes are shown in Fig.3.4. There can be another conversion process due to the interactions shown in the Feynman diagram of Fig.3.1. This can occur due to coannihilation processes, not shown in above Boltzmann equations. In our model, however, singlet scalar DM can, in principle, coannihilate with other particles involved in the same

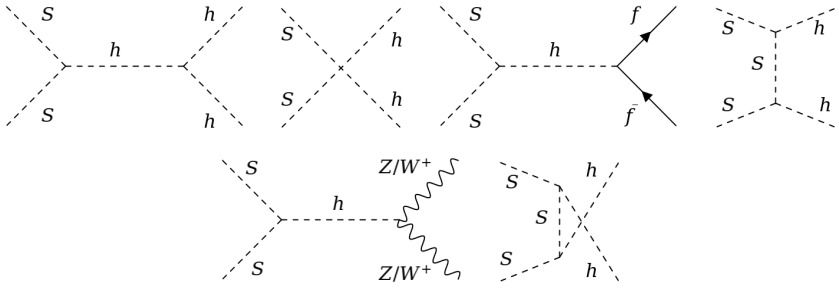

Figure 3.2: Feynman diagrams for relevant annihilation processes for singlet scalar DM.

Feynman diagram of Fig.3.1. Since the two DM candidates are stabilised by two separate Z_2 symmetries, their coannihilation can only led to ψ which is odd under both the Z_2 symmetries. Alternatively, one of the DM can also coannihilate with ψ and convert into the other DM. These processes are shown in Fig.3.4. Since we consider ψ to be heavier than both the DM candidates, we do not show it in the final states.

In order to cover all the features of annihilations, coannihilations as well as conversions, we use `micrOMEGAs` [235] to calculate the relic abundance of two component DM in our model. The model information has been supplied to `micrOMEGAs` using `FeynRules` [236] while all the relevant annihilation and coannihilation cross sections of dark matter number changing processes required to solve the coupled equations are calculated using `CaLCHEP` [237]. While singlet scalar DM annihilates either through four point scalar interactions or SM Higgs mediated processes, the scalar doublet DM can annihilate (coannihilate) via Higgs as well as electroweak gauge boson portals apart from the four point interactions with Higgs as well as gauge bosons. Additionally, the conversion coupling λ_6 as well as Yukawa coupling y_i can play significant role in individual as well as total DM relic densities.

Just like the SM Higgs boson mediates DM annihilation into SM particles, similarly, it can also mediate spin independent DM-nucleon scatterings. Different ongoing experiments like Xenon1T [89,90], LUX [87], PandaX-II [91,92] are trying to detect the DM in the lab-based experiments and give a strong upper bound on the spin-independent (SI) direct detection (DD) cross-section as a function of DM mass. We have extracted the SI elastic scattering cross-section for both the DM candidates from `micrOMEGAs`. DD analysis for two-component DM is slightly different from the single component scenario. To compare the result of our model with Xenon1T bound, we have multiplied the elastic scattering cross-section by the relative number density of each DM candidate and used the following conditions

$$\begin{aligned}\sigma_1^{\rm eff} &= \frac{\rm n_1}{\rm n_1+n_2}\sigma_1^{\rm SI} \leq \sigma_{\rm Xenon1T}\\ \sigma_2^{\rm eff} &= \frac{\rm n_2}{\rm n_1+n_2}\sigma_2^{\rm SI} \leq \sigma_{\rm Xenon1T}\end{aligned} \tag{3.31}$$

Further details related to the direct detection of multi component DM can be found in [238,239].

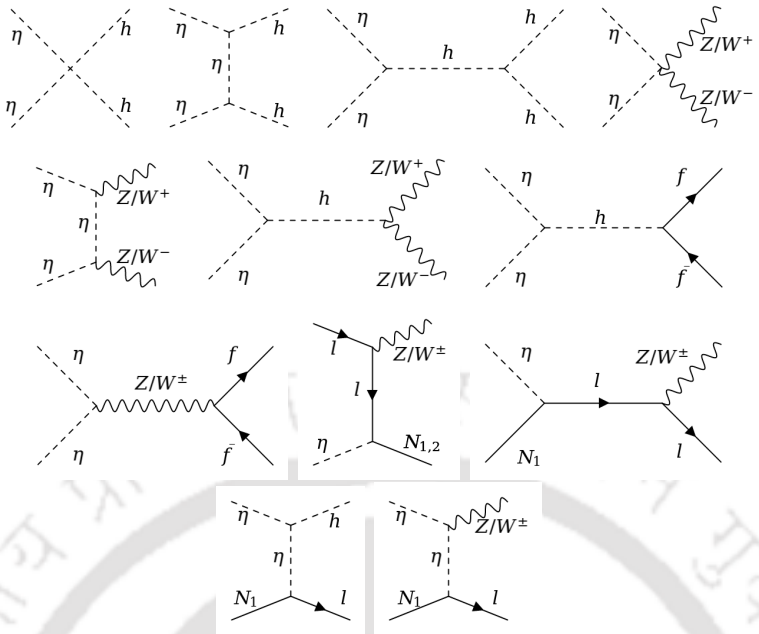

Figure 3.3: Feynman diagrams of all the relevant processes for scalar doublet dark matter in scotogenic model. Here DM is chosen to be the real scalar component of the doublet.

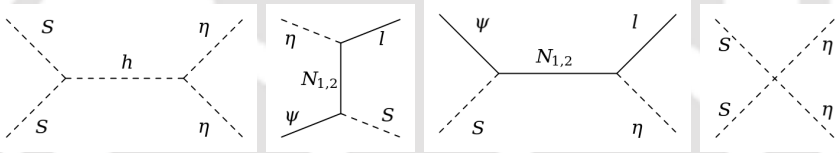

Figure 3.4: Feynman diagrams of all the relevant processes determining the DM relic density which emerged due to the extension of the scotogenic model.

3.4 Results and Discussion

In this section, we discuss our numerical results for leptogenesis as well as dark matter separately.

3.4.1 Leptogenesis

To calculate the lepton asymmetry, we first solve the coupled Boltzmann Eqs.(3.17), (3.18) and (3.19) numerically to estimate the final B-L asymmetry. We considered two possible ranges for N_1 mass M_1.

In the first case we have chosen a benchmark as $M_1 = 2 \times 10^5$ GeV and in the other case we choose $M_1 = 2 \times 10^7$ GeV while keeping $M_2 = 10M_1$ and other parameters fixed for both the cases. Using the first choice of benchmark values for M_1 and M_2, in Fig.3.5, the evolution of the comoving number densities of ψ, N_1 and $B - L$ are shown with $z = \dfrac{m_\psi}{T}$ for

different values of λ_5 and $y_{1,2}$. Similarly in Fig.3.6, the second benchmark for RHN masses is chosen and the evolution of the comoving number densities of ψ, N_1 and $B-L$ are shown with $z = \frac{m_\psi}{T}$ for different values of λ_5 and $y_{1,2}$. The parameter λ_5 decides the strength of Dirac Yukawa coupling of neutrinos via Casas-Ibarra parametrisation as (3.12) discussed earlier.

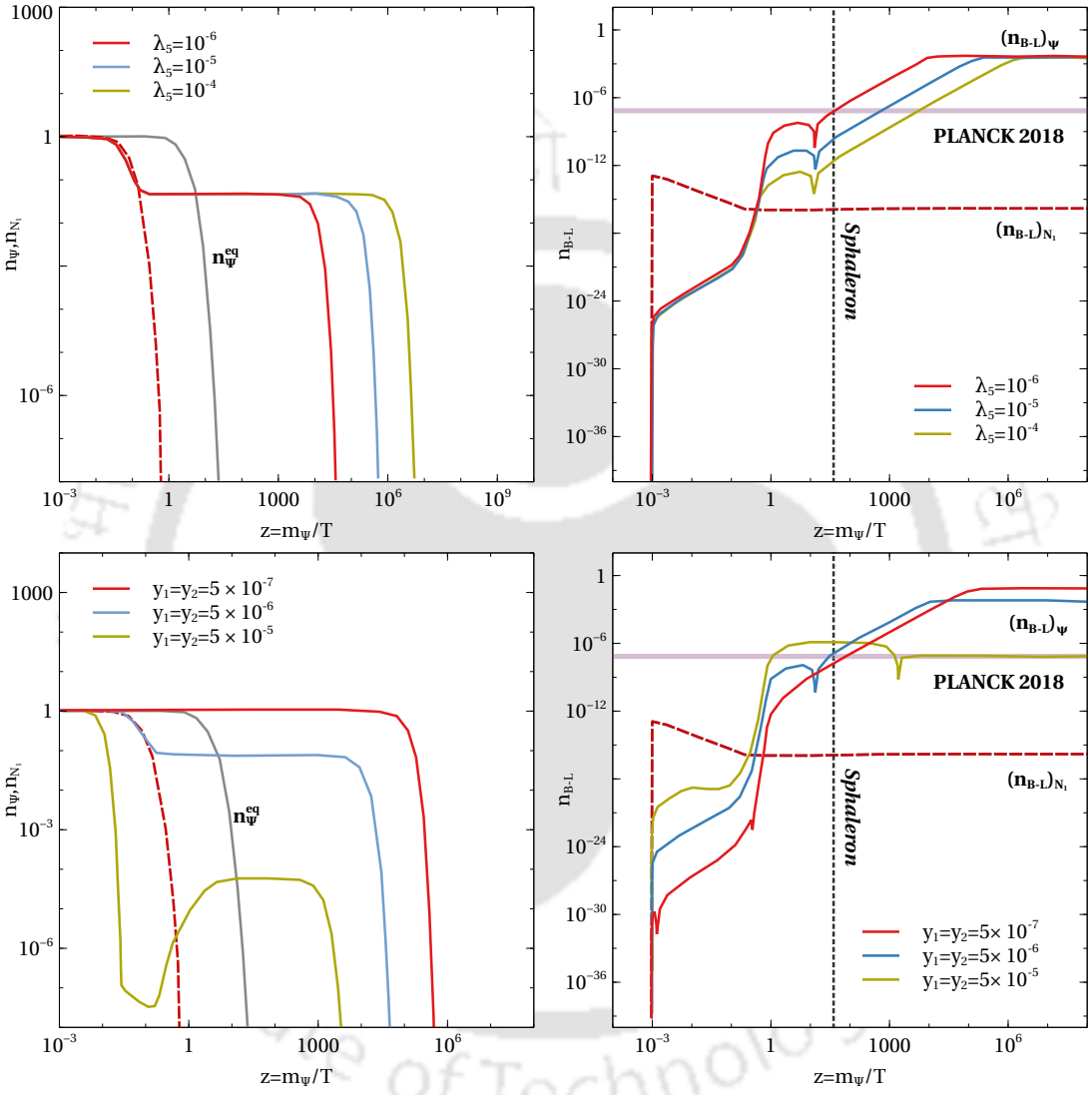

Figure 3.5: Evolution of comoving number densities of ψ and N_1 (left panel) and $B-L$ (right panel) with $z = \frac{m_\psi}{T}$ for different values of λ_5 (upper panel), Yukawa couplings $y_{1,2}$ (lower panel). The other parameters are set at benchmark values: $M_1 = 2\times10^5$ GeV, $M_2 = 2\times10^6$ GeV, $m_\eta = 100$ GeV, $m_S = 500$ GeV, $m_\psi = 5$ TeV and $y_1 = y_2 = 5\times10^{-6}$ (upper panel) and $\lambda_5 = 10^{-6}$ (lower panel).

In the three-body decay width $\Gamma_{\psi\longrightarrow lS\eta}$, apart from Dirac Yukawa couplings of active neutrinos, we also have other Yukawa couplings $y_{1,2}$ which can affect leptogenesis, without affecting neutrino mass. In this section we discuss the effect of these two types of Yukawa

couplings on the asymmetry. In the upper left panel of Fig.3.5 we show the evolution of the comoving number densities of ψ (solid lines) and N_1 (dashed lines) for different benchmark values of λ_5. In the upper right panel of Fig.3.5, we show the evolution of $B-L$ for different λ_5. We have taken both ψ and N_1 to be in equilibrium at very high temperatures and numerically solved the coupled Boltzmann equations up to a temperature when the asymmetry gets saturated.

From the evolution of the comoving number densities of ψ and N_1 we can see that initially both the particles follow their equilibrium number densities but soon after the ψ abundance deviates from its equilibrium abundance while the N_1 abundance remains very close to its equilibrium number density and therefore vanishes shortly after it becomes non-relativistic. It is mainly because N_1 has very strong two-body decays ($N_1 \longrightarrow l\eta$ and $N_1 \longrightarrow \psi S$) and corresponding inverse decays and therefore its abundance remains very close to its equilibrium abundance. On the other hand, ψ has relatively feeble three-body decay $\psi \longrightarrow S\eta l$ and a strong inverse decay $\psi S \longrightarrow N_1$. Because of the strong two-body inverse decay of ψ the abundance of ψ decreases sharply. This inverse decay stops when the temperature drops to a value such that the process $\psi S \longrightarrow N_1$ becomes kinematically forbidden. After this point the ψ abundance gets saturated and goes out of equilibrium before finally decaying through the three-body decay at a low temperature. The effect of this strong inverse decay ($\psi S \longrightarrow N_1$) can also be seen in the asymmetry evolution shown on the right panel plot. The solid lines represent the asymmetry generated from the ψ decay and the dashed line represents the asymmetry generated from the two-body decay of N_1. From asymmetry plots on right panel of Fig.3.5, it can be seen that asymmetry generated from the N_1 decay is very less compared to the one generated from the three-body decay of ψ, which is expected as N_1 remains very close to its equilibrium abundance. Another important point is the asymmetry generated from N_1 gets saturated at a very high temperature as N_1 abundance vanishes when it becomes non-relativistic. However, the asymmetry generated from the ψ decay keep evolving up to a very low temperature because of the small decay width of ψ. Because of the small decay parameter for the decay $\psi \longrightarrow S\eta l$, the inverse decay rate is also very small and we are always in a weak washout regime ($K_\psi \ll 1$). However, the asymmetry generation from the two-body decay of N_1 is always is in strong washout regime as we have only two RHNs (for two RHNs scenarios, $K_{N_1} > 1$) [113, 176]. Because of this, the resultant asymmetry is mainly determined by the three-body decay.

In the upper panel plot of Fig.3.5 it is observed that abundance of ψ become less than its equilibrium abundance because of the inverse decay $\psi \longrightarrow N_1 S$ (while N_1 has strong two-body decays into both ψS and ηl final states) and therefore the asymmetry generated from the ψ decay remains suppressed initially. However, when the inverse decay stops, the ψ abundance saturates and finally the asymmetry becomes overabundant before its decay is complete. When the ψ becomes more compared to its equilibrium abundance then the $B-L$ asymmetry starts rising steadily, as can be seen by comparing left and right panel plots of Fig.3.5. In upper left panel plot of Fig.3.5 we can see that the decay of ψ happens earlier for smaller value of λ_5, which is expected as smaller value of λ_5 led to larger Dirac Yukawa couplings. For the same reason the saturation of asymmetry happens earlier for smaller value values of λ_5, as seen from upper right panel plot. The asymmetry generated up to the sphaleron epoch ($T_{\rm sphaleron} \simeq 131$ GeV, shown by vertical dashed line) is important as the asymmetry generated after the sphaleron freeze-out temperature can not be converted into

a baryon asymmetry. It can be seen from upper right panel plot of Fig.3.5 that for smaller λ_5 the asymmetry generated up to sphaleron temperature is more compared to the ones for larger λ_5. In the lower left panel plot of Fig.3.5 we observe that for larger values of the Yukawa couplings $y_{1,2}$, the effect of the inverse decay $\psi S \longrightarrow N_1$ is more. For larger Yukawa coupling $y_{1,2}$ the ψ abundance decreases sharply because of the very strong inverse decay $\psi S \longrightarrow N_1$ and at later epochs also when its abundance is more compared to equilibrium abundance, smaller Yukawa leads to larger abundance as expected. For the same reason, the $B-L$ asymmetry also increases more sharply for larger Yukawa couplings leading to larger asymmetry at the epoch of sphaleron freeze-out, as seen from the lower right panel plot of Fig.3.5. It should be noted that, we are showing only the absolute value of $B-L$ asymmetry on the right panel plots; in reality, the points towards the left of the dip in solid lines correspond to negative asymmetry. Clearly, for large Yukawa $y_{1,2}$, the asymmetry remains negative even at the sphaleron epoch, as seen from lower right panel plot. Therefore, we can not make Yukawa coupling $y_{1,2}$ arbitrarily large to get more asymmetry at the epoch of shpaleron decoupling.

Similarly, in Fig.3.6 we have shown the evolution ψ, N_1 and $B-L$ number densities with $z = m_\psi/T$ for different values of λ_5 (upper panel) and $y_{1,2}$ (lower panel) but with heavier mediator masses namely, $M_1 = 2\times10^7$ GeV and $M_2 = 10M_1$, keeping other parameters fixed as in Fig.3.5. It can be seen that for the same value of $m_\psi, \lambda_5, m_\eta, m_S$ and $y_{1,2}$ the effect of the inverse decay $\psi S \longrightarrow N_1$ is much less in this case. This is expected as for larger value of N_1 will make the inverse decay $\psi S \longrightarrow N_1$ inefficient even at very high temperatures. The variation of the $B-L$ asymmetry with λ_5 and $y_{1,2}$ can be understood in a way similar to the Fig.3.5 discussed earlier. Also, comparing Fig.3.5 and Fig.3.6 we can see that for the same set of parameters the decay of ψ and generation of asymmetry occur slowly making the asymmetry less in Fig.3.6 than in 3.5 at the epoch of sphaleron decoupling. This is expected as larger $N_{1,2}$ masses make the three-body decay width of ψ smaller due to propagator suppression.

Finally, we perform a numerical scan to find the relevant parameter space in $m_\psi - \lambda_5$ plane that can give rise to the observed baryon asymmetry for both $M_1 = 2\times10^5$ GeV and $M_1 = 2\times10^7$ GeV. While varying these parameters, we keep the masses of other relevant particles to be fixed at $m_S = 500$ GeV, $m_\eta = 100$ GeV. The parameter space in $m_\psi - \lambda_5$ plane for benchmark choices of $y_{1,2}$ is shown in Fig.3.7 for $M_1 = M_2/10 = 2\times10^5$ GeV (left panel) and for $M_1 = M_2/10 = 2\times10^7$ GeV (right panel). In Fig.3.7 we can see that for a benchmark value of $y_{1,2}$ the mass required of ψ become large for larger values of λ_5, which is expected as larger values of λ_5 make the Dirac Yukawa couplings $h_{i\alpha}$ smaller making the three-body decay width of ψ smaller. For similar reason, for a particular value of λ_5, the required mass of ψ for a small Yukawa coupling $y_{1,2}$ is more compared to that for larger Yukawa coupling. However, as mentioned earlier we can not take arbitrarily large values of the new Yukawa couplings $y_{1,2}$ to lower the scale of leptogenesis. As discussed earlier, beyond a certain value of $y_{1,2}$ the inverse decay $\psi S \longrightarrow N_1$ will become so dominant that the asymmetry become negative at the time of sphaleron. We found that for a TeV scale leptogenesis with moderately high $M_{1,2}$ it is safe to take $y_{1,2} \leq 10^{-5}$ such that the asymmetry become positive at the sphaleron freeze-out temperature. From Fig.3.7 we can conclude that successful TeV scale leptogenesis is possible dominantly from the three-body decay for appropriate choice of the model parameters. Also we can see that the scale of

leptogenesis is slightly higher in the right panel plot of 3.7 compared to the left plot of Fig.3.7. This is because with the increases in $M_{1,2}$ the three-body decay width encounters propagator suppression as discussed earlier.

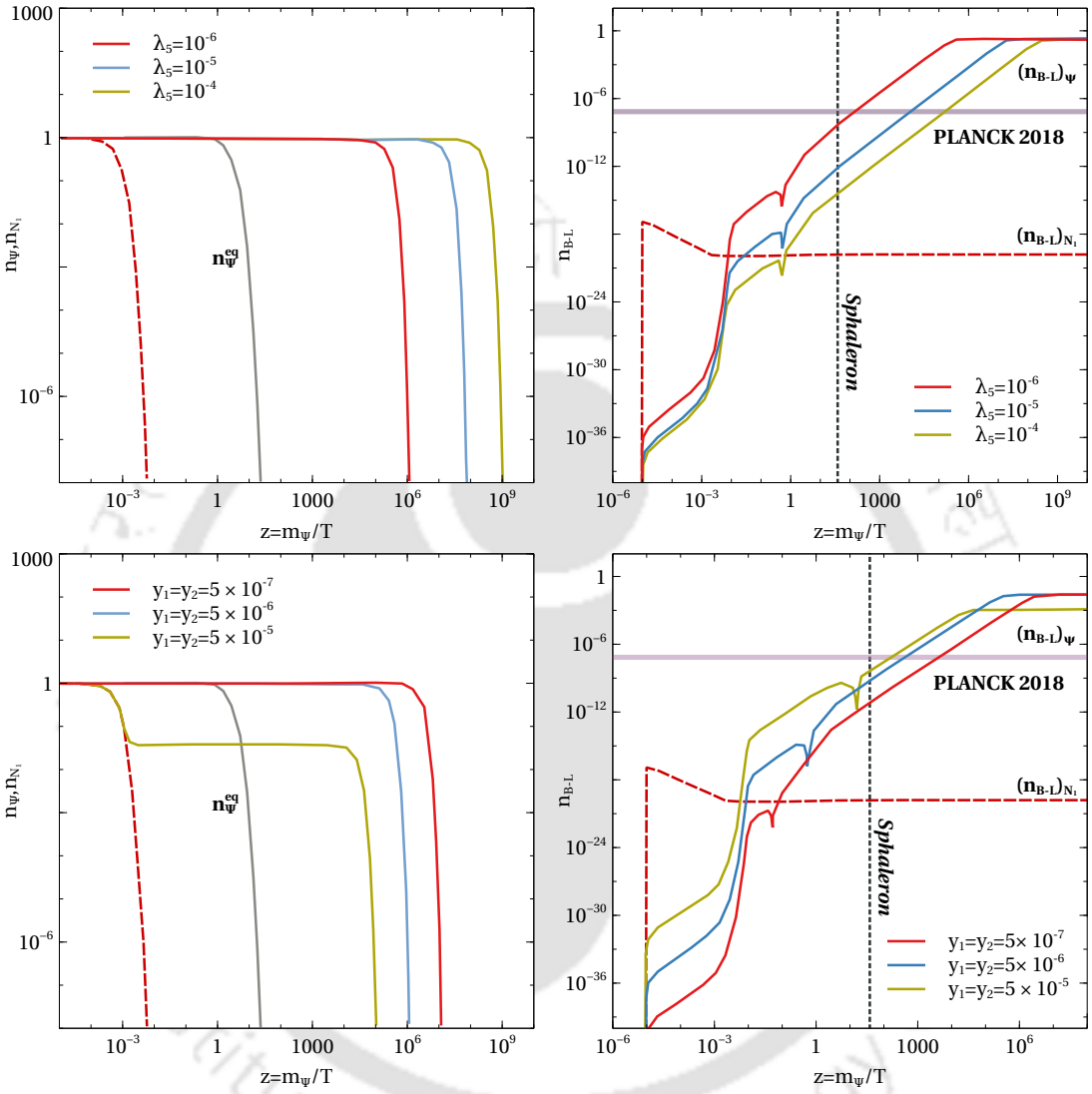

Figure 3.6: Evolution of comoving number densities of ψ and N_1 (left panel) and $B-L$ (right panel) with $z = \dfrac{m_\psi}{T}$ for different values of λ_5 (upper panel), Yukawa couplings $y_{1,2}$ (lower panel). The other parameters are set at benchmark values: $M_1 = 2\times10^7$ GeV, $M_2 = 2\times10^8$ GeV, $m_\eta = 100$ GeV, $m_S = 500$ GeV, $m_\psi = 5$ TeV and $y_1 = y_2 = 5\times10^{-6}$ (upper panel) and $\lambda_5 = 10^{-6}$ (lower panel).

3.4.2 Flavour effects on leptogenesis

It should be noted that while discussing leptogenesis in the above sections, we did not consider the effects of lepton flavours. Since we are considering leptogenesis at low scale,

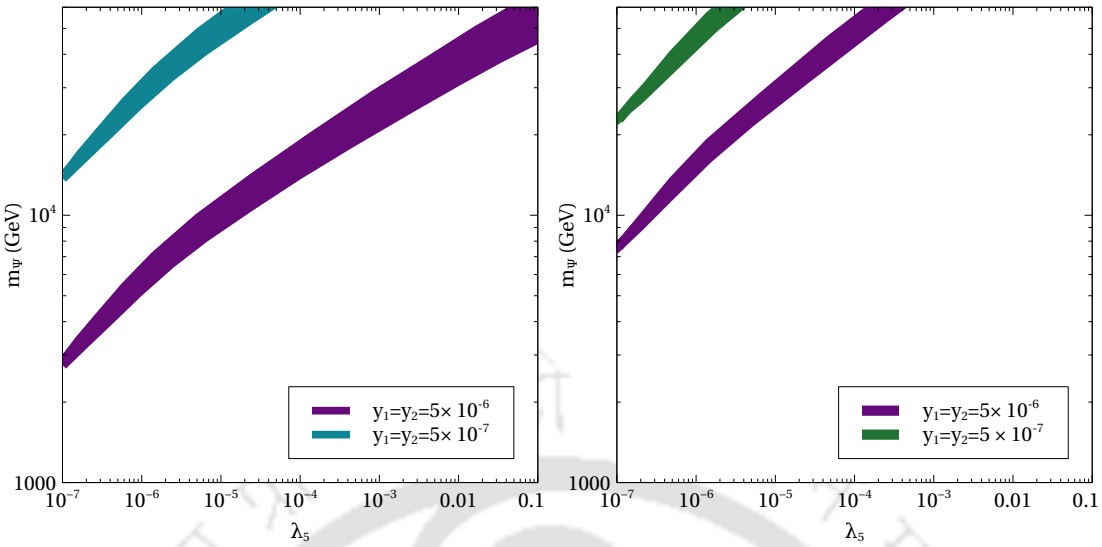

Figure 3.7: The variation of m_ψ with λ_5, required to satisfy the observed asymmetry. For the left panel the $M_1 = 2\times10^5$ GeV, $M_2 = 2\times10^6$ GeV and for the right panel $M_1 = 2\times10^7$ GeV, $M_2 = 2\times10^8$ GeV. The other parameters are set at $m_\eta = 10$ GeV, $m_S = 500$ GeV.

lepton flavour effects may play non-trivial roles as pointed out by several earlier works on flavoured leptogenesis [55–58], also summarised in a recent review article [159]. Adopting the notations of [58], the Boltzmann equations for flavoured leptogenesis can be written as

$$\begin{aligned}\frac{dn_\psi}{dz} &= -D_\psi(n_\psi - n_\psi^{\rm eq}) + D_{N_1\longrightarrow\psi S}(n_{\rm N_1} - n_{\rm N_1}^{\rm eq}) - W_{ID_{N_1}\longrightarrow\psi S}n_\psi \\ &- \frac{s}{\mathbf{H}(z)z}[(n_\psi n_\eta - n_\psi^{\rm eq}n_\eta^{\rm eq})\langle\sigma v\rangle_{\psi\eta\longrightarrow Sl} + (n_\psi n_S - n_\psi^{\rm eq}n_S^{\rm eq})\langle\sigma v\rangle_{\psi S\longrightarrow l\eta} \\ &(n_\psi - n_\psi^{\rm eq})n_l^{\rm eq}\langle\sigma v\rangle_{\psi l\longrightarrow\eta S}],\end{aligned} \tag{3.32}$$

$$\begin{aligned}\frac{dn_{\rm N_1}}{dz} &= -D_{N_1}(n_{\rm N_1} - n_{\rm N_1}^{\rm eq}) - D_{N_1\longrightarrow\psi S}(n_{\rm N_1} - n_{\rm N_1}^{\rm eq}) - \frac{s}{\mathbf{H}(z)z}[(n_{\rm N_1}^2 - (n_{\rm N_1}^{\rm eq})^2)\langle\sigma v\rangle_{N_1N_1\longrightarrow ll} \\ &+ [n_{\rm N_1}n_{SM} - n_{\rm N_1}^{\rm eq}n_{SM}^{\rm eq}]\langle\sigma v\rangle_{\eta l\longrightarrow N_1(W^\pm,Z)}],\end{aligned} \tag{3.33}$$

$$\begin{aligned}\frac{dn_{B/3-L_i}}{dz} &= -\epsilon_{\psi_i}D_\psi(n_\psi - n_\psi^{\rm eq}) - \epsilon_{N_1i}D_{N_1}(n_{\rm N_1} - n_{\rm N_1}^{\rm eq}) - (W_{N_1}P_{1i} + W_{\psi_i}P_{\psi i})n_{(B-L)_i} \\ &- \frac{s}{\mathbf{H}(z)z}[P_{\psi i}\Gamma_{Sl_i\longrightarrow\psi\eta} + P_{\psi i}\Gamma_{l_i\eta\longrightarrow\psi S} + P_{\psi i}\sum_j P_{\psi j}\Gamma_{l_il_j\longrightarrow\eta\eta} + P_{\psi i}\sum_j P_{\psi j}\Gamma_{l_il_j\longrightarrow N_1N_1} + \\ &P_{\psi i}\Gamma_{l_i\eta\longrightarrow(N_1W^\pm,Z)} + P_{\psi i}\sum_j\Gamma_{\eta l_i\longrightarrow\eta^*\bar{l_j}} + P_{\psi i}\Gamma_{\psi l_i\longrightarrow S\eta}]n_{B/3-L_i},\end{aligned} \tag{3.34}$$

where the projectors $P_{\psi i}$ and P_{1i} are defined, respectively, as

$$P_{\psi i} = \frac{\Gamma_{\psi\longrightarrow S\eta l_i}}{\sum_j\Gamma_{\psi\longrightarrow S\eta l_j}}, \tag{3.35}$$

$$P_{1i} = \frac{\Gamma_{N_1 \longrightarrow l_i \eta}}{\sum_j \Gamma_{N_1 \longrightarrow l_j \eta}}. \tag{3.36}$$

In the projectors, the denominator indicates the total decay width of ψ, N_1 whereas the numerators correspond to partial decay width into a particular lepton flavour. The washout terms remain same as before. We fix the benchmarks same as the ones used in scanning the parameter space of unflavoured leptogenesis. The resulting parameter space in $m_\psi - \lambda_5$ plane for both the cases are shown in Fig.3.8. Comparing with scan plots for unflavoured leptogenesis shown in Fig.3.7 , it is seen that the scale of leptogenesis can be be lowered after inclusion of lepton flavour effects, as expected. Thus, successful leptogenesis can occur at a scale just above 1 TeV for $M_1 = 2 \times 10^5$ GeV and can be as low as approximately 5 TeV for case $M_1 = 2 \times 10^7$ GeV.

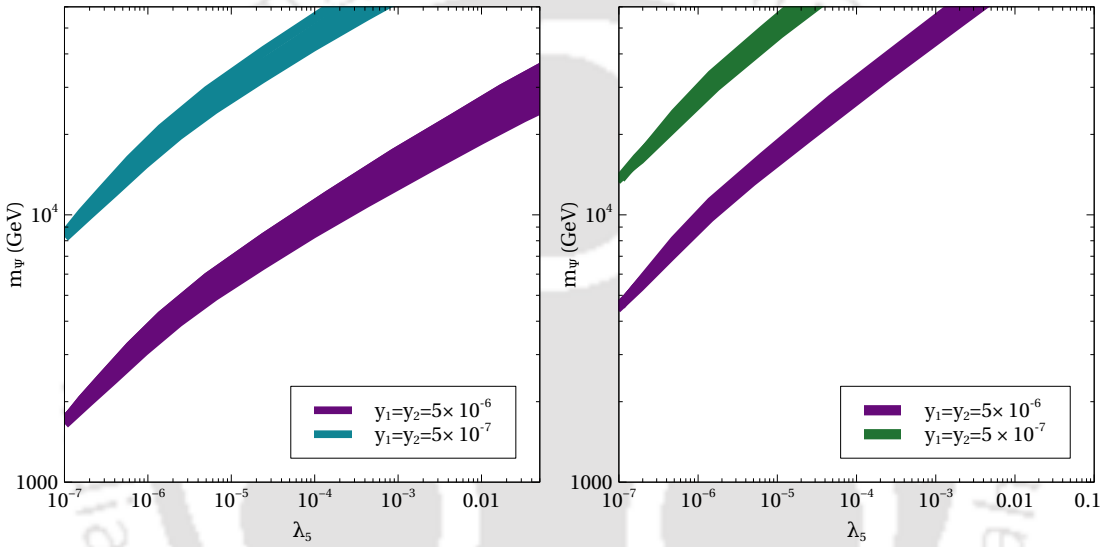

Figure 3.8: The variation of m_ψ with λ_5, required to satisfy the observed asymmetry using lepton flavour effects. For the left panel, $M_1 = 2 \times 10^5$ GeV and $M_2 = 2 \times 10^6$ GeV and for the right panel, $M_1 = 2 \times 10^7$ GeV and $M_2 = 2 \times 10^9$ GeV. The other parameters are set at $m_\eta = 10$ GeV, $m_S = 500$ GeV.

3.4.3 Dark Matter

We briefly discuss our dark matter results in this subsection. As mentioned earlier, a two component scalar singlet and scalar doublet DM has been recently discussed in details within a type-I seesaw model [196]. Instead of showing the details in general, here we focus on possible differences due to new couplings of these two DM candidates in relation to leptogenesis and neutrino mass as discussed above. We first discuss the behaviour of DM relic density with its mass for various possible combinations of relevant benchmark parameters. In Fig.3.9, we show the variation in individual and total DM relic densities for different mass relations between two DM candidates. While the overall features agree with the known results of scalar singlet and scalar doublet DM, there are some interesting differences due to inter-conversions and coannihilations here which we highlight.

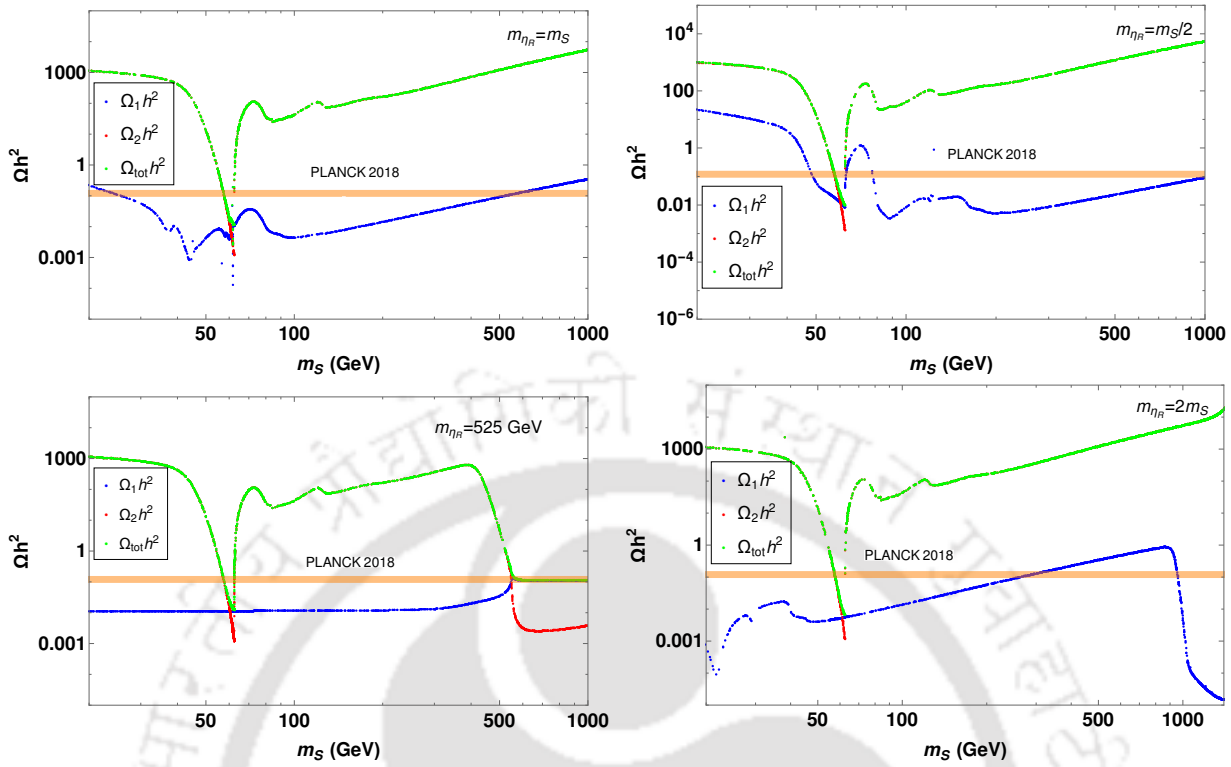

Figure 3.9: Relic abundance versus DM mass for various mass relations between two DM candidates. The other parameters are fixed at the following benchmark values $\lambda_L = 10^{-4}$, $\lambda_6 = 10^{-3}$, $\lambda_7 = 0$, $y_{1,2} = 10^{-4}$, $\Delta m_{\eta_I} = 2$ GeV and $\Delta m_{\eta_\pm} = 2$ GeV.

In top left panel of Fig.3.9, the two DM candidates are assumed to have equal masses. The Higgs portal interactions of both the DM candidates are open due to the chosen non-zero couplings $\lambda_6, \lambda_L = \lambda_3 + \lambda_4 + \lambda_5$. Although the Higgs portal coupling of doublet DM is relatively smaller, the coannihilation channels are very efficient due to tiny mass splittings $\Delta m_{\eta_I} = m_{\eta_I} - m_{\eta_R}, \Delta m_{\eta^\pm} = m_{\eta^\pm} - m_{\eta_R}$, keeping its relic abundance suppressed compared to the singlet DM. In the top right panel plot of Fig.3.9, a noticeable change in doublet DM relic abundance is observed. While all relevant couplings have the same value as those on the top left panel plot, the doublet DM relic increases as singlet DM mass is twice the mass of doublet DM and hence there can be efficient conversions from singlet to doublet DM through Higgs portal interactions. Note that in both of these plots, the direct conversion coupling λ_7 is switched off and hence all possible DM conversions can occur only via Higgs portal interactions. To show the effect of DM conversion more clearly, we keep the mass of doublet DM fixed in the bottom left panel plot of Fig.3.9. As the singlet DM mass approaches the doublet DM mass, there is a sharp fall in its relic while at the same time the doublet relic increases due to relative conversions. In this plot, such conversions can occur via both Higgs portal and direct coupling λ_7. Finally, on the bottom right panel of Fig.3.9, we show one interesting feature where doublet DM relic density suddenly drops as its mass becomes close to 1.5 TeV. This particular feature is not due to DM conversions via Higgs portal or direct coupling λ_7 as that can happen at any mass, given the fact that doublet mass is twice that of singlet mass all throughout. This happens due to doublet DM coannihilation with ψ whose

mass is fixed at 1.5 TeV. Due to this coannihilation $\eta_R\psi \to S\ell$, the singlet relic density also increases, though it is not as prominent as the depletion of doublet relic density in the figure.

After discussing the general features of DM relic dependence on various relevant parameters, in Fig.3.10, we specifically show the effects of direct conversion coupling λ_7 and Yukawa coupling $y_{1,2}$ of $\psi - S - N_{1,2}$ vertices. Mass of doublet dark matter is assumed to be twice of singlet dark matter mass. Comparing top panel plots of Fig.3.10 where $y_{1,2} = 0$, it is seen that turning on the direct conversion coupling λ_7 leads to sharp fall in heavier DM relic density. Same effect is visible while comparing the bottom panel plots also where the effect of $y_{1,2} \neq 0$ is also shown leading to depletion of doublet DM relic as its mass approaches m_ψ.

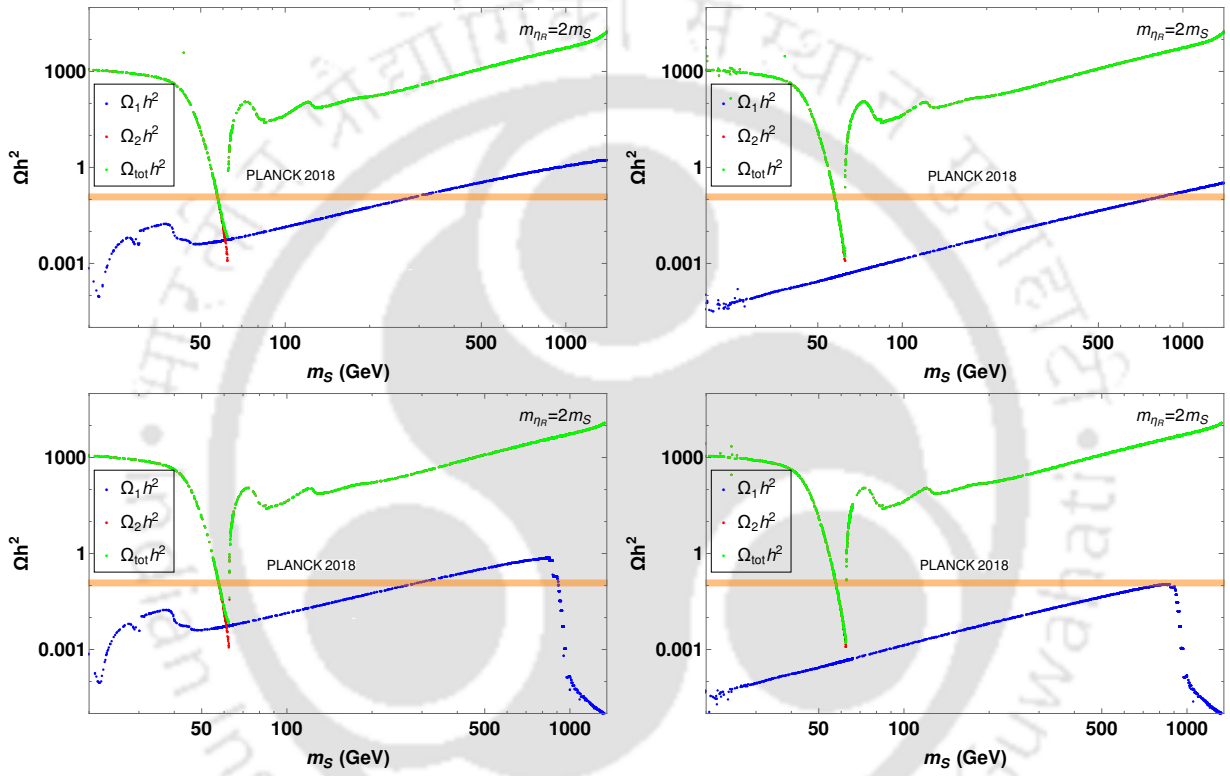

Figure 3.10: Relic abundance versus DM mass showing the effects of direct conversion coupling λ_7 and Yukawa coupling $y_{1,2}$ of $\psi - S - N_{1,2}$ vertices. The benchmark parameters fixed for all the four plots are $\lambda_6 = 10^{-3}$ and $\lambda_L = 10^{-4}$. The conversion coupling and the new Yukawa coupling are fixed at $y_{1,2} = 0$, $\lambda_7 = 0$ (upper left panel plot), $y_{1,2} = 0$, $\lambda_7 = 1$ (upper right panel plot), $y_{1,2} = 10^{-2}$, $\lambda_7 = 0$ (lower left panel plot) $y_{1,2} = 10^{-2}$, $\lambda_7 = 1$ (lower right panel plot).

To find the relevant parameter space of DM that gives rise to the observed relic density, we perform a numerical scan of the relevant parameter space favoured from the requirement of successful leptogenesis. For the first case ($M_1 = 2 \times 10^5$ GeV), the parameter space in terms of two DM masses is shown on left panel plot of Fig.3.11 . To be in agreement with the parameter space chosen for leptogenesis, here we fix $m_{\eta_R} < m_\psi$ and vary other parameters in the range $10\,\text{GeV} < m_S, m_\eta < 1000$ GeV, $10^{-6} < \lambda_5 < 10^{-1}$, $10^{-4} < \lambda_6, \lambda_7 < 10^{-2}$, $10^{-7} < y_{1,2} < 10^{-5}$. While singlet DM masses are evenly distributed across the range,

there seems to be an upper bound on doublet DM mass near 500 GeV. This is due to the chosen mass splitting within doublet components. As earlier studies of inert scalar doublet DM shows [115, 118–131, 229], for such small mass splitting, the DM is overproduced in the high mass regime. While the underproduction of one DM component in our model can be compensated by the second DM component, overabundance of one is difficult to reconcile with. Choosing a larger mass splitting within inert doublet components will allow more region of parameter space in terms of doublet DM mass. The right panel plot of Fig.3.11 shows the spin independent DM-nucleon scattering rate of both the DM components, compared against the latest bound from Xenon1T experiment [90]. Clearly, all the points satisfy the direct detection bounds. This is due to the fact that, we have kept the Higgs portal coupling of both the DM candidates fixed at small value. We varied $10^{-6} < \lambda_6 < 10^{-2}$ and fixed $\lambda_L = 10^{-3}$. Since tree level DM-nucleon scattering arises through Higgs portal couplings only, the corresponding rates remain low enough to survive Xenon1T bounds. The colour code on left panel plot of Fig.3.11 shows the value of $y = |y_1| = |y_2^*|$. Similar scan plot for case 2 is shown on the left panel of Fig.3.12. While we notice a similar upper bound on doublet DM mass due to chosen mass splitting, the parameter space remains safe from direct detection bounds.

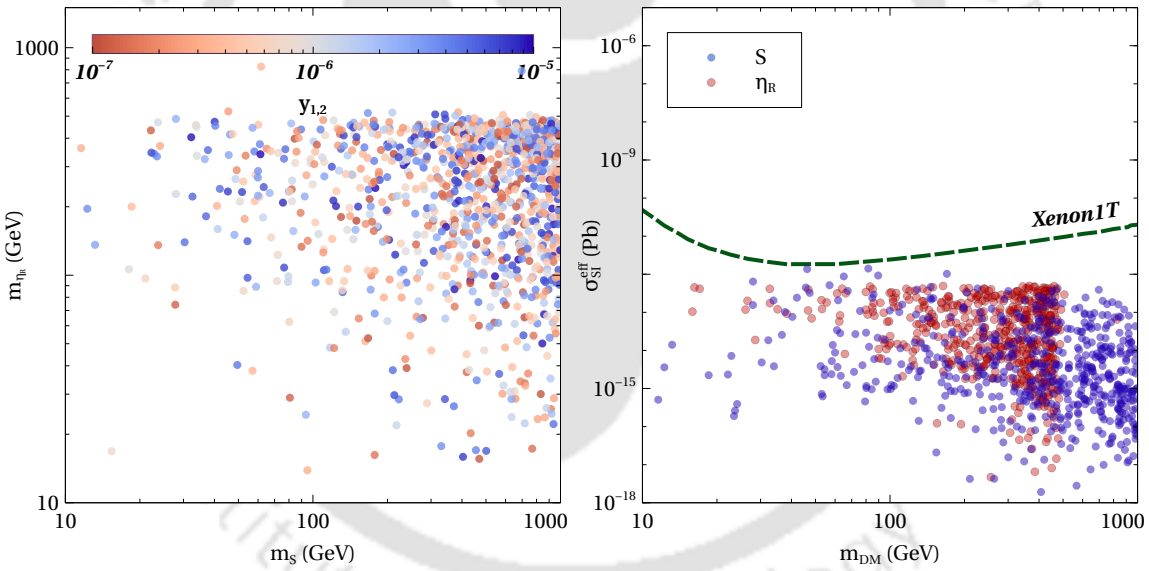

Figure 3.11: Scan plot showing the parameter space in $m_S - m_{\eta_R}$ plane allowed from total DM relic abundance (left panel) and $m_{\rm DM} - \sigma_{\rm SI}$ plot for all the points satisfying the total relic (right panel). For this scan the RHN masses are set at $M_1 = 2 \times 10^5$ GeV and $M_2 = 2 \times 10^6$ GeV. The other important parameters are randomly varied within the ranges $10^{-7} < \lambda_5 < 10^{-1}$, $10^{-4} < \lambda_6 < 10^{-2}$, $10^{-4} < \lambda_7 < 10^{-2}$ and $10^{-7} < y_{1,2} < 10^{-5}$.

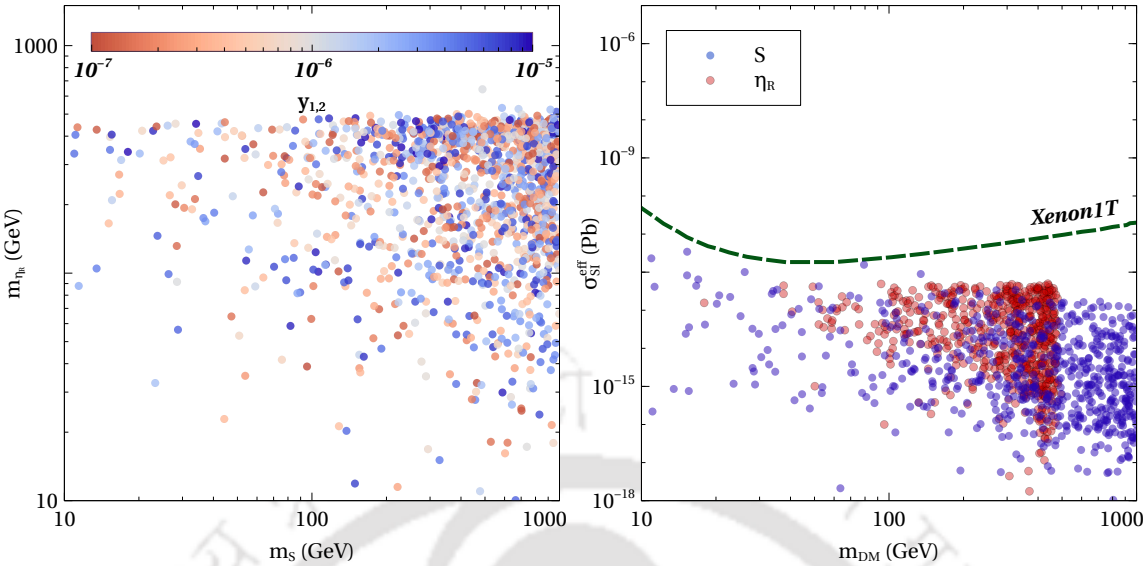

Figure 3.12: Scan plot showing the parameter space in $m_S - m_{\eta_R}$ plane allowed from total DM relic abundance (left panel) and $m_{\rm DM} - \sigma_{\rm SI}$ plot for all the points satisfying the total relic (right panel). For this scan the RHN masses are set at $M_1 = 2 \times 10^7$ GeV and $M_2 = 2 \times 10^8$ GeV. The other important parameters are randomly varied within the ranges $10^{-7} < \lambda_5 < 10^{-1}$, $10^{-4} < \lambda_6 < 10^{-2}$, $10^{-4} < \lambda_7 < 10^{-2}$ and $10^{-7} < y_{1,2} < 10^{-5}$.

CHAPTER 4

Low scale Dirac leptogenesis and dark matter with observable N_{eff}

In this chapter, we study the possibility of low scale leptogenesis and DM with light neutrinos being of Dirac nature. It is worth mentioning that the typical seesaw models give rise to Majorana light neutrinos as they violate lepton number by 2 units. However, the nature of light neutrinos: Dirac or Majorana, is not yet known. While neutrino oscillation experiments can not settle this issue, there are other experiments like the ones looking for neutrinoless double beta decay ($0\nu\beta\beta$) [240], a promising signature of Majorana neutrinos. However, there have been no such observations yet which can confirm Majorana nature of light neutrinos. While null result at $0\nu\beta\beta$ does not necessarily rule out Majorana nature of light neutrinos, it has led to growing interests in Dirac neutrino models in the last few years. For different seesaw realisations to generate light Dirac neutrino masses, please see [174, 241–281] and references therein. While Dirac neutrinos may imply conservation of lepton number and absence of a viable leptogenesis mechanism, there are interesting ways to circumvent this. As proposed in [282,283], one can have successful leptogenesis even with light Dirac neutrino scenarios where total lepton number or $B - L$ is conserved just like in the SM. Popularly known as Dirac leptogenesis scenario, it involves the creation of an equal and opposite amount of lepton asymmetry in left handed and right handed neutrino sectors followed by the conversion of left sector asymmetry into baryon asymmetry via electroweak sphalerons. The lepton asymmetries left and right handed sectors are prevented from equilibration due to the tiny effective Dirac Yukawa couplings. [260, 284–295]. In few other works [296, 297] light Dirac neutrinos with $B - L$ violation was considered in such a way that the latter does not give any Majorana mass for light neutrinos. We find this interesting due to the role $B - L$ gauge symmetry or the corresponding gauge boson after spontaneous symmetry breaking can play in phenomenology and other experimental signatures. It should be noted that leptogenesis with light Dirac neutrinos have been referred to as Dirac leptogenesis, Dirac neutrinogenesis among others in the above-mentioned works depending upon the particular realisations. Here, we simply call it Dirac leptogenesis for simplicity.

Motivated by these, we consider a gauged $B - L$ model with light Dirac neutrinos and lepton number violating heavy chiral fermions whose out-of-equilibrium decay into leptons lead to generation of lepton asymmetry. In contrast with earlier works [296, 297], here lepton asymmetry is generated by decay processes similar to usual type-I seesaw [45–50]

leptogenesis except for the fact that there are no $\Delta(B-L)=2$ processes ensuring Dirac nature of light neutrinos. The $B-L$ gauge boson plays important role in leptogenesis, specially in determining the abundance of the decaying particle and also in the wash-out processes. The same $B-L$ gauge interactions also lead to thermalisation of right handed neutrinos contributing to relativistic degrees of freedom $N_{\rm eff}$ which is tightly constrained from Planck 2018 data. We also consider $B-L$ portal fermion singlet DM whose relic density depends crucially upon its annihilation channels mediated by $B-L$ gauge bosons. We consider a typical WIMP type DM which gets thermally produced in the early universe from the standard bath by virtue of $B-L$ gauge interaction followed by freeze-out leaving a relic. Thus, the requirements of successful leptogenesis and correct dark matter relic abundance without overproducing $N_{\rm eff}$ tightly constrain the $B-L$ gauge sector parameter space, in addition to the constraints from collider experiments. While collider bounds rule out some parts of the parameter space, the Planck 2018 bound on $N_{\rm eff}$ rules out some additional parameter space consistent with leptogenesis and dark matter requirements. We show that future CMB experiments with much more sensitivity to $N_{\rm eff}$ will be able to probe the entire parameter space currently favoured from low scale leptogenesis and dark matter requirements. We also show that the fermion singlet DM candidates with exotic $B-L$ charges keep the model anomaly free, adding another motivation to consider DM in this setup. We find one minimal framework of this type where two Dirac fermion DM candidates are sufficient to cancel the anomalies. This allowed parameter space consistent with DM, leptogenesis and $N_{\rm eff}$ criteria while satisfying collider bounds can still be probed at near future CMB experiments, keeping the model very predictive and testable.

4.1 The Basic Framework

In this section, we consider a minimal setup based on gauge $B-L$ extension of the SM to highlight our key findings. Gauged $B-L$ extension of the SM [298–303] has been a popular framework studied in the context of neutrino mass, leptogenesis for a long time. In addition to the SM fermion content with usual gauge charges, we consider three right handed neutrinos ν_R having $B-L$ charge -1 which form massive Dirac neutrinos with ν_L after electroweak symmetry breaking (EWSB). The scalar content is chosen in a way that prevents ν_R from acquiring Majorana masses. To realise leptogenesis, we introduce two heavy singlet fermions N_R having $B-L$ charge $n_1 \neq \pm 1$ so that generating Majorana mass term of N_R (generated by singlet scalar ϕ_1) does not lead to Majorana mass of ν_R. Since lepton doublet ℓ_L and N_R have different $B-L$ charges, we introduce another scalar doublet η with appropriate non-zero $B-L$ charge so that the required Yukawa coupling can be realised. The neutral component of this new scalar doublet does not acquire any vacuum expectation value (VEV), a requirement to ensure that light neutrinos do not receive any Majorana mass contribution via type-I seesaw. Note that, this particle content will not lead to an anomaly free gauged $B-L$ model. We will later show how additional chiral fermions with non-trivial $B-L$ charges can lead to vanishing anomalies while playing the role of dominant dark matter component of the universe at the same time.

With the particle content mentioned above, the relevant Yukawa Lagrangian is

$$-\mathcal{L}_Y \supset Y_D \bar{L}\tilde{H}\nu_R + Y_\eta \bar{L}\tilde{\eta}N_R + Y_N \phi_1 N_R N_R + \text{h.c.} \tag{4.1}$$

Thus, light Dirac neutrino masses arise purely from the Yukawa coupling with the SM Higgs. While it requires fine-tuned Yukawa coupling to generate sub-eV Dirac neutrino masses, we do not pursue dynamical realisations of such small Yukawa couplings in the minimal models discussed here. Details of such Dirac neutrino models can be found in [174,241,243–281,304].

The gauge invariant scalar interactions can be written as

$$\begin{aligned}\mathcal{L}_{\text{scalar}} = &\left(D_{H\mu}H\right)^\dagger \left(D_H{}^\mu H\right) + \left(D_{\eta_\mu}\eta\right)^\dagger \left(D_\eta{}^\mu \eta\right) + \left(D_{\phi_\mu}\phi_1\right)^\dagger \left(D_\phi{}^\mu \phi_1\right) + \mu_H^2|H|^2 \\ &- \lambda_H|H|^4 - \left(\mu_\eta^2|\eta|^2 + \lambda_\eta|\eta|^4\right) - \lambda_{H\eta}(\eta^\dagger\eta)(H^\dagger H) - \lambda'_{H\eta}(\eta^\dagger H)(H^\dagger \eta) \\ &+ \mu_{\phi_1}^2|\phi_1|^2 - \lambda_{\phi_1}|\phi_1|^4 - \lambda_{H\phi_1}(H^\dagger H)(\phi_1^\dagger\phi_1) - \lambda_{\eta\phi_1}(\eta^\dagger\eta)(\phi_1^\dagger\phi_1)\end{aligned} \tag{4.2}$$

where $\mathrm{D_H}{}^\mu$, $\mathrm{D}_\eta{}^\mu$ and $\mathrm{D}_\phi{}^\mu$ denote the covariant derivatives for the scalar doublets H, η and scalar singlets ϕ_i respectively and can be written as

$$\begin{aligned} D_{H\mu}\, H &= \left(\partial_\mu + i\,\frac{g}{2}\,\sigma_a\, W_\mu^a + i\,\frac{g'}{2}\,B_\mu\right) H\,, \\ D_{\eta_\mu}\,\eta &= \left(\partial_\mu + i\,\frac{g}{2}\,\sigma_a\, W_\mu^a + i\,\frac{g'}{2}\,B_\mu + i\,g_{BL}\,n_\eta Z_{BL\mu}\right)\eta\,, \\ D_{\phi_\mu}\,\phi_1 &= \left(\partial_\mu + i\,g_{BL}\,n_{\phi_1} Z_{BL\mu}\right)\phi_1\,. \end{aligned} \tag{4.3}$$

Here $\mathrm{g_{BL}}$ is the new gauge coupling and n_η and n_{ϕ_1} are the charges under $\mathrm{U(1)_{B-L}}$ for η and ϕ_1 respectively. The kinetic term of the $B-L$ gauge boson can be written as

$$\mathcal{L}_{\text{kin}} \supset -\frac{1}{4} B'_{\alpha\beta} B'^{\alpha\beta} \tag{4.4}$$

where $B'^{\alpha\beta} = \partial^\alpha Z_{BL}^\beta - \partial^\beta Z_{BL}^\alpha$ is the corresponding field strength tensor. The symmetry of the model also allows kinetic mixing between $U(1)_Y$ of SM and $U(1)_{B-L}$ of the form $\epsilon B^{\alpha\beta}B'_{\alpha\beta}/2$ where $B^{\alpha\beta} = \partial^\alpha B^\beta - \partial^\beta B^\alpha$ and ϵ is the kinetic mixing parameter. We ignore such tree level mixing in this work. The mixing at one loop can be approximated as $\epsilon \approx g_{BL}g'/(16\pi^2)$ [305]. As we will see while discussing our numerical results, our final allowed parameter space for g_{BL} will correspond to tiny one-loop kinetic mixing (smaller than $\mathcal{O}(10^{-3})$) and has very little effect on the phenomenology discussed here. Therefore, we ignore such kinetic mixing in our work.

After both $B-L$ and electroweak symmetries get broken by the VEVs of H and ϕ_1 the doublet and all three singlets are given by

$$H = \begin{pmatrix} H^+ \\ \dfrac{h' + v + iz}{\sqrt{2}} \end{pmatrix}, \quad \eta = \begin{pmatrix} \eta^+ \\ \dfrac{\eta'_R + i\eta'_I}{\sqrt{2}} \end{pmatrix}, \quad \phi_1 = \frac{s'_1 + u_i + A'_1}{\sqrt{2}} \quad , \tag{4.5}$$

The details of the scalar mass spectrum can be found in Appendix C.1.

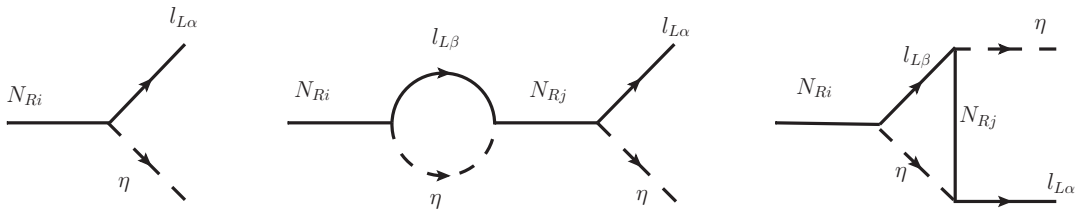

Figure 4.1: Processes creating lepton asymmetry.

4.1.1 Dirac leptogenesis

As can be seen from the Yukawa Lagrangian mentioned above, the out-of-equilibrium decay of N_R to lepton doublet and additional scalar doublet η can generate lepton asymmetry in our model. Compared to usual Dirac leptogenesis scenarios, here the generation of lepton asymmetry is much simpler and only requires the steps followed in type-I seesaw leptogenesis known for decades. The Feynman diagrams for this decay process, including one-loop corrections are shown in Fig.4.1.

The relevant Boltzmann equations can be written as

$$\frac{dn_{\rm N_1}}{dz} = -D_1(n_{N_1} - n_{\rm N_1}^{\rm eq}) - \frac{s}{\mathbf{H}(z)z}[(n_{N_1}^2 - (n_{\rm N_1}^{\rm eq})^2)\langle\sigma v\rangle_{N_{R_1}N_{R_1}\longrightarrow XX}], \tag{4.6}$$

$$\frac{dn_{\rm B-L}}{dz} = -\epsilon_1 D_1(n_{\rm N_1} - n_{\rm N_1}^{\rm eq}) - W^{\rm Total} n_{\rm B-L} \tag{4.7}$$

where n_{N_1} denotes the comoving number density of N_{R_1} (to be denoted as N_1 hereafter) and $n_{N_1}^{\rm eq} = \frac{z^2}{2}K_2(z)$ is its equilibrium number density (with $K_i(z)$ being the modified Bessel function of i-th kind). The quantity on the right hand side of the above equations

$$D_1 \equiv \frac{\Gamma_1}{\mathbf{H}z} = K_{N_1} z \frac{K_1(z)}{K_2(z)} \tag{4.8}$$

measures the total decay rate of N_1 with respect to the Hubble expansion rate, and similarly, $W^{\rm Total} \equiv \frac{\Gamma_W}{\mathbf{H}z}$ measures the total washout rate. Here, $K_{N_1} = \Gamma_1/\mathbf{H}(z=1)$ is the decay parameter. In the second term on right hand side of Eq.(4.6), we consider N_1 annihilations into all SM fermions mediated by Z_{BL} along with N_1 annihilations to pair of Z_{BL} as well as η. Similarly, $n_{\rm B-L}$ in Eq.(4.7) denotes the comoving number density of $B-L$ generated from CP violating out-of-equilibrium decay of N_1. The CP asymmetry parameter on the right hand side of Eq.(4.7) is defined as

$$\epsilon_i = \frac{\sum_\alpha \Gamma(N_i \to l_\alpha \eta) - \Gamma(N_i \to \bar{l_\alpha}\bar{\eta})}{\sum_\alpha \Gamma(N_i \to l_\alpha \eta) + \Gamma(N_i \to \bar{l_\alpha}\bar{\eta})}. \tag{4.9}$$

We consider a hierarchical limit of right handed neutrinos N_R and hence only the lightest of them namely, $N_{R_1} \equiv N_1$ contribute dominantly to the generation of lepton asymmetry. In the Boltzmann equation of N_1 above, we have considered two types of dilution terms on the

right hand side: one due to its decay into leptons and the other due to its annihilation into lighter particles. We consider the singlet scalar to be much heavier than the right handed neutrinos and hence the corresponding processes involving singlet scalars are sub-dominant compared to the ones mediated by $B-L$ gauge bosons. Such additional dilution terms for right handed neutrinos also appear in type-I seesaw leptogenesis with Majorana light neutrinos and $B-L$ gauge symmetry, see [306–309] for details. In the Boltzmann equation for lepton asymmetry, in addition to the inverse decay, we consider the following scattering processes responsible for washing out the generated lepton asymmetry:

$$lZ_{BL} \longrightarrow \eta N_1, lW^{\pm}(Z) \longleftarrow \eta N_1, \eta l \longleftarrow N_1 Z_{BL}, l\eta \longleftarrow \bar{l}\eta^*, lN_1 \longrightarrow \bar{l}N_1^*.$$

All the relevant cross sections and decay widths are given in Appendix C.2. Note that, apart from the usual Yukawa or SM gauge coupling related processes, we also have washout processes involving $B-L$ gauge bosons. Since interactions involving $B-L$ gauge bosons can cause dilution of N_1 abundance as well as wash out the generated lepton asymmetry, one can tightly constrain the $B-L$ gauge sector couplings from the requirement of successful leptogenesis at low scale. Also, the Yukawa couplings involved in CP asymmetry generation are not related to light neutrino mass generation, unlike in vanilla leptogenesis scenario. Therefore, we do not have any strict lower bound on the scale of leptogenesis like the Davidson Ibarra bound of vanilla leptogenesis scenario [64].

We first show the CP asymmetry parameter ϵ_1 and the decay parameter $K_{N_1} = \Gamma_1/H(z=1)$ with heavy Majorana neutrino mass M_1 for different benchmark values Yukawa couplings. We consider flavour universal Yukawa couplings of N_i for simplicity. From the left panel plot of Fig.4.2 we can see that with a fixed value of the N_2 Yukawa coupling $(Y_\eta)_{\alpha 2}$ the decay parameter K_{N_1} increases with the increase in N_1 Yukawa coupling as expected whereas the CP asymmetry parameter ϵ_1 remains constant. The CP asymmetry parameter ϵ_1 does not change with the change in $(Y_\eta)_{\alpha 1}$ as $(Y_\eta)_{\alpha 2}$ decides the imaginary part of Yukawa coupling products appearing in CP asymmetry ϵ_1, as described the Appendix C.3. In the right panel plot of Fig.4.2 one can see that with the increase in $(Y_\eta)_{\alpha 2}$ the CP asymmetry parameter ϵ_1 increases while K_{N_1} remains same due to the fixed Yukawa coupling $(Y_\eta)_{\alpha 1}$. The increase in CP asymmetry with the increase in $(Y_\eta)_{\alpha 2}$ can be understood from the description of Appendix C.3. The constancy of the decay parameter with respect to $(Y_\eta)_{\alpha 2}$ is trivially understood as N_1 decay width depends on $(Y_\eta)_{\alpha 1}$ only. From this Fig.4.2 we can understand that for a fixed value of $(Y_\eta)_{\alpha 1}$ one need relatively large value of the $(Y_\eta)_{\alpha 2}$ to have enough CP asymmetry ϵ_1. In both the plots, the decay parameter K_{N_1} remains very large for some part of the parameter space. Such large values will lead to wash-out of the $B-L$ asymmetry via inverse decay. We mark the points as stars which correspond to the combination of Yukawa as well as M_1 that can give rise to correct final asymmetry. Clearly, both these points correspond to small K_{N_1} which can be ensured for smaller Yukawa coupling $(Y_\eta)_{\alpha 1}$ and larger M_1. The washout effects are also visible in the evolution plots 4.3, 4.4, 4.5. It should be noted that in a strong washout region ($K_{N_1} > 1$), the generated asymmetry can be made large by choosing large enough $(Y_\eta)_{\alpha 2}$ (within perturbative limit) such that it gives the correct asymmetry after the washout process become negligible. Since both the Yukawa couplings in our model are completely free from the light neutrino sector we can tune them accordingly to give the observed asymmetry. This is in sharp contrast with type-I seesaw leptogenesis where Yukawa couplings are constrained by light neutrino mass data for

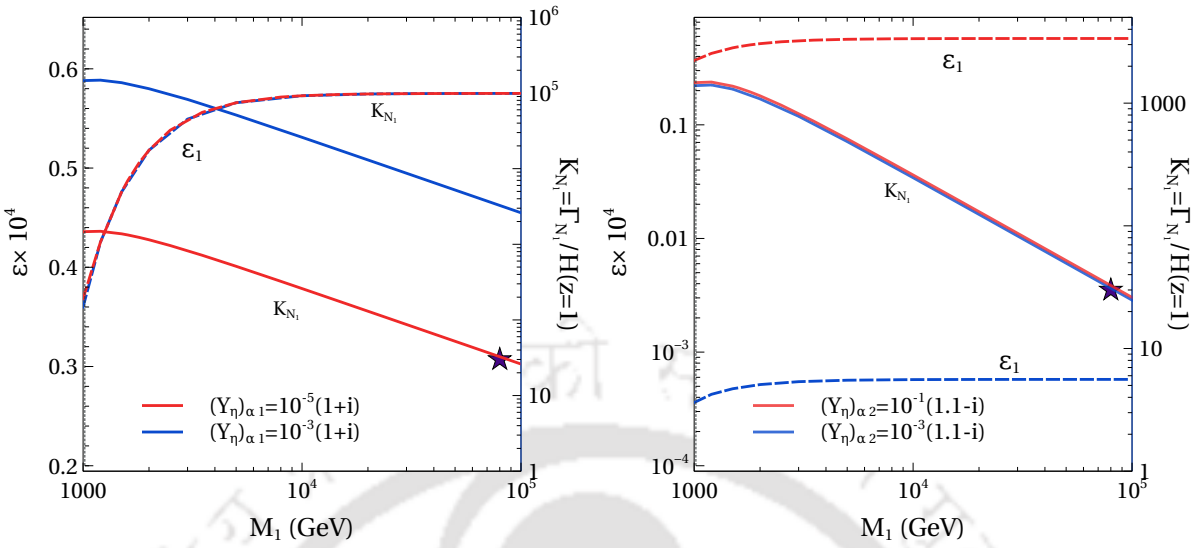

Figure 4.2: Variation of CP asymmetry parameter ϵ_1 and the decay parameter K_{N_1} with M_1 for different values of the N_1 Yukawa coupling (left panel) and for different values of the N_2 Yukawa coupling (Right panel). K_{N_1} is shown by the solid lines and the ϵ_1 is shown with the dashed lines. We fix the $(Y_\eta)_{\alpha 2} = 10^{-1}(1.1 - i)$ for the left panel and $(Y_\eta)_{\alpha 1} = 10^{-5}(1 + i)$ for the right panel. The points marked as stars correspond to successful leptogenesis scale and couplings.

a fixed scale of leptogenesis, leading to the Davidson Ibarra bound $M_1 \geq 10^9$ GeV [64]. Note that increase in Yukawa coupling also increases the inverse decay, decreasing the asymmetry generated, the details of which we discuss below.

In left panel plot of Fig.4.3, we show the evolution of lepton asymmetry for different values of $B - L$ gauge couplings while fixing other parameters at benchmark values. Note that, for the numerical analysis we consider $n_1 = -3/2$. The right panel plot of the same figure shows the corresponding evolution of N_{R_1} number density n_{N_1}. The evolution of comoving number densities of N_1 for different values of g_{BL} do not show significant differences as they are primarily governed by their decay. However, presence of additional gauge interactions can lead to significant changes in N_1 number density as they tend to keep N_1 in equilibrium for longer duration. We show these details in Appendix C.2. The effect of the N_1 annihilations is visible in the evolution plots of the comoving number density of $B - L$ asymmetry in Fig.4.3 and Fig.4.4. With the increase in g_{BL} and $M_{Z_{BL}}$ the N_1 annihilation cross section increases which brings the N_1 number density closer to its equilibrium number density and therefore the $B - L$ asymmetry decreases. We observe similar behavior of the asymmetry with g_{BL} and $M_{Z_{BL}}$ because of the washout process $lZ_{BL} \longrightarrow N_1\eta$. The details of the relevant washout is shown in Appendix C.2. However, we noticed that in the determination of the $B - L$ asymmetry the N_1 annihilation plays more dominant role than the washout $lZ_{BL} \longrightarrow N_1\eta$. In the left panel plot of Fig.4.3, the horizontal line shows the required final comoving lepton asymmetry at the epochs of sphaleron transition which gets converted into

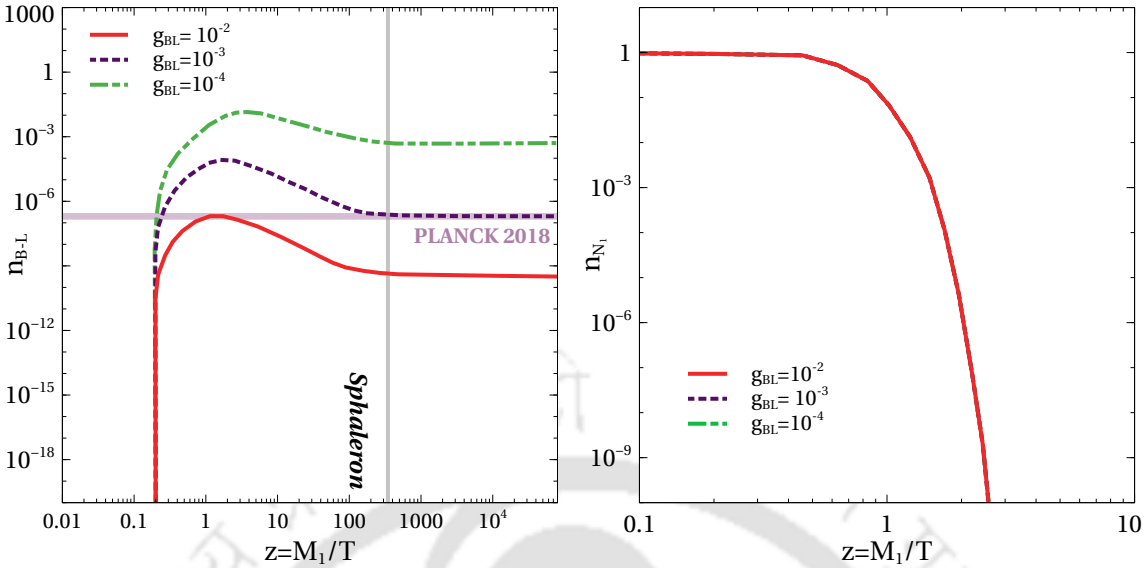

Figure 4.3: Comoving density of B-L asymmetry (left panel) and comoving number density of N_{R_1} (right panel) with $z = \dfrac{M_1}{T}$ for different g_{BL}. The Yukawa couplings relevant for Leptogenesis are taken to be $(Y_\eta)_{\alpha 1} = 10^{-5}(1+i)$ and $(Y_\eta)_{\alpha 2} = 10^{-1}(1.1-i)$. The other important parameters used are $M_1 = 45$ TeV, $M_2 = 450$ TeV, $m_\eta = 5$ TeV and $M_{Z_{BL}} = 4$ GeV. The horizontal line in left panel plot denotes the required $B-L$ asymmetry to generate for observed baryon asymmetry (Planck 2018) after sphaleron transition.

the observed baryon asymmetry. The final $B-L$ asymmetry $n^f_{\rm B-L}$ just before electroweak sphaleron freeze-out is converted into the observed baryon to photon ratio by the standard formula

$$\eta_B \;=\; \frac{3}{4}\frac{g^0_*}{g_*} a_{\rm sph} n^f_{\rm B-L} \;\simeq\; 9.2\times 10^{-3}\, n^f_{\rm B-L}\,, \tag{4.10}$$

where $a_{\rm sph} = \frac{8}{23}$ is the sphaleron conversion factor (taking into account two Higgs doublets). The effective relativistic degrees of freedom is taken to be $g_* = 116$, slightly higher than that of the SM at such temperatures as we are including the contribution of the inert Higgs doublet and ν_R's too. In the above expression $g^0_* = \frac{43}{11}$ is the effective relativistic degrees of freedom at the recombination epoch. Using observed η_B from Eq.(4.10), the required final $B-L$ asymmetry can be found as $n^f_{\rm B-L} \approx 7\times 10^{-8}$ corresponding to the horizontal line labelled as Planck 2018 in Fig.4.3 (left panel).

In Fig.4.5 the evolution of comoving number density of $B-L$ and N_1 are shown for different values of $(Y_\eta)_{\alpha 1}$ keeping the other parameters fixed. One can see a two-way behavior of the asymmetry with $(Y_\eta)_{\alpha 1}$ in the left panel plot of figure 4.5. With the decrease in the Yukawa coupling $(Y_\eta)_{\alpha 1}$ the asymmetry increases, it is mainly because with the decrease in $(Y_\eta)_{\alpha 1}$ the scattering washouts as well as the inverse decay rate decrease significantly. However, beyond a certain small value of $(Y_\eta)_{\alpha 1}$ the asymmetry decreases with the decrease in $(Y_\eta)_{\alpha 1}$. The is because even though the washout rates decrease with a decrease in the

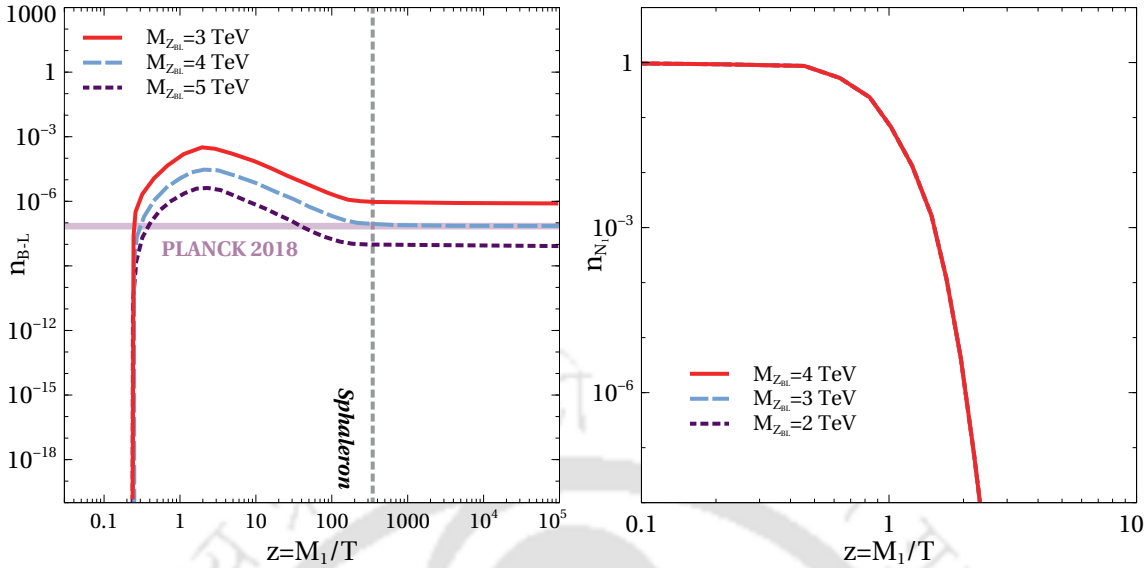

Figure 4.4: Comoving density of B-L asymmetry (left panel) and comoving number density of N_{R_1} (right panel) with $z = \dfrac{M_1}{T}$ for different $M_{Z_{BL}}$. The Yukawa couplings relevant for Leptogenesis are taken to be $(Y_\eta)_{\alpha 1} = 10^{-5}(1+i)$ and $(Y_\eta)_{\alpha 2} = 10^{-1}(1.1-i)$. The other important parameters used are $M_1 = 45$ TeV, $M_2 = 450$ TeV, $m_\eta = 5$ TeV and $g_{BL} = 10^{-3}$. The horizontal line in left panel plot denotes the required $B-L$ asymmetry to generate for observed baryon asymmetry (Planck 2018) after sphaleron transition.

Yukawa couplings, the generation of the asymmetry itself decreases because of the decrease in the decay width of N_1. Thus, the interplay of production and washout dictate the strength of required Yukawa couplings for a given scale of leptogenesis. Unlike the negligible dependence of N_1 number density on $B-L$ sector parameters discussed above, variation in Yukawa coupling leads to noticeable changes in N_1 abundance, as can be seen from the right panel plot of Fig.4.5. This is due to strong dependence of N_1 lifetime on the Yukawa coupling. Larger the Yukawa coupling, quicker is the fall of N_1 abundance, as expected.

In Fig.4.6, we show the final baryon asymmetry against the scale of leptogenesis namely, the mass of N_1. As seen from this figure, scale of leptogenesis can be tens of TeV depending upon the values of g_{BL} as well as $M_{Z_{BL}}$. We also check the evolution of lepton asymmetry for superheavy Z_{BL} (much above the scale of leptogenesis M_1) and find that variation in $M_{Z_{BL}}$ in such a case does not lead to any noticeable change in $n_{\mathrm{B-L}}$ evolution, as expected.

4.1.2 Relativistic degrees of freedom N_{eff}

The Dirac nature of light neutrinos introduces additional relativistic degrees of freedom which can be thermalised in the early universe by virtue of $B-L$ gauge interactions. Such additional light degrees of freedom can be probed by precise measurements of the CMB anisotropies. Recent 2018 data from the CMB measurement by the Planck satellite [3]

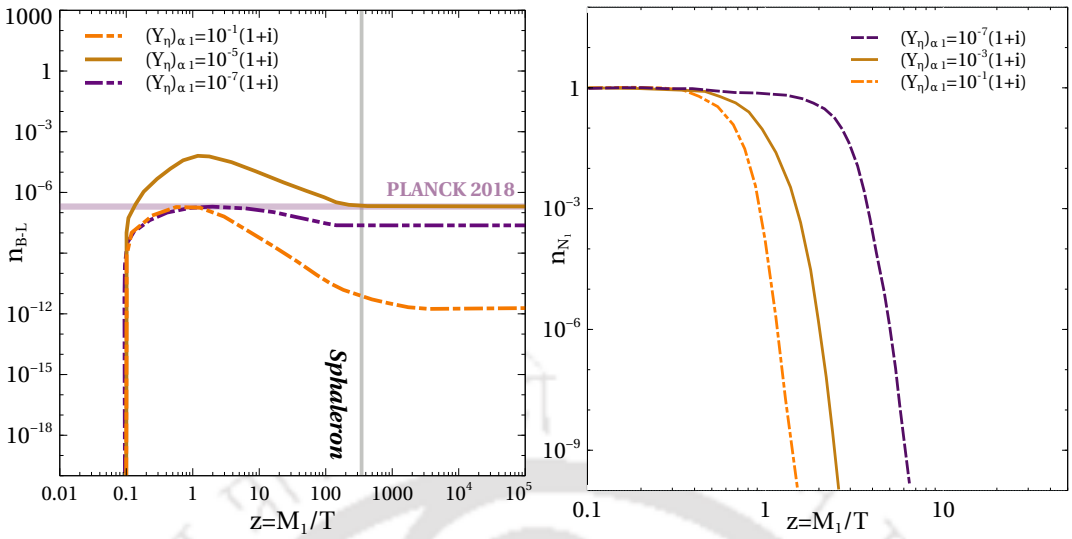

Figure 4.5: Comoving density of B-L asymmetry (left panel) and comoving number density of N_{R_1} (right panel) with $z = \dfrac{M_1}{T}$ for different $(Y_\eta)_{\alpha 1}$. The $B-L$ gauge coupling relevant for Leptogenesis are taken to be $g_{BL} = 10^{-3}$ and $(Y_\eta)_{\alpha 2} = 10^{-1}(1.1 - i)$. The other important parameters used are $M_1 = 45$ TeV, $M_2 = 450$ TeV, $m_\eta = 5$ TeV and $M_{Z_{B-L}} = 4$ TeV. The horizontal line in left panel plot denotes the required $B-L$ asymmetry to generate for observed baryon asymmetry (Planck 2018) after sphaleron transition.

suggests that the effective degrees of freedom for neutrinos as

$$\mathrm{N_{eff}} = 2.99^{+0.34}_{-0.33} \tag{4.11}$$

at 2σ or 95% CL including baryon acoustic oscillation (BAO) data. At 1σ CL it becomes more stringent to $N_{\rm eff} = 2.99 \pm 0.17$. Both these bounds are consistent with the standard model (SM) prediction $N_{\rm eff}^{\rm SM} = 3.045$ [310–312]. Upcoming CMB Stage IV (CMB-S4) experiments are expected to put much more stringent bounds than Planck due to their potential of probing all the way down to $\Delta N_{\rm eff} = N_{\rm eff} - N_{\rm eff}^{\rm SM} = 0.06$ [313]. For some recent studies on light Dirac neutrinos and enhanced $\Delta N_{\rm eff}$ in different contexts, please see [174, 314–320].

Effective number of relativistic degrees of freedom is defined as

$$N_{\rm eff} \equiv \frac{8}{7}\left(\frac{11}{4}\right)^{4/3}\left(\frac{\rho_{\rm rad} - \rho_\gamma}{\rho_\gamma}\right)$$

where $\rho_{\rm rad} = \rho_\gamma + \rho_\nu$ is the net radiation content of the universe. As mentioned earlier, the SM prediction is $N_{\rm eff}^{\rm SM} = 3.045$ [310–312]. In our model, $\Delta N_{\rm eff}$ can be estimated by finding the decoupling temperature T_{ν_R} of right handed neutrinos (ν_R) using

$$\Gamma(T^{\rm d}_{\nu_R}) = \mathbf{H}(T^{\rm d}_{\nu_R}) \tag{4.12}$$

where $\Gamma(T)$ is the interaction rate and $\mathbf{H}(T)$ is the expansion rate of the universe. It should be noted that the decoupling is never instantaneous in reality and non-instantaneous decoupling can also lead to spectral distortions of neutrino distributions. However such spectral

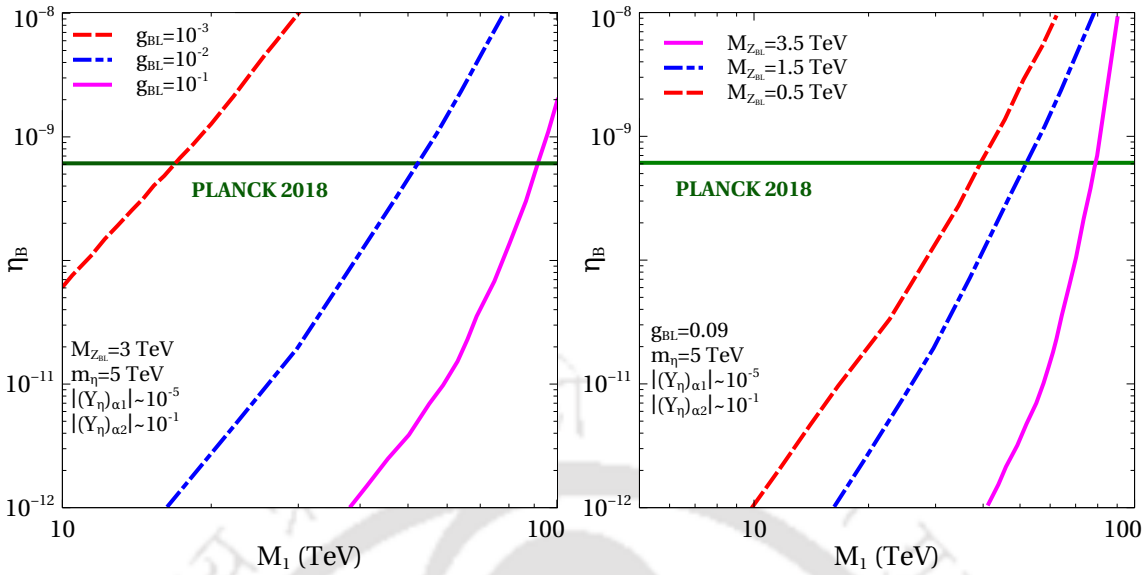

Figure 4.6: Baryon to photon ration with mass of N_1 for different benchmark values of g_{BL} (left panel) and $M_{Z_{BL}}$ (right panel). The Yukawas taken are $(Y_\eta)_{\alpha 1} = 10^{-5}(1+i)$ and $(Y_\eta)_{\alpha 2} = 3 \times 10^{-1}(1.1-i)$.

distortions have been found to be very small 0.01% (see [317], for example). Also, the decoupling temperature calculated using instantaneous decoupling approximation above remains in qualitative agreement with full treatment incorporating relevant Boltzmann equations [317]. Therefore, we stick to this simplistic approach in our work here.

We show the constraints on model parameters $g_{BL} - M_{Z_{BL}}$ from Planck 2σ bound on $\Delta N_{\rm eff}$ in Fig.4.7. The same plot also shows the LEP II limit $M_{Z_{BL}}/g_{BL} \geq 7$ TeV [321, 322]. The LHC bound is implemented by considering the 13 TeV limit from the ATLAS experiment [323, 324] and CMS experiment [325]. Clearly, the Planck 2σ bound on $\Delta N_{\rm eff}$ remains stronger than the LEP II as well as the LHC bounds for Z_{BL} mass heavier than around 3 TeV. We finally show the parameter space giving rise to successful leptogenesis for two different masses of N_1 while keeping N_2 mass ten times higher. Clearly, lower the scale of leptogenesis, lower should be the gauge coupling g_{BL} in order to keep the washout processes suppressed. Additionally, for fixed g_{BL} the scale of leptogenesis gets pushed up for larger values of $M_{Z_{BL}}$ as heavier Z_{BL} leads to increase in $lZ_{BL} \longrightarrow N_1\eta$ washout process noted earlier.

While it is possible to obtain successful leptogenesis at a scale as low as a TeV, the required gauge coupling g_{BL} for such scenarios will be insufficient to generate correct WIMP DM phenomenology as we discuss below. Interestingly, the next generation CMB experiments like CMB-S4 [326], SPT-3G [327] (whose sensitivities are shown as dashed and solid lines respectively) will be able to probe the entire parameter space consistent with successful Dirac leptogenesis.

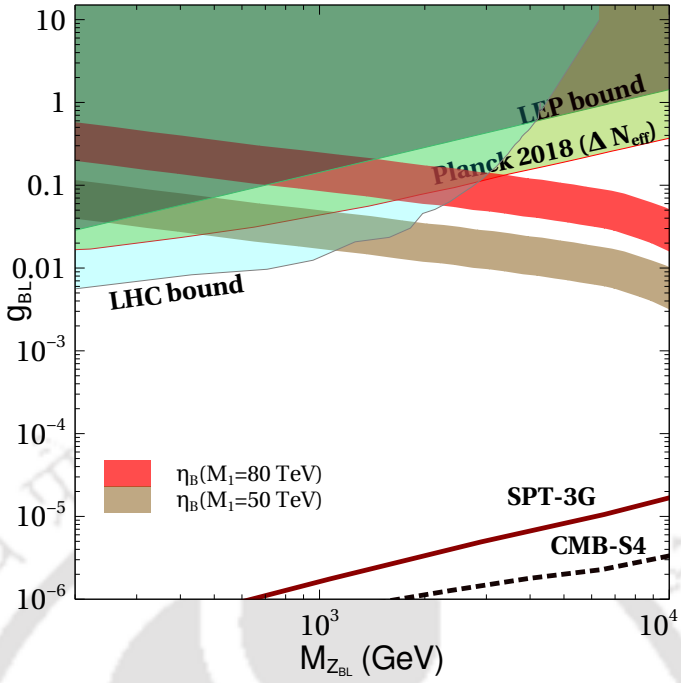

Figure 4.7: Allowed parameter space in $g_{BL} - M_{Z_{BL}}$ plane. The red and brown coloured bands correspond to regions of successful leptogenesis for two different scales. Bounds from LEP, LHC and future sensitivities of CMB experiments are shown. The Yukawa couplings chosen for this scan are $(Y_\eta)_{\alpha 1} = 10^{-5}(1+i)$ and $(Y_\eta)_{\alpha 2} = 3 \times 10^{-1}(1.1-i)$.

4.2 Anomaly Free $B - L$ Model

After discussing the interesting features related to Dirac leptogenesis and observable $\Delta N_{\rm eff}$ in previous section, we now move onto discussing the complete model, which is required to be anomaly free. While the SM fermion content with gauged B-L symmetry leads to triangle anomalies, including three right handed neutrinos make the model anomaly free. Therefore, including additional heavy fermions for realising successful Dirac leptogenesis introduces new anomalies as well. In this section, we briefly discuss one such possibility where the anomalies introduced by heavy chiral fermions required for Dirac leptogenesis as well as dark matter cancel among themselves leading to an anomaly free scenario.

Sticking to a minimal setup, we consider two heavy Majorana fermions N_R, sufficient to produce non-vanishing CP asymmetry. Since we do not want to violate lepton number by two units, therefore, we assign $B - L$ charge $-3/2$ each to N_R, as earlier. This is just a choice for numerical calculations, any other $B - L$ gauge charge for N_R will not change our results drastically, as long as we can ensure Dirac nature of light neutrinos. In order to make it couple to usual leptons, we introduce another Higgs doublet η having $B - L$ charge $-1/2$ and its neutral component does not acquire any VEV. A singlet scalar ϕ_1 having $B-L$ charge 3 is introduced in order to give mass to N_R after spontaneous gauged $B-L$ symmetry breaking. However, the introduction of these two heavy Majorana fermions again gives rise

Particles	$SU(3)_c \times SU(2)_L \times U(1)_Y \times U(1)_{B-L}$
$q_L = \begin{pmatrix} u_L \\ d_L \end{pmatrix}$	$(3, 2, \frac{1}{6}, \frac{1}{3})$
u_R	$(3, 1, \frac{2}{3}, \frac{1}{3})$
d_R	$(3, 1, -\frac{1}{3}, \frac{1}{3})$
$\ell_L = \begin{pmatrix} \nu_L \\ e_L \end{pmatrix}$	$(1, 2, -\frac{1}{2}, -1)$
e_R	$(1, 1, -1, -1)$
ν_R	$(1, 1, 0, -1)$
N_{R1}	$(1, 1, 0, -3/2)$
N_{R2}	$(1, 1, 0, -3/2)$
χ_L	$(1, 1, 0, \frac{9}{4})$
χ_R	$(1, 1, 0, \frac{5}{4})$
ψ_L	$(1, 1, 0, -\frac{15}{8})$
ψ_R	$(1, 1, 0, \frac{17}{8})$

Table 4.1: Fermion Content of the Model

to triangle anomalies as

$$\begin{aligned} \mathcal{A}_1\left[U(1)^3_{B-L}\right] &= 54/8 \\ \mathcal{A}_2\left[(\text{gravity})^2 \times U(1)_{B-L}\right] &= 3. \end{aligned} \tag{4.13}$$

These anomalies can be cancelled after introducing four chiral fermions $\chi_L, \chi_R, \psi_L, \psi_R$ having $B-L$ charges $9/4, 5/4, -15/8, 17/8$ respectively. This can be seen as

$$\begin{aligned} \mathcal{A}_1\left[U(1)^3_{B-L}\right] &= \left(\frac{9}{4}\right)^3 + \left(-\frac{5}{4}\right)^3 + \left(-\frac{15}{8}\right)^3 + \left(-\frac{17}{8}\right)^3 = -54/8 \\ \mathcal{A}_2\left[(\text{gravity})^2 \times U(1)_{B-L}\right] &= \left(\frac{9}{4}\right) + \left(-\frac{5}{4}\right) + \left(-\frac{15}{8}\right) + \left(-\frac{17}{8}\right) = -3 \end{aligned} \tag{4.14}$$

While this solution is not unique, we stick to this minimal solution which leads to the desired phenomenology without requiring arbitrarily large $B-L$ charges or more chiral fermions than the above-mentioned ones. One can also pursue non-minimal scenarios which can explain tiny Dirac neutrino masses dynamically, as done in earlier works [174,241,243–281,304]. We, however, stick to the minimal way of generating Dirac neutrino masses from SM Higgs at the cost of fine-tuned Dirac Yukawa coupling.

The fermion and scalar content of the model are shown in table 4.1 and 4.2 respectively. The necessity of the individual scalar fields will be discussed later.

The relevant Yukawa Lagrangian is

$$\mathcal{L}_Y \supset Y_D \bar{L}\tilde{H}\nu_R + Y_\eta \bar{L}\tilde{\eta}N_R + Y_N \phi_1 N_R N_R + Y_\chi \bar{\chi_L}\chi_R\phi_3 + Y_\psi \bar{\psi}_L \psi_R \phi_2^\dagger + \text{h.c.} \tag{4.15}$$

Here also, Dirac leptogenesis may occur through out-of-equilibrium decay of N_R's. There are several DM candidates here in terms of χ, ψ, η.

Particles	$SU(3)_c \times SU(2)_L \times U(1)_Y \times U(1)_{B-L}$
$H = \begin{pmatrix} H^+ \\ H^0 \end{pmatrix}$	$(1, 2, \frac{1}{2}, 0)$
$\eta = \begin{pmatrix} \eta^+ \\ \eta^0 \end{pmatrix}$	$(1, 2, \frac{1}{2}, -\frac{1}{2})$
ϕ_1	$(1, 1, 0, 3)$
ϕ_2	$(1, 1, 0, 4)$
ϕ_3	$(1, 1, 0, 1)$

Table 4.2: Scalar content of the Minimal Model

The gauge invariant scalar interactions described by $\mathcal{L}_{scalar}$ can be written as

$$\begin{aligned}\mathcal{L}_{scalar} = &\left(D_{H\mu}H\right)^\dagger \left(D_H{}^\mu H\right) + \left(D_{\eta_\mu}\eta\right)^\dagger \left(D_\eta{}^\mu \eta\right) + \sum_{i=1}^{3}\left(D_{\phi_i\,\mu}\phi_i\right)^\dagger \left(D_{\phi_i}{}^\mu \phi_i\right) - \Big\{ -\mu_H^2|H|^2 \\ &+ \lambda_H|H|^4 + \left(\mu_\eta^2|\eta|^2 + \lambda_\eta|\eta|^4\right) + \sum_{i=1,2,3}\left(-\mu_{\phi_i}^2|\phi_i|^2 + \lambda_{\phi_i}|\phi_i|^4\right) + \lambda_{H\eta}(\eta^\dagger\eta)(H^\dagger H) \\ &+ \lambda'_{H\eta}(\eta^\dagger H)(H^\dagger \eta) + \sum_{i=1,2,3}\lambda_{H\phi_i}(\phi_i^\dagger\phi_i)(H^\dagger H) + \sum_{i=1,2,3}\lambda_{\eta\phi_i}(\eta^\dagger\eta)(\phi_i^\dagger\phi_i) \\ &+ \lambda_{12}(\phi_1^\dagger\phi_1)(\phi_2^\dagger\phi_2) + \lambda_{13}(\phi_1^\dagger\phi_1)(\phi_3^\dagger\phi_3) + \lambda_{23}(\phi_2^\dagger\phi_2)(\phi_3^\dagger\phi_3) \\ &+ \left(\mu_\phi\phi_1\phi_2^\dagger\phi_3 + \text{h.c.}\right)\Big\} \end{aligned} \tag{4.16}$$

Where $D_H{}^\mu$, $D_\eta{}^\mu$ and $D_\phi{}^\mu$ denote the covariant derivatives for the scalar doublets H, η and scalar singlets ϕ_i respectively and can be written as

$$\begin{aligned} D_{H\mu}\,H &= \left(\partial_\mu + i\,\frac{g}{2}\,\sigma_a\,W_\mu^a + i\,\frac{g'}{2}\,B_\mu\right)H\,, \\ D_{\eta_\mu}\,\eta &= \left(\partial_\mu + i\,\frac{g}{2}\,\sigma_a\,W_\mu^a + i\,\frac{g'}{2}\,B_\mu + i\,g_{BL}\,n_\eta Z_{BL\mu}\right)\eta\,, \\ D_{\phi_\mu}\,\phi_i &= \left(\partial_\mu + i\,g_{BL}\,n_{\phi_i} Z_{BL\mu}\right)\phi_i\,. \end{aligned} \tag{4.17}$$

where g_{BL} is the new gauge coupling and n_η and n_{ϕ_i} are the charges under $U(1)_{B-L}$ for η and ϕ_i respectively. After both $B-L$ and electroweak symmetries get broken by the VEVs of H and ϕ_is the doublet and all three singlets are given by

$$H = \begin{pmatrix} H^+ \\ \dfrac{h' + v + iz}{\sqrt{2}} \end{pmatrix}\,, \quad \eta = \begin{pmatrix} \eta^+ \\ \dfrac{\eta'_R + i\eta'_I}{\sqrt{2}} \end{pmatrix}\,, \quad \phi_i = \frac{s'_i + u_i + A'_i}{\sqrt{2}} \;\; (i = 1,\, 2,\, 3)\,, \tag{4.18}$$

The details of the scalar mass spectrum can be found in Appendix C.1.

Since none of the scalar field acquiring non-zero VEV has $B-L$ charge ± 2, there is no possibility of generating Majorana light neutrino masses. However, out-of-equilibrium decay

$N_R \to L\eta$ can give rise to non-zero CP asymmetry in a way similar to vanilla leptogenesis, as seen from Fig.4.1. However, the corresponding Yukawa couplings do not play any role in neutrino mass generation and hence are unconstrained. This allows the possibility of low scale leptogenesis that too with Dirac neutrinos. Additionally, the model also offers several dark matter candidates in terms of η, χ, ψ. Out of them, the scalar doublet can not give rise to desired DM phenomenology due to large direct detection cross section mentioned earlier. Therefore, we keep its mass fixed at benchmark values where its relic abundance is sub-dominant.

Similar to the proposal in [296], one can also generate light Dirac neutrino mass by a neutrinophillic Higgs doublet which gets induced VEV after EWSB. An additional Z_2 symmetry was introduced in addition to $U(1)_{B-L}$ gauge symmetry. However, we stick to this minimal field content at the cost of fine-tuned Yukawa couplings. The conclusions reached here will not change significantly if we adopt such non-minimal scenarios. Additionally, generation of lepton asymmetry in our proposal is different from earlier works on Dirac leptogenesis. For example, in [296] the CP asymmetry was generated by scalar singlet decay into right handed neutrinos ν_R through $\Delta(B-L) = 4$ process. The lepton asymmetry in ν_R then gets transferred to the left sector via Yukawa interactions with the neutrinophillic Higgs doublet. This is in a way complementary to the proposal in [282, 283] where an equal and opposite amount of lepton asymmetry were generated in right and left sectors (vanishing net lepton number violation) which were prevented from equilibration by virtue of tiny Dirac Yukawa couplings. On the other hand, in our proposal, leptogenesis remains very similar to vanilla leptogenesis except for the fact that the couplings involved do not play any role in neutrino mass generation and we do not have $\Delta(B-L) = 2$ processes. Additional advantage is that the model also predicts stable dark matter candidates in terms of additional chiral fermions added to cancel chiral anomalies.

Thermal dark matter in gauged $B-L$ model has been discussed by several authors, see [138, 171, 173, 174, 328–333] for example. If we consider SM singlet fermions with non-trivial $B-L$ charges to be DM candidates, the only interaction between DM and SM particles is the $B-L$ gauge interactions [1]. In order to calculate thermal averaged cross sections as well as relic abundance numerically, we use the package `micrOMEGAs` [235] where the necessary model information have been provided using package `FeynRules` [236]. Since DM interacts with the SM bath only via $B-L$ gauge portal interactions, relic abundance is typically satisfied only around the resonance regime $2m_{\rm DM} = M_{Z_{BL}}$. Note that the scalar doublet η is also stable and hence its neutral component can, in principle, be DM candidate as well. However, the neutral scalar and pseudoscalar components of η namely $\eta_R^{'}, \eta_I^{'}$ are degenerate and hence will lead to a large DM-nucleon scattering cross section (mediated by both Z and Z_{BL}) ruled out by direct detection experiments like XENON1T [89, 90]. The situation is similar to sneutrino DM in minimal supersymmetric standard model (MSSM) [334]. The only way to keep our model consistent with direct detection data is to choose η mass and other model parameters in such a way that leads to a sub-dominant contribution to DM. While scalar doublet DM has a mass regime giving rise to under-abundant relic abundance [122, 229], we find that usual SM portal interactions are not sufficient to keep relic abundance of η sub-

[1] Singlet scalars can also mediate DM-SM interactions due to their mixing with the SM Higgs. However, we neglect such scalar portal interactions in order to obtain maximum constraints on $B-L$ gauge sector.

dominant in required amount. Interestingly, it turns out that the under-abundance criteria for η also restricts the $B-L$ gauge sector parameters. In fact, η abundance decreases sharply, once $\eta\eta \longrightarrow Z_{BL}Z^*_{BL} \longrightarrow Z_{BL}f\bar{f}$ and $\eta\eta \longrightarrow Z_{BL}Z_{BL}$ open up. Therefore, we keep η mass above the required threshold ($M_{Z_{BL}}/2$) to allow at least one of these processes to contribute significantly to its thermal relic.

While the details of leptogenesis remain same as before, we incorporate additional constraints from required DM phenomenology here for the anomaly free $B-L$ model. The relevant interactions of extra chiral fermions can be written as

$$\begin{aligned}\mathcal{L}_{DM} = i\left[\bar{\chi_L}\not{D}(Q^L_\chi)\chi_L + \bar{\chi_R}\not{D}(Q^R_\chi)\chi_R + \bar{\psi_L}\not{D}(Q^L_\psi)\psi_L + \bar{\psi_R}\not{D}(Q^R_\psi)\psi_R +\right] - \\ (f_1\bar{\chi_L}\chi_R\phi_3 + f_2\bar{\psi_L}\psi_R\phi_2^\dagger + \text{h.c.})\end{aligned} \tag{4.19}$$

We now rewrite the above Lagrangian in the basis $\xi_1 = \chi_L + \chi_R$ and $\xi_2 = \psi_L + \psi_R$, identified as the two Dirac fermion DM candidates. In the basis of ξ_1 and ξ_2 , the above Lagrangian can be written as

$$\begin{aligned}\mathcal{L}_{\mathcal{DM}} = i\bar{\xi}_1\not{\partial}\xi_1 + i\bar{\xi}_2\not{\partial}\xi_2 - g_{BL}\left(\frac{9}{4}\right)\bar{\xi}_1\not{Z}_{B-L}P_{\rm L}\xi_1 - g_{BL}\left(\frac{-15}{8}\right)\bar{\xi}_2\not{Z}_{B-L}P_{\rm L}\xi_2 \\ - g_{BL}\left(\frac{5}{4}\right)\bar{\xi}_1\not{Z}_{B-L}P_{\rm R}\xi_1 - g_{BL}\left(\frac{17}{8}\right)\bar{\xi}_2\not{Z}_{B-L}P_{\rm R}\xi_2 - f_1\bar{\xi}_1P_{\rm R}\xi_1\phi_3 \\ - f_1\bar{\xi}_1P_{\rm L}\xi_1\phi_3^\dagger - f_2\bar{\xi}_2P_{\rm R}\xi_2\phi_2^\dagger - f_2\bar{\xi}_2P_{\rm L}\xi_2\phi_2.\end{aligned} \tag{4.20}$$

Since we have two stable DM candidates i.e. ξ_1 and ξ_2 in this model comprising the dominant part of DM, the total relic abundance can be expressed as the sum of the individual candidates, $\Omega_{\rm DM}h^2 = \Omega_{\xi_1}h^2 + \Omega_{\xi_2}h^2$. Note that we focus particularly on $B-L$ gauge portal interactions of DM and accordingly show the parameter space satisfying total DM relic abundance in $g_{BL} - M_{Z_{BL}}$ plane of summary plot shown in Fig.4.8. We also found that the DM parameter space shown in Fig.4.8 survives the direct detection bounds from XENON1T experiment. To be more quantitative, all the blue dots in Fig.4.8 corresponds to correct total DM relic, dominantly from two fermion DM candidates and effective DM-nucleon cross section below XENON1T upper bound. The same points also correspond to sub-dominant η (at least four to five order of magnitudes suppressed compared to observed DM relic) and hence an acceptable DM-nucleon scattering rate. Interestingly, even though η's contribution to DM relic is negligible, its direct detection rate still lies within two to three order of magnitudes below XENON1T upper limit and should be accessible at future direct search experiments. For details of such multi-component Dirac fermion DM studies in gauge $B-L$ models, one may refer to [173, 174, 224]. Here we show only the final parameter space and compare it with the ones required for other desired phenomenology like leptogenesis and $\Delta N_{\rm eff}$.

In order to generate the summary plot of Fig.4.8, we randomly vary $M_{Z_{BL}}, g_{BL}$ in range 0.5 TeV $- 10$ TeV and $0.0001 - 10$ respectively. Then we define $m_\eta = M_{Z_{BL}} - \Delta M$, where we randomly vary the mass splitting as 0.5 TeV $< \Delta M < 0.5M_{Z_{BL}}$ so that the minimum value of η mass remains $M_{Z_{BL}}/2$ in order to allow its annihilation into at at least one on-shell Z_{BL}

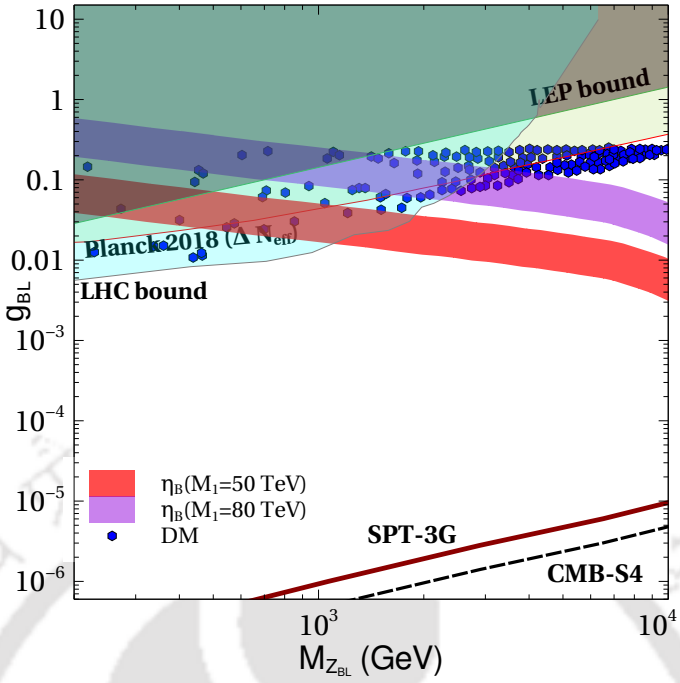

Figure 4.8: Summary plot showing allowed parameter space in $g_{BL} - M_{Z_{BL}}$ plane. In addition to the parameter space shown already in Fig.4.7, the allowed points from DM phenomenology are indicated by blue dots. The Yukawa couplings chosen for this scan are $(Y_\eta)_{\alpha 1} = 10^{-5}(1+i)$ and $(Y_\eta)_{\alpha 2} = 3 \times 10^{-1}(1.1 - i)$.

discussed earlier. Note that the scalar potential of the model still allows us to choose the mass of charged component of η to be much heavier while keeping the neutral components degenerate at m_η. Finally we select the points which satisfy the Planck 2018 relic bound for the total DM relic with each DM component satisfying direct detection bounds. Similarly, for the same variation of parameters, we check the parameter space giving rise to successful leptogenesis for two different scale of leptogenesis.

In the summary plot of Fig.4.8, we show the parameter space for successful leptogenesis with scale $M_1 = 50$ TeV, 80 TeV respectively. Also, for simplicity, we have considered the singlet scalars to be much heavier than DM as well as Z_{BL} so that the scalar portal interactions are sub-dominant. Including scalar portal interactions will widen up the DM parameter space further due to less dependence on gauge portal annihilations. Thus, as expected, one can achieve successful leptogenesis even with hierarchical heavy neutrinos as light as a few tens of TeV. This is particularly due to the fact that the Yukawa couplings as well as heavy fermion masses which dictate the dynamics of leptogenesis are decoupled from light neutrino mass generation in our model. In fact, the scale of leptogenesis can be as low as a TeV also, with smaller values of g_{BL}. However, this will not be sufficient to keep the abundance of η sub-dominant in order to keep its direct detection rate within limits.

We also show the bounds from collider experiments as well as Planck bound on $\Delta N_{\rm eff}$ at 2σ in the plot of Fig.4.8. Clearly, a large part of the parameter space satisfying correct DM phenomenology and leptogenesis criteria is disfavoured by these bounds. In fact, for

$M_1 = 50$ TeV, the common parameter space satisfying DM and leptogenesis criteria are ruled out while a small part of the parameter space for $M_1 = 80$ TeV still remains allowed. On the other hand, the currently allowed parameter space can be completely probed by future measurements of $\Delta N_{\rm eff}$ at upcoming CMB experiments, keeping the model testable at the near future.

CHAPTER 5

TeV scale leptogenesis with dark matter in non-standard cosmology

In this chapter, we study the consequence of some non-standard cosmological epochs in the early universe on the generation of baryon asymmetry through leptogenesis as well as dark matter abundance. One common feature of the BSM proposals for leptogenesis and DM is that both are high scale phenomena. While the generation of lepton asymmetry must occur before the electroweak scale $T \sim \mathcal{O}(100\,\text{GeV})$, WIMP DM having mass M_{DM} usually freezes out at temperature corresponding to $M_{\text{DM}}/T \sim \mathcal{O}(20-30)$. Both these temperatures correspond to radiation dominated era of standard ΛCDM cosmology. However, there is no experimental evidence to suggest that the universe was radiation dominated prior to the BBN era that is typically around 1 s after the big bang, corresponding to temperature of order $T \sim \mathcal{O}(1\,\text{MeV})$. Since the predictions of leptogenesis and DM freeze-out crucially depends upon the rate of expansion of the universe, the standard predictions can change significantly if the universe expands at a rate different from usual radiation dominated one. This can happen in two different ways, one in which there was an early matter dominated (EMD) phase and the other in which the universe is dominated by a component that redshifts faster than radiation often dubbed as a fast expanding universe (FEU). There have been several works considering the DM relic abundance calculation in such non-standard cosmologies [335–357]. Similarly, there have been some works studying leptogenesis with non-standard cosmologies. In [358], authors studied high scale type-I seesaw leptogenesis in a fast expanding universe. A relatively earlier work [359] considered the effects of non-standard cosmology (braneworld scenario and non-thermal production of right handed neutrinos from inflaton decay) on generation of lepton asymmetry in a TeV scale inverse seesaw model. Low scale leptogenesis in scalar-tensor theories of gravity was studied in [360] while the implications of such non-standard cosmology on DM relic were studied in several earlier works including [361–365]. Our work is different from both these two works due to the non- standard cosmological scenarios considered, different way of generating neutrino mass as well as connection to dark matter.

Our goal is to study popular scenarios of leptogenesis and dark matter and check if the scale of leptogenesis can be further lowered due to the presence of non-standard cosmological histories. This is motivating due to enhanced detection prospects for such low scale leptogenesis. We first study the impact of such non-standard cosmology on the parameter space

of minimal scotogenic model discussed earlier from the requirement of successful N_1 decay leptogenesis and scalar doublet DM. In the later half of this chapter, we consider a cogenesis scenario, popularly known as WIMPy leptogenesis and check the impact of non-standard cosmological histories.

5.1 A fast expanding universe

In this non-standard cosmological scenario, prior to the BBN era that is typically around 1 s after the big bang, the universe was dominated by some scalar field ϕ instead of usual radiation such that the energy density red-shifts with the scale factor a as follows

$$\rho_\phi \propto a^{-(4+n)}. \tag{5.1}$$

In the above expression, $n > 0$. Such a possibility (coined as fast expanding universe) where the energy density at early epochs redshifts faster than radiation leading to ϕ domination at early universe but negligible at later epochs was first discussed in the context of WIMP dark matter by the authors of [353]. This is also extended to non-thermal or freeze-in DM models in [354]. In the above expression, $n = 0$ corresponds to a universe similar to the usual radiation dominated universe.

The expansion rate of the universe, quantified by the Hubble parameter **H**, is controlled by the total energy density through the Friedmann equations. In FEU scenario where two different species populate the early universe, the total energy density in the very early epochs can be written as

$$\rho(T) = \rho_{\rm rad}(T) + \rho_\phi(T), \tag{5.2}$$

where the usual radiation energy density $\rho_{\rm rad}$ can be written as

$$\rho_{\rm rad} = \frac{\pi^2}{30} g_*(T)\, T^4. \tag{5.3}$$

If we consider the equation of state for the ϕ field to be $p_\phi = \omega_\phi \rho_\phi$ then Friedmann equation leads to $\rho_\phi \propto a^{-3(1+\omega_\phi)}$. Therefore, one can connect ω_ϕ and n by the relation $n = 3\omega_\phi - 1$. Here, we always consider $n > 0$, which implies that the ϕ energy always dominates over the radiation at early enough epochs. To express the energy density ρ_ϕ in terms of the radiation temperature, we consider that this new field ϕ does not have any interactions with SM particles and hence it only contribute to the energy density of the universe but not to the entropy density of the universe. This leads to the conservation of entropy in a comoving volume $S = sa^3$ =constant, where the entropy density reads the standard one,

$$s(T) = \frac{2\pi^2}{45} g_{*s}(T) T^3, \tag{5.4}$$

with g_{*s} being the effective relativistic degrees of freedom contributing to the entropy density. Taking the BBN constraints into account we argue that the equality between the energy density of ϕ and radiation must happen at a temperature $T_{\rm r} \gtrsim T_{\rm BBN}$. From Eq.(5.4) and scaling the Eq.(5.1) one can write ρ_ϕ in terms of temperature as

$$\rho_\phi(T) = \rho_\phi(T_{\rm r}) \left(\frac{g_{*s}(T)}{g_{*s}(T_{\rm r})}\right)^{(4+n)/3} \left(\frac{T}{T_{\rm r}}\right)^{4+n}. \tag{5.5}$$

Then the full energy density at any temperature reads

$$\rho(T) = \rho_{\rm rad}(T) + \rho_\phi(T) = \rho_{\rm rad}(T)\left[1 + \frac{g_*(T_r)}{g_*(T)}\left(\frac{g_{*s}(T)}{g_{*s}(T_{\rm r})}\right)^{(4+n)/3}\left(\frac{T}{T_{\rm r}}\right)^n\right]. \tag{5.6}$$

Considering $g_{*s}(T) = g_*(T)$ for most of the history of the universe the Hubble parameter can be calculated to be

$$\mathbf{H}(T) \simeq \frac{\pi g_*^{1/2}(T)T^2}{3\sqrt{10}M_{\rm Pl}}\left[1 + \left(\frac{g_*(T)}{g_*(T_{\rm r})}\right)^{(1+n)/3}\left(\frac{T}{T_{\rm r}}\right)^n\right]^{1/2}. \tag{5.7}$$

5.2 Early matter dominated universe

In this scenario, we consider an epoch in the early universe (prior to the BBN era) to be dominated by a matter component instead of a purely radiation dominated era of ΛCDM cosmology. The total energy density of the universe in this epoch was dominated by a scalar field ϕ, which behaves like an ordinary pressure-less matter, known as early matter dominated universe. In an EMD universe the energy density of the matter field ρ_ϕ falls with the expansion of the universe at a slower rate compared to the radiation energy density $\rho_{\rm rad}$ as long as ϕ does not decay. In principle ϕ can decay to both SM radiation and dark sector particles like DM. In the early universe the evolution of ρ_ϕ, the SM entropy density s, as well as the DM number density n are governed by the system of coupled Boltzmann equations [347]

$$\frac{d\rho_\phi}{dt} + 3(1+\omega)\mathbf{H}\rho_\phi = -\Gamma_\phi\rho_\phi, \tag{5.8}$$

$$\frac{ds}{dt} + 3\mathbf{H}s = \frac{\Gamma_\phi\rho_\phi}{T}\left(1 - b\frac{E}{m_\phi}\right) + 2\frac{E}{T}\langle\sigma v_{\rm rel}\rangle\left(n^2 - n_{\rm eq}^2\right), \tag{5.9}$$

$$\frac{dn}{dt} + 3\mathbf{H}n_{\rm DM} = \frac{b}{m_\phi}\Gamma_\phi\rho_\phi - \langle\sigma v_{\rm rel}\rangle(n^2 - n_{\rm eq}^2), \tag{5.10}$$

where $\langle\sigma v_{\rm rel}\rangle$ is the total DM annihilation cross-section into SM particles and $E^2 \simeq m^2 + 3T^2$ is the averaged energy per DM particle. Here, b is twice the branching ratio ϕ decaying into a couple of DM particles and thus b controls the proportion at which ϕ decays to SM radiation and DM. $\left(1 - b\frac{E}{m_\phi}\right)$ is the fraction of ϕ energy that goes into radiation. The second term on the RHS of Eq.(5.9) is the entropy injection due to DM annihilations which is subdominant compared to the first term and hence can be ignored. Also we assume that the branching ratio of ϕ decaying to DM particles is very small so that effectively $b = 0$. This simplifies the calculation of DM abundance very simple as it is governed by usual annihilation and coannihilation processes, similar to the WIMP paradigm. It also keeps the

model minimal. Eq.(5.9) plays an important role to track the temperature of the SM plasma through the entropy density s

$$s(T) = \frac{\rho_R + p_R}{T} = \frac{2\pi^2}{30} g_{*s}(T) T^3. \tag{5.11}$$

The evolution of the SM radiation temperature is given by

$$\frac{dT}{da} = \left(1 + \frac{T}{3g_{*s}} \frac{dg_{*s}}{dT}\right)^{-1} \left[-\frac{T}{a} + \frac{\Gamma_\phi \rho_\phi}{3\mathbf{H}sa}\left(1 - \frac{Eb}{m_\phi}\right) + \frac{2}{3}\frac{E\langle\sigma v_{\rm rel}\rangle}{\mathbf{H}sa}(n^2 - n_{\rm eq}^2)\right]. \tag{5.12}$$

In order not to alter the successful predictions of BBN in standard ΛCDM cosmology, the temperature at the end of the ρ_ϕ dominated phase has to be $T_{\rm end} \gtrsim 4$ MeV [366–368], where $T_{\rm end}$ is given by the total decay width Γ_ϕ as

$$T_{\rm end}^4 = \frac{90}{\pi^2 g_*(T_{\rm end})} M_{\rm Pl}^2 \Gamma_\phi^2. \tag{5.13}$$

Since we are not defining the specific interactions of ϕ with SM particles, its decay width can be kept as a free parameter for a model independent analysis. Therefore, this type of EMD universe can be characterised by two free parameters, $T_{\rm end}$ and $k = \left.\frac{\rho_\phi}{\rho_{\rm rad}}\right|_{a=a_0}$ as adopted by the authors of [347] for DM analysis. Before proceeding to analyse different scenarios in the context of leptogenesis and DM in an EMD universe, we show the evolution of radiation and ϕ energy densities as well as radiation temperature in Fig.5.1. Clearly, the energy density of ϕ evolves like usual matter until ϕ decays completely into radiation giving a sudden increase in radiation energy density. The effect of ϕ decay is also visible in the evolution of temperature as radiation temperature increases suddenly due to entropy injection from ϕ decay into radiation. The results also matches with the ones shown in [347].

5.3 Dark matter and leptogenesis from decay in non-standard cosmologies

In this section, we briefly discuss the model and summarise the details of dark matter and leptogenesis calculations in a standard cosmological scenario. In chapter 2 we already discussed the details of the minimal scotogenic model and therefore we avoid it in this chapter. Here we study the scalar DM scenario within the minimal scotogenic model where the lepton asymmetry is mainly generated from the decay of the lightest right handed neutrino (N_1). The N_1 leptogenesis with scalar DM is already studied in [113], where the authors have shown that the scale of leptogenesis can be $\mathcal{O}$ (10 TeV). We extend the same discussion in the fast expanding universe and early matter dominated universe scenarios.

5.3.1 Dark matter in standard cosmology

As pointed out earlier, the DM candidate in our model is one of the neutral components of the Z_2 odd scalar doublet η. By virtue of its SM gauge interactions, DM can be thermally

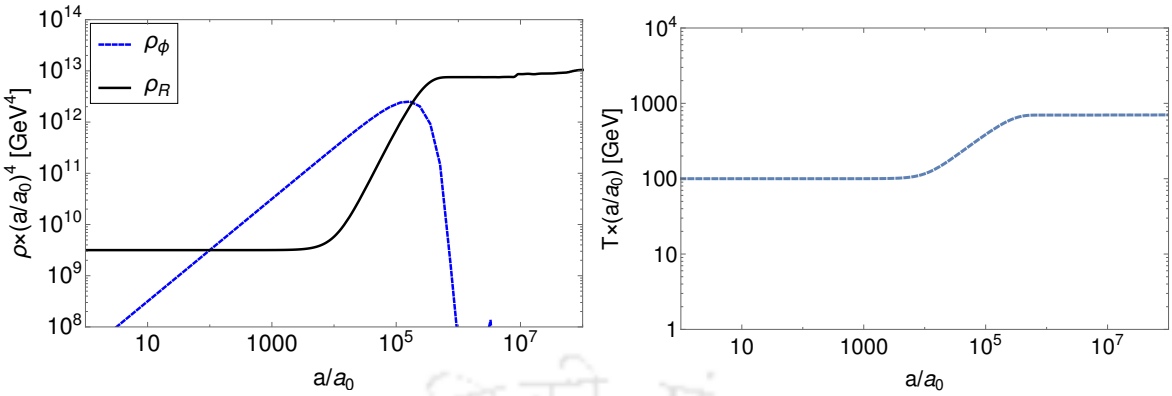

Figure 5.1: Evolution of the energy densities for radiation and the ϕ field (left panel), and evolution of radiation temperature T (right panel) as a function of scale factor a, for $\omega = 0$, $T_{\rm end} = 7 \times 10^{-3}$ GeV and $\dfrac{\rho_\phi(T = 100\text{GeV})}{\rho_{rad}(T = 100\text{GeV})} = 10^{-2}$. Here we assume that at $a = a_0$, $T = 100$ GeV.

produced in the early universe and hence give rise to a WIMP type scenario. Apart from gauge interactions, the Higgs portal interactions can also play a non-trivial role in generating thermal relic abundance.

For WIMP type DM which is produced thermally in the early universe, its thermal relic abundance can be obtained by solving the Boltzmann equation for the evolution of the DM number density $n_{\rm DM}$:

$$\frac{dn_{\rm DM}}{dt} + 3\mathbf{H}n_{\rm DM} \;=\; -\langle\sigma v\rangle\left[n_{\rm DM}^2 - (n_{\rm DM}^{\rm eq})^2\right], \tag{5.14}$$

where $n_{\rm DM}^{\rm eq}$ is the equilibrium number density of DM and $\langle\sigma v\rangle$ is the thermally averaged annihilation cross section, given by [136]

$$\langle\sigma v\rangle \;=\; \frac{1}{8m_{\rm DM}^4 T K_2^2\left(\frac{m_{\rm DM}}{T}\right)} \int_{4m_{\rm DM}^2}^{\infty} \sigma(s - 4m_{\rm DM}^2)\sqrt{s}\, K_1\left(\frac{\sqrt{s}}{T}\right) ds\,, \tag{5.15}$$

where $K_i(z)$'s are modified Bessel functions of order i. In the presence of coannihilation, one follows the recipe given by [137] to calculate the relic abundance. Apart from the gauge mediated coannihilations, there can be coannihilations due to lepton portal interactions as well, if the mass of η remain very close to that of N_1. We have used `micrOMEGAs` package [158] to calculate the freeze-out details of DM in our work.

5.3.2 Leptogenesis in standard cosmology

Successful leptogenesis is possible in this model due to the presence of heavy singlet neutrinos N_i whose out-of-equilibrium decay into SM leptons and η can generate the required non-zero lepton asymmetry [113, 121, 139–143]. In the hierarchical spectrum of $N_i, i = 1 - 3$ one can

significantly lower the usual Davidson-Ibarra bound to around 10 TeV [113, 143] without any need of resonance enhancement [54, 144]. Although $N_{2,3}$ decay can also generate lepton asymmetry, in principle, we consider the asymmetry generated by $N_{2,3}$ decay or any pre-existing asymmetry to be negligible due to strong washout effects mediated either by N_1 or $N_{2,3}$ themselves.

The details of CP asymmetry parameter ϵ_i, in right handed neutrino N_i decay in the minimal scotogenic model is already discussed in section 2.3 of chapter 2. The difference is, here we are looking for leptogenesis from the lightest right handed neutrino N_1, therefore it is important to define the decay parameter as

$$K_{N_1} = \frac{\Gamma_1}{\mathbf{H}(z=1)} \tag{5.16}$$

where Γ_1 is the N_1 decay width, $\mathbf{H}$ is the Hubble parameter and $z = M_1/T$ with T being the temperature of the thermal bath. Since leptogenesis occurs far above the electroweak scale where the universe was radiation dominated the Hubble expansion rate is expressed by Eq.(2.28) . The decay width Γ_1 can be calculated as

$$\Gamma_1 = \frac{M_2}{8\pi}(Y^\dagger Y)_{11}(1-\eta_1)^2. \tag{5.17}$$

Here Y denotes the Dirac Yukawa coupling of neutrinos $Y^N_{i\alpha}\overline{\ell_\alpha}\tilde{\eta}N_i$ in the scotogenic model. The frequently appearing $Y^\dagger Y$ is calculated using Casas-Ibarra parametrisation mentioned earlier in Eq.(2.30). Now, the Boltzmann equations for N_1 leptogenesis are given by [62]

$$\frac{dn_{N_1}}{dz} = -D_1(n_{N_1} - n^{\rm eq}_{N_1}), \tag{5.18}$$

$$\frac{dn_{\rm B-L}}{dz} = -\epsilon_1 D_1(n_{N_1} - n^{\rm eq}_{N_1}) - W^{\rm Total} n_{\rm B-L}, \tag{5.19}$$

where $n^{\rm eq}_{N_1} = \frac{z^2}{2}K_2(z)$ is the equilibrium number density of N_1 (with $K_i(z)$ being the modified Bessel function of i-th kind). The quantity on the right hand side of the above equations

$$D_1 \equiv \frac{\Gamma_1}{\mathbf{H}z} = K_{N_1} z \frac{K_1(z)}{K_2(z)} \tag{5.20}$$

measures the total decay rate of N_1 with respect to the Hubble expansion rate, and similarly, $W^{\rm Total} \equiv \frac{\Gamma_W}{\mathbf{H}z}$ measures the total washout rate. The washout term is the sum of two contributions, i.e. $W^{\rm Total} = W_1 + W_{\Delta L}$, where the washout due to the inverse decays $\ell\eta$, $\bar{\ell}\eta^* \to N_1$ is given by

$$W_1 = W_{\rm ID} = \frac{1}{4}K_{N_1} z^3 K_1(z). \tag{5.21}$$

The other contribution to washout $W_{\Delta L}$ originates from scatterings which violate lepton number by $\Delta L = 1, 2$. The contribution from $\Delta L = 2$ scatterings $\ell\eta \leftrightarrow \bar{\ell}\eta^*$, $\ell\ell \leftrightarrow \eta^*\eta^*$ is given by [113]

$$W_{\Delta L=2} \simeq \frac{18\sqrt{10}\, M_{\rm Pl}}{\pi^4 g_\ell \sqrt{g_*} z^2 v^4}\left(\frac{2\pi^2}{\lambda_5}\right)^2 M_1 \bar{m}_\zeta^2, \tag{5.22}$$

where η_i, g_ℓ, and $\bar{m}_\zeta$ are same as defined in section 2.3 of chapter 2. Upon solving the above Boltzmann Eqs. (5.18) and (5.19) simultaneously, the final $B-L$ asymmetry $n^f_{\rm B-L}$ just before electroweak sphaleron freeze-out is converted into the observed baryon to photon ratio by the standard formula given in Eq.2.40.

Before studying the changes in leptogenesis results due to non-standard cosmological history, we first solve the above Boltzmann equations assuming a standard radiation dominated epoch. While more details can be found in earlier works [113, 143], we show the evolution of lepton asymmetry and number density of N_1 in Fig.5.2 for three different values of λ_5. As the number density of N_1 decreases due to its decay, the lepton asymmetry grows. The decrease in lepton asymmetry subsequently due to washout effects are clearly visible from left panel plot of Fig.5.2, where the parameter λ_5 plays a crucial role. For this as well as remaining calculations, the R matrix is chosen to have the following structure

$$R = \begin{pmatrix} \cos z & 0 & \sin z \\ 0 & 1 & 0 \\ -\sin z & 0 & \cos z \end{pmatrix} \tag{5.23}$$

where z is a complex angle with, $z_R = z_I = \sqrt{\dfrac{m_1}{2m_3}}$ [113]. We also consider normal ordering of light neutrino mass with vanishingly small lightest neutrino mass $m_1 = 10^{-13}$ eV. Effect of changing lightest neutrino mass on final asymmetry was investigated in earlier works mentioned above, we will discuss this in the context of non-standard cosmology in upcoming sections. To have an overall picture of leptogenesis in standard radiation dominated universe, we perform a numerical scan, the result of which is shown in Fig.5.3 which shows that the scale of leptogenesis M_1 can be as low as 7 TeV in this case. Similar results can be obtained for inverted ordering of light neutrino mass as well. We will compare the results of leptogenesis in non-standard cosmology in upcoming sections with the plot shown in Fig.5.3.

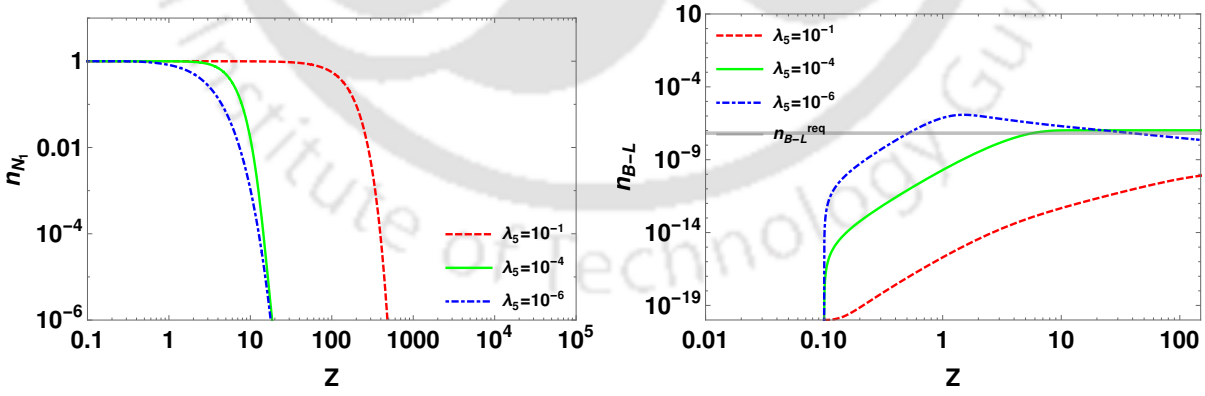

Figure 5.2: Comoving number densities of N_1 (left panel) and $B-L$ (right panel) respectively with $z = M_1/T$ for different benchmark parameters. The parameters used for this results are $M_1 = 10$ TeV, $m_1 = 10^{-13}$ eV, and $M_{i+1}/M_i = 10^{0.5}$.

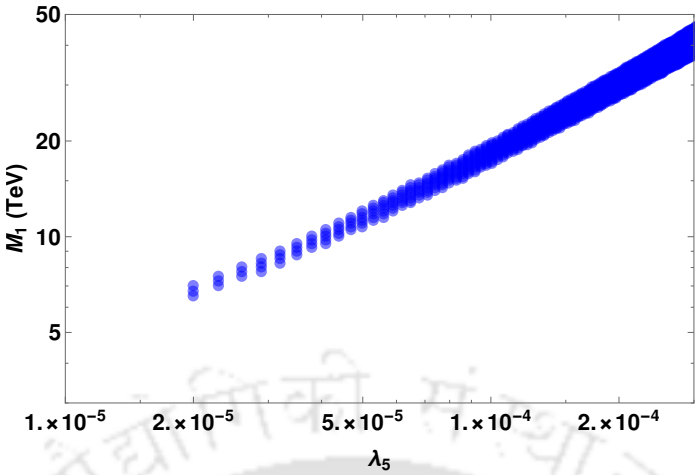

Figure 5.3: Parameter space in the $M_1 - \lambda_5$ plane that gives rise to observed baryon asymmetry in the standard radiation dominated universe. The parameters used for this results are $m_1 = 10^{-13}$ eV, and $M_{i+1}/M_i = 10^{0.5}$.

5.3.3 Dark matter in FEU

In a FEU scenario the Boltzmann equation to calculate the abundance of thermally produced DM is derived to be [353]

$$\frac{dn_{\rm DM}}{dz} = -A\frac{\langle\sigma v_{\rm rel}\rangle}{z^3 L\left[n, z, z_r\right]}\left[n_{\rm DM}^2 - (n_{\rm DM})_{\rm eq}^2\right], \tag{5.24}$$

where, $n_{\rm DM}$ is the comoving number density of DM and $z = m_{DM}/T$. The $\langle\sigma v_{rel}\rangle$ is the total annihilation cross-sectin of DM, $A = \dfrac{s(z=1)}{\mathbf{H}_{\rm rad}(z=1)} = \dfrac{2\sqrt{2}\pi}{3\sqrt{5}} g_*^{1/2} m_{\rm DM} M_{\rm Pl}$ and the function $L\left[n, z, z_r\right]$ has the form

$$L\left[n, z, z_r\right] = (n+4)\left[\frac{1}{z^4} + \left(\frac{g_*(z)}{g_*(z_r)}\right)^{(1+n)/3}\frac{z_r^n}{z^{n+4}}\right]^{3/2}\left[\frac{4}{z^5} + (4+n)\left(\frac{g_*(z)}{g_*(z_r)}\right)^{(1+n)/3}\frac{z_r^n}{z^{n+5}}\right]^{-1}. \tag{5.25}$$

In the limit $T \gg T_{\rm r}$ the Boltzmann equation reduces to

$$\frac{dn_{\rm DM}}{dz} = -A\frac{\langle\sigma v_{\rm rel}\rangle}{z^{2-n/2} z_r^{n/2}}\left[n_{\rm DM}^2 - (n_{\rm DM})_{\rm eq}^2\right]. \tag{5.26}$$

Borrowing this basic setup from [353] we first apply it to scalar doublet DM in our model. Note that, we do not ignore the sub-dominant radiation part in the calculation and use the most general Boltzmann equations to calculate DM relic. Similar to the earlier scenario, here also the annihilation cross sections of DM $\langle\sigma v_{\rm rel}\rangle$ are evaluated using `micrOMEGAs` package [158]. We first show the evolution of DM density in Fig.5.4 by choosing some benchmark values of DM parameters and for different integral values of n. The overall behaviour matches

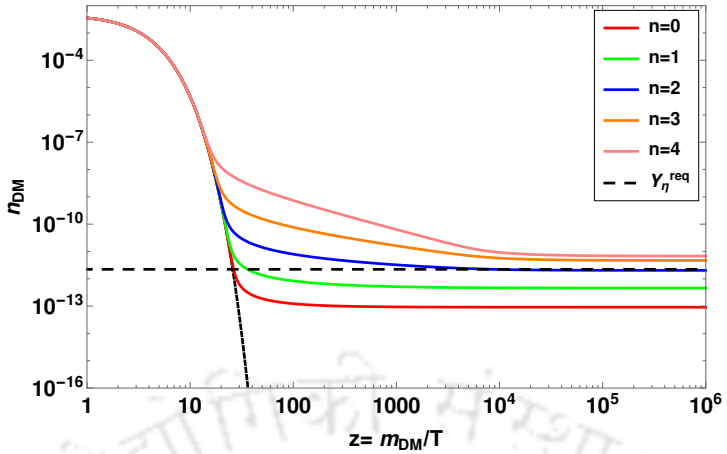

Figure 5.4: Comoving number density of DM (η) with z for different cosmological histories. The parameters used for this results are $m_{DM} = 200$ GeV, $m_{H_0} = 200.076$ GeV ($\lambda_5 = 0.0005$), $m_{H^\pm} = 205$ GeV, $T_r = 20$ MeV and $\lambda_L = 10^{-8}$. The black dashed line represents the required DM abundance with 200 GeV mass to satisfy the correct Planck 2018 limit on DM abundance [3].

with the model independent analysis of earlier work [353]. Clearly, with increase in the values of n, the final DM relic abundance increases. While for $n = 0$ or the usual radiation dominated universe, the DM remains under-abundant, $n = 2$ FEU scenario generates the correct DM abundance for same benchmark DM parameters. We therefore, choose DM parameters in such a way that the usual thermal relic remains under-abundant. This justifies the choice of DM mass 200 GeV which falls in the range of inert Higgs doublet DM mass $\in (80 - 550)$ GeV where thermal abundance in usual radiation dominated universe remains suppressed. Thus, FEU scenario provides another way of generating correct relic in this intermediate mass range of inert Higgs doublet DM. Other possibilities by invoking non-thermal contribution and multi-component DM scenario can be found in [229], [226] respectively.

5.3.4 Leptogenesis in FEU

After applying the basic recipe of FEU to the specific DM model we have, we now proceed to derive the Boltzmann equations for leptogenesis. The Boltzmann equation for leptogenesis in this scenario can be written as

$$\frac{dn_{N_1}}{dz} = -D_1^{'}(n_{N_1} - n_{N_1}^{\rm eq}), \tag{5.27}$$

$$\frac{dn_{\rm B-L}}{dz} = -\epsilon_1 D_1^{'}(n_{N_1} - n_{N_1^{eq}}) - W_{\rm Total}^{'} n_{\rm B-L}, \tag{5.28}$$

with the $z = M_1/T$ dependent quantities

$$D_1^{'} = K_{N_1} \frac{\kappa_1(z)}{\kappa_2(z)} \frac{1}{L\,[n, z, z_r]}, \tag{5.29}$$

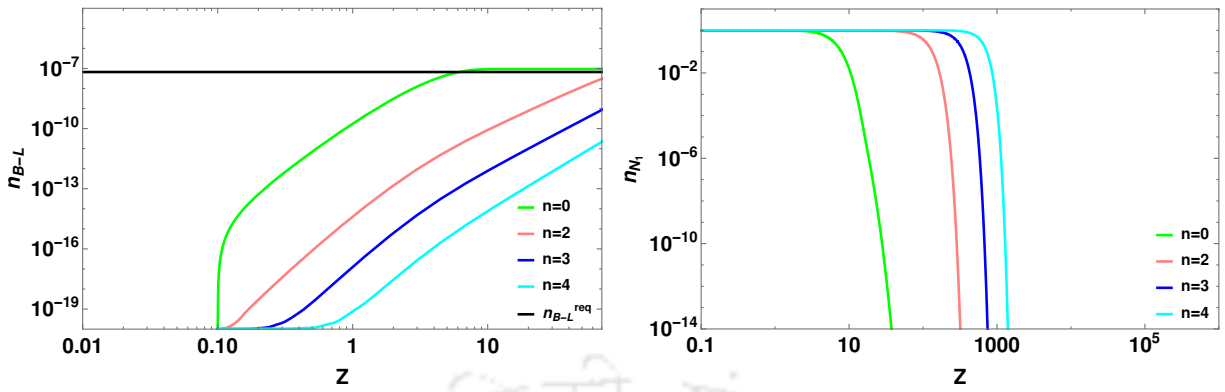

Figure 5.5: Evolution of comoving number density of $B-L$ with z for different values of n for FEU scenario (left panel), and evolution of the comoving number density of N_1 with z for different values of n for FEU scenario (right panel). Here we choose the parameters $m_1 = 10^{-13}$ eV, $M_1 = 10^4$ GeV, $M_{i+1}/M_i = 10^{0.5}$ and $\lambda_5 = 10^{-4}$ and $T_{\rm r} = 10$ MeV.

$$W^{'}_{\rm Total} = W^{'}_1 + \Delta W^{'}, \tag{5.30}$$

$$W^{'}_1 = \frac{1}{4} z^2 K_{N_1} \kappa_1(z) \frac{1}{L\left[n, z, z_r\right]}, \tag{5.31}$$

$$n_{N_1} = \frac{z^2}{2} \kappa_2(z). \tag{5.32}$$

Here the term $\Delta W^{'}$ is taking care about the washouts coming from the $\Delta L = 2$ scattering processes, $l\eta \longleftrightarrow \bar{l}\eta^*$ and $ll \longleftrightarrow \eta^*\eta^*$. This term can be calculated to be

$$\Delta W^{'} = \frac{36\sqrt{5} M_{\rm Pl}}{\pi^{1/2} g_l \sqrt{g_*} v^4} \frac{1}{z^3 L\left[n, z, z_r\right]} \frac{1}{\lambda_5^2} M_1 \bar{m_\zeta}^2. \tag{5.33}$$

Other parameters are defined in a way similar to the usual leptogenesis in scotogenic model discussed in section 5.3.2.

Using the equations derived above, we first show the evolution of lepton asymmetry and N_1 abundance for different values of n in Fig.5.5 by choosing some benchmark values of model parameters. Clearly, there is a delay in generation of asymmetry as well as depletion in N_1 abundance with increase in the values of n. Here, $n = 0$ or the standard cosmological scenario overproduces lepton asymmetry. In order to see the overall parameter space allowed from the requirement of generating correct baryon asymmetry, we fix $n = 2$ and perform a numerical scan over $M_1 - \lambda_5$ by keeping other model parameters fixed. The resulting parameter space is shown in Fig.5.6. While we are not showing scans for other possible values of n here, the overall behaviour is similar. For $n = 2$ and $T_{\rm r} = 20$ MeV the scale of leptogenesis gets pushed up to $M_1 = 40$ TeV. A more rigorous numerical scan can be performed to find the complete parameter space that can generate correct baryon asymmetry of the universe.

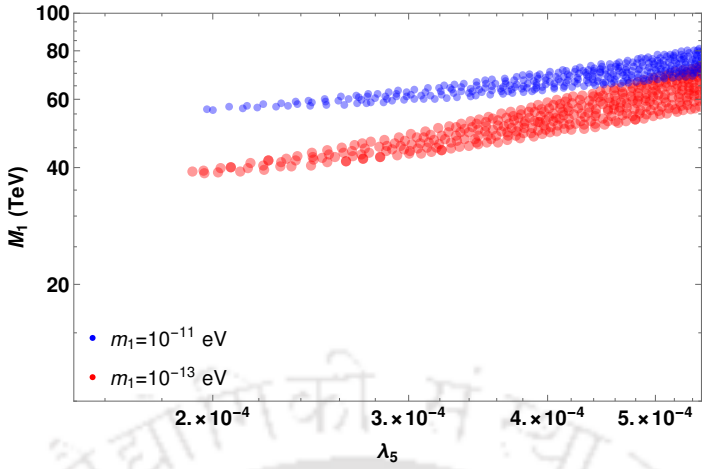

Figure 5.6: Parameter space in the $M_1 - \lambda_5$ plane giving rise to observed baryon asymmetry. The parameters used for this results are $n = 2$, $M_{i+1}/M_i = 10^{0.5}$ and $T_{\rm r} = 20$ MeV.

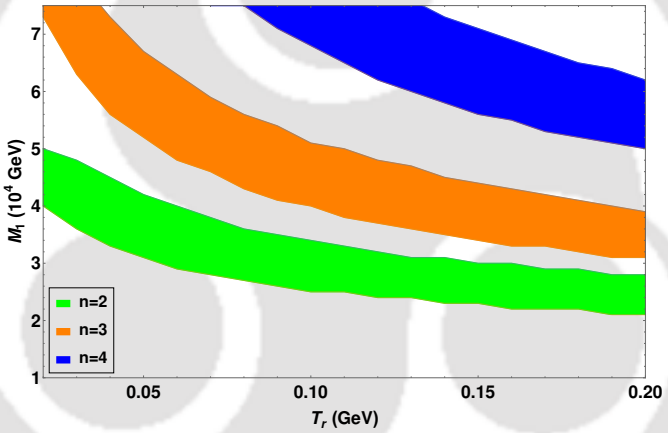

Figure 5.7: Parameter space in $M_1 - T_{\rm r}$ plane with different values of n for successful leptogenesis in FEU scenario. The parameters used for this result are $\lambda_5 = 0.0003$, and $m_1 = 10^{-13}$ eV.

We then constrain the cosmological parameters in FEU scenario from the requirement of producing the correct baryon asymmetry. We show it in $M_1 - T_{\rm r}$ plane for different values of n in Fig.5.7. We can see from this plot that for larger values n, we require large M_1 to satisfy the correct baryon asymmetry. Again for non-zero n, large $T_{\rm r}$ pushes the cosmological history at and below the scale of leptogenesis more towards usual radiation like, bringing down the scale of leptogenesis (as in the standard case discussed earlier).

5.3.5 Leptogenesis in EMD universe

Since the entropy per comoving volume of the universe is not constant in this case, we can no longer write the usual Boltzmann equations for leptogenesis in terms of the comoving number densities. Also, during the decay of the matter field finding an analytical relation between

time (t) and temperature (T) is not possible and therefore we can not write the Boltzmann equations in terms of the dimensionless variable $z = M_1/T$. Rather, it is convenient to write the equations in terms of the number N and the scale factor a. In such a case, the relevant Boltzmann equations are found to be

$$\frac{dN_{N_1}}{da} = -\frac{\langle\Gamma_1\rangle}{\mathbf{H}a}\left(N_{N_1} - N_{N_1}^{eq}\right), \tag{5.34}$$

$$\frac{dN_{\rm B-L}}{da} = \epsilon_1\frac{\langle\Gamma_1\rangle}{\mathbf{H}a}\left(N_{N_1} - N_{N_1}^{eq}\right) - \frac{W_{\rm ID}}{\mathbf{H}a}N_{\rm B-L} - \frac{\Delta W}{Ta}M_1 N_{\rm B-L}, \tag{5.35}$$

where we define the thermal decay width $\langle\Gamma_1\rangle$, the inverse decay term $W_{\rm ID}$, the $\Delta L = 2$ washout term ΔW, and the equilibrium number of N_1 in terms of temperature as follows,

$$\langle\Gamma_1\rangle = \Gamma_1\frac{\kappa_1(M_1/T)}{\kappa_2(M_1/T)}, \tag{5.36}$$

$$W_{\rm ID} = \frac{1}{4}\langle\Gamma_1\rangle\kappa_1\left(M_1/T\right), \tag{5.37}$$

$$\Delta W = \frac{36\sqrt{5}M_{\rm Pl}}{\pi^{1/2}g_l\sqrt{g_*}v^4}\left(\frac{T^2}{M_1}\right)\frac{1}{\lambda_5^2}\bar{m}_\xi^2, \tag{5.38}$$

$$N_{N_1}^{eq} = \frac{g_N}{2\pi^2}T^3\left(\frac{M_1}{T}\right)^2\kappa_2\left(M_1/T\right). \tag{5.39}$$

The Eqs.(5.34) and (5.35) have to be solved simultaneously with Eqs.(5.8) and (5.12) which we rewrite as

$$\frac{d\rho_\phi}{da} = -\frac{\Gamma_\phi}{a\mathbf{H}}\rho_\phi - 3\frac{\rho_\phi}{a}, \tag{5.40}$$

$$\frac{dT}{da} = \left(1 + \frac{T}{g_{*s}}\frac{dg_{*s}}{dT}\right)^{-1}\left[-\frac{T}{a} + \frac{\Gamma_\phi\rho_\phi}{3\mathbf{H}as(T)}\right] \tag{5.41}$$

respectively. The Boltzmann equation for DM, Eq.(5.10) is also solved simultaneously, the results of which will be discussed in upcoming section. Here the Hubble parameter, in general, is given by

$$\mathbf{H} = \sqrt{\frac{\rho_\phi(a) + \rho_{\rm rad}(a)}{3M_{\rm Pl}^2}}. \tag{5.42}$$

Here, the equation of state parameter for the matter field ω is taken to be zero and k is the ratio between ρ_ϕ and $\rho_{\rm rad}$ at the starting point $a = a_0$. It is important to mention here that we have solved the Bolztamnn equations from a temperature of $T = 10M_1$. We use the exact Hubble parameter in our numerical analysis. Depending upon equilibrium temperature of N_1 ($T_{\rm eq}$), the decay temperature of the ϕ field ($T_{\rm end}$) and the Sphaleorn freeze-out temperature ($T_{\rm sphaleron}$), we study three different cases below.

Case 1: $T_{\rm end} \ll T_{\rm sphaleron} \ll T_{\rm eq}$

Here, we have taken $T_{\rm end} = 10$ GeV such that the ϕ field decays after the sphaleron freeze-out temperature. The early matter domination gives rise to two kinds of effects in the evolution of $B - L$ asymmetry. The presence of the matter field enhances the Hubble expansion rate and also provides additional entropy into the plasma when it decays. These two effects are distinctly visible in the upper panel plots of Fig.5.8. For the chosen benchmark of cosmological parameters, the sphaleron freeze-out temperature corresponds to a scale factor $a/a_0 \simeq 7660$ and therefore we plot $n_{\rm B-L}$ up to a scale factor $a/a_0 \simeq 7660$ and η_B after that. In the upper left panel plot, it can be seen that with the increase in the ϕ field energy density the $B - L$ asymmetry increases. This is due to the fact that with the addition of extra energy density the Hubble expansion rate increases which leads to a larger deviation of the N_1 abundance from its equilibrium abundance leading to an increase in asymmetry. On the other hand, later, when the ϕ field decays it releases more entropy into the plasma with the increase in k leading to more entropy dilution of the asymmetry. This is clearly visible in the upper right panel plot of Fig.5.8.

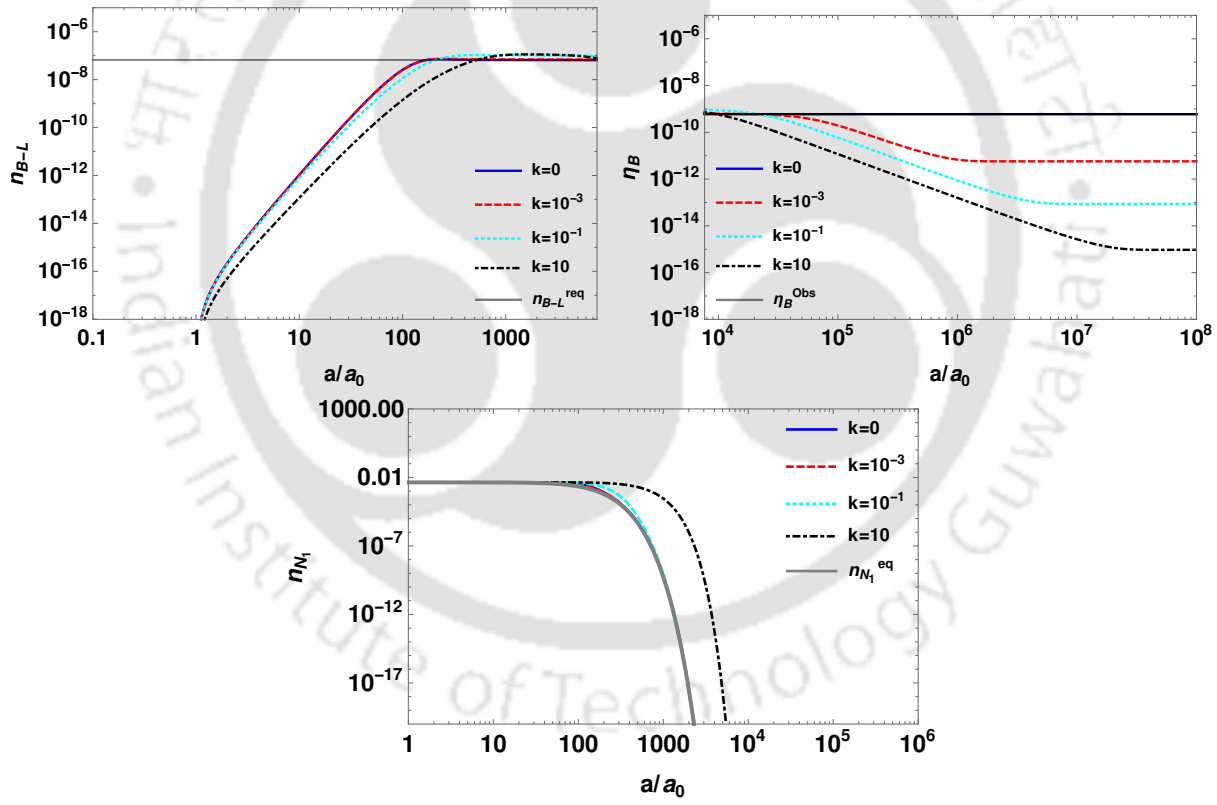

Figure 5.8: Evolution of $n_{\rm B-L}$ (Upper left panel), η_B (Upper right panel) and n_{N_1} (lower panel) with a/a_0 in EMD universe (Case 1). The parameters used for these plots are $m_1 = 10^{-13}$ eV, $M_1 = 2 \times 10^4$ GeV, $M_i/M_{i+1} = 10^{0.5}$, $\lambda_5 = 10^{-4}$ and $T_{\rm end} = 10$ GeV.

We then perform a parameter scan over the parameters λ_5 and M_1 and show the viable parameter space in Fig.5.9. It can be seen that even with a very small initial value of ρ_ϕ the

scale of leptogenesis is pushed up to $\mathcal{O}(10^8)$ GeV. This is due to the strong entropy dilution coming from the decay of the ϕ field. To get the correct asymmetry after entropy dilution, one needs to generate a large amount of asymmetry prior to the decay of ϕ. This can be understood from the evolution plots of $n_{\rm B-L}$ and η_B in Fig.5.8. From Fig.5.9 one can see that for $k = 10^{-4}$ we need larger values of M_1 to satisfy the observed asymmetry compared to $k = 10^{-5}$. This is expected as the entropy dilution will be more for $k = 10^{-4}$ compared to that for $k = 10^{-5}$. The lowest possible scale of leptogenesis is found out to be $M_1 \simeq 1.5 \times 10^8$ GeV for $k = 10^{-4}$ and $M_1 \simeq 5 \times 10^7$ GeV for $k = 10^{-5}$ in case of $T_{\rm end} = 10$ GeV.

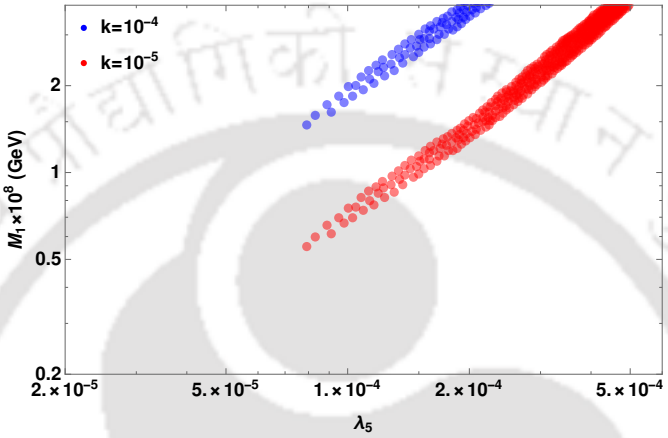

Figure 5.9: Scan plot in $\lambda_5 - M_1$ plane for case 1 with $T_{\rm end} = 10$ GeV. The other important parameters are fixed at $m_1 = 10^{-13}$ eV and $M_{i+1}/M_i = 10^{0.5}$.

Case 2: $T_{\rm sphaleron} \lesssim T_{\rm end} \ll T_{\rm eq}$

In the previous case, we found that keeping $T_{\rm end}$ much below $T_{\rm sphaleron}$ leads to significant dilution of lepton asymmetry resulting in negligible baryon asymmetry after sphaleron transitions. Therefore, we now choose $T_{\rm end} = 150$ GeV such that it is much closer to $T_{\rm sphaleron}$ and show the results in Fig.5.10. Here $T_{\rm sphaleron}$ corresponds to a scale factor $a/a_0 \simeq 1 \times 10^4$, and therefore we show $n_{\rm B-L}$ up to that epoch and η_B after that. The similar effect of the modified Hubble expansion rate can be seen similar to Fig.5.8 in case 1. However, here the entropy dilution is occurring much earlier compared to case 1. This is expected as we keep $T_{\rm end} = 150$ GeV in this case. Comparing the $B - L$ evolution plot in Fig.5.10 with that of Fig.5.8 it can be seen that, the entropy dilution in case 2 is less compared to case 1. This is expected as the ϕ field is decaying at a time when the universe is much hotter compared to case 1. However, the entropy dilution is significant enough to dilute the generated asymmetry.

Similar to case 1, we show the viable parameter space in $\lambda_5 - M_1$ plane in Fig.5.11. Here, we see the similar push of the leptogenesis scale due to entropy dilution. However, the scale of leptogenesis is slightly lower than case 1. This is expected as the entropy dilution should be weaker for $T_{\rm end} = 150$ GeV compared to $T_{\rm end} = 10$ GeV. However, the scale of leptogenesis is still significantly higher $\mathcal{O}$ (10^7 GeV), compared to that in standard radiation case $\mathcal{O}$ (10 TeV). In particular, it is found that the scale of leptogenesis can be as low as $M_1 \simeq 5.5 \times 10^7$ GeV for $k = 10^{-4}$ and $M_1 \simeq 1.8 \times 10^7$ GeV for $k = 10^{-5}$ in case of $T_{\rm end} = 150$ GeV.

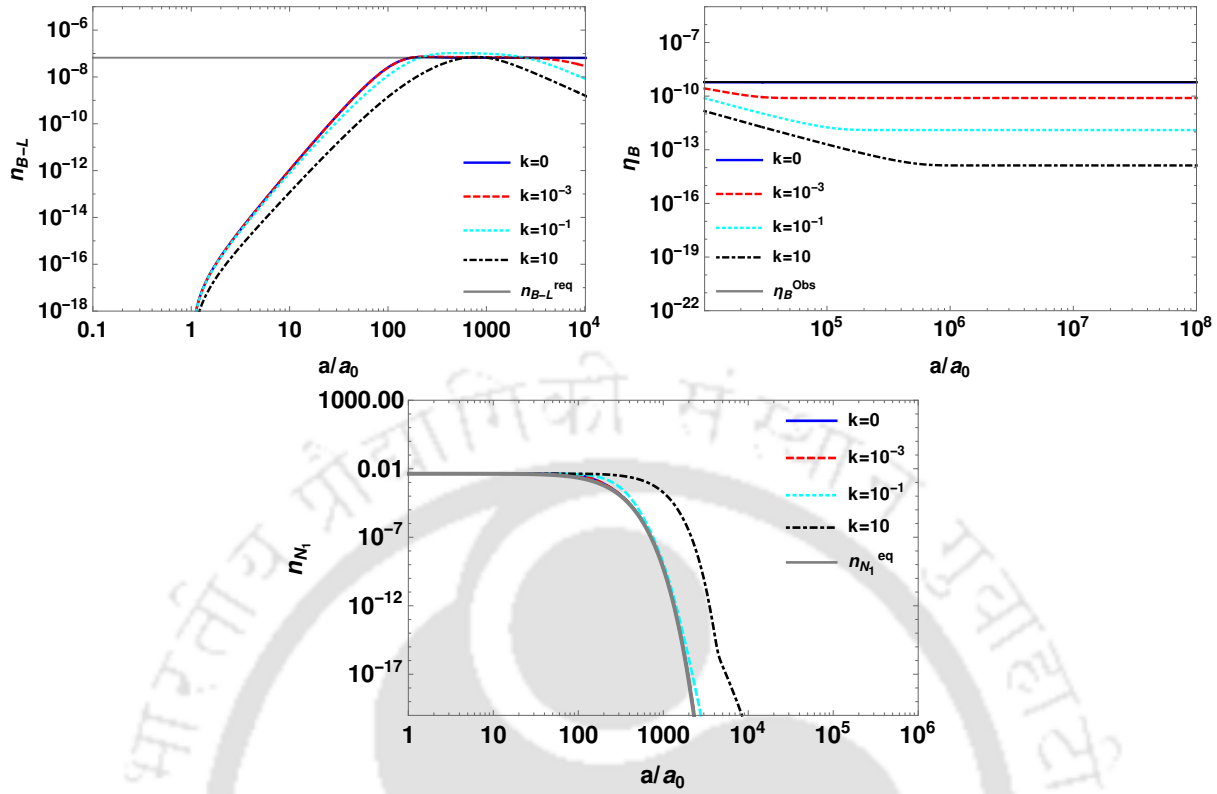

Figure 5.10: Evolution of $n_{\mathrm{B-L}}$ (Upper left panel), η_B (Upper right panel) n_{N_1} (lower panel) with a/a_0 in EMD universe (Case 2). The parameters used for these plots are $m_1 = 10^{-13}$ eV, $M_1 = 2 \times 10^4$ GeV, $M_i/M_{i+1} = 10^{0.5}$, $\lambda_5 = 10^{-4}$ and $T_{\mathrm{end}} = 150$ GeV.

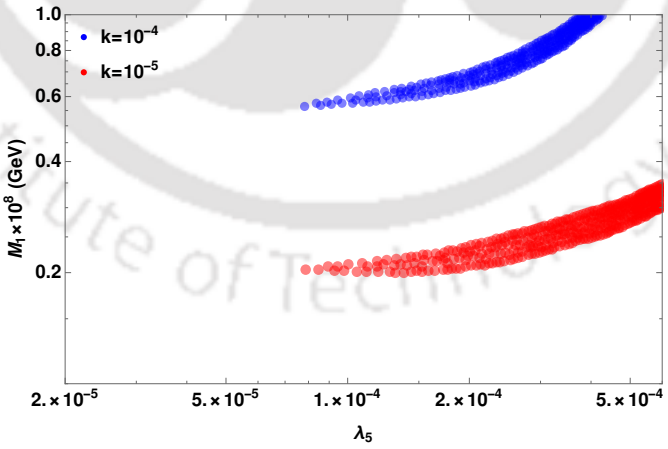

Figure 5.11: Scan plot in $\lambda_5 - M_1$ plane for case 2 with $T_{\mathrm{end}} = 150$ GeV. The other important parameters are fixed at $m_1 = 10^{-13}$ eV and $M_{i+1}/M_i = 10^{0.5}$.

Case 3: $T_{\rm sphaleron} \ll T_{\rm end} \lesssim T_{\rm eq}$

We further increase $T_{\rm end}$ and consider the scenario where $T_{\rm end} \lesssim T_{\rm eq}$. For that we keep $T_{\rm end} = 5 \times 10^5$ GeV and show the results in Fig.5.12. Here $T_{\rm sphaleron}$ corresponds to a scale factor $a/a_0 = 7600$, and therefore we have shown the evolution plot of $n_{\rm B-L}$ up to the scale factor $a/a_0 = 7600$ and don't show the evolution of η_B since the ϕ field decays much earlier to that. In Fig.5.12 it can be seen that the entropy dilution happens much earlier and it also impacts the number density of N_1. For sufficiently large values of k the increase in entropy dilutes the number density of the RHN N_1 below its equilibrium number density ($n_{N_1}^{eq}$). This results in a negative asymmetry and after the end of entropy dilution the N_1 become overabundant making the $B-L$ asymmetry positive. We plot the absolute values of $n_{\rm B-L}$ in the left panel plot of Fig.5.12. The kinks can be seen for $k = 10^{-1}$ and $k = 10$ because of the sign change of the $B-L$ asymmetry at the points when N_1 is becoming overabundant. Interestingly, for $T_{\rm end} \lesssim T_{\rm eq}$ scenario, we can have more asymmetry generation compared to the standard domination for small values of k. It is because, for small values of k, the increases in Hubble expansion rate can be the dominant factor in determining the asymmetry compared to the entropy dilution. For example, the red dashed line corresponds to $k = 10^{-3}$ and $T_{\rm end} = 5 \times 10^5$ GeV in the left panel plot of Fig.5.12 goes slightly above the blue solid line corresponds to the asymmetry in standard radiation case. However, this increase in asymmetry is found to be very small and would not change the results of leptogenesis from the standard radiation case. Therefore we can conclude that for sufficiently large values of $T_{\rm end}$ the leptogenesis results would converge with the results of standard cosmology.

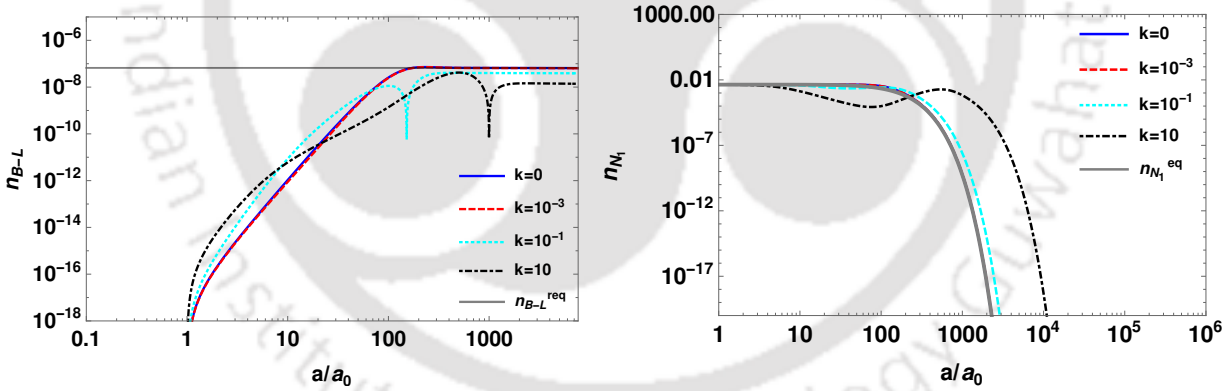

Figure 5.12: Evolution of $n_{\rm B-L}$ (Left panel), and n_{N_1} (Right panel) with a/a_0 in EMD universe (Case 3). The parameters used for these plots are $m_1 = 10^{-13}$ eV, $M_1 = 2 \times 10^4$ GeV, $M_i/M_{i+1} = 10^{0.5}$, $\lambda_5 = 10^{-4}$ and $T_{\rm end} = 5 \times 10^5$ GeV.

In Fig.5.13 we show the viable parameter space in $\lambda_5 - M_1$ plane for $k = 10^{-5}$ and $k = 10^{-1}$ with $T_{\rm end} = 5 \times 10^5$ GeV. It can be noticed that for $k = 10^{-5}$ the parameter space remains the same as that in standard cosmology. This is expected as for such a small value of k and a high value of $T_{\rm end}$ the effect of the matter field becomes very minimal and hence the leptogenesis result converges to the standard cosmology result. For $k = 10^{-1}$ the parameter space shifts towards the higher values of M_1. However, the change of the scale of

leptogenesis with k is small compared to case 1 and case 2. Even for $k = 10^{-1}$ the lowest possible scale of leptogenesis can be around $M_1 \simeq 10$ TeV.

Finally, in Fig.5.14 we show the viable parameter space in $k - T_{\rm end}$ plane by fixing the particle physics parameters at benchmark values. It is observed that with the increase of k one would require larger $T_{\rm end}$ values to satisfy the observed asymmetry. As higher values of k result in more entropy dilution, one needs to increase the $T_{\rm end}$ to compensate for it.

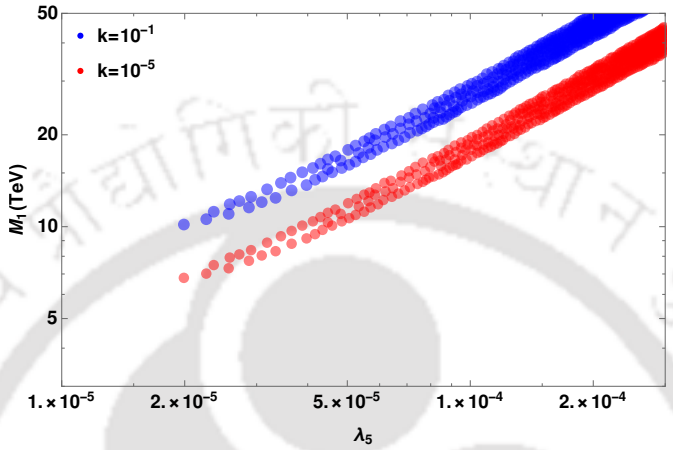

Figure 5.13: Scan plot in $\lambda_5 - M_1$ plane for case 3 with $T_{\rm end} = 5 \times 10^5$ GeV. The other important parameters are fixed at $m_1 = 10^{-13}$ eV and $M_{i+1}/M_i = 10^{0.5}$.

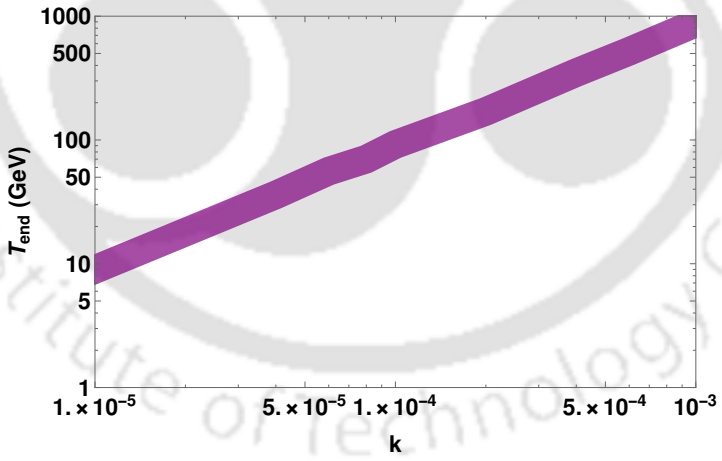

Figure 5.14: Scan plot showing the viable parameter space in $k - T_{\rm end}$ plane from the requirement of observed baryon asymmetry. The relevant parameters are fixed at $M_1 = 10.5 \times 10^7$ GeV, $M_{i+1}/M_i = 10^{0.5}$, $\lambda_5 = 10^{-4}$ and $m_1 = 10^{-13}$ eV.

5.3.6 Dark Matter in EMD universe

Although the calculation of DM relic abundance in the EMD universe has already been done, here we calculate it for the DM candidate specific to our model and corresponding to the

scenarios for leptogenesis discussed above. The relic abundance of DM can be calculated by solving the corresponding Boltzmann equation for the number of DM N_η,

$$\frac{dN_\eta}{da} = -\frac{\langle\sigma v\rangle_{\eta\eta\longrightarrow SMSM}}{\mathbf{H}a^4}\left[N_\eta^2 - (N_\eta)^2\right]. \tag{5.43}$$

Similar to leptogenesis we solve Eqs.(5.8), and (5.12) with Eq.(5.43) simultaneously to calculate the abundance of dark matter for benchmark values of DM mass and other relevant parameters. The annihilation cross sections of DM ($\langle\sigma v_{\eta\eta\longrightarrow SMSM}\rangle$) are evaluated using `micrOMEGAs` package [158], as mentioned before. We now consider three different scenarios adopted for leptogenesis earlier.

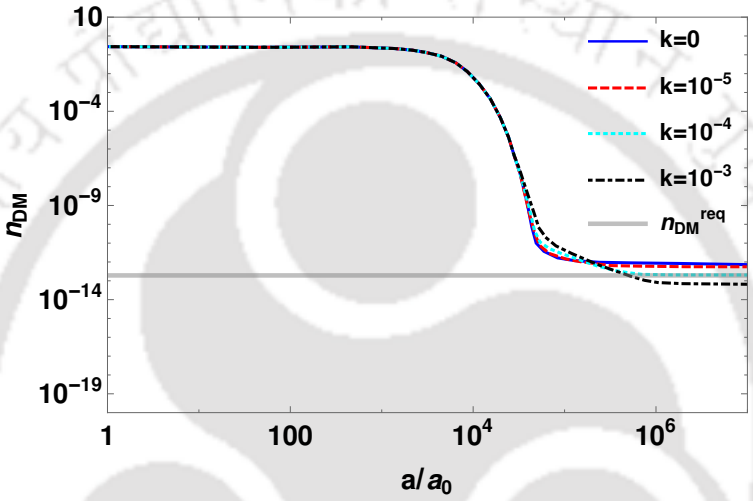

Figure 5.15: Evolution plot for the comoving number density of DM with scale factor for case 1 ($T_{\rm end} = 10$ GeV). The relevant parameters are fixed at $m_{\eta_R} = 2500$ GeV, $m_{\eta_I} = 2500.001$ GeV, $m_{\eta^\pm} = 2520$ GeV and $\lambda_L = 10^{-6}$.

The benchmark values are chosen in such a way that it also gives correct lepton asymmetry. For case 1 chosen for leptogensis we show the corresponding evolution of the comoving number density of DM in Fig.5.15. Similar to leptogenesis the two distinct effects of early matter domination are visible in DM abundance. With the increase in k the early deviation from the equilibrium abundance can be seen for $n_{\rm DM}$. This is due to the increase in Hubble expansion rate with the increase in k. On the other hand, with the increase in k the entropy dilution also increases leading to a suppression of $n_{\rm DM}$. Therefore to satisfy the correct DM relic in case 1 of EMD universe we need to fix the model parameters in a region where it is overabundant in standard cosmology. For case 2, we fix $T_{\rm end} = 150$ GeV and show the evolution plot of DM abundance in Fig.5.16. For the chosen values k, the entropy dilution is found out to be very minimal. It is due to the fact that we are fixing $T_{\rm end} = 150$ GeV which is far above the freeze-out temperature for a DM of mass 600 GeV. This is similar to the evolution plot of n_{N_1} in Fig.5.12 for case 3. For higher values of k, the entropy dilution effect will be dominant which will decrease the DM abundance below its equilibrium abundance, however, we don't choose such high values of k as it is not favourable from leptogenesis. Also, since the matter field decays much earlier than the freeze-out temperature the final abundance of

DM relic is found to be the same irrespective of k values. The DM mass and other important model parameters required to satisfy the correct relic for case 2 are similar to the standard radiation dominated universe. However, the difference occurs on the frreze-out epochs. After the decay of the matter field, the universe got heated up due to the entropy injection and then the temperature red-shifts as in the case of standard cosmology. Therefore for higher values of k the universe reaches the freeze-out temperature at later times leading to a delay in freeze-out.

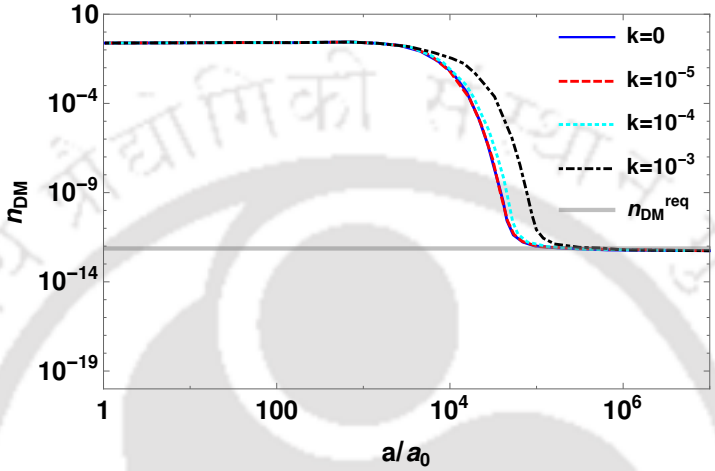

Figure 5.16: Evolution plot for the comoving number density of DM with scale factor for case 2 ($T_{\rm end} = 150$ GeV). The relevant parameters are fixed at $m_{\eta_R} = 550$ GeV, $m_{\eta_I} = 550.005$ GeV, $m_{\eta^\pm} = 551$ GeV and $\lambda_L = 10^{-6}$.

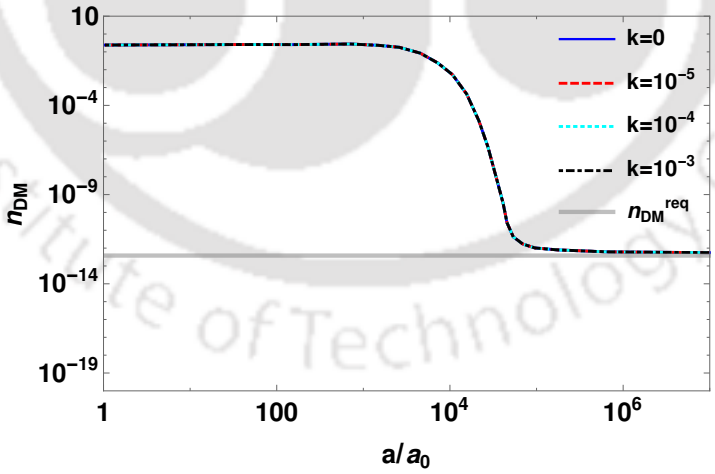

Figure 5.17: Evolution plot for the comoving number density of DM with scale factor for case 3 ($T_{\rm end} = 5 \times 10^5$ GeV). The relevant parameters are fixed at $m_{\eta_R} = 550$ GeV, $m_{\eta_I} = 550.005$ GeV, $m_{\eta^\pm} = 551$ GeV and $\lambda_L = 10^{-6}$.

In Fig.5.17 we show the evolution plot for case 3, keeping $T_{\rm end} = 5 \times 10^5$ GeV. It can be seen that for such large values of $T_{\rm end}$ the DM abundance follows the abundance in the usual

radiation-dominated universe irrespective of the value of k. If $T_{\rm end}$ is very large compared to the DM freeze-out abundance it will leave no information of the matter field on DM abundance. The temperature of the universe also red shifts enough to dilute the effect of entropy injection by the matter field. Therefore both DM and leptogenesis results converge with the standard radiation cosmology results.

5.3.7 Leptogenesis with flavour effects

In the discussions above, we have not considered the effects of lepton flavours. In this section, we briefly summarise the role of lepton flavour effects on our results. For earlier works on flavoured leptogenesis, please refer to [55–58] while a recent review may be found in [159]. Here we adopt the notations adopted by [58] and calculate the baryon asymmetry for all the non-standard cosmological scenarios mentioned earlier, including lepton flavour effects.

The Boltzmann equations for flavoured leptogenesis in EMD universe can be written as,

$$\frac{dN_{N_1}}{da} = -\frac{\langle\Gamma_1\rangle}{\mathbf{H}a}\left(N_{N_1}-N_{N_1}^{eq}\right), \tag{5.44}$$

$$\frac{dN_{\Delta_\alpha}}{da} = -\frac{\epsilon_{1\alpha}\langle\Gamma_1\rangle}{\mathbf{H}a}\left(N_{N_1}-N_{N_1}^{eq}\right) - P_{1\alpha}\left(\frac{W_{\rm ID}}{\mathbf{H}a} - \sum_{\beta=e,\mu,\tau} P_{1\beta}\frac{M_1(\Delta W)_{\alpha\beta}}{Ta}\right)N_{\Delta_\alpha}, \tag{5.45}$$

Here $\alpha = e, \mu, \tau$ corresponds to lepton flavours resulting in three coupled equations. $N_{\Delta\alpha}$ is the number of $B/3 - L_\alpha$ (for each flavour of leptons) and $P_{1\alpha}$ are the projectors defined by

$$P_{1\alpha} = \frac{\Gamma_{1\alpha}}{\Gamma_1}, \tag{5.46}$$

where Γ_1 is the total decay width of N_1 while $\Gamma_{1\alpha}$ is the corresponding partial decay width to a particular lepton flavour denoted by α. The flavoured CP asymmetry parameter $\epsilon_{1\alpha}$ and the washout terms can be found in a way similar to the unflavoured leptogenesis discussed earlier. In the EMD scenario, they are solved simultaneously with Eqs.(5.40), and (5.41) like in unflavored case. Since case 1 lead to relatively high scale leptogenesis due to the strong entropy dilution and case 3 results are very similar to standard cosmology results, here we show the flavour effects in leptogenesis for case 2. For case 2, we have significant effects of the early matter domination on leptogenesis as well as DM. By including lepton flavour effects we look for the possible changes on the scale of leptogenesis. After doing a parameter scan in $M_1 - \lambda_5$ plane we show the allowed parameter space in Fig.5.18. It should be noted that while comparing flavoured leptogenesis with unflavoured ones (that is, comparing Fig.5.18 with Fig.5.11), we have used the lightest active neutrino mass to be $m_1 = 10^{-13}$ eV which corresponds to the weak washout regime $K_{N_1} = \Gamma_1/\mathbf{H}(T = M_1) \ll 1$ [58]. In such weak washout regimes the projection operator $P_{1\alpha} \to 1$ takes the flavoured leptogenesis towards the unflavoured regime. Therefore, the quantitative difference after the inclusion of flavour effects in this weak wash-out regime is less compared to the difference brought out by non-standard cosmological epoch (EMD) over standard cosmology. Here the lowest possible scale for succesful leptogenesis is found to be $M_1 \simeq 1.5 \times 10^7$ GeV. Going to a strong washout regime will show the significance of flavour effects in a clear way.

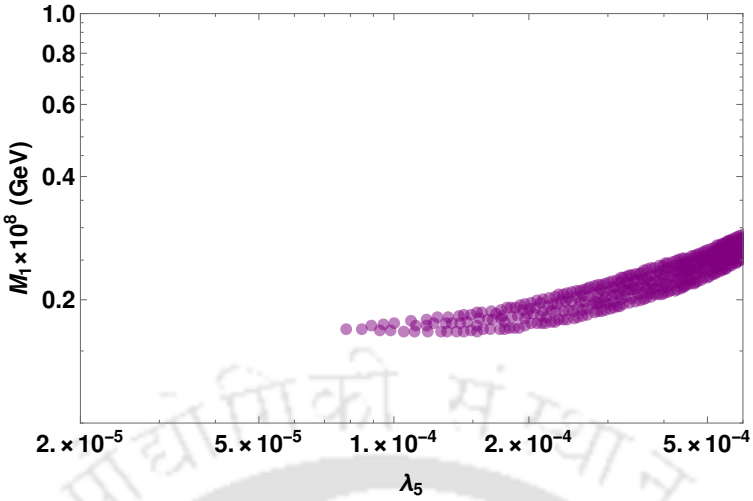

Figure 5.18: Allowed parameter space in $\lambda_5 - M_1$ plane in EMD universe with $T_{\rm end} = 150$ GeV and $k = 10^{-5}$. The relevant model parameters are fixed at $m_1 = 10^{-13}$ eV, $M_{i+1}/M_i = 10^{0.5}$

Similarly, the Boltzmann equations for flavoured leptogenesis in fast expanding universe scenario can be written as

$$\frac{dn_{N_1}}{dz} = -D_1^{'}(n_{N_1} - n_{N_1}^{\rm eq}), \tag{5.47}$$

$$\frac{dn_{\Delta_\alpha}}{dz} = -\epsilon_{1\alpha} D_1^{'}(n_{N_1} - n_{N_1}^{\rm eq}) - P_{1\alpha} W_1^{'} n_{\Delta_\alpha} - P_{1\alpha} n_{\Delta\alpha} \sum_{\beta=e,\mu,\tau} P_{1\beta} (\Delta W^{'})_{\alpha\beta}. \tag{5.48}$$

The notations have their usual meaning as adopted throughout the discussions. The allowed parameter space in $M_1 - \lambda_5$ plane is shown in Fig.5.19. The allowed parameter space reveals that the scale of leptogenesis can be as low as $M_1 \simeq 30$ TeV, which is 10 TeV less compared to $M_1 \simeq 40$ TeV for the unflavoured case.

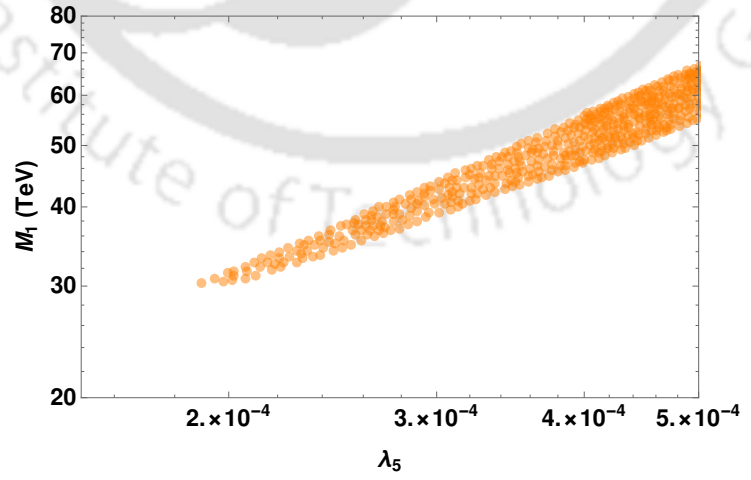

Figure 5.19: Allowed parameter space in $M_1 - \lambda_5$ plane in a FEU with $n = 2$ and $T_r = 20$ MeV. The relevant model parameters are fixed at $m_1 = 10^{-13}$ eV, $M_{i+1}/M_i = 10^{0.5}$

5.4 WIMPy leptogenesis in non-standard cosmologies

After studying the effect of non-standard cosmologies on N_1 decay leptogenesis along with dark matter in the minimal scotogenic model, we study the effect of such non-standard cosmologies on a cogenesis scenario known as WIMPy leptogenesis. Such cogenesis mechanisms are motivated by the similarity between DM and baryon abundances $\Omega_{\rm DM} \approx 5\Omega_{\rm B}$. Ignoring the possibility of any numerical coincidence or anthropic origin behind this similarity, one can provide a dynamical origin of it by uniting their production mechanisms. A brief review of such cogenesis mechanisms for DM and BAU can be found in [369]. Such cogenesis mechanisms can be classified into two broad categories. In the first one, the DM sector is also assumed to be asymmetric like the visible one, known as the asymmetric dark matter (ADM) scenario [370–374], where out-of-equilibrium decay of the same heavy particle is responsible for generating similar asymmetries $n_{\rm B} - n_{\overline{\rm B}} \sim |n_{\rm DM} - n_{\overline{\rm DM}}|$ in the two sectors. In the second class of this cogenesis scenario, the asymmetry is produced from annihilations [25, 375, 376], where one or more particles involved in the process eventually go out of thermal equilibrium to generate a net asymmetry. The so-called WIMPy baryogenesis [377–379] belongs to this category, where a DM particle freezes out to generate its own relic abundance while simultaneously producing an asymmetry in the baryon sector. This idea has also been extended to leptogenesis, known as the WIMPy leptogenesis scenario [193, 380–384]. Here we consider a simple WIMPy leptogenesis framework and study the impact of three non-standard cosmological histories namely, (a) a fast expanding universe scenario, (b) an early matter dominated phase and (c) scalar-tensor theory of gravity (STG). While leptogenesis from decay has been studied in the context of non-standard cosmology mentioned before, WIMPy baryogenesis or WIMPy leptogenesis has not been studied in this context earlier and ours is a first of its kind attempt in this direction.

As pointed out in earlier works on WIMPy baryogenesis or WIMPy leptogenesis, one can satisfy all the Sakharov's conditions with DM annihilations such that some of the processes responsible for WIMP freeze-out can also create a baryon or lepton asymmetry. In order to keep the washout scatterings under control, one has to ensure that the washout scatterings freeze out before WIMP freeze-out [379]. Based on this central criteria, several WIMPy baryogenesis and leptogenesis models have been constructed. In order to illustrate the effects of non-standard cosmological histories, we consider the model considered in [164] for simplicity although choosing a more complicated model will not change the generic conclusions reached in this work.

Similar to usual leptogenesis scenarios, WIMPy leptogenesis models are also constructed in a way which explains non-zero neutrino mass too, another observed phenomena which the SM fails to explain. The model proposed in [164] is an extension of the minimal scotogenic model [112] by a scalar triplet. The minimal scotogenic model extends the SM by three gauge singlet right handed neutrinos $N_i, (i = 1 - 3)$ and a scalar doublet η, all of which are odd under an unbroken Z_2 symmetry. While this minimal field content can account for neutrino mass, DM as well as leptogenesis from RHN decay, the extension by a scalar triplet is necessary to realise a WIMPy leptogenesis setup with the neutral real component of inert scalar doublet η playing the role of WIMP DM. The scalar triplet is kept Z_2 even like SM particles are, in order to realise the necessary interactions. The relevant leptonic Lagrangian

can be written as follows.

$$-\mathcal{L} \supset Y^{N}_{i\alpha}\overline{\ell_\alpha}\tilde{\eta}N_i + Y^{\Delta}_{\alpha\beta}\overline{\ell^c_\alpha}\Delta\ell_\beta + \text{h.c.}, \tag{5.49}$$

with $\ell = (\nu, l)^T$ being the SM lepton doublet, C in superscript denotes the charge conjugation, $\tilde{\eta} = i\sigma_2\eta^*$. The scalar potential of the model is given in Appendix D.1. The term $\lambda''_{H\eta}(H^\dagger\eta)^2$ in the scalar potential given in Eq.(D.1) plays a crucial role in generating radiative neutrino mass as well as DM phenomenology, by generating the mass splitting of scalar and pseudoscalar components of η, the details of which is given in Appendix D.1. On the other hand, the trilinear term $\mu_{H\Delta}\tilde{H}^\dagger\Delta H$ leads to an induced vacuum expectation value (VEV) of neutral component of Δ (denoted as v_Δ) after electroweak symmetry breaking generating the well known type-II seesaw contribution to neutrino mass [48, 50, 66–69]. The other trilinear term in the scalar potential namely, $\mu_{\eta\Delta}\eta^\dagger\Delta^\dagger\tilde{\eta}$ plays an important role in WIMPy leptogenesis as it opens up new WIMP annihilation channels into leptons which violate lepton number. The trilinear coupling $\mu_{\eta\Delta}$ is a free parameter of the model and can be complex in general. To generate a net leptonic asymmetry, the coupling $\mu_{\eta\Delta}$ is assumed to be purely imaginary while all other parameters in Eq.(D.1) are considered real.

5.4.1 WIMPy leptogenesis in standard cosmology

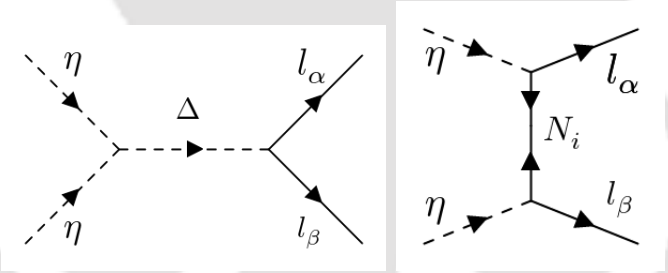

Figure 5.20: Feynman diagrams for the scattering process $\eta\eta \longrightarrow ll$.

We consider the lightest neutral component of the scalar doublet η as the WIMP DM candidate. While there exist several gauge and scalar portal diagrams for inert scalar DM annihilations, as discussed in earlier works [115, 122–131], there are fewer diagrams which violate lepton number in our setup. Such CP and lepton number violating DM annihilation processes are responsible for generating a non-zero lepton asymmetry, as shown in Fig.5.20. In this model, the lepton number violating DM annihilation is $\eta\eta \longrightarrow \ell\ell$, which violates the lepton number by two units ($\Delta L = 2$). Due to the existence of multiple Feynman diagrams for this process as shown in Fig.5.20, it is possible to generate a non-zero CP asymmetry from the interference. Although we show the tree level diagrams only, the propagators are resummed taking the radiative corrections into account, similar to [385] where three-body decay involving DM in the final state was considered instead of DM annihilation to source lepton asymmetry. In order to enhance the CP asymmetry, we consider the resonance regime $m_\eta \simeq m_\Delta/2$ such that the scale of WIMPy leptogenesis can be as low as possible with the washout scatterings under control.

In order to implement the constraints from neutrino data, we use the Casas-Ibarra parametrisation [65] to write the Yukawa couplings Y^N, Y^Δ in terms of neutrino parameters as well as physical masses of different BSM particles. As can be seen from Eq.(D.7) in Appendix D.1, the mass difference between η_R and η_I depends on $\mu_{\eta\Delta}$, $\lambda''_{H\eta}$ and v_Δ. On the other hand, from Eq.(D.10) and Eq.(D.11) it is clear that increasing mass difference between η_R and η_I decreases the Yukawa coupling Y^N. For leptogenesis one needs large enough Y^N to generate the correct asymmetry. Therefore we need to choose $\lambda''_{H\eta}$, v_Δ and $\mu_{\eta\Delta}$ carefully such that the mass difference between η_R and η_I remains small. Also one can not make the mass difference $\Delta m_{\eta^0} = m_{\eta_R} - m_{\eta_I}$ arbitrarily small as it will make the direct detection cross-section for the DM very large [334], ruled out by stringent direct detection constraints [93]. In this work, we choose the all mentioned parameters in such a way that $\Delta m_{\eta^0} > 200$ keV, large enough to forbid tree level Z mediated inelastic scattering of DM off nucleons.

The Boltzmann equations (BEs) for comoving number densities of DM and lepton number respectively, can be identified to be

$$\frac{dY_\eta}{dz} = -\frac{s}{\mathbf{H}(z)z}\left[(Y_\eta^2 - (Y_\eta^{\rm eq})^2)\langle\sigma v\rangle_{\eta\eta\longrightarrow \rm SM\,SM}\right], \tag{5.50}$$

$$\frac{dY_{\Delta L}}{dz} = \frac{s}{\mathbf{H}(z)z}\left[(Y_\eta^2 - (Y_\eta^{\rm eq})^2)\langle\sigma v\rangle^\delta_{\eta\eta\longrightarrow\ell\ell}\right] - 2Y_{\Delta L}Y_l^{\rm eq}r_\eta^2\langle\sigma v\rangle_{\eta\eta\longrightarrow\ell\ell} - 2Y_{\Delta L}Y_\eta^{\rm eq}\langle\sigma v\rangle_{\eta\bar{\ell}\longrightarrow\eta\ell}, \tag{5.51}$$

where $z = m_\eta/T \equiv m_{\rm DM}/T$ and $Y_i^{\rm eq} = n_i^{\rm eq}/s$ are the normalised number densities (in equilibrium) for the particle species i (s being the entropy density of the universe). The $Y_{\Delta L}$ is the comoving number density of lepton asymmetry and is defined by $Y_{\Delta L} = Y_L - Y_{\bar{L}}$. Here $r_\eta = Y_\eta^{\rm eq}/Y_l^{\rm eq}$ and $\mathbf{H}(z) = \sqrt{8\pi^3 g_*/90}m_\eta^2/(z^2 M_{\rm Pl})$ is the Hubble expansion rate for the standard radiation dominated universe with $M_{\rm Pl} \simeq 1.22\times10^{19}$ GeV being the Planck mass. Here the $\langle\sigma v\rangle$ represents the thermally averaged cross sections for the mentioned processes. On the other hand, $\langle\sigma v\rangle^\delta_{\eta\eta\longrightarrow\ell\ell}$ on the right hand side of Eq.(5.51) includes the difference between $\eta\eta \longrightarrow \ell\ell$ and $\eta\eta \longrightarrow \bar{\ell}\bar{\ell}$ processes responsible for generating a net lepton asymmetry, the details of which are shown in Appendix D.2. The lepton asymmetry is converted into baryon asymmetry via sphaleron factor $Y_{\Delta B} = c_{\rm sph}Y_{\Delta L}$ where $c_{\rm sph} = -\frac{16}{39}$ for our model, as shown in Appendix D.4.

In Fig.5.21 we show the evolution of the comoving number densities of DM and L asymmetry with $z = m_{\rm DM}/T$ for different benchmark values of $\mu_{\eta\Delta}$ (upper panel) and v_Δ (lower panel). The grey vertical lines labelled as "sphaleron" in the right panel plots of Fig.5.21 (and the subsequent evolution plots for lepton asymmetry) correspond to the sphaleron freeze-out temperature $T_{\rm Sph} = (131.7\pm2.3)$ GeV [386]. In the upper left panel plot of Fig.5.21, it can be seen that with a change in $\mu_{\eta\Delta}$ there is no change in the evolution of the comoving number density of DM, which is expected as it is governed by total annihilation rates dominated by electroweak gauge portal interactions. However, in the upper right panel of Fig.5.21, sharp variation in comoving lepton number density is seen for different values of $\mu_{\eta\Delta}$. This is expected as this trilinear term is assumed to be the only term violating CP and hence the lepton asymmetry initially increases with an increase in $\mu_{\eta\Delta}$. However, it is found that beyond a certain value of $\mu_{\eta\Delta}$ the asymmetry starts decreasing with further increase in $\mu_{\eta\Delta}$.

This is because beyond a certain value of $\mu_{\eta\Delta}$, the mass difference between η_R and η_I starts increasing, which in turn decreases the neutrino Dirac Yukawa couplings Y^N to maintain the radiative seesaw contribution to neutrino mass. Since the CP asymmetry depends upon both $\mu_{\eta\Delta}$ and Y^N, their relative increase and decrease lead to an overall decrease in lepton asymmetry at some point.

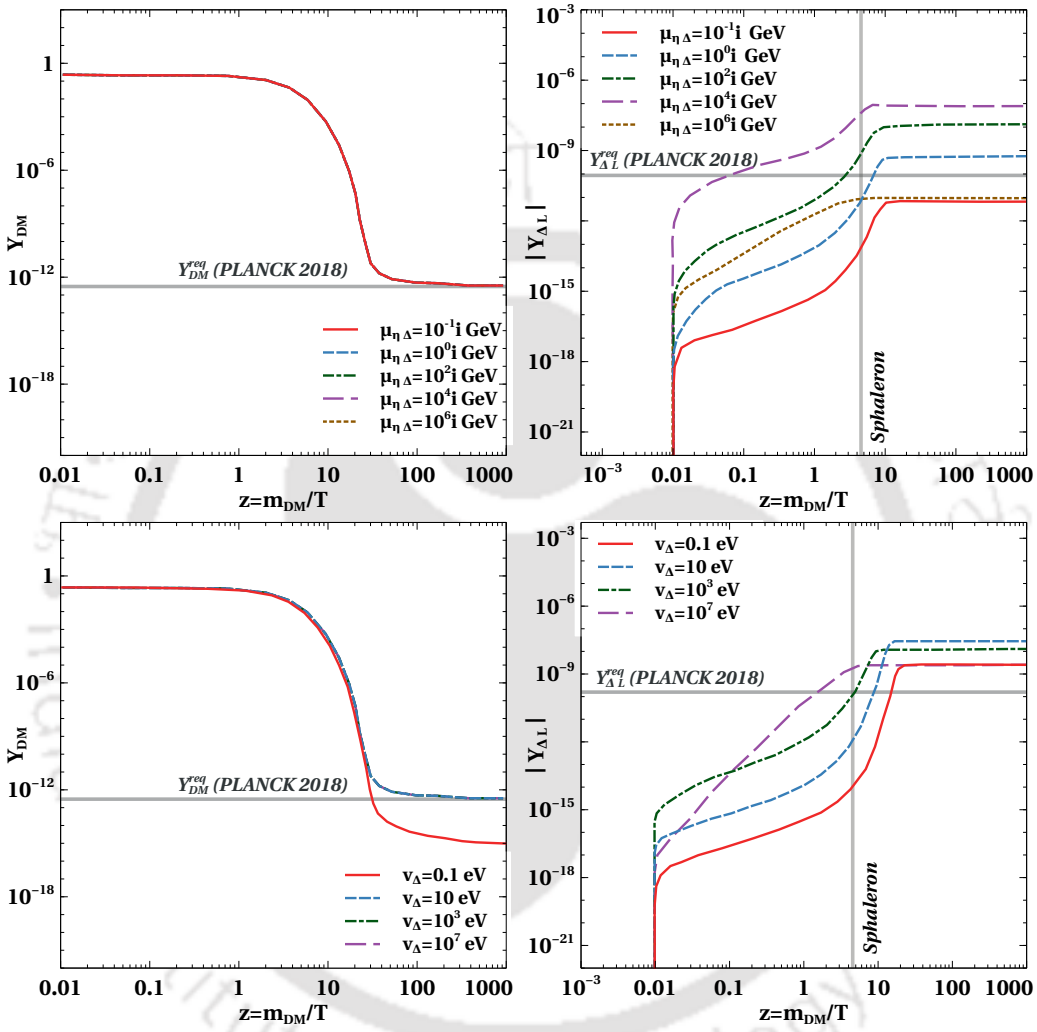

Figure 5.21: Evolution of the comoving number density of dark matter (left panel) and L asymmetry (right panel) with $z = m_{\rm DM}/T$ for different values of $\mu_{\eta\Delta}$ (top panel) and v_Δ (bottom panel) respectively. The other relevant parameters are set at $m_{\eta_R} = m_{\rm DM} = 600$ GeV, $m_{\Delta^\pm} = m_{\Delta^{\pm\pm}} = m_{\Delta^0} = 1.2$ TeV, $M_1 = 6$ TeV, $M_{j+1}/M_j = 1.1$, $\lambda''_{H\eta} = 1 \times 10^{-5}$, $v_\Delta = 1$ keV (for the top panel) and $\mu_{\eta\Delta} = 10i$ GeV (for the bottom panel).

On the other hand, in the lower left panel plot of Fig.5.21 we can see that the DM relic decreases beyond a certain small value of v_Δ. This is because, beyond a certain small value of v_Δ, the Yukawa coupling of leptons with triplet scalar namely, $Y^\Delta \propto v_\Delta^{-1}$ become large enough (for a fixed contribution of type-II seesaw to neutrino mass) such that the annihilation of η through the scalar triplet becomes much more dominant compared to the annihilations

involving the electroweak gauge bosons. Therefore, the DM relic is primarily determined by the strong annihilations involving the Yukawa Y^{Δ}. From the lower right plot of Fig.5.21 it can be seen that with the increase in v_{Δ}, the asymmetry first increases, but beyond a certain value of v_{Δ} the asymmetry decreases with increasing v_{Δ}. As v_{Δ} increases, the Yukawa Y^{Δ} decreases (for a fixed contribution of type-II seesaw to neutrino mass) and therefore the washout due to $\ell\ell \longrightarrow \eta\eta$ decreases which leads to an increase in the asymmetry. However, beyond a certain large value of v_{Δ} the washout effects become very small. At the same time due to the decrease in Y^{Δ} the generation of asymmetry itself becomes small leading to a decrease in asymmetry with further increase in v_{Δ}.

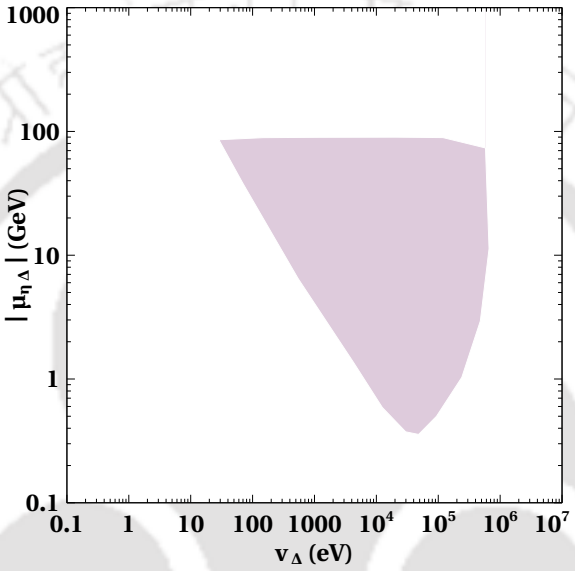

Figure 5.22: Viable parameter space in $\mu_{\eta\Delta}$ versus v_{Δ} plane which can generate the observed baryon asymmetry as well as correct DM relic. The other important parameters are fixed at $m_{\eta_R} = 600$ GeV, $m_{\Delta^{\pm}} = m_{\Delta^{\pm\pm}} = m_{\Delta^0} = 1.2$ TeV, $\lambda''_{H\eta} = 1 \times 10^{-5}$, $M_1 = 6$ TeV, and $M_{j+1}/M_j = 1.1$.

In Fig.5.22 we show the viable parameter space from successful WIMPy leptogenesis and correct DM relic in $\mu_{\eta\Delta}$ versus v_{Δ} plane while other relevant parameters are fixed at benchmark values and assuming a standard radiation dominated universe. From Fig.5.22 one can clearly see that there is an upper limit as well as a lower limit on the allowed values of v_{Δ} and $\mu_{\eta\Delta}$. Quantitatively the bounds on v_{Δ} and $\mu_{\eta\Delta}$ are found to be 30 eV $\lesssim v_{\Delta} \lesssim$ 0.7 MeV and 0.25 GeV $\lesssim \mu_{\eta\Delta} \lesssim$ 88 GeV respectively. When v_{Δ} is very small, the Yukawa coupling $Y^{\Delta} \propto v_{\Delta}^{-1}$ is so large that the washout effects coming from the processes $\ell\ell \longrightarrow \eta\eta$ are too strong to give rise to correct asymmetry. On the other hand when v_{Δ} is large the Yukawa coupling Y^{Δ} become too small to generate sufficient asymmetry. One would expect that the decrease in Y^{Δ} due to the increase in v_{Δ} can be compensated by increasing $\mu_{\eta\Delta}$, however, that is not to be true as increasing $\mu_{\eta\Delta}$ also increases the mass splitting between η_R and η_I which in turn decreases the Yukawa coupling Y^N. It should be noted that lepton asymmetry can, in principle, be generated from Δ decay as well. However, since WIMP annihilation is generating asymmetry at a lower scale, the high scale production of lepton

asymmetry remains sub-dominant, as we show in Appendix D.3.

In Fig.5.23, we show how the viable parameter space in $\mu_{\eta\Delta}$ versus v_Δ plane changes with the change in the mass of N_1 (left panel plot) and with the change in the mass hierarchy among the RHNs (right panel plot). It is observed that with the increase in M_1 as well as the mass hierarchy we require larger $\mu_{\eta\Delta}$ to generate the desired asymmetry. This is due to the propagator suppression of the CP asymmetry coming from the t-channel diagram shown in Fig.5.20. This can be compensated by increasing the value of $\mu_{\eta\Delta}$. Also with the increase in $\mu_{\eta\Delta}$ the washouts increase which results in a requirement of a larger v_Δ. There exists an interplay of these two effects as a result of which the parameter space shifts towards the higher values of $\mu_{\eta\Delta}$ as well as v_Δ.

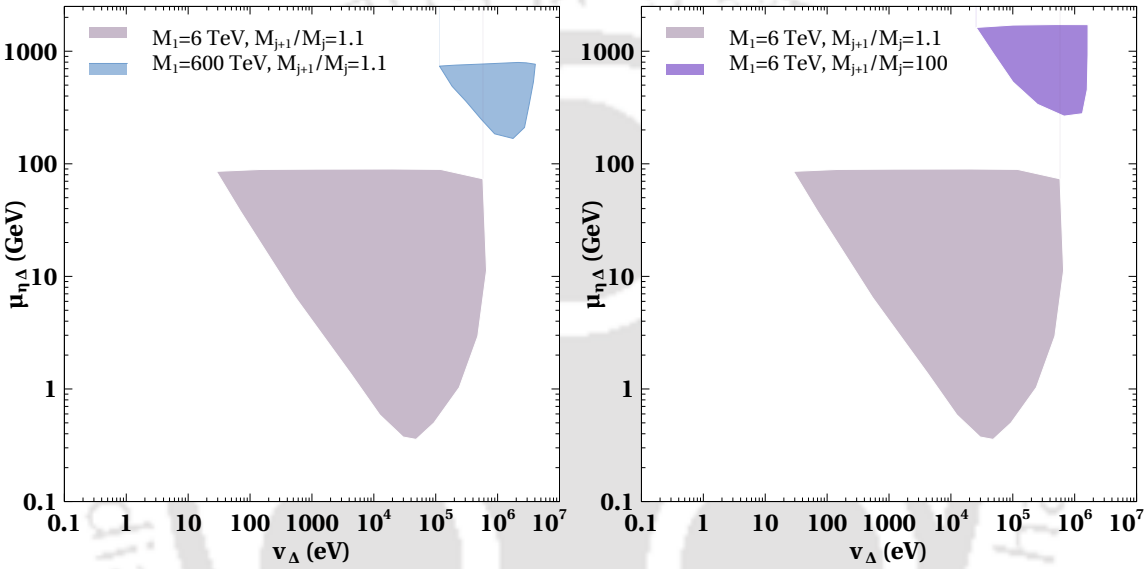

Figure 5.23: Viable parameter space in $\mu_{\eta\Delta}$ versus v_Δ plane which can generate the observed baryon asymmetry as well as correct DM relic. The other important parameters are fixed at $m_{\eta_R} = 600$ GeV, $m_\Delta^\pm = m_{\Delta^{\pm\pm}} = m_{\Delta^0} = 1.2$ TeV, $\lambda''_{H\eta} = 1 \times 10^{-5}$.

5.4.2 WIMPy leptogenesis in FEU

In WIMPy leptogenesis scenario, we need to write the Boltzmann equation for L asymmetry too along with the one for DM. Assuming the universe to be dominated by the ϕ field only till the WIMP freeze-out that is, $T \gg T_{\rm r}$, we can simply write the relevant Boltzmann equations as

$$\frac{dY_\eta}{dz} = -\frac{s(z=1)}{z^{2-n/2} z_r^{n/2} \mathbf{H}_{\rm rad}(z=1)} \langle\sigma v\rangle_{\eta\eta\longrightarrow \rm SM\ SM} \left[Y_\eta^2 - (Y_\eta^{\rm eq})^2\right], \tag{5.52}$$

$$\frac{dY_{\Delta L}}{dz} = \frac{s(z=1)}{z^{2-n/2} z_r^{n/2} \mathbf{H}_{\rm rad}(z=1)} \Big(\langle\sigma v\rangle^\delta_{\eta\eta\longrightarrow\ell\ell} \left[Y_\eta^2 - (Y_\eta^{\rm eq})^2\right] - Y_{\Delta L} Y_l^{\rm eq} r_\eta^2 \langle\sigma v\rangle_{\eta\eta\longrightarrow\ell\ell} - Y_{\Delta L} Y_\eta^{\rm eq} \langle\sigma v\rangle_{\eta\bar{\ell}\longrightarrow\eta\ell} \Big). \tag{5.53}$$

While we write the simplified form of equations here, we consider the complete function $L(n, z, z_r)$ in the numerical calculations. In Fig.5.24 we show the evolution of the comoving number density of dark matter and L asymmetry for different values of the FEU parameter n keeping the other important parameters fixed.

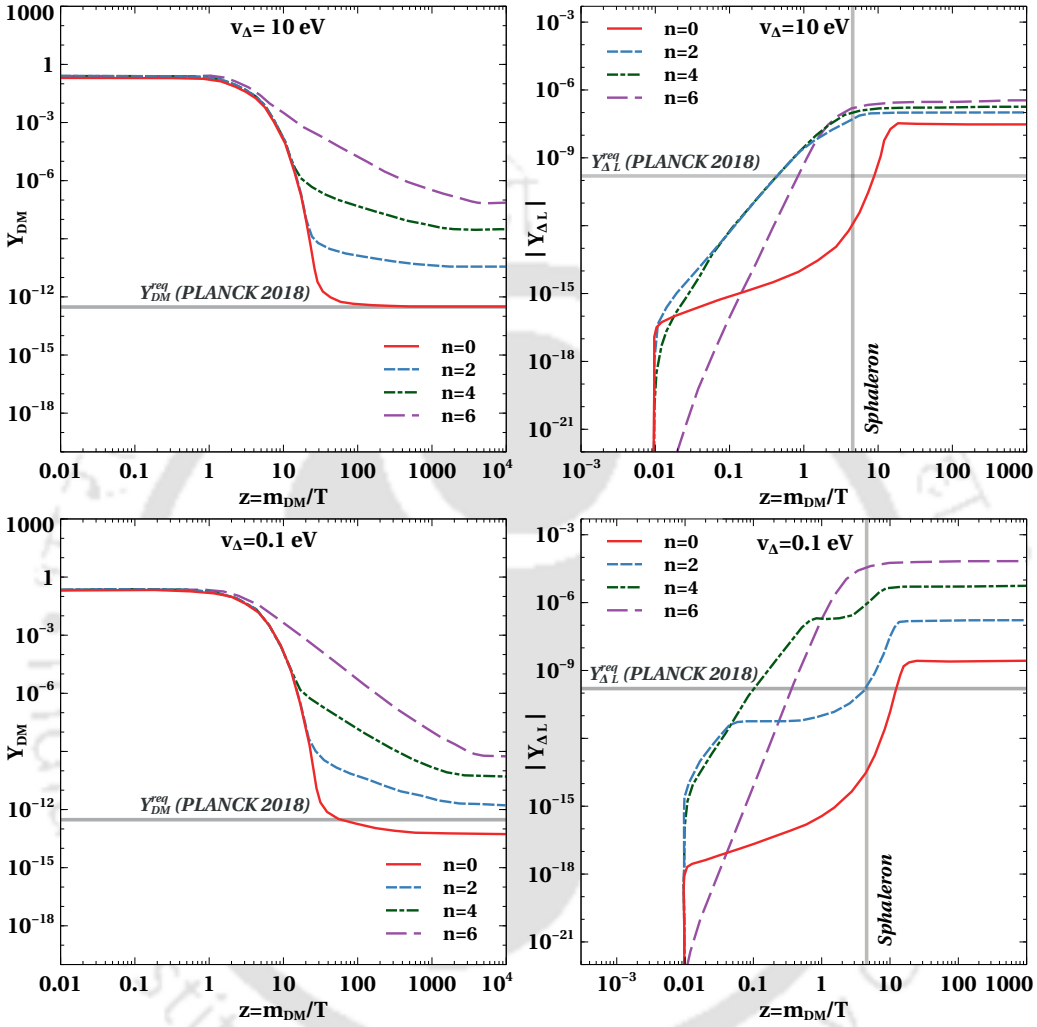

Figure 5.24: Evolution of the comoving number densities of dark matter (left panel) and L asymmetry (right panel) with $z = m_{\rm DM}/T$ for different values of FEU parameter n. The relevant parameters are set at $m_{\eta R} = 600$ GeV, $m_{\Delta^\pm} = m_{\Delta^{\pm\pm}} = m_{\Delta^0} = 1.2$ TeV,$M_1 = 6$ TeV, $M_{j+1}/M_j = 1.1$, $\mu_{\eta\Delta} = 10i$ GeV, $\lambda''_{H\eta} = 1 \times 10^{-5}$ and $v_\Delta = 10$ eV (upper panel) and $v_\Delta = 0.1$ eV (lower panel). Here we have taken $T_r = 30$ MeV ($z_r \simeq 2 \times 10^4$).

From the DM relic plots one can see that with increasing values of n, the DM abundance also increases. It is because, larger the value of n, larger is the expansion rate and therefore the decoupling of the DM particles happens much earlier. However, since the decoupling occurs at a time when the rate of annihilations is sufficiently large, a few DM particles keep on annihilating up to a much later time giving rise to a relentless nature of the DM

abundance, as pointed out in [353]. Due to the early deviation of η from its equilibrium abundance the asymmetry also increases with the increase in n. Also, the rates of washout processes become relatively suppressed with the increase in n because of the faster expansion. This effect is clearly visible in the lower right panel plot of Fig.5.24 where the washouts are relatively strong compared to the upper right panel plot. In the lower panel plots of Fig.5.24 we choose relatively smaller value of $v_\Delta = 0.1$ eV which leads to very strong annihilations of η by the process $\eta\eta \longrightarrow ll$. This leads to two distinct effects on DM abundance as well as in asymmetry. For such value of v_Δ the DM relic is primarily determined by the process $\eta\eta \longrightarrow ll$ involving Y^Δ. For small v_Δ, the DM relic is less than the observed value in standard cosmolgy as can be seen in the lower left plot of Fig.5.24 (keeping in mind that $n = 0$ leads to standard cosmological history). Since faster expansion leads to an increase in DM relic we expect to achieve the correct relic by increasing the value of n. Similarly smaller value of v_Δ increases the washout coming from the process $ll \longrightarrow \eta\eta$. This results in a decrease of the asymmetry for standard history ($n = 0$) as can be seen in the lower right panel plot of Fig.5.24. Therefore, increasing the value of n can open up new regions of parameter space consistent with the correct DM relic and the observed baryon asymmetry. In Fig.5.25 we show evolution plots of comoving number densities of DM and L for three benchmark points which can satisfy the observed relic density of DM and also the correct L asymmetry in a FEU.

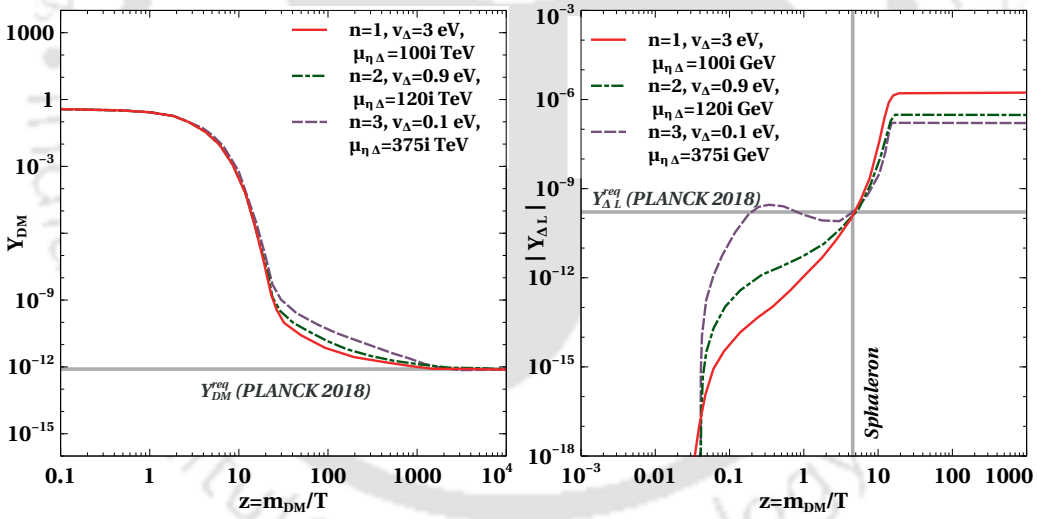

Figure 5.25: Evolution of the comoving number densities of DM and L asymmetry for few benchmark points which can generate the correct DM relic and the observed asymmetry. The other relevant parameters are fixed at $m_{\eta_R} = 600$ GeV, $\lambda''_{H\eta} = 10^{-5}$,$m_{\Delta^0} = m_{\Delta^\pm} = m_{\Delta^{\pm\pm}} = 1.2$ TeV,$M_1 = 6$ TeV, $M_{j+1}/M_j = 1.1$ and $z_r = 2 \times 10^4$.

In Fig.5.26 we show the viable parameter space in $\mu_{\eta\Delta}$ versus v_Δ plane in a FEU scenario. We consider two different values of the FEU parameter namely, $n = 1$ and $n = 3$. One can see that the viable parameter space changes in FEU from the standard radiation case. More specifically, the parameter space gets squeezed in this plane compared to the same in standard cosmology shown in Fig.5.22. This is due to the different interplay of these two parameters on DM relic as well as washout processes discussed earlier. While we choose $T_r = 30$ MeV,

choosing larger values will reduce the effect of non-standard cosmology and bring the results closer to the ones in standard radiation dominated scenario discussed earlier. Finally we found the limits on v_Δ and $\mu_{\eta\Delta}$ to be 0.2 eV $\lesssim v_\Delta \lesssim$ 4 eV and 67 GeV $\lesssim \mu_{\eta\Delta} \lesssim$ 143 GeV for $m_{\rm DM} = 600$ GeV in a FEU with $n = 1$. Similarly the limits are found to be 0.068 eV $\lesssim v_\Delta \lesssim$ 0.13 eV, 285 GeV $\lesssim \mu_{\eta\Delta} \lesssim$ 390 GeV respectively for $m_{\rm DM} = 600$ GeV in a FEU with $n = 3$.

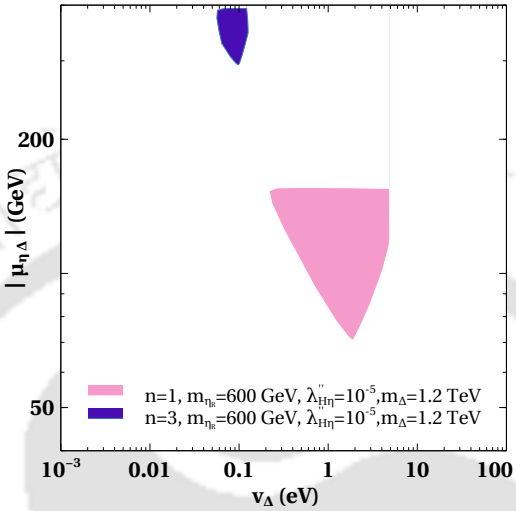

Figure 5.26: Scan plot showing the available parameter space in $\mu_{\eta\Delta}$ vs v_Δ plane from the requirement of observed baryon asymmetry and the correct DM relic. z_r is fixed at 2×10^4. The other important parameters are fixed at $m_{\eta_R} = 600$ GeV, $m_{\Delta^\pm} = m_{\Delta^{\pm\pm}} = m_{\Delta^0} = 1.2$ TeV, $\lambda''_{H\eta} = 1 \times 10^{-5}$, $M_1 = 6$ TeV, and $M_{j+1}/M_j = 1.1$.

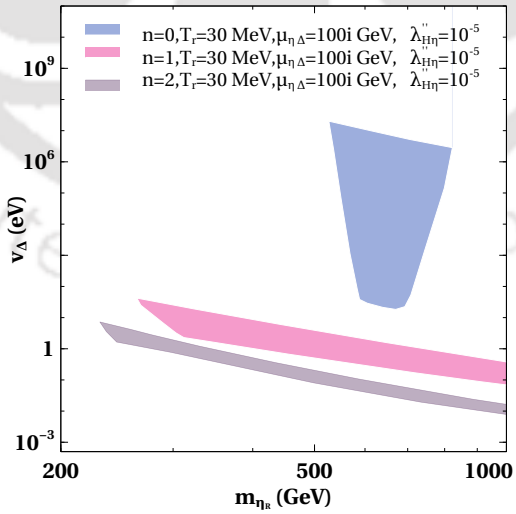

Figure 5.27: Scan plot showing the viable parameter space in m_{η_R} Vs v_Δ plane for different possible FEU. The other important parameters are fixed at $m_{\Delta^\pm} = m_{\Delta^{\pm\pm}} = m_{\Delta^0} = 1.2$ TeV, $M_1 = 6$ TeV, and $M_{j+1}/M_j = 1.1$.

In Fig.5.27 we show the viable parameter space in m_{η_R} versus v_Δ plane from the requirement of correct DM relic and the observed baryon asymmetry for different FEU parameter n. In this figure, the region shown by the blue colour corresponds to the $n = 0$ case or equivalently to the standard radiation dominated universe. For $n = 1, 2$ we can see that the scale of leptogenesis can be lower than the standard radiation case. For the standard radiation dominated universe the DM mass required to satisfy the correct relic is very specific due to strong gauge portal annihilations and therefore the viable parameter space is appearing around a specific value of m_{η_R}. However, as seen from Fig.5.24 for FEU, the DM relic and asymmetry both increase with the increase in n and therefore with increase in n we need stronger DM annihilations to satisfy DM relic and baryon asymmetry. Hence for FEU, the viable parameter space is appearing with smaller values of v_Δ, which makes the Yukawa mediated annihilations stronger. This also opens up parameter space with smaller m_{η_R} compared to the standard case as smaller m_{η_R} leads to stronger annihilations. Also, we observed that with increase in v_Δ the required DM mass decreases, which is expected. However, we can not increase the value of v_Δ arbitrarily to lower the DM mass, because, beyond a certain large value of v_Δ the Yukawa mediated annihilations of DM become subdominant and we have to rely on the standard gauge sector to achieve the correct relic. We found that the lowest possible DM mass is $m_{\eta_R} = 230$ GeV for $n = 1$ and is $m_{\eta_R} = 275$ GeV for $n = 2$ case keeping the other particle physics parameters fixed as shown in Fig.5.27. This is significantly lower than the standard radiation case with the same benchmark parameters. Such low DM mass as well as low scale of leptogenesis can have promising detection prospects from colliders to direct and indirect DM detection experiments.

5.4.3 WIMPy leptogenesis in EMD universe

In this section, we study the impact of early matter domination on WIMPy leptogenesis based on the model discussed in the last two sections. Since entropy is not conserved, we do not consider the ratio of number density to entropy density while writing the relevant Boltzmann equations for an EMD universe. Instead, we write in terms of $N = na^3$ where n, a denotes the number density and scale factor respectively. Accordingly, we track the variation in terms of scale factor only. The coupled Boltzmann equations for WIMPy leptogenesis in an EMD universe can be written as follows

$$\frac{dN_\eta}{da} = -\frac{\langle\sigma v\rangle_{\eta\eta\longrightarrow \mathrm{SM\,SM}}}{\mathbf{H}a^4}\left[N_\eta^2 - (N_\eta^{\mathrm{eq}})^2\right], \tag{5.54}$$

$$\frac{dn_{\Delta\mathrm{L}}}{da} = \frac{\langle\sigma v\rangle^{\delta}_{\eta\eta\longrightarrow ll}}{\mathbf{H}a^4}\left[N_\eta^2 - (N_\eta^{\mathrm{eq}})^2\right] - \frac{n_{\Delta\mathrm{L}}}{\mathbf{H}a^4}N_l^{\mathrm{eq}} r_\eta^2 \langle\sigma v\rangle_{\eta\eta\longrightarrow ll} - \frac{n_{\Delta\mathrm{L}}}{\mathbf{H}a^4}N_\eta^{\mathrm{eq}}\langle\sigma v\rangle_{\eta\bar{l}\longrightarrow\eta l}. \tag{5.55}$$

Here, r_η is defined by $r_\eta = N_\eta^{\mathrm{eq}}/N_l^{\mathrm{eq}}$. Eqs.(5.54) and (5.55) have to be solved simultaneously with Eqs.(5.40) and (5.41). The Hubble parameter and the relativistic degrees of freedom contributing to the entropy density of the universe are represented by the usual symbols $\mathbf{H}$ and g_{*s} respectively. As discussed earlier in section 5.2, there are two important cosmological parameters in this scenario which are the ratio of ϕ energy density to that of the radiation at the initial temperature $k = \rho_\phi^{\mathrm{in}}/\rho_{\mathrm{rad}}^{\mathrm{in}}$ and the T_{end}. Therefore we study the impact of these parameters on the asymmetry and DM relic.

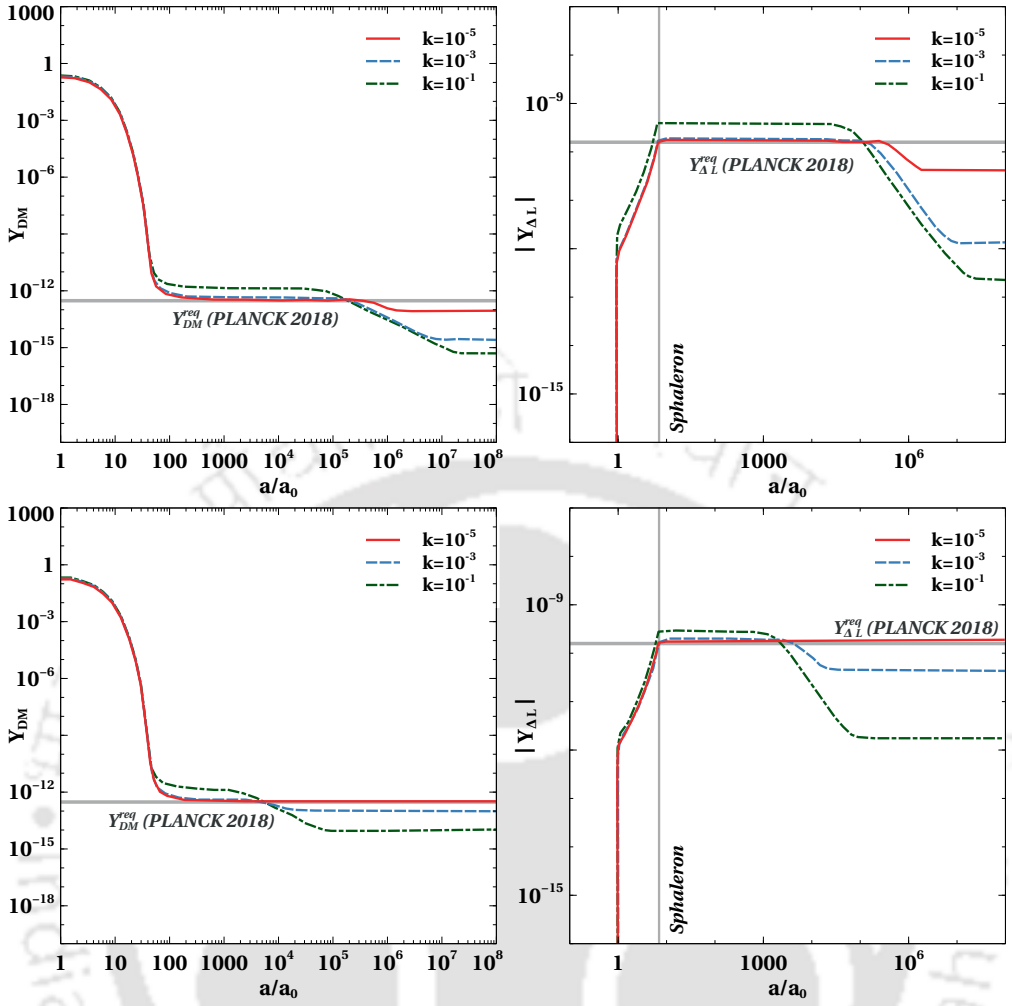

Figure 5.28: The comoving number densities of DM and L asymmetry with the relative scale factor a/a_0 for different values of k. The model parameters are fixed at $m_{\eta_R} = 600$ GeV, $v_\Delta = 1$ keV, $\lambda''_{H\eta} = 1 \times 10^{-5}$, $\mu_{\eta\Delta} = 10i$, $M_1 = 6$ TeV, $M_{j+1}/M_j = 1.1$, and $m_{\Delta^0} = m_{\Delta^\pm} = m_{\Delta^{\pm\pm}} = 1.2$ TeV. Here $T_{\rm end}$ is fixed at 2 MeV for the upper panel plots, and at 200 MeV for the lower panel plots.

Case 1: $T_{\rm end} < T_{\rm Sph}$

Here we consider the evolution of the DM relic and the L asymmetry by taking two different values of $T_{\rm end}$ such that $T_{\rm end} < T_{\rm Sph}$. In Fig.5.28 we show the evolution of the comoving number densities of DM and the L asymmetry with the scale factor for the case when $T_{\rm end} = 2$ MeV and $T_{\rm end} = 200$ MeV respectively. While we solve the equations in terms of N as written above, we convert it to $Y = n/s = N/(a^3 s(a))$ for both DM and L asymmetry, shown in these plots. The entropy dilution effect on DM abundance and baryon asymmetry is clearly visible in Fig.5.28. In an EMD universe, larger value of k makes the expansion rate larger since the Hubble expansion rate is determined by both ρ_ϕ and $\rho_{\rm rad}$. Therefore, the DM abundance starts deviating from the equilibrium abundance at earlier epochs for larger k, as can be seen in the left panel plots of Fig.5.28. As a consequence, the generated asymmetry

also increases slightly. However, for larger k the late entropy dilution effect on DM abundance and lepton asymmetry is much more dominant compared to the enhancement coming due to the change in the expansion rate of the universe and therefore with the increase in k both final DM abundance as well as the asymmetry decreases.

It is important to note that the entropy dilution effect in the lower panel plots of Fig.5.28 is less compared to that in the upper panel plots. The is because, we have chosen $T_{\rm end} = 200$ MeV for the lower panel plot whereas $T_{\rm end} = 2$ MeV for the upper panel plots, implying that the ϕ field decays when the universe is much hotter for the lower panel plots compared to the upper panel plots. Therefore, upon the decay of the scalar field, the entropy injection into the plasma is small compared to the entropy the plasma has. Hence it is expected that as we increase $T_{\rm end}$ the entropy dilution effect will become weaker.

We run a parameter scan over the parameter v_Δ and $|\mu_{\eta\Delta}|$, by taking $T_{\rm end} = 2$ MeV and $T_{\rm end} = 200$ MeV respectively while keeping the other particle physics parameters fixed. Due to the strong entropy dilution effect, we found no available parameter space that can satisfy the correct DM relic and the observed baryon asymmetry irrespective of the value of k (for $k \geq 10^{-5}$) with $T_{\rm end} = 2$ MeV and $T_{\rm end} = 200$ MeV. Increasing $T_{\rm end}$ to 2 GeV allows some parameter space in $v_\Delta - \mu_{\eta\Delta}$ plane, to be discussed below.

Case 2: $T_{\rm end} \simeq T_{\rm Sph}$

Now we redo the analysis for DM abundance and L asymmetry by considering $T_{\rm end} \simeq T_{\rm Sph}$. Here we have chosen $T_{\rm end} = 150$ GeV to illustrate the phenomenology near $T_{\rm end} \simeq T_{\rm Sph}$. The results for the evolution of DM abundance and the L asymmetry are shown in Fig.5.29. In this case, we can see that the entropy dilution effect is very feeble. It is observed that near a particular value of $k \simeq 10^{-3}$ the generated asymmetry can be even more than the required asymmetry.

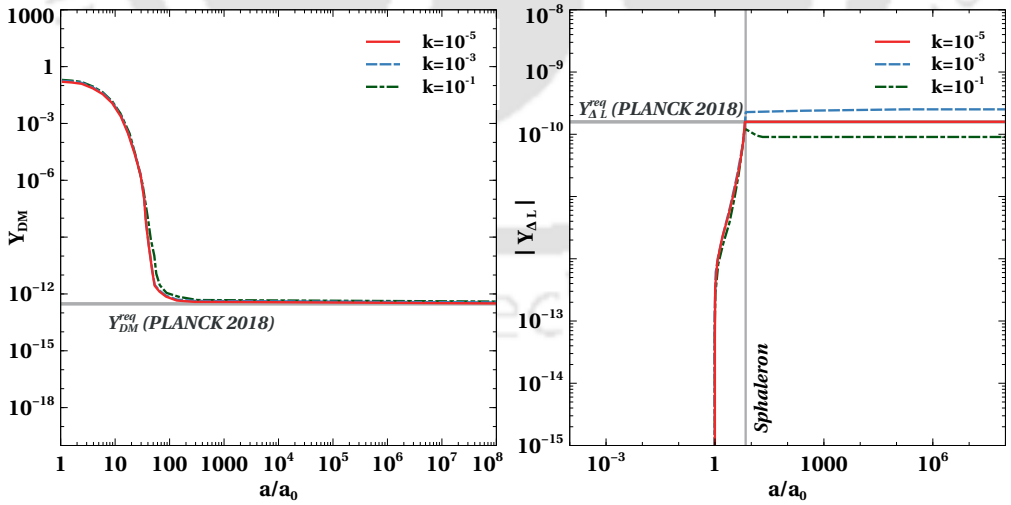

Figure 5.29: The comoving number densities of DM and L asymmetry with the relative scale factor a/a_0 for different values of k. The model parameters are fixed at $m_{\eta_R} = 600$ GeV, $v_\Delta = 1$ keV, $\lambda''_{H\eta} = 1 \times 10^{-5}$, $\mu_{\eta\Delta} = 10i$, $M_1 = 6$ TeV, $M_{j+1}/M_j = 1.1$, and $m_{\Delta^0} = m_{\Delta^\pm} = m_{\Delta^{\pm\pm}} = 1.2$ TeV. Here $T_{\rm end}$ is fixed at 150 GeV.

Case 3: $T_{\rm end} > T_{\rm Sph}$

Finally, we consider $T_{\rm end} = 250$ GeV such that $T_{\rm end} > T_{\rm Sph}$. The evolution of the comoving number densities of DM and the L asymmetry are shown in Fig.5.30. It is clearly seen from the figure that the entropy dilution effect is not evident in this case even for large k namely, $k = 10^{-1}$. On the other hand, it is observed that at least up to $k \simeq 10^{-1}$, the L asymmetry increases with the increase in k.

After studying the evolution of number densities for three different cases, we do a parameter scan over the parameters v_Δ and $|\mu_{\eta\Delta}|$ by keeping $T_{\rm end}$ fixed for each of these cases. The resulting parameter space in Case 1, for $T_{\rm end} = 2$ GeV is shown by the grey coloured patch in Fig.5.31. The limits on the parameter are found to be 0.008 MeV $\lesssim v_\Delta \lesssim$ 0.05 MeV, 700 GeV $\lesssim |\mu_{\eta\Delta}| \lesssim 9 \times 10^4$ GeV in an EMD universe with $k = 10^{-3}$ and $T_{\rm end} = 2$ GeV for $m_{\eta_R} = 600$ GeV.

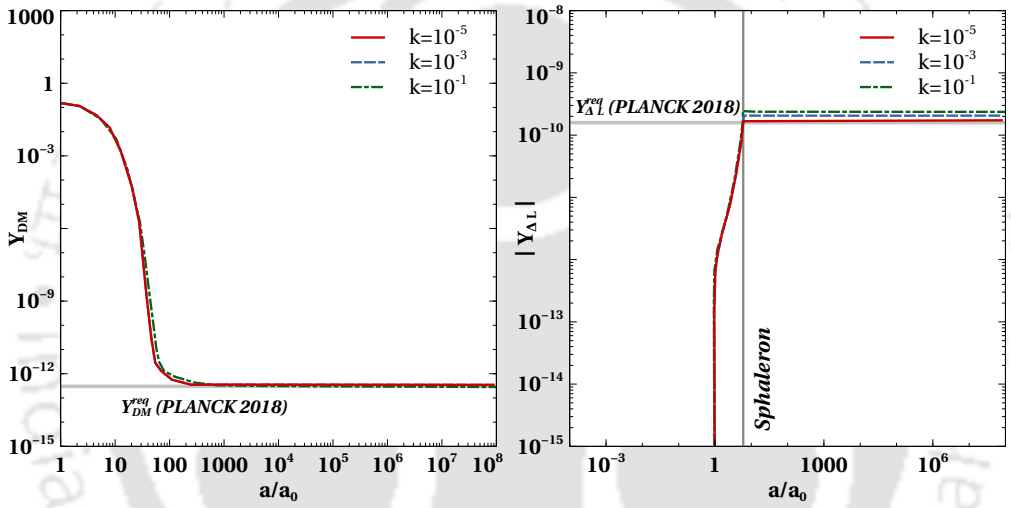

Figure 5.30: The comoving number density of DM and L asymmetry with the relative scale factor a/a_0 for different values of k. The model parameters are fixed at $m_{\eta_R} = 600$ GeV, $v_\Delta = 1$ keV, $\lambda''_{H\eta} = 1 \times 10^{-5}$, $\mu_{\eta\Delta} = 10i$, $M_1 = 6$ TeV, $M_{j+1}/M_j = 1.1$, and $m_{\Delta^0} = m_{\Delta^\pm} = m_{\Delta^{\pm\pm}} = 1.2$ TeV. Here $T_{\rm end}$ is fixed at 250 GeV.

The same in Case 2, for $T_{\rm end} = 150$ GeV is shown by the blue coloured patch in Fig.5.31. For Case 2, the limits on the v_Δ and $\mu_{\eta\Delta}$ are found to be 0.07 MeV $\lesssim v_\Delta \lesssim$ 26 MeV, 0.02 GeV $\lesssim |\mu_{\eta\Delta}| \lesssim$ 85 GeV respectively while keeping DM mass fixed at $m_{\eta_R} = 600$ GeV. Repeating the same for Case 3 while keeping $T_{\rm end} = 250$ GeV results in the light green coloured patch in Fig.5.31. In this case the bounds on v_Δ and $\mu_{\eta\Delta}$ are found to be 2 MeV $\lesssim v_\Delta \lesssim$ 260 MeV and 0.35 GeV $\lesssim |\mu_{\eta\Delta}| \lesssim$ 80 GeV. One can clearly see that the viable parameter space changes for the EMD universe compared to the standard radiation dominated universe. We also found that for larger value of k we need larger $T_{\rm end}$ to satisfy the correct asymmetry. In particular, we found that the correct baryon asymmetry and DM relic can not be achieved for $k \gtrsim 10^{-2}$ due to the strong entropy dilution coming from the matter field ϕ, irrespective of $T_{\rm end}$. As discussed above, there is a range of k near 10^{-3} where the asymmetry can be even more than the standard radiation case for sufficiently large $T_{\rm end} \sim 100$ GeV. Therefore,

we have shown the viable parameter space in $\mu_{\eta\Delta}$ versus v_Δ plane keeping $k = 10^{-3}$ for all the three cases. It is clearly visible that the allowed parameter space reduces for $T_{\rm end} = 2$ GeV compared to $T_{\rm end} = 150, 250$ GeV, because for higher $T_{\rm end}$, the entropy dilution effect is very minimal on both comoving number densities of DM and L asymmetry.

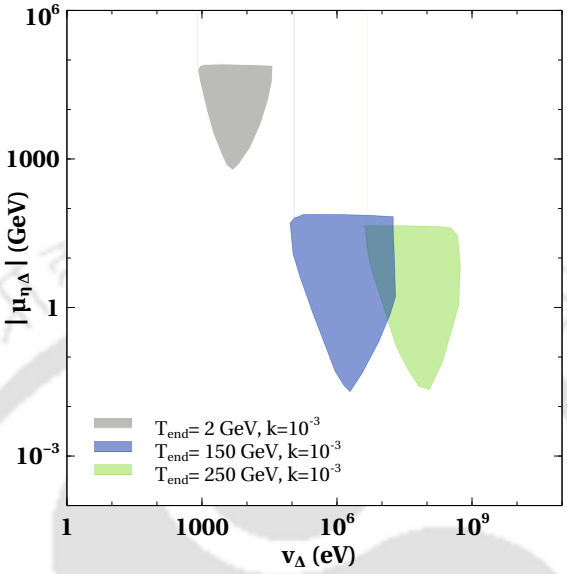

Figure 5.31: Scan plot showing the available parameter space in $\mu_{\eta\Delta}$-v_Δ plane from the requiremnet of correct DM relic and the observed baryon asymmetry for two different possible scenario of early matter dominated universe. The other relevant parameters are set at $m_{\eta_R} = 600$ GeV, $\lambda''_{H\eta} = 10^{-5}$, $m_{\Delta^0} = m_{\Delta^\pm} = m_{\Delta^{\pm\pm}} = 1.2$ TeV, $M_1 = 6$ TeV, $M_{j+1}/M_j = 1.1$.

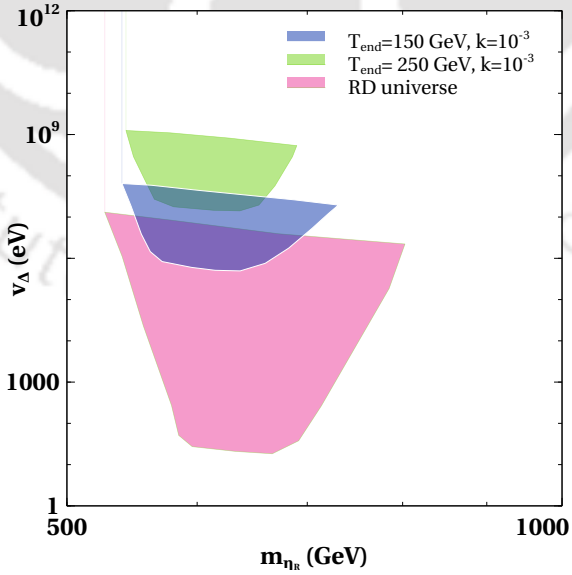

Figure 5.32: Scan plot showing the allowed parameter space in m_{η_R} versus v_Δ plane. The relevant parameters are fixed at $\mu_{\eta\Delta} = 80i$ GeV, $\lambda''_{H\eta} = 1 \times 10^{-5}$, $M_1 = 6$ TeV, $M_{j+1}/M_j = 1.1$.

We then do another scan over the parameters v_Δ and m_{η_R} by keeping the other relevant parameters fixed. The result is shown in Fig.5.32 for case 2, 3 along with the result for standard cosmology. We found that no parameter space is allowed for smaller values of $T_{\rm end} \leq \mathcal{O}(100\,{\rm MeV})$ where the entropy dilution effect is very dominant. However, near $T_{\rm end} \sim T_{\rm Sph}$, when the entropy dilution effect is very minimal we found available parameter space as shown in Fig.5.32. The region shown by pink colour in Fig.5.32 is for $k = 0$ which represents the standard radiation dominated universe. We can clearly see an upward shift of the parameter space along v_Δ axis in case of EMD universe from the standard radiation dominated scenario. This is expected because for case 2, 3 with less effects of entropy dilution, we get more asymmetry than the standard radiation case. Therefore a larger v_Δ is required to satisfy the correct asymmetry. However, the mass of DM needed to satisfy the correct relic does not change much from that in standard radiation domination. This is because, for such large values of v_Δ, required to satisfy the correct asymmetry the annihilations of DM is mainly through the gauge interactions. Therefore the DM relic is determined by the usual gauge interactions and hence the lower limit on DM mass remains the same. The upper bound on DM mass, however, gets reduced visibly in the EMD scenario compared to the standard case. From these results, we can conclude that early matter domination can not lower the scale of WIMPy leptogenesis unlike in the FEU scenario discussed before.

5.4.4 WIMPy leptogenesis in a Scalar-Tensor theory of gravity

In this section, we study the impact of the modified expansion rate of the universe on WIMPy leptogenesis within the framework of a class of Scalar-Tensor theories of gravity (STG) [387, 388]. In STG, gravity is described by both metric and a scalar field. In such theories, the cosmological expansion rate deviates from the standard general relativity (GR) and an attractor mechanism relaxes it to the standard expansion era prior to the onset of the BBN. STG is often formulated in either the Einstein frame or in the Jordan frame with the most general transformation between the two frames is given by

$$\tilde{g}_{\mu\nu} \;=\; C(\phi) g_{\mu\nu} + D(\phi)\partial_\mu\phi\partial_\nu\phi, \tag{5.56}$$

where $\tilde{g}_{\mu\nu}$ and $g_{\mu\nu}$ represent the metrics in Jordan frame and in Einstein frame respectively. Here $C(\phi)$ and $D(\phi)$ are so called the conformal and disformal couplings respectively. In Jordan frame, the matter fields Ψ are directly coupled to the metric, $\tilde{g_{\mu\nu}}$ and therefore the action of the matter sector can be written as $S_{\rm Matter} = S_{\rm Matter}(\tilde{g}_{\mu\nu}, \Psi)$. The effect of modified gravity enters only through the expansion rate of the universe and usual particle physics observables remain unchanged. However, in Einstein frame the scenario becomes completely opposite. Therefore the Jordan frame is considered throughout this work. Leptogenesis in scalar-tensor theories of gravity was studied in [360] while the implications of such non-standard cosmology on DM relic were studied in several earlier works including [361–365]

Following the procedure of [360, 364] the master equation for the evolution of the scalar field in the conformal limit ($D(\phi) = 0$) while ignoring its potential energy is found to be

$$\frac{2}{3B\left[1-\alpha(\varphi)\varphi'\right]^3}\left(\varphi'' + \frac{d\alpha}{d\varphi}(\varphi')^3\right) + \frac{1-\tilde{\omega}}{\left[1-\alpha(\varphi)\varphi'\right]}\varphi' + 2(1-3\tilde{\omega})\alpha(\varphi) = 0. \tag{5.57}$$

Here $\varphi = \kappa\phi$ is a dimensionless scalar introduced for convenience and $B = 1 - \frac{1}{6}\frac{\varphi^{'}}{(1-\alpha(\varphi)\varphi^{'})^2}$. The derivatives are taken with respect to the number of e-folds ($d\tilde{N} = \tilde{\mathbf{H}}dt$) in the Jordan frame, which is defined with a prime $f^{'} = df/d\tilde{N}$. The $\tilde{\mathbf{H}}$ is the modified Hubble expansion rate in the Jordan frame. Here the function $\alpha(\varphi) = \frac{d\ln C^{1/2}}{d\varphi}$, where $C(\varphi)$ is the conformal coupling. We have considered the conformal coupling to be $C(\varphi) = (1 + 0.1\exp(-8\varphi))^2$. The choice of such a conformal function is motivated from earlier works [360, 361, 364]. The number of e-folds can be expressed as a function of the Jordan frame temperature as follows,

$$\tilde{N} = \ln\left[\frac{\tilde{T}_0}{\tilde{T}}\left(\frac{g_{*s}(\tilde{T}_0)}{g_{*s}(\tilde{T})}\right)^{1/3}\right]. \tag{5.58}$$

The modified expansion rate $\tilde{\mathbf{H}}$ in the Jordan frame can be written as [360, 364]

$$\tilde{\mathbf{H}}^2 = \frac{k^2}{k^2_{\rm GR}}\frac{C(1+\alpha(\phi)\phi^{'})^2}{1-\varphi^{'2}/6}H^2, \tag{5.59}$$

where $\mathbf{H}^2 = \frac{k^2_{\rm GR}}{3}\tilde{\rho}$, $k^2 \simeq k^2_{\rm GR} = 8\pi G$ and $\tilde{\rho} \sim g(\tilde{T})\tilde{T}^4$ for the radiation dominated era. From Eq.(5.59) the ratio of the new expansion rate to the standard GR expansion rate is defined as the speed-up parameter,

$$\xi = \frac{\tilde{\mathbf{H}}}{\mathbf{H}} = \left[\frac{k^2}{k^2_{\rm GR}}\frac{C(1+\alpha(\phi)\phi^{'})^2}{1-\phi^{'2}/6}\right]^{1/2}. \tag{5.60}$$

The third term of the master equation shown in Eq.(5.57) behaves like an effective potential term which is given by $V_{\rm eff} = \ln C^{1/2}$. During the radiation dominated era, $\tilde{\omega} = 1/3$ due to which the effective potential term disappears. Later, when the particles start becoming non-relativistic, $\tilde{\omega}$ slightly deviates from 1/3 and the effective potential kicks in. In absence of the effective potential, the master equation predicts a solution of the type $\varphi^{'} \propto e^{-\tilde{N}}$. This means that any initial value of velocity will instantly become zero. As discussed in [360, 364], positive initial value of φ and negative initial value of $\varphi^{'}$ lead to a very interesting scenario where the field moves to negative values until its velocity becomes zero and then becomes positive again as the field rolls back down the effective potential. This change in pattern in the evolution of the scalar field leads to a peak in the conformal function C which gives rise to a non-trivial change in the Jordan's frame Hubble expansion rate. Later the conformal factor becomes one and the standard GR expansion rate is recovered.

To calculate the equation of state parameter $\tilde{\omega}$ throughout the early stages of the universe we start writing [361, 363]

$$1 - 3\tilde{\omega} = \frac{\tilde{\rho} - 3\tilde{p}}{\tilde{\rho}} = \sum_A \frac{\tilde{\rho_A} - 3\tilde{p_A}}{\tilde{\rho}} + \frac{\tilde{\rho_m}}{\tilde{\rho}}, \tag{5.61}$$

where the sum runs over all the particles in thermal equilibrium during the early stages of the universe. The $\tilde{\rho_m}$ is the contribution from the non-relativistic pressureless matter. During the radiation dominated era the $\tilde{\rho_m}$ is negligible. Therefore the equation of state parameter becomes

$$\tilde{\omega} = \frac{1}{3}\left(1 - \sum_A \frac{\tilde{\rho_A} - 3\tilde{p_A}}{\tilde{\rho}}\right). \tag{5.62}$$

The energy density and pressure of any particle A are given by

$$\tilde{\rho_A}(\tilde{T}) = \frac{g_A}{2\pi^2}\int_{m_A}^{\infty} \frac{(E^2 - m_A^2)^{1/2}}{\exp(E/\tilde{T}) \pm 1} E^2 dE \tag{5.63}$$

$$\tilde{p}_A(\tilde{T}) = \frac{g_A}{6\pi^2}\int_{m_A}^{\infty} \frac{(E^2 - m_A^2)^{3/2}}{\exp(E/\tilde{T} \pm 1)} dE, \tag{5.64}$$

where g_A is the number of internal degrees of freedom of species A and the plus (minus) sign inside the integrals correspond to fermions (bosons). In the calculation of $\tilde{\omega}$ we have taken all the relevant particles in our model into consideration. Apart from the particles considered in [364], we have three additional Majorana neutrinos, one inert doublet scalar and one triplet scalar. We show the result for the evolution of $\tilde{\omega}$ in Fig.5.33, between temperature $1\,\text{MeV} \leq \tilde{T} \leq 100$ TeV. As the individual particles are becoming non-relativistic at different temperatures, the kicks are appearing in $\tilde{\omega}$. We then solve the Boltzmann equations for Wimpy leptogenesis. The relevant BEs are given below.

$$\frac{dY_\eta}{dz} = -\frac{s(z)}{z\xi(z)\mathbf{H}(z)}\langle\sigma v\rangle_{\eta\eta\longrightarrow \text{SM SM}}\left[Y_\eta^2 - (Y_\eta^{\text{eq}})^2\right] \tag{5.65}$$

$$\begin{aligned}\frac{dY_{\Delta L}}{dz} &= \frac{s(z)}{z\xi(z)\mathbf{H}(z)}\langle\sigma v\rangle^{\delta}_{\eta\eta\longrightarrow ll}\left[Y_\eta^2 - (Y_\eta^{\text{eq}})^2\right] \\ &\quad - \frac{s(z)}{z\xi(z)\mathbf{H}(z)} Y_{\Delta L} Y_l^{\text{eq}} r_\eta^2 \langle\sigma v\rangle_{\eta\eta\longrightarrow ll} \\ &\quad - \frac{s(z)}{z\xi(z)\mathbf{H}(z)} Y_{\Delta L} Y_\eta^{\text{eq}} \langle\sigma v\rangle_{\eta\bar{l}\longrightarrow \eta l}.\end{aligned} \tag{5.66}$$

Here the speed-up parameter can be written in terms of the parameter z as follows

$$\xi(z) = \frac{C^{1/2}(\varphi)}{C^{1/2}(\varphi_0)} \frac{1}{(1 - \alpha(\varphi)\, z\, d\varphi/dz)\sqrt{B}\sqrt{1+\alpha^2(\varphi_0)}}. \tag{5.67}$$

where $B = 1 - \frac{1}{6}\frac{1}{(1-\alpha(\varphi)\, z\, d\varphi/dz)^2}\left(z\frac{d\varphi}{dz}\right)^2$. Here $s(z)$ is the entropy density defined in the Jordan frame. In terms of the Jordan frame temperature it is given by $s(\tilde{T}) = \frac{2\pi}{45} g_{*s}(\tilde{T})\tilde{T}^3$.

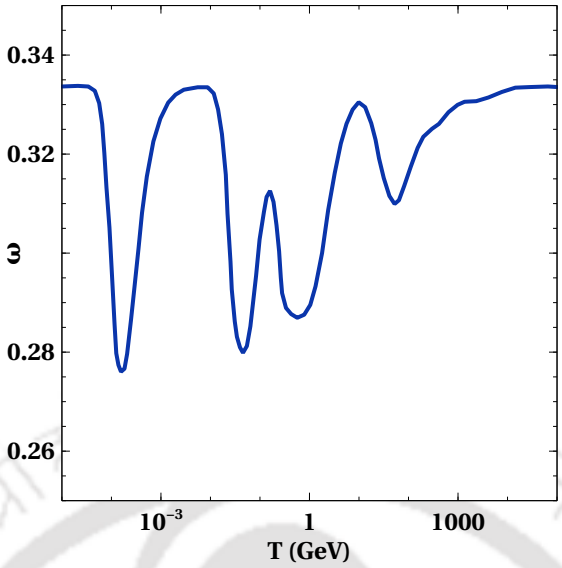

Figure 5.33: Equation of state parameter as a function of temperature. Here T in x-axis is equivalent to $\tilde{T}$, the temperature in the Jordan frame.

Solving the φ equation we show the evolution of the field φ, the conformal factor $C(\varphi)$, the speed-up parameter and the Hubble $\tilde{H}$ with $z = m_{\rm DM}/\tilde{T}$ in Fig.5.34. It can be seen that the field φ changes the nature of its evolution at a particular value of $\tilde{T}$ depending on the initial conditions chosen. This change in φ brings a non-trivial change in the conformal factor as well as in $\tilde{H}$ and hence the speed-up parameter. From the evolution plot it can be seen that as the field moves down the potential there is an increase in the Hubble $\tilde{H}$ compared to the standard GR expansion rate, as shown in the lower right panel of Fig.5.34. A sharp enhancement in the speed-up parameter can also be seen. But as the field rolls back and settles at a positive value, both the conformal factor and the speed-up parameter become one relaxing back to the standard GR case. Thereafter the Hubble $\tilde{H}$ settles with standard GR expansion rate.

We then solve the BEs together with the φ equation to look for the possible changes in DM relic and L asymmetry due to the enhancement of the expansion rate. From the L asymmetry evolution plots in Fig.5.35, it can be seen that the asymmetry increases in such a scenario compared to the standard case. However, it is observed that the DM relic is unaffected for $m_{\rm DM} = 600$ GeV. The reason for this is the following. For $\tilde{T}_0 = 1$ TeV, the enhancement in ξ is occurring near $z \simeq 1$ and during that period the DM particles are in equilibrium and the freeze-out of DM occurs near $20 \lesssim z \lesssim 30$. Hence their abundance does not change much. But, with the increase in ξ the washout processes of the asymmetry get relatively weaker and a rise in the asymmetry results. Also it can be seen that with the increase in $\varphi_0^{'}$ and with the decrease in φ_0 the asymmetry increases. It is because, with the increase in $\varphi_0^{'}$ and with the decrease in φ_0, the conformal factor and the ξ increases. However, one can not increase the $\varphi_0^{'}$ arbitrarily. There is an upper limit on $\varphi_0^{'}$ ($\varphi_0^{'} \lesssim \pm\sqrt{6}$) coming from the Friedmann equation [364].

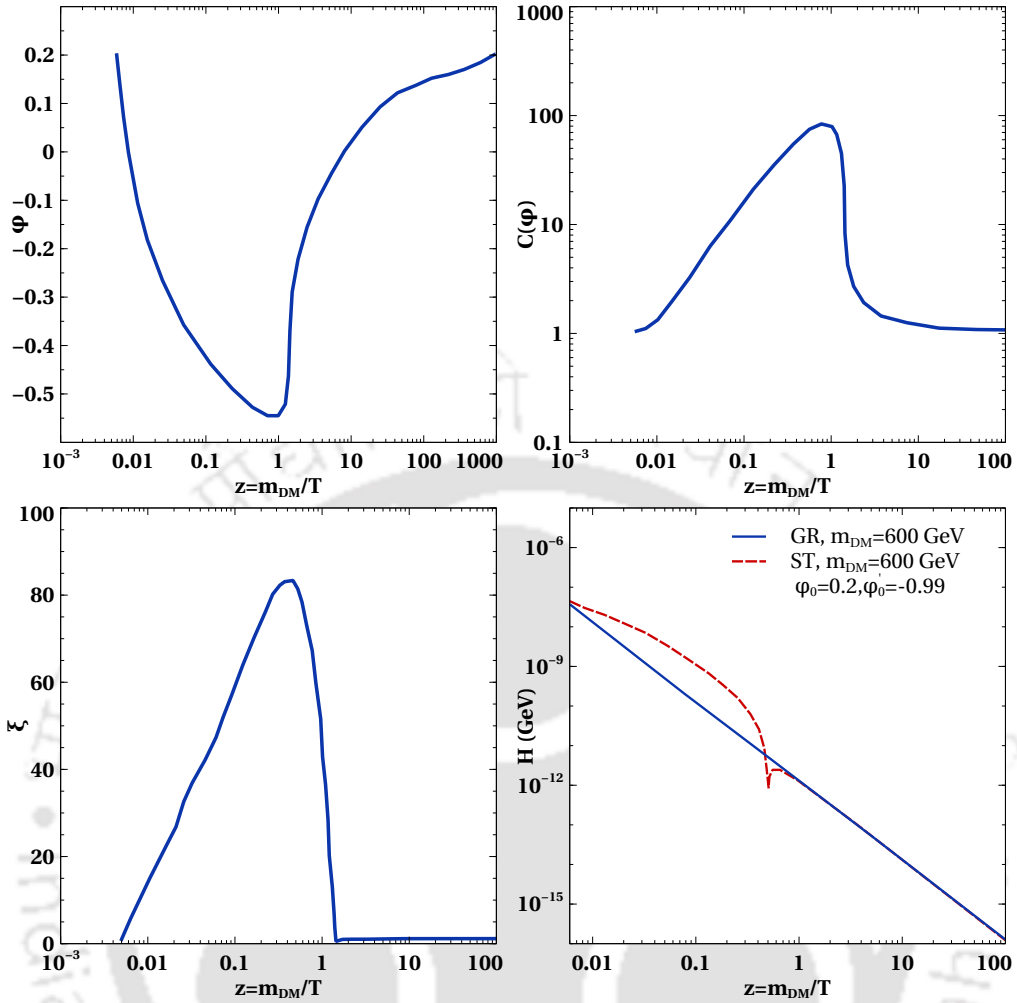

Figure 5.34: Plots showing the evolution of the field (upper left plot), the conformal factor (upper right plot), speed-up parameter ξ (lower left plot) and Hubble expansion rate (lower right plot) with $z = m_{\rm DM}/\tilde{T}$. Here $m_{\rm DM} = 600$ GeV and the initial conditions are chosen to be $(\varphi_0, \varphi_0^{'}) = (0.2, -0.72)$ and $\tilde{T}_0 = 100$ TeV. Here T in x-axis is equivalent to $\tilde{T}$, the temperature in the Jordan frame.

We then look for the possibility of lowering the scale of leptogenesis by choosing the appropriate cosmological parameters. We fix the mass of the DM to be $m_{\rm DM} = 400$ GeV (keeping in mind that it is not allowed with standard GR expansion due to suppressed relic). Keeping the other particle physics parameters at benchmark values as described in Fig.5.36, we change the cosmological parameters $\varphi_0, \varphi_0^{'}$ and $\tilde{T}_0$. From the evolution plot of DM shown on the left panel of Fig.5.36, it can be seen that both the benchmark values give rise to relic lower than the observed one in the case of standard GR expansion (dashed lines). Apart from the strong gauge portal annihilations, the chosen value of $v_\Delta = 1$ eV, also leads to strong DM annihilations via the processes $\eta\eta \longrightarrow ll$ leading to further suppression in relic.

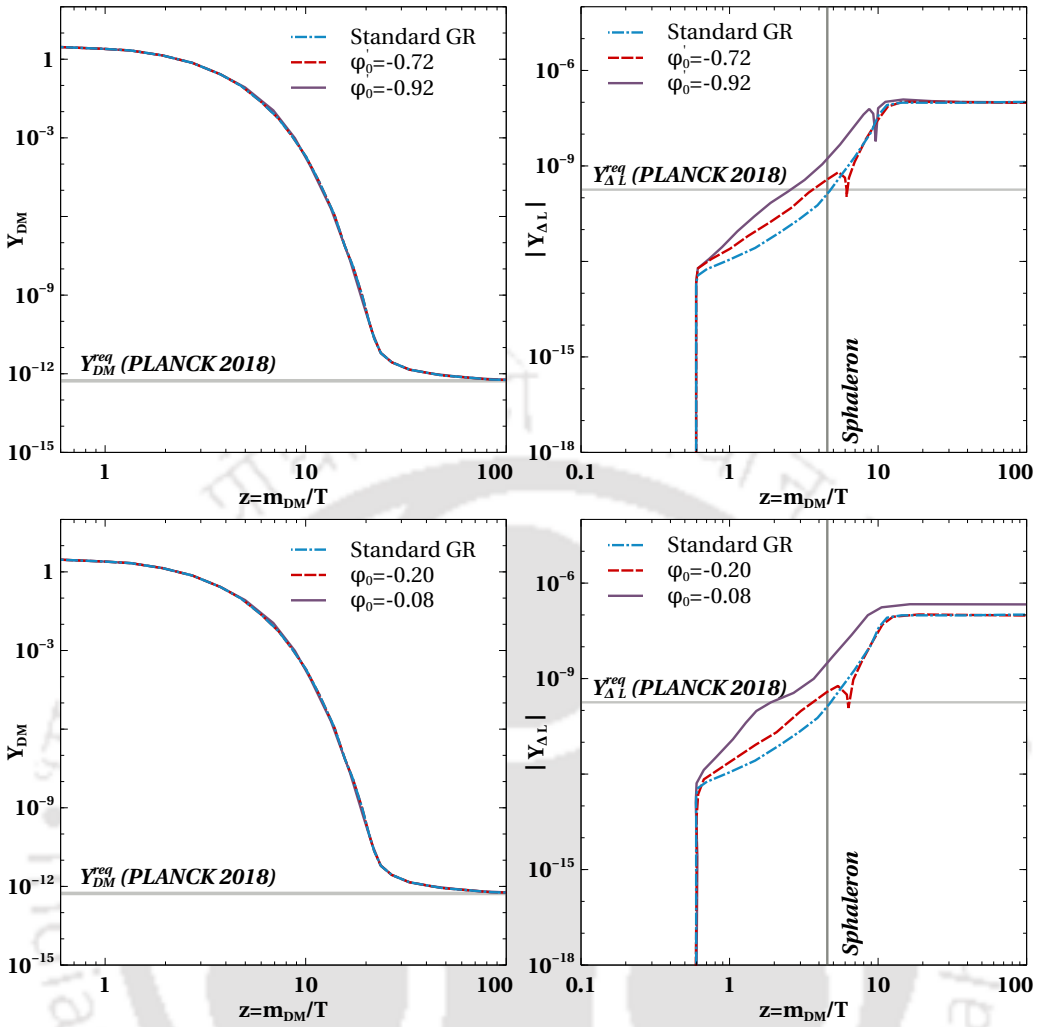

Figure 5.35: Evolution plot for the comoving number density of DM and L asymmetry with different value of for $\varphi_0^{'}$ with $\varphi_0 = 0.2$ (left panel plots) and for different φ_0 with $\varphi_0^{'} = -0.72$ (right panel plot) with $\tilde{T}_0 = 1$ TeV. The particle physics parameter are fixed at $m_{\eta_R} = m_{\rm DM} = 600$ GeV, $\lambda_{H\eta}^{''} = 1 \times 10^{-5}$, $\mu_{\eta\Delta} = 10i$ GeV, $v_\Delta = 1$ keV, $m_{\Delta^0} = m_{\Delta^\pm} = m_{\Delta^{\pm\pm}} = 1.2$ TeV, $M_1 = 6$ TeV, and $M_{j+1}/M_j = 1.1$. Here T in x-axis is equivalent to $\tilde{T}$, the temperature in the Jordan frame.

However, with the enhancement of the Hubble expansion rate in STG, both these benchmark points give rise to the correct relic (solid lines). Similarly, from the evolution plot of the L asymmetry on the right panel of Fig.5.36, we can see that both these benchmark points lead to insufficient L asymmetry at the time of sphaleron decoupling. But with the modified expansion rate, they generate the correct L asymmetry. Therefore, we can conclude that in scalar-tensor theory of gravity a new viable parameter space will open up with lower scales of WIMPy leptogenesis. Finally we do a parameter scan over the parameters $m_{\rm DM} \equiv m_{\eta_R}$ and v_Δ by keeping the other parameters fixed. We show the result in Fig.5.37. From Fig.5.37 we can see that the viable parameter space changes significantly from that in standard GR case. This can be understood from the fact that enhanced background expansion rate in

STG leads to an increase in DM relic as well as the L asymmetry.

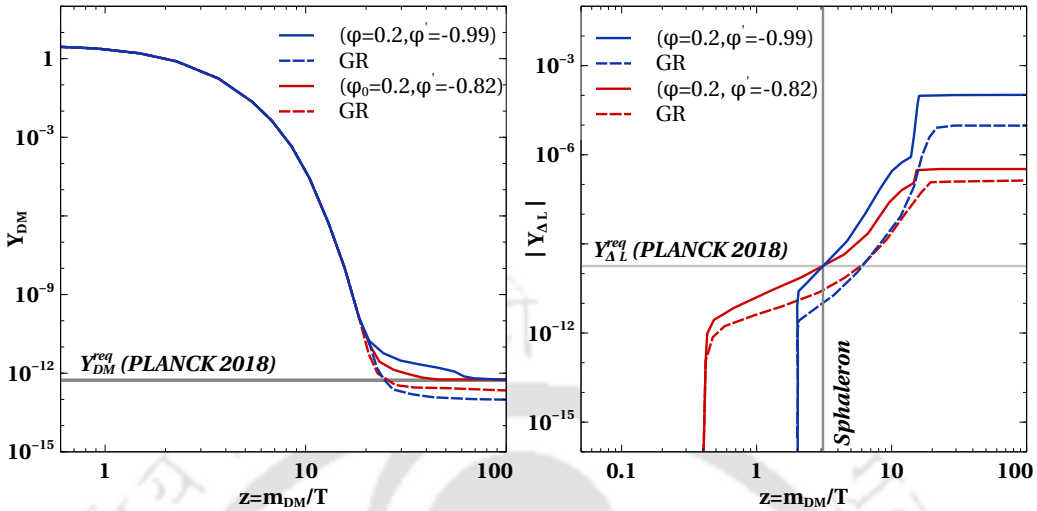

Figure 5.36: Evolution plot of the comoving number density of DM and L asymmetry with $z = m_{\rm DM}/\tilde{T}$ for different benchmark values of the cosmological parameters. Here the particle Physics parameters are fixed at $m_{\rm DM} = 400$ GeV, $\lambda''_{H\eta} = 1 \times 10^{-5}$, $m_{\Delta^0} = m_{\Delta^\pm} = m_{\Delta^{\pm\pm}} =$ 800 GeV, $M_1 = 6$ TeV, $M_{j+1}/M_j = 1.1$, $\mu_{\eta\Delta} = 100i$ GeV and $v_\Delta = 1$ eV. The initial temperature ($\tilde{T}_0$) are taken to be 1 TeV (for the red lines) and 200 GeV (for the blue lines). Here T in x-axis is equivalent to $\tilde{T}$, the temperature in the Jordan frame.

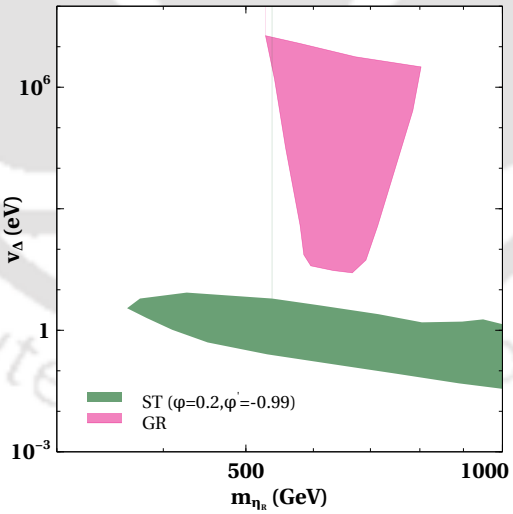

Figure 5.37: Scan plot showing the viable parameter space in $m_{\eta_R} - v_\Delta$ plane by keeping the other parameters fixed. The important cosmological parameters are fixed at $\varphi_0 = 0.2$, $\varphi' = -0.99$ and $T_0 = 200$ GeV. The other relevant particle physics parameters were set at $\mu_{\eta\Delta} = 80i$ GeV, $\lambda''_{H\eta} = 1 \times 10^{-5}$, $M_1 = 6$ TeV, $M_{j+1}/M_j = 1.1$.

This leads to a requirement of large Y^Δ such that the annihilation of DM through the Yukawa interaction ($\eta\eta \longrightarrow ll$) is more compared to the usual gauge portal channels. This

also makes the washout processes stronger which help in reducing the asymmetry. Hence the parameter space can be seen to be shifted towards smaller values of the v_Δ. Also since we are no longer relying on the standard gauge portal interactions to satisfy the DM relic, a broader range of $m_{\rm DM}$ is allowed compared to the standard GR case. For the specific values of other parameters mentioned in the caption of Fig.5.37 the limits on m_{η_R} and v_Δ are found to be 320 GeV $\lesssim m_{\eta_R} \lesssim$ 1.55 TeV and 0.02 eV $\lesssim v_\Delta \lesssim$ 9.6 eV.

CHAPTER 6

Summary

In this chapter, we finally summarise the key results obtained in this thesis. We have studied some minimal particle physics scenarios which provide a common framework for leptogenesis as well as dark matter while being consistent with neutrino mass and other phenomenological constraints. We have particularly focused on the possibility of having a low scale leptogenesis contrary to high scale vanilla leptogenesis setups, such that the detection prospects of such scenarios get enhanced.

In chapter 2 of this thesis, we have studied the possibility of fermion singlet dark matter in the minimal scotogenic model along with explaining the origin of the baryon asymmetry of the universe through leptogenesis. The stable nature of the lightest right handed neutrino, being the dark matter candidate, leaves us with the possibility of next to lightest right handed neutrino N_2 decay as the source of lepton asymmetry. Compared to the vanilla leptogenesis scenario with N_1 decay as the main source of lepton asymmetry in the minimal scotogenic model, here the scale of leptogenesis gets pushed above to $M_2 \sim 10^{10}$ GeV, in the case of normal ordering of light neutrino masses. However, in the case of inverted ordering of light neutrino mass, the scale of leptogenesis can be significantly lower by several orders of magnitude to $M_2 \sim 50$ TeV. While both thermal as well as non-thermal DM is feasible with NO, we show that IO does not allow non-thermal N_1 dark matter due to the neutrino mass constraints on Dirac Yukawa coupling structures. While the scale of N_2 leptogenesis still remains moderately high with IO and very high with NO of light neutrino masses, there exists interesting physics at low scale in terms of fermion singlet DM and inert scalar doublet which can be probed at experiments.

In chapter 3 of this thesis, we have proposed a model to implement the idea of leptogenesis from three-body decay of a heavy particle with some of the final state particles playing the role of dark matter. Non-zero CP asymmetry arises due to interference of multiple three-body decay diagrams with resummed propagators. The minimal setup consists of three singlet fermions and two scalar fields: one singlet and one doublet beyond the standard model field content. While two of these singlet fermions and the additional scalar doublet help in generating light neutrino masses one-loop level, the other two particles help in realising the desired three-body decay leptogenesis. Due to the presence of new parameters which affect CP asymmetry but not neutrino mass, and phase space suppression of three-body decay, the scale of leptogenesis was found to be lower than usual two-body decay leptogenesis in scotogenic model. The minimal setup also leads to a two-component dark matter scenario

in terms of scalar singlet and neutral component of scalar doublet, giving rise to a rich dark matter phenomenology. Possibility of leptogenesis at a scale as low as 2 TeV without any resonant enhancement or fine-tuned mass spectrum, keeps the discovery prospects of such models very promising at near future experiments.

In chapter 4 of this thesis, we have proposed a minimal scenario to achieve successful Dirac leptogenests at a scale of few tens of TeV along with dark matter by considering a gauged $B-L$ extension of the standard model. While light Dirac neutrino mass is assumed to arise from SM Higgs coupling for simplicity, additional heavy Majorana fermions are introduced in such a way that leads to $\Delta(B-L) \neq 2$ processes, required to prevent Majorana mass contribution to light neutrinos. These heavy neutrinos can couple to SM lepton doublets via an additional Higgs doublet and hence can lead to the generation of lepton asymmetry through standard out-of-equilibrium decays. Since the relevant Yukawa couplings involved in such decays remain decoupled from light neutrino mass generation, they can be tuned freely so as to realise successful Dirac leptogenesis at low scale. Since these heavy Majorana fermions have gauged $B-L$ interactions, the corresponding gauge washout effects play non-trivial role thereby giving constraints on $g_{BL} - M_{Z_{BL}}$ parameter space from successful leptogenesis criteria. Additionally, the Dirac nature of light neutrinos leads to additional relativistic degrees of freedom which can be thermalised due to gauged $B-L$ interactions and hence can be constrained further from Planck 2018 bounds on such additional thermalised relativistic degrees of freedom $\Delta N_{\rm eff}$. While the additional scalar doublet η can be a stable DM candidate by itself, its degenerate neutral components give rise to a large direct detection rate, similar to sneutrino DM in MSSM. This requires sub-dominant contribution of η to DM relic and we show that it can be achieved only when its annihilations into Z_{BL} becomes kinematically allowed, further constraining $g_{BL}-M_{Z_{BL}}$ parameter space from the requirement of its under-abundance. On the other hand, additional chiral fermions are needed to make the model anomaly free. We show one possible way of cancelling these anomalies with the inclusion of four chiral fermions with fractional $B-L$ charges. With an appropriate choice of singlet scalars, these fermions give rise to two Dirac fermions, eligible for being DM candidates. We show that the criteria of correct DM relic from fermion DM along with sub-dominant scalar doublet while being in agreement with direct detection data constrains the $g_{BL}-M_{Z_{BL}}$ parameter space significantly. For two different scales of leptogenesis we considered, only the higher one namely, $M_1 = 80$ TeV gives rise to some common parameter space consistent with all criteria and experimental bounds. Future LHC runs as well as CMB measurements will be able to probe the entire parameter space consistent with successful Dirac leptogenesis and thermal dark matter.

In chapter 5 of this thesis, we have studied the possibility of generating correct baryon asymmetry and dark matter relic in the universe by considering non-standard cosmological epochs prior to the BBN era. While leptogenesis in non-standard cosmology has not been studied much in the literature, we also looked for the possibility of lowering the scale of leptogenesis compared to the one in standard ΛCDM cosmology. In the first part of this chapter, we consider the usual leptogenesis from heavy neutrino decay in the scotogenic model discussed earlier with the inert scalar doublet being the DM candidate. We incorporated two different non-standard cosmological histories namely, a fast expanding universe and an early matter dominated universe. While DM relic calculation in such non-standard cosmological epochs were studied earlier, the detailed calculations for leptogenesis were missing. We

find that the fast expanding universe scenario allows a low scale leptogenesis in this model, keeping it around a few tens of TeV. However, the early matter domination scenario pushes the scale of leptogenesis to high scale. While the modified Hubble parameter affects the rates of decays and scattering relevant for leptogenesis in a complicated manner, the requirement of a higher scale of leptogenesis in EMD scenario is primarily due to the need of overproducing the lepton asymmetry initially to survive the subsequent entropy dilution.

In the second part of chapter 5 we have studied the impact of three different non-standard cosmology scenarios on leptogenesis while considering the lepton asymmetry to be originating from WIMP type DM annihilations. Unlike the earlier studies in this thesis, this provides a stronger connection between the origin of baryon asymmetry and DM, giving rise to a cogenesis setup which can explain the baryon-DM coincidence. Since the minimal scotogenic model discussed before does not allow for this possibility, we extend it by a complex scalar triplet field such that light neutrino mass can arise from a combination of type-II and scotogenic seesaw. The neutral component of the Z_2-odd scalar doublet is considered to be the WIMP DM having both lepton number violating and lepton number conserving annihilation processes. After reproducing the known results for WIMPy leptogenesis in standard cosmology, we implement it in three different non-standard cosmology scenario namely, fast expanding universe, early matter domination and scalar-tensor theory of gravity. Apart from the shift in parameter space compared to the standard cosmology scenario, we also found the scale of leptogenesis or equivalently the WIMP DM mass to be lower in FEU and STG scenarios. This can open up interesting detection prospects of such lighter DM at both direct as well as indirect detection experiments together with colliders. This is in sharp contrast with canonical seesaw or leptogenesis scenarios where the scale remains out of reach from direct experimental probes.

The minimal scenarios studied in this thesis not only provide a unified framework for leptogenesis and dark matter together with light neutrino masses, providing a solution to three longstanding problems in the standard model of particle physics. While some of these scenarios also lead to a low scale leptogenesis around the TeV corner bringing it within the reach of colliders, all the models we have studied can have several interesting and complementary detection aspects. For example, most of these models should face further scrutiny with future data from collider, neutrino, cosmology as well as rare decay experiments looking for charged lepton flavour violation, neutrinoless double beta decay etc. In fact, future observation of neutrinoless double beta decay can rule out the Dirac leptogenesis scenario we have discussed in chapter 4. Charged lepton flavour violation like $\mu \to e\gamma, \mu \to 3e$ and $\mu \to e$ (Ti) conversion in scotogenic type models can be sizeable and saturate experimental upper bounds on corresponding branching ratios as discussed in several works including [138, 389, 390]. Another interesting prospect could be to the role of additional scalars in driving cosmic inflation. As shown in the recent work [143], the Z_2-odd scalar doublet in the scotogenic model can give rise to an inflationary phase of expansion at very early epochs of the universe through its non-minimal coupling to gravity, while playing the role of DM at the same time. Another interesting prospect of probing our model can be in the form of gravitational waves (GW) from a strongly first order phase transition (SFOPT). In a recent work [390], it was shown that in the minimal scotogenic model, the criteria of SFOPT constrains the scalar sector a lot, leading to a scalar DM parameter space in tension with direct detection bounds. Presence of an additional singlet scalars, as in the model studied in chapter 3, whose

mass is not as constrained as the inert doublet components, the SFOPT criteria is likely to be satisfied with more freedom. The the non-standard cosmological scenarios, discussed in chapter 5 can also have interesting GW signatures [391, 392]. In fact, such non-standard cosmological era leads to tilts in GW spectrum with amplification of amplitude in high or low frequency regime depending upon the equation of state [392–394]. Accordingly, such non-standard era can be constrained from its effect on primordial GW spectra generated by inflationary dynamics or by other sources like topological defects. Firstly, this can be constrained from non-observation of primordial GW at existing experiments. Secondly, if GW starts dominating the radiation energy density of the universe it can give rise to additional $\Delta N_{\rm eff}$ which is constrained from BBN and CMB measurements. Such bound on $\Delta N_{\rm eff}$ can be used to put upper bound $\Omega_{\rm GW}h^2 \lesssim 10^{-6}$. In order to keep the amplified GW amplitude in non-standard cosmology within these bounds, the inflationary scale has to be lower than the maximum allowed value in standard cosmology $\mathbf{H}_{\rm inf} \leq 10^{-6} M_{\rm Pl}$. These bounds can be strong in scenarios where the equation of state parameter is much stiffer than radiation, like in FEU. It will be interesting to study such complementary probes of these models while also improving them theoretically to solve other puzzles in particle physics and cosmology.

APPENDIX A

Here we explain the details of the R matrix used in chapter 2

A.1 Choice of R matrix and N_2 leptogenesis

The choice of complex orthogonal matrix R that appears in the Casas-Ibarra parametrisation of Yukawa couplings (3.12), is crucial for both leptogenesis and dark matter phenomenology. In general, it can be parametrised by three complex parameters. In case of only two right handed neutrinos, the R matrix is a function of only one complex rotation parameter $z = z_R + iz_I, z_R \in [0, 2\pi], z_I \in \mathbb{R}$ [178]. This does not leave much freedom in choosing R and gives rise to a lower bound on the scale of leptogenesis very similar to the Davidson-Ibarra bound $M_1 > 10^9$ GeV [64] even in scotogenic model with two right handed neutrinos [113]. However, in our case, although leptogenesis is due to N_2 decay, we still have more freedom in choosing R compared to the two right handed neutrino scenario. As discussed in the main text, our choice of R matrix is

$$R = \begin{pmatrix} 1 & 0 & 0 \\ 0 & \cos z & \sin z \\ 0 & -\sin z & \cos z \end{pmatrix} \tag{A.1}$$

Recalling the relation between Yukawa and R (3.12) that is, $Y = UD_\nu^{1/2} R^\dagger \Lambda^{1/2}$ and the product of Yukawas relevant for CP asymmetry $(Y^\dagger Y)_{ij} = \sqrt{\Lambda_i \Lambda_j}(RD_\nu R^\dagger)_{ij}$, we calculate, for the above choice of R matrix, the following quantity

$$RD_\nu R^\dagger = \begin{pmatrix} m_1 & 0 & 0 \\ 0 & m_2 \cos z(\cos z)^* + m_3 \sin z(\sin z)^* & -m_2(\sin z)^* \cos z + m_3(\cos z)^* \sin z \\ 0 & -m_2(\cos z)^* \sin z + m_3 \cos z(\sin z)^* & -m_2(\sin z)^* \sin z + m_3 \cos z(\cos z)^* \end{pmatrix} \tag{A.2}$$

This clearly gives a non-zero complex entry in $(Y^\dagger Y)_{23}$ which will contribute to net CP asymmetry ϵ_2 in accordance with Eq.(C.27). This choice of R also explains the reason behind the difference in the scale of leptogenesis we obtained for NO and IO. As can be seen from the CP asymmetry parameter ϵ_2 given in (C.27), it is also inversely proportional to $(Y^\dagger Y)_{22}$. Therefore, for maximum CP asymmetry $(Y^\dagger Y)_{22}$ should be smaller and imaginary

part of $((Y^\dagger Y)_{23})^2$ should be larger. As can be seen from the matrix given in Eq.(A.2), the (22) element can be made very small for IO by choosing z in such a way that makes $\cos z$ small. The term containing $\sin z$ can be small by choosing m_3 arbitrarily small. Since we are not making $\sin z$ arbitrarily small, we can still have a larger (23) term of the matrix (A.2) to enhance the CP asymmetry parameter ϵ_2. However, in case of NO, we can not choose either m_2 or m_3 to be small and hence it is not possible to get a hierarchy between (23) and (22) terms of the matrix (A.2). Therefore, the only way that can increase the CP asymmetry parameter is by pushing the scale M_2 up. This results in higher scale of leptogenesis in NO compared to that in IO.

If we had taken a different choice of R, with the rotation parameters either in $1-3$ plane or $1-2$ plane, we will get

$$RD_\nu R^\dagger = \begin{pmatrix} m_1\cos z(\cos z)^* + m_3 \sin z(\sin z)^* & 0 & -m_1\cos z(\sin z)^* + m_3(\cos z)^*\sin z \\ 0 & m_2 & 0 \\ -m_1(\cos z)^*\sin z + m_3\cos z(\sin z)^* & 0 & m_1(\sin z)^*\sin z + m_3\cos z(\cos z)^* \end{pmatrix} \tag{A.3}$$

and

$$RD_\nu R^\dagger = \begin{pmatrix} m_1\cos z(\cos z))^* + m_2 \sin z(\sin z)^* & -m_1\cos z(\sin z)^* + m_3(\cos z)^*\sin z & 0 \\ -m_1(\cos z)^*\sin z + m_2\cos z(\sin z)^* & m_1\sin z(\sin z)^* + m_3\cos z(\cos z))^* & 0 \\ 0 & 0 & m_3 \end{pmatrix} \tag{A.4}$$

respectively. Clearly, the rotation only in $1-3$ plane can not give rise to non-vanishing CP asymmetry in our case, as both $(Y^\dagger Y)_{23}$ and $(Y^\dagger Y)_{21}$ terms appearing in CP asymmetry formula (C.27) are vanishing as seen from (A.3). A rotation in $1-2$ plane can however, give rise to a net CP asymmetry, as seen from (A.4). We now try to estimate the strength of the resulting lepton asymmetry from such a choice of R. Let us choose the R matrix to be

$$R = \begin{pmatrix} \cos z & \sin z & 0 \\ -\sin z & \cos z & 0 \\ 0 & 0 & 1 \end{pmatrix} \tag{A.5}$$

with $z = 0.82 + 1.42i$ for NO and $z = 0.48 - 0.58i$ for IO. We then solve the coupled Boltzmann equations to find the evolution of N_2 number density and $B-L$ asymmetry for both NO and IO. The resulting plots are shown in Fig.2.2 and 2.9 respectively. As can be seen from these two plots, the net lepton asymmetry generated for such a choice of R matrix remain several order of magnitudes smaller than the required one [1]. Therefore, it justifies the use of $2-3$ rotation in R matrix as was done in the main text. We also check that, it still remains suppressed even if we push the scale of leptogenesis higher say $M_2 \sim 10^{14}$ GeV. Apart from the R matrix, another factor which affects the resulting asymmetry is the loop function $F(r_{ji}, \eta_i)$ in CP asymmetry formula (C.27). For $1-2$ rotation, it is effectively the contribution from N_1 in loop which is contributing the net CP asymmetry from N_2 decay. Since N_1 is lighter than N_2 we have $r_{ji} \equiv r_{12} < 1$ and the loop factor $F(r_{12}, \eta_2)$ gets suppressed in this regime. On the other hand for $2-3$ rotation the loop factor $F(r_{32}, \eta_2)$ can be large as we are in the regime $r_{ji} \equiv r_{32} > 1$.

[1] Here, for simplicity, we have not considered $\Delta L = 1$ washout processes, including which, will lower the asymmetries further.

Now, coming to the implications for dark matter sector, let us consider the R matrix to be a multiplication of two different rotation matrices $R = R_{23}R_{13}$ given by

$$R = \begin{pmatrix} \cos z' & 0 & \sin z' \\ -\sin z \sin z' & \cos z & \sin z \cos z' \\ -\cos z \sin z' & -\sin z & \cos z \cos z' \end{pmatrix} \tag{A.6}$$

This choice of R matrix will give us the following Yukawa couplings for N_1 to the three lepton generations

$$Y_{i1} = \begin{pmatrix} \sqrt{m_1}\sqrt{\Lambda_1}(\cos z')^* U_{11} + \sqrt{m_3}\sqrt{\Lambda_1}(\sin z')^* U_{13} \\ \sqrt{m_1}\sqrt{\Lambda_1}(\cos z')^* U_{21} + \sqrt{m_3}\sqrt{\Lambda_1}(\sin z')^* U_{23} \\ \sqrt{m_1}\sqrt{\Lambda_1}(\cos z')^* U_{31} + \sqrt{m_3}\sqrt{\Lambda_1}(\sin z')^* U_{33} \end{pmatrix} \tag{A.7}$$

where U_{ij} are the PMNS matrix elements. If we set $z' = 0$, we recover the first column of Yukawa matrix given in Eq.(2.41). In that case, as we mentioned earlier, if we have normal ordering of light neutrino masses, we can have small Yukawa couplings of N_1 by choosing small m_1. Or else, we can choose sizeable Yukawa by choosing large values of m_1. These two scenarios can lead to thermal and non-thermal dark matter possibilities respectively. Now, for inverted ordering, we can not have arbitrarily small Yukawa in the $z' = 0$ limit which we discussed in the main text above. Since for inverted ordering m_3 can be arbitrarily small, we can choose z' in such a way that $\cos z'$ is very small. This can in principle give rise to tiny Yukawa couplings of N_1 in inverted ordering case, realising the non-thermal dark matter scenario. Since 13 rotation parameter z' does not produce non-vanishing CP asymmetry as mentioned earlier, we did not discuss it in this work.

APPENDIX B

Here we show the details of CP asymmetry derivation in three-body decay used in chapter 3.

B.1 CP asymmetry from three-body decay of ψ

Let us start deriving the most general expression of asymmetry from an out of equilibrium process. The usual amplitude for a process is given as

$$i\mathcal{M}_{i\to f} = \mathcal{E} \times \mathcal{A} \times \omega, \tag{B.1}$$

where $\mathcal{E}$ comprises of all the couplings and ω comprises of all the wave functions of outgoing and incoming particles. Finally $\mathcal{A}$ contains all the rest of the term of the amplitude. For a non-zero CP asymmetry to be created one need at least two amplitudes for a process as shown in Fig.B.1.

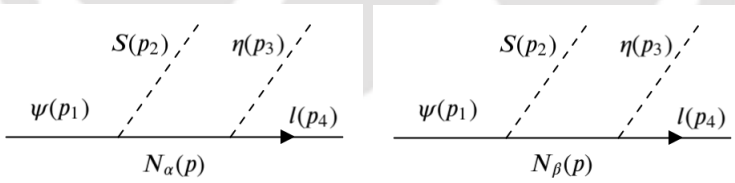

Figure B.1: Two processes for the three-body decay.

Then the total amplitude for the process can be written as,

$$i\mathcal{M}_{i\to f} = [\mathcal{E}_1\mathcal{A}_1 + \mathcal{E}_2\mathcal{A}_2]\omega. \tag{B.2}$$

Similarly, the amplitude for the process corresponding to its antiparticle counterpart is given as,

$$i\mathcal{M}_{\bar{i}\to\bar{f}} = [\mathcal{E}_1^*\mathcal{A}_1 + \mathcal{E}_2^*\mathcal{A}_2]\omega^\dagger. \tag{B.3}$$

The corresponding amplitude squared terms are given as,

$$|\,\mathcal{M}_{i\to f}\,|^2 = \left(|\,\mathcal{E}_1\,|^2|\,\mathcal{A}_1\,|^2 + |\,\mathcal{E}_2\,|^2|\,\mathcal{A}_2\,|^2 + 2\mathrm{Re}[\mathcal{E}_1^*\mathcal{E}_2]\mathrm{Re}[\mathcal{A}_1^*\mathcal{A}_2] - 2\mathrm{Im}[\mathcal{E}_1^*\mathcal{E}_2]\mathrm{Im}[\mathcal{A}_1^*\mathcal{A}_2]\right)|\,\omega\,|^2 \tag{B.4}$$

$$\mid \mathcal{M}_{\bar{i}\to\bar{f}} \mid^2 = \left(\mid \mathcal{E}_1 \mid^2 \mid \mathcal{A}_1 \mid^2 + \mid \mathcal{E}_2 \mid^2 \mid \mathcal{A}_2 \mid^2 + 2\mathrm{Re}[\mathcal{E}_1\mathcal{E}_2^*]\mathrm{Re}[\mathcal{A}_1^*\mathcal{A}_2] - 2\mathrm{Im}[\mathcal{E}_1\mathcal{E}_2^*]\mathrm{Im}[\mathcal{A}_1^*\mathcal{A}_2] \right) \mid \omega \mid^2 \tag{B.5}$$

and therefore, the asymmetry is calculated to be,

$$\delta = \mid \mathcal{M}_{i\to f} \mid^2 - \mid \mathcal{M}_{\bar{i}\to\bar{f}} \mid^2 = -4\mathrm{Im}[\mathcal{E}_1^*\mathcal{E}_2]\mathrm{Im}[\mathcal{A}_1^*\mathcal{A}_2] \mid \omega \mid^2 . \tag{B.6}$$

In the following subsections we first calculate the CP asymmetry by using the resummed propagators and then verify the same by tree-loop diagram interference calculation.We have adopted the two spinor notations from [395] throughout the derivations.

B.1.1 Calculation of the CP asymmetry using resummed propagator

Before doing the CP asymmetry calculation using resummed propagator let's calculate the resummed propagators first. In Fig.B.2 we show the diagrammatic representations of the full loop corrected propagators for two component fermions. For a detailed calculation on resummed propagator please see [395].

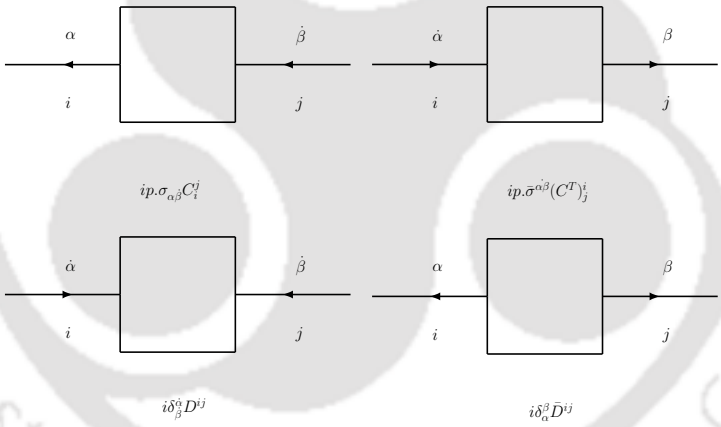

Figure B.2: The full loop corrected propagators for two component fermions are associated with functions $C(p^2)_i^j$ and its matrix transpose, $D(p^2)^{ij}$ and $\bar{D}(p^2)_{ij}$. The square boxes represent all the sum of all connected Feynman diagrams, with external legs included. The four-momentum p flows from right to left.

The full propagators can be organised in terms of one particle irreducible (1PI) self-energy functions [395]. These are defined as the sum of Feynman diagrams to all orders in perturbation theory (with the corresponding tree level graph excluded) that contribute to the 1PI two-point Green functions.

$$\begin{pmatrix} i\bar{\mathbf{D}} & ip.\sigma\mathbf{C} \\ ip.\bar{\sigma}\mathbf{C}^T & i\mathbf{D} \end{pmatrix} = \begin{pmatrix} i(m+\Omega) & -ip.\sigma(1-\Xi^T) \\ -ip.\bar{\sigma}(1-\Xi) & i(\bar{m}+\bar{\Omega}) \end{pmatrix}^{-1} \tag{B.7}$$

The right hand side of the above equation can be evaluated by employing the following identity for the inverse of a block diagonal matrix,

$$\begin{pmatrix} P & Q \\ R & S \end{pmatrix}^{-1} = \begin{pmatrix} (P-QS^{-1}R)^{-1} & (R-SQ^{-1}P)^{-1} \\ (Q-PR^{-1}S)^{-1} & (S-RP^{-1}Q)^{-1} \end{pmatrix} \tag{B.8}$$

under the assumption that all inverses, appearing in the Eq.(B.8) exist. Applying this result to the Eq.(B.7) we get,

$$C^{-1} = s(1-\Xi) - (\bar{m}+\bar{\Omega})(1-\Xi^T)^{-1}(m+\Omega), \tag{B.9}$$

$$D^{-1} = s(1-\Xi)(m+\Omega)^{-1}(1-\Xi^T) - (\bar{m}+\bar{\Omega}), \tag{B.10}$$

$$\bar{D}^{-1} = s(1-\Xi^T)(\bar{m}+\bar{\Omega})^{-1}(1-\Xi) - (m+\Omega), \tag{B.11}$$

where $s = p^2$. Taking the inverse and keeping the calculation up to one-loop order,

$$\begin{aligned} C &= \left[s(1-\Xi)(1-\Xi^T) - (\bar{m}m + \bar{m}\Omega + m\bar{\Omega})\right]^{-1}(1-\Xi^T) = C^T \\ &= \frac{1-\Xi^T}{s(1-(\Xi+\Xi^T)) - (\bar{m}m + \bar{m}\Omega + m\bar{\Omega})} \\ &= \frac{1-\Xi^T}{\left[s - m^2 - (s(\Xi+\Xi^T) + m\bar{\Xi} + \bar{m}\Omega)\right]} \\ &= \frac{1-\Xi^T}{(s-m^2)\left[1 - \dfrac{(s(\Xi+\Xi^T) + m\bar{\Omega} + \bar{m}\Omega)}{s-m^2}\right]} \\ &= \frac{1-\Xi^T}{(s-m^2)}\left[1 + \frac{s(\Xi+\Xi^T) + m\bar{\Omega} + \bar{m}\Omega}{s-m^2}\right] \\ &= \frac{1}{s-m^2} + \frac{s\Xi + m^2\Xi^T + m\bar{\Omega} + \bar{m}\Omega}{(s-m^2)^2} \end{aligned} \tag{B.12}$$

Similarly, for the mass insertion section it can found out that,

$$D = \frac{m}{s-m^2} + \frac{s(m\Xi + m\Xi^T + \Omega) + m^2\bar{\Omega}}{(s-m^2)^2} \tag{B.13}$$

$$\bar{D} = \frac{\bar{m}}{s-m^2} + \frac{\bar{m}s(\Xi+\Xi^T) + s\bar{\Omega} + \bar{m}^2\Omega}{(s-m^2)^2} = (D)^*. \tag{B.14}$$

To calculate the CP asymmetry let us consider the tree level diagrams with the resummed propagators. The amplitudes for the tree level diagrams with the resummed propagators (denoted by subscript i and j) can be written as

$$\mathcal{M}_i = D_{ii}x_l^\dagger y_\Psi^\dagger y_i^* h_{i\alpha}^* + C_{ii}x_l^\dagger \bar{\sigma} p x_\Psi y_i h_{i\alpha}^*, \tag{B.15}$$

$$\mathcal{M}_j = D_{jj}x_l^\dagger y_\Psi^\dagger y_j^* h_{j\alpha}^* + C_{jj}x_l^\dagger \bar{\sigma} p x_\Psi y_j h_{j\alpha}^*. \tag{B.16}$$

With the total amplitude $\mathcal{M}$ being,

$$\mathcal{M} = \mathcal{M}_i + \mathcal{M}_j. \tag{B.17}$$

Taking the interference, the asymmetry in the amplitude level can be found to be

$$\begin{aligned}\delta =& \mid \mathcal{M} \mid^2 - \mid \bar{\mathcal{M}} \mid^2 \\ &= \mathrm{Im}[y_i^* h_{i\alpha}^* y_j h_{j\alpha}]\mathrm{Im}[D_i D_j^*]\mathrm{Tr}[P_{\mathrm{L}}.\sigma p_\Psi.\bar{\sigma}] \\ &+ \mathrm{Im}[y_i y_j^* h_{i\alpha}^* h_{j\alpha}]\mathrm{Im}[C_i C_j^*]\mathrm{Tr}[P_{\mathrm{L}}.\sigma\overline{\sigma}.pp_\Psi.\sigma\bar{\sigma}.p] \\ &+ \left[\mathrm{Im}[y_i h_{i\alpha}^* y_j h_{j\alpha}]\mathrm{Im}[C_i D_j^*] + \mathrm{Im}[y_i^* h_{i\alpha}^* y_j^* h_{j\alpha}]\mathrm{Im}[D_i C_j^*]\right]\mathrm{Tr}[P_{\mathrm{L}}.\sigma\bar{\sigma}.p]m_\Psi.\end{aligned} \tag{B.18}$$

The relevant quantities coming from the interference of the resummed propagators can be found out to be (keeping the calculation up to one-loop order),

$$\begin{aligned}\mathrm{Im}[D_i D_j^*] = \mathrm{Im}&\left[\frac{M_i}{p^2 - M_i^2}\left(\frac{p^2(M_j\Xi_j^* + M_j\Xi_j) + p^2\Omega_j^* + M_j\bar{\Omega}_j^*}{(p^2 - M_j^2)^2}\right)\right] \\ &+ \mathrm{Im}\left[\frac{M_j}{p^2 - M_j^2}\left(\frac{p^2(M_i\Xi_i + M_i\Xi_i^*) + p^2\Omega_j + M_i^2\Omega_i^*}{(p^2 - M_i^2)^2}\right)\right]\end{aligned} \tag{B.19}$$

Similarly,

$$\mathrm{Im}[C_i C_j^*] = \mathrm{Im}\left[\frac{p^2\Xi_j^* + M_j^2\Xi_j + M_j\Omega_j + M_j\Omega_j^*}{(p^2 - M_i^2)(p^2 - M_j^2)^2} + \frac{p^2\Xi_i + M_i\Xi_i^* + M_i\Omega_i^* + M_i\Omega_i}{(p^2 - M_i^2)^2(p^2 - M_j^2)^2}\right], \tag{B.20}$$

$$\mathrm{Im}[C_i D_j^*] = \mathrm{Im}\left[\frac{p^2(M_i\Xi_i^* + M_i\Xi_i^* + \Omega_i^*) + M_i\Omega_i^*}{(p^2 - M_j^2)(p^2 - M_i^2)^2} + \frac{M_i(p^2\Xi_j^* + M_j^2\Xi_j + M_j\Omega_j + M_j\Omega_j^*)}{(p^2 - M_i^2)(p^2 - M_j^2)^2}\right], \tag{B.21}$$

$$\mathrm{Im}[D_i C_j^*] = \mathrm{Im}\left[\frac{p^2(M_i\Xi_i + M_i\Xi_i^* + \Omega_i) + M_i^2\Omega_j^*}{(p^2 - M_j^2)(p^2 - M_i^2)^2} + \frac{M_i(p^2\Xi_j^* + M_j^2\Xi_j + M_j\Omega_j + M_j\Omega_j^*)}{(p^2 - M_i^2)(p^2 - M_j^2)^2}\right]. \tag{B.22}$$

For our case the self-energy functions in two component spinor notation are diagrammatically shown in Fig.B.3, B.4 and B.5 and they can be found out to be,

$$(\Xi)_j^i = \frac{y_i^* y_j}{16\pi^2} I_{\mathrm{FS}}(s, m_\Psi^2, m_S^2) + \sum_l \frac{h_{il}^* h_{jl}}{16\pi^2} I_{\mathrm{FS}}(s, m_l^2, m_\eta^2) = (\Xi), \tag{B.23}$$

$$(\Xi^T)_j^i = \frac{y_i y_j^*}{16\pi^2} I_{\mathrm{FS}}(s, m_\Psi^2, m_S^2) + \sum_l \frac{h_{il} h_{jl}^*}{16\pi^2} I_{\mathrm{FS}}(s, m_l^2, m_\eta^2) = (\Xi^T), \tag{B.24}$$

$$(\Omega)^{ij} = \frac{y_i y_j}{16\pi^2} m_\Psi I_{\overline{\mathrm{FS}}}(s, m_\Psi^2, m_S^2) = (\Omega), \tag{B.25}$$

$$(\bar{\Omega})_{ij} = \frac{y_i^* y_j^*}{16\pi^2} m_\Psi I_{\overline{\mathrm{FS}}}(s, m_\Psi^2, m_S^2) = (\bar{\Omega}). \tag{B.26}$$

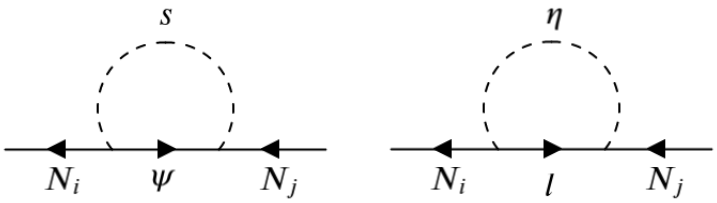

Figure B.3: Diagrammatic representation of $(\Xi)^j_i$.

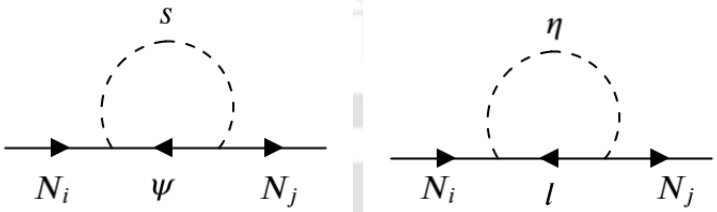

Figure B.4: Diagrammatic representation of $(\Xi)^i_j$.

Here,

$$I_{\rm FS}(s,x,y) = \frac{1}{2\epsilon} + \left[\frac{(s+x-y)B_0(s;x,y) + A_0(x) - A_0(y)}{2s}\right]. \tag{B.27}$$

$$I_{\overline{\rm FS}}(s,x,y) = \frac{1}{\epsilon} - B_0(s;x,y) \tag{B.28}$$

where, A_0 and B_0 are the Passarino-Veltman functions. For identical right handed neutrinos N_i on external legs, we use the notation Ξ_i, Ω_i, as seen in Eqs.(B.19), (B.20), (B.21), (B.22) mentioned above.

Using Eqs.(B.19),(B.20),(B.21) and (B.22) in Eq.(B.18) we get final expression of the CP asymmetry. To find the CP asymmetry parameter ϵ_ψ, defined in Eq.(3.16) we perform the three-body phase space integration numerically without any assumption. While we do not write the final CP asymmetry expression in this subsection, it is identical to the one derived using the interference of tree-loop diagrams as we show in the next subsection.

B.1.2 CP asymmetry calculation from tree-loop interference

In this appendix we calculate asymmetry parameter from the interference of tree and one-loop diagrams. The relevant diagrams in the tree level are shown in Fig.B.6. The amplitudes for the tree level diagram can be written as,

$$i\mathcal{M}^i_0 = y^*_i h^*_{i\alpha} \frac{x^\dagger_l y^\dagger_\Psi}{(p^2 - M_i^2)} M_i + y_i h^*_{i\alpha} \frac{x^\dagger_l \overline{\sigma}.p x_\Psi}{(p^2 - M_i^2)}. \tag{B.29}$$

For a Majorana fermion ψ there are two sets of diagrams contributing to the three-body decay at one-loop. These diagrams are shown in Fig.B.7 and B.8 respectively. For the

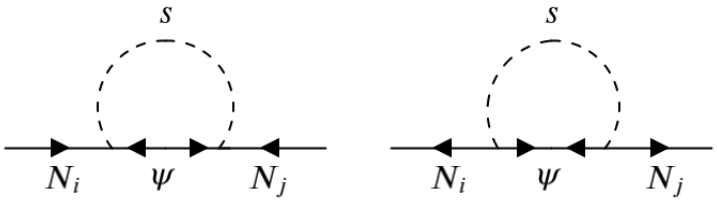

Figure B.5: Diagrammatic representation of $(\Omega)^{ij}$ and $(\overline{\Omega})_{ij}$.

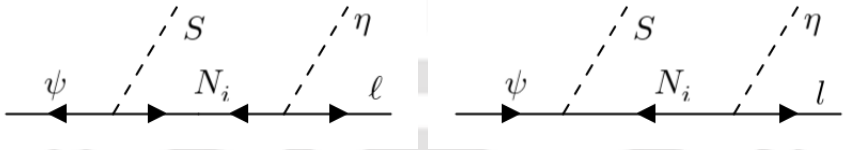

Figure B.6: Tree level diagram contributing to the three-body decay of ψ.

diagrams in Fig.B.7, the corresponding amplitudes can be written as,

$$\begin{aligned} i\mathcal{M}_j^{1'} &= y_j^* h_{j\alpha}^* \frac{x_l^\dagger \overline{\sigma}.p\sigma.p y_\Psi^\dagger (\Xi)_j^T M_j}{(p^2-M_j^2)^2} + y_j^* h_{j\alpha}^* \frac{x_l^\dagger \overline{\sigma}.p(\Omega)_j \sigma.p y_\Psi^\dagger}{(p^2-M_j^2)^2} \\ &+ y_j^* h_{j\alpha}^* \frac{x_l^\dagger \overline{\sigma}.p\sigma.p y_\Psi^\dagger M_j (\Xi)_j}{(p^2-M_j^2)^2} + y_j^* h_{j\alpha}^* \frac{x_l^\dagger M_j^2 (\overline{\Omega})_j y_\Psi^\dagger}{(p^2-M_j^2)^2} \\ &= y_j^* h_{j\alpha}^* \frac{x_l^\dagger y_\Psi^\dagger}{(p^2-M_j^2)} \left[p^2 [M_j (\Xi)_j^T + M_j (\Xi)_j + (\Omega)_j] + M_j^2 (\overline{\Omega})_j\right]. \end{aligned} \tag{B.30}$$

Similarly, for the other set of four one-loop diagrams in Fig.B.8, the amplitude can be written as,

$$\begin{aligned} i\mathcal{M}_j^{1''} &= y_j h_{j\alpha}^* \frac{x_l^\dagger \overline{\sigma.p}\sigma.p\overline{\sigma}.p(\Xi)_j x_\Psi}{(p^2-M_j^2)^2} + y_j h_{j\alpha}^* \frac{x_l^\dagger \overline{\sigma}.p M_j (\overline{\Omega})_j x_\Psi}{(p^2-M_j^2)^2} \\ &+ y_j h_{j\alpha}^* \frac{x_l^\dagger \overline{\sigma}.p x_\Psi M_j^2 (\Xi)_j^T}{(p^2-M_j^2)^2} + y_j h_{j\alpha}^* \frac{x_l^\dagger \overline{\sigma}.p x_\Psi M_j (\Omega)_j}{(p^2-M_j^2)^2} \\ &= y_j h_{j\alpha}^* \frac{x_l^\dagger \overline{\sigma}.p x_\Psi}{(p^2-M_j^2)} \left[p^2 (\Xi)_j + M_j^2 (\Xi)_j^T + M_j (\Omega)_j + M_j (\overline{\Omega})_j\right]. \end{aligned} \tag{B.31}$$

Therefore, the total amplitude for the decay at one-loop level can be written as,

$$\mathcal{M}_j^1 = \mathcal{M}_j^{1'} + \mathcal{M}_j^{1''}. \tag{B.32}$$

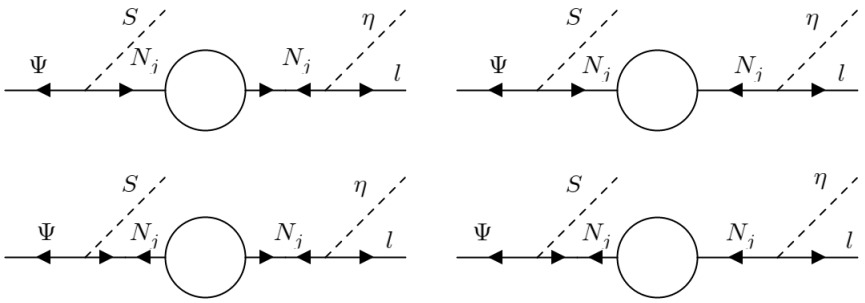

Figure B.7: Feynman diagrams contributing to the three-body decay of Ψ at one-loop level.

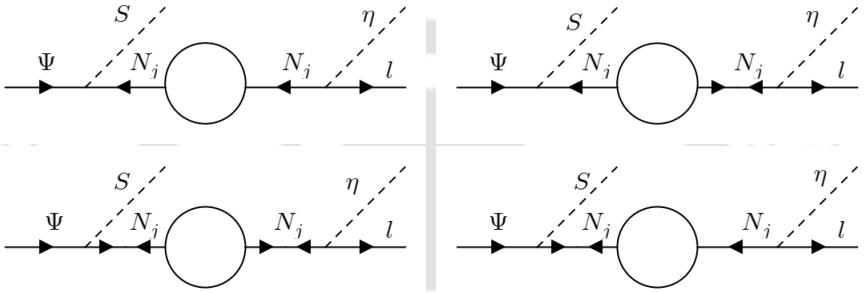

Figure B.8: Feynman diagrams contributing to the three-body decay of Ψ at one-loop level.

The asymmetry parameter is given by

$$
\begin{aligned}
\delta =& \mid \mathcal{M} \mid^2 - \mid \overline{\mathcal{M}} \mid^2 \\
&= 4\mathrm{Im}[\mathcal{M}_i^0 \mathcal{M}_j^{1*} + \mathcal{M}_i^1 \mathcal{M}_j^{0*}] \\
&= 4\mathrm{Im}[y_i^* h_{i\alpha}^* y_j h_{j\alpha}] \left[\frac{\mathrm{Im}[M_i(p^2[M_j(\Xi)_j^T + M_j(\Xi)_j^* + \Omega_j^*] + M_j^2 \bar{\Omega}_j^*)]}{(p^2 - M_i^2)(p^2 - M_j^2)^2} \right] \mathrm{Tr}[P_\mathrm{L}.\sigma p_\Psi.\bar{\sigma}] \\
&+ 4\mathrm{Im}[y_i^* h_{i\alpha}^* y_j h_{j\alpha}] \left[\frac{\mathrm{Im}[M_j(p^2[M_i(\Xi)_i^T + M_i(\Xi)_i + \Omega_i] + M_i^2 \overline{\Omega}_i)]}{(p^2 - M_j^2)(p^2 - M_i^2)^2} \right] \mathrm{Tr}[P_\mathrm{L}.\sigma p_\Psi.\bar{\sigma}] \\
&+ 4\mathrm{Im}[y_i h_{i\alpha}^* y_j^* h_{j\alpha}] \left[\frac{\mathrm{Im}[p^2(\Xi)_j^* + M_j^2(\Xi)_j + M_j \Omega_j^* + M_j \overline{\Omega_j^*}]}{(p^2 - M_i^2)(p^2 - M_j^2)^2} \right] \mathrm{Tr}[P_\mathrm{L}.\sigma p.\bar{\sigma} p_\Psi.\sigma p.\bar{\sigma}] \\
&+ 4\mathrm{Im}[y_i h_{i\alpha}^* y_j^* h_{j\alpha}] \left[\frac{Im[p^2(\Xi)_i + M_i^2(\Xi)_i^T + M_i \Omega_i + M_i \overline{\Omega_i}]}{(p^2 - M_i^2)^2(p^2 - M_j^2)} \right] \mathrm{Tr}[P_\mathrm{L}.\sigma p.\bar{\sigma} p_\Psi.\sigma p.\bar{\sigma}] \\
&+ 4\mathrm{Im}[y_i^* h_{i\alpha}^* y_j^* h_{j\alpha}] \left[\frac{\mathrm{Im}[p^2(\Xi)_j^* + M_j^2(\Xi^T)_j^* + M_j \Omega_j + M_j \overline{\Omega_j}]}{(p^2 - M_i^2)(p^2 - M_j^2)^2} \right] M_i m_\Psi \mathrm{Tr}[P_\mathrm{L}.\sigma \bar{\sigma}.p] \\
&+ 4\mathrm{Im}[y_i^* h_{i\alpha}^* y_j^* h_{j\alpha}] \left[\frac{\mathrm{Im}[p^2(M_i(\Xi)_i^T + M_i(\Xi)_i + \Omega_i) + M_i^2(\overline{\Omega})_i]}{(p^2 - M_i^2)^2(p^2 - M_j^2)} \right] m_\Psi \mathrm{Tr}[P_\mathrm{L}.\sigma \bar{\sigma}.p] \\
&+ 4\mathrm{Im}[y_i h_{i\alpha}^* y_j h_{j\alpha}] \left[\frac{\mathrm{Im}[p^2[M_j(\Xi)_j^* + M_j(\Xi^T)_j^* + \Omega_j^*] + M_j^2 \bar{\Omega}_j^*}{(p^2 - M_i^2)(p^2 - M_j^2)^2]} \right] \mathrm{Tr}[P_\mathrm{L}.\sigma \bar{\sigma}.p] m_\Psi \\
&+ 4\mathrm{Im}[y_i h_{i\alpha}^* y_j h_{j\alpha}] \left[\frac{\mathrm{Im}[p^2(\Xi)_i + M_i^2(\Xi)_i^T + M_i \Omega_i + M_i \overline{\Omega_i}]}{(p^2 - M_i^2)^2(p^2 - M_j^2)} \right] M_j m_\Psi \mathrm{Tr}[P_\mathrm{L}.\sigma \bar{\sigma}.p]. \qquad \text{(B.33)}
\end{aligned}
$$

Note that for the full loop corrected propagators $(\Xi^T)^* = \Xi$ and $\overline{\Omega} = \Omega^*$. One can easily figure out that the asymmetry we have from tree-loop interference calculation matches with the asymmetry we got in Eq.(B.18) after replacing the resummed propagators.

B.2 Two-body decay of N_i

The decay width for the decay $N_1 \longrightarrow \eta l$ is given by

$$\Gamma_{N_1 \longrightarrow \eta l} = \frac{M_1}{8\pi}(h^\dagger h)_{11}\left(1 - \frac{m_\eta^2}{M_1^2}\right)^2 \tag{B.34}$$

The CP asymmetry parameter for $N_1 \to l_i\eta, \bar{l}_i\bar{\eta}$ is given by

$$\epsilon_{(N_1)_i} = \frac{1}{8\pi(h^\dagger h)_{11}}\left[f\left(\frac{M_2^2}{M_1^2}, \frac{m_\eta^2}{M_1^2}\right)\mathrm{Im}[h_{i1}^* h_{i2}(h^\dagger h)_{12}] - \frac{M_1^2}{M_2^2 - M_1^2}\left(1 - \frac{m_\eta^2}{M_1^2}\right)^2 \mathrm{Im}[h_{i1}^* h_{i2} H_{12}]\right] \tag{B.35}$$

where, the function $f(r_{ji}, \eta_i)$ is coming from the interference of the tree-level and one-loop diagrams and has the form

$$f(r_{ji}, \eta_i) = \sqrt{r_{ji}}\left[1 + \frac{(1 - 2\eta_i + r_{ji})}{(1 - \eta_i^2)^2}\ln\left(\frac{r_{ji} - \eta_i^2}{1 - 2\eta_i + r_{ji}}\right)\right] \tag{B.36}$$

with $r_{ji} = M_j^2/M_i^2$ and $\eta_i = m_\eta^2/M_i^2$. The self energy contribution H_{ij} is given by

$$H_{ij} = (h^\dagger h)_{ij}\frac{M_j}{M_i} + (h^\dagger h)_{ij}^* \tag{B.37}$$

Now, the CP asymmetry parameter, neglecting the flavour effects (summing over final state flavours α) is

$$\epsilon_{N_1} = \frac{1}{8\pi(h^\dagger h)_{11}}\mathrm{Im}[((h^\dagger h)_{12})^2]\frac{1}{\sqrt{r_{21}}}F(r_{21}, \eta_1) \tag{B.38}$$

where the function $F(r_{ji}, \eta)$ is defined as

$$F(r_{ji}, \eta_i) = \sqrt{r_{ji}}\left[f(r_{ji}, \eta_i) - \frac{\sqrt{r_{ji}}}{r_{ji} - 1}(1 - \eta_i)^2\right]. \tag{B.39}$$

APPENDIX C

Here we show the details of a few calculations relevant for chapter 4.

C.1 Scalar mass matrix diagonalisation

After putting Eq.(4.18) in Eq.(4.16) we have found out the 5×5 mixing matrix for the real scalar fields in the basis $\frac{1}{\sqrt{2}}\begin{pmatrix} h^{'} & \eta_R^{'} & S_1^{'} & S_2^{'} & S_3^{'} \end{pmatrix}$ which has the following form

$$\begin{pmatrix} m_{hh}^{'} & 0 & m_{hS_1} & m_{hS_2}^{'} & m_{hS_3}^{'} \\ 0 & m_{\eta_R\eta_R}^{'} & 0 & 0 & 0 \\ m_{S_1h}^{'} & 0 & m_{S_1S_1}^{'} & m_{S_1S_2}^{'} & m_{S_1S_3}^{'} \\ m_{S_2h}^{'} & 0 & m_{S_2S_1}^{'} & m_{S_2S_2}^{'} & m_{S_2S_3}^{'} \\ m_{S_3h}^{'} & 0 & m_{S_3S_1}^{'} & m_{S_3S_2}^{'} & m_{S_3S_3}^{'} \end{pmatrix} \tag{C.1}$$

$$\begin{aligned}
m_{hh}^{'} &= 2v^2\lambda_H, \\
m_{hS_1}^{'} &= vu_1\lambda_{H\phi_1} = m_{S_1h}^{'}, \\
m_{hS_2}^{'} &= vu_2\lambda_{H\Phi_2} = m_{S_2h}^{'}, \\
m_{hS_3}^{'} &= vu_3\lambda_{H\Phi_3} = m_{S_3h}^{'}, \\
m_{S_1S_1}^{'} &= \frac{4u_1^3\lambda_{\phi_1} - \sqrt{2}u_2u_3\mu_\phi}{2u_1}, \\
m_{S_1S_2}^{'} &= u_1u_2\lambda_{\phi_1\phi_2} + \frac{u_3\mu_\phi}{\sqrt{2}} = m_{S_2S_1}^{'}, \\
m_{S_1S_3}^{'} &= u_1u_3\lambda_{\phi_1\phi_3} + \frac{u_2\mu_\phi}{\sqrt{2}} = m_{S_3S_1}^{'}, \\
m_{S_2S_2}^{'} &= \frac{4u_2^3\lambda_{\phi_2} - \sqrt{2}u_1u_3\mu_\phi}{2u_2}, \\
m_{S_2S_3}^{'} &= u_2u_3\lambda_{\phi_2\phi_3} + \frac{u_1\mu_\phi}{\sqrt{2}} = m_{S_3S_2}^{'},
\end{aligned}$$

where

$$\begin{aligned} m^{'}_{S_3S_3} &= \frac{4u_3^3\lambda_{\phi_3} - \sqrt{2}u_1u_2\mu_\phi}{2u_3}, \\ m^{'}_{\eta_R\eta_R} &= \frac{1}{2}\left(v^2(\lambda_{H\eta} + \lambda^{'}_{H\eta}) + u_1^2\lambda_{\eta\phi_1} + u_2^2\lambda_{\eta\phi_2} + u_3^2\lambda_{\eta\phi_3} + 2\mu_\eta^2\right). \end{aligned} \tag{C.2}$$

Diagonalising this real symmetric matrix by the orthogonal matrix $\mathcal{O}_s$ the physical states can be identified as

$$\begin{pmatrix} h' \\ \eta'_R \\ S'_1 \\ S'_2 \\ S'_3 \end{pmatrix} = \mathcal{O}_s \begin{pmatrix} h \\ \eta_R \\ S_1 \\ S_2 \\ S_3 \end{pmatrix}. \tag{C.3}$$

where

$$\mathcal{O}_s = \mathcal{O}_{12}\mathcal{O}_{13}\mathcal{O}_{14}\mathcal{O}_{15} \tag{C.4}$$

Similarly for the pseudo scalar the 4×4 mass matrix is found to be

$$\begin{pmatrix} m^{'}_{\eta_I\eta_I} & 0 & 0 & 0 \\ 0 & m^{'}_{A_1A_1} & m^{'}_{A_1A_2} & m^{'}_{A_1A_3} \\ 0 & m^{'}_{A_2A_1} & m^{'}_{A_2A_2} & m^{'}_{A_2A_3} \\ 0 & m^{'}_{A_3A_1} & m^{'}_{A_3A_2} & m^{'}_{A_3A_3} \end{pmatrix} \tag{C.5}$$

where

$$\begin{aligned} m^{'}_{\eta_I\eta_I} &= \frac{1}{2}\left(v^2(\lambda_{H\eta} + \lambda^{'}_{H\eta}) + u_1^2\lambda_{\eta\phi_1} + u_2^2\lambda_{\eta\phi_2} + u_3^2\lambda_{\eta\phi_3} + \mu_\eta^2\right), \\ m^{'}_{A_1A_1} &= -\frac{u_2u_3\mu_\phi}{\sqrt{2}u_1}, \\ m^{'}_{A_1A_2} &= \frac{u_3\mu_\phi}{\sqrt{2}} = m^{'}_{A_2A_1}, \\ m^{'}_{A_1A_3} &= -\frac{u_2\mu_\phi}{\sqrt{2}} = m^{'}_{A_3A_1}, \\ m^{'}_{A_2A_2} &= -\frac{u_1u_3\mu_\phi}{\sqrt{2}u_2}, \\ m^{'}_{A_2A_3} &= \frac{u_1\mu_\phi}{\sqrt{2}} = m^{'}_{A_3A_2}. \end{aligned} \tag{C.6}$$

C.2 Relevant cross sections and decay widths

The cross section for the process $N_1N_1 \longrightarrow f\bar{f}$ is found out to be

$$\sigma_{N_1N_1\longrightarrow f\bar{f}} = \frac{n_1^2g_{BL}^4}{48\pi\{(s - M^2_{Z_{BL}})^2 + \Gamma^2_{Z_{BL}}M^2_{Z_{BL}}\}} \sum_f n_f^2N_f^C\sqrt{1 - \frac{4m_f^2}{s}}\left(2m_f^2 + s\right), \tag{C.7}$$

where $n_f(n_1)$ is the charge of the SM fermion f (N_1) under the $U(1)_{B-L}$ and N_f^C is the colour multiplicity of the fermions.

The total washout term $W^{\rm Total}$ given in Eq.(4.7) contains multiple washout processes and can be identified to be

$$W^{\rm Total} = W_{\rm ID} + W_{lZ_{BL}\longrightarrow\eta N_1} + W_{\eta l\longrightarrow N_1 Z_{BL}} + W_{l\eta\longleftarrow\bar{l}\eta^*} + W_{lW^{\pm}(Z)\longrightarrow\eta N_1} \\ W_{lN_1\longrightarrow\bar{l}N_1^*}. \tag{C.8}$$

Here $W_{\rm ID}$ is the inverse decay term and it is given by

$$W_{\rm ID} = \frac{1}{4}K_{N_1}z^3\kappa_1(z_1), \tag{C.9}$$

where $K_{N_1} = \dfrac{\Gamma_1}{\mathbf{H}(z=1)}$ is the decay parameter and the corresponding decay width of N_1 is given by

$$\Gamma_1 = \frac{M_1}{8\pi}\left(Y_\eta^\dagger Y_\eta\right)_{11}\left(1-\frac{m_\eta^2}{M_1^2}\right). \tag{C.10}$$

The other relevant washout terms are defined by

$$W_{lZ_{BL}\longrightarrow\eta N_1} = \frac{zs}{\mathbf{H}(z=1)}n^{\rm eq}_{Z_{BL}}\langle\sigma v\rangle_{lZ_{BL}\longleftarrow\eta N_1}, \tag{C.11}$$

$$W_{l\eta\longleftrightarrow N_1 Z_{BL}} = \frac{zs}{\mathbf{H}(z=1)}n^{\rm eq}_{\eta}\langle\sigma v\rangle_{l\eta\longrightarrow N_1 Z_{BL}}, \tag{C.12}$$

$$W_{l\eta\longrightarrow\bar{l}\eta^*} = \frac{zs}{\mathbf{H}(z=1)}n^{\rm eq}_{\eta}\langle\sigma v\rangle_{l\eta\longrightarrow\bar{l}\eta^*}, \tag{C.13}$$

$$W_{lW^{\pm}(Z)\longleftarrow\eta N_1} = \frac{zs}{\mathbf{H}(z=1)}n^{\rm eq}_{W(Z)}\langle\sigma v\rangle_{lW^{\pm}(Z)\longrightarrow\eta N_1}, \tag{C.14}$$

$$W_{lN_1\longleftarrow\bar{l}N_1^*} = \frac{zs}{\mathbf{H}(z=1)}n^{\rm eq}_{\rm N_1}\langle\sigma v\rangle_{lN_1\longleftarrow\bar{l}N_1^*}. \tag{C.15}$$

Where, $\langle\sigma v\rangle_{ij\longrightarrow k,l}$ is the thermal averaged cross section for the process $i,j\longrightarrow k,l$ and is given by

$$\langle\sigma v\rangle_{i,j\longrightarrow k,l} = \frac{z}{8m_i^2m_j^2K_2\left(\dfrac{m_i}{M_1}z\right)K_2\left(\dfrac{m_j}{M_1}z\right)}\int_{(m_i+m_j)^2}^{\infty}\sigma_{ij\longleftarrow kl}(s-(m_i+m_j)^2) \\ \sqrt{s}K_1(\sqrt{s}z/M_1). \tag{C.16}$$

The relevant cross sections (assuming $n_1 = -3/2$ as in the UV complete model) for the washouts are given below.

$$\sigma_{lZ_{BL}\longleftarrow\eta N_1} = \frac{Y_\eta^2 g_{BL}^2}{8\pi s}\left[\frac{(s-(m_\eta+M_1)^2)(s-(m_\eta-M_1)^2)}{(s-(m_l+M_{Z_{BL}})^2)(s-(m_l-M_{Z_{BL}})^2)}\right]^{1/2} \frac{(m_l^2+2M_{Z_{BL}}^2)}{s^2}\left(\frac{s-M_{Z_{BL}}^2}{2\sqrt{s}}\left(\frac{s-m_\eta^2+M_1^2}{2\sqrt{s}}+\sqrt{\left(\frac{s-m_\eta^2+M_1^2}{2\sqrt{s}}\right)^2-M_1^2}\right)\right) \tag{C.17}$$

$$\sigma_{l\eta\longrightarrow N_1 Z_{BL}} = \frac{9Y_\eta^2 g_{BL}^2}{32\pi s}\left[\frac{(s-(M_1+M_{Z_{BL}})^2)(s-(M_1-M_{Z_{BL}})^2)}{(s-(m_l+m_\eta)^2)(s-(m_l-m_\eta)^2)}\right]^{1/2} \frac{1}{(s-M_1^2)^2}\left(\frac{s+M_1^2-M_{Z_{BL}}^2}{2\sqrt{s}}.\frac{s-M_1^2+M_{Z_{BL}}^2}{2\sqrt{s}}+\sqrt{\left(\frac{s-m_\eta^2}{2\sqrt{s}}\right)}\sqrt{\left(\frac{s-m_\eta^2}{2\sqrt{s}}\right)^2-M_1^2}\right) \left(\frac{s-m_\eta^2}{2\sqrt{s}}\frac{s-M_1^2+M_{Z_{BL}}^2}{2\sqrt{s}}+\frac{s-m_\eta^2}{2\sqrt{s}}\sqrt{\left(\frac{s-m_\eta^2}{2\sqrt{s}}\right)^2-M_1^2}\right) \tag{C.18}$$

For the processes $\sigma_{lZ_{BL}\longrightarrow N_1 Z_{BL}}$ and $\sigma_{l\eta\longrightarrow N_1 Z_{BL}}$, we have written the cross sections coming from the s-channel diagram only as they are the dominant ones in this case. However, in our numerical analysis we have taken the contribution from both s and t channel diagrams and their interferences.

$$\sigma_{lW^\pm(Z)\longleftarrow\eta N_1} = \frac{Y_\eta^2 g^2}{64\pi s}\left[\frac{(s-(m_\eta+M_1)^2)(s-(m_\eta-M_1)^2)}{(s-(m_l+M_W)^2)(s-(m_l-M_W)^2)}\right]^{1/2} \frac{(m_l^2+2M_W^2)}{s^2}\left(\frac{s-M_W^2}{2\sqrt{s}}\left(\frac{s-m_\eta^2+M_1^2}{2\sqrt{s}}+\sqrt{\left(\frac{s-m_\eta^2+M_1^2}{2\sqrt{s}}\right)^2-M_1^2}\right)\right) \tag{C.19}$$

$$\sigma_{l\eta\longrightarrow\bar{l}\eta^*} = \frac{Y_\eta^4}{4\pi s}\frac{M_1^2}{(s-M_1^2)^2}\left[\frac{s-m_\eta^2+m_l^2}{2\sqrt{s}}\frac{s-m_l^2+m_\eta^2}{2\sqrt{s}}\right] \tag{C.20}$$

$$\sigma_{lN_1\longrightarrow\bar{l}N_1} = \frac{Y_\eta^4}{4\pi s}\frac{m_\eta^2}{(s-m_\eta^2)^2}\left[\frac{s-M_1^2}{2\sqrt{s}}\frac{s-m_l^2+M_1^2}{2\sqrt{s}}+\frac{s-m_l^2+M_1^2}{2\sqrt{s}}\sqrt{\left(\frac{s-m_l^2+M_1^2}{2\sqrt{s}}\right)^2-M_1^2}\right] \tag{C.21}$$

In Fig.C.1, we show the behaviour of thermal averaged cross section for $lZ_{BL}\longrightarrow N_1\eta$, a key washout process involving $B-L$ gauge boson. The analytical estimate matches with the numerical estimates extracted from `micrOMEGAs` quite well. Clearly, with rise in Z_{BL} mass,

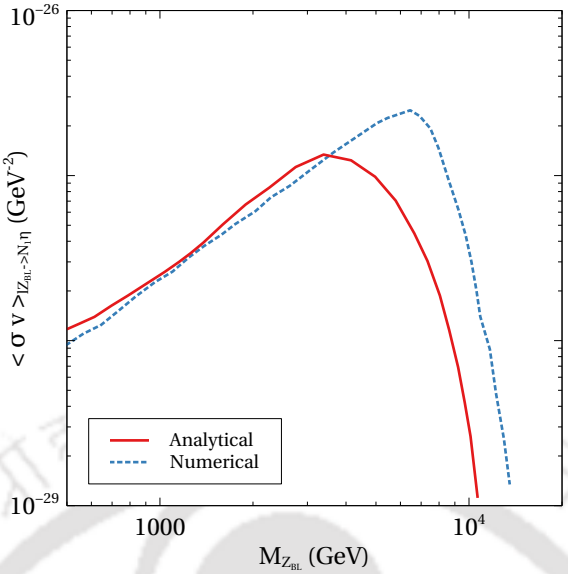

Figure C.1: Comparison of analytical and numerical results for the thermal averaged cross section of the key washout process $lZ_{BL} \longrightarrow N_1\eta$ at temperature $T = 100M_1$. The relevant benchmark parameters are fixed at the following values $m_\eta = 500$ GeV, $M_1 = 10$ TeV, $g_{BL} = 0.1$, $(Y_\eta)_{\alpha 1} \simeq 10^{-4}$.

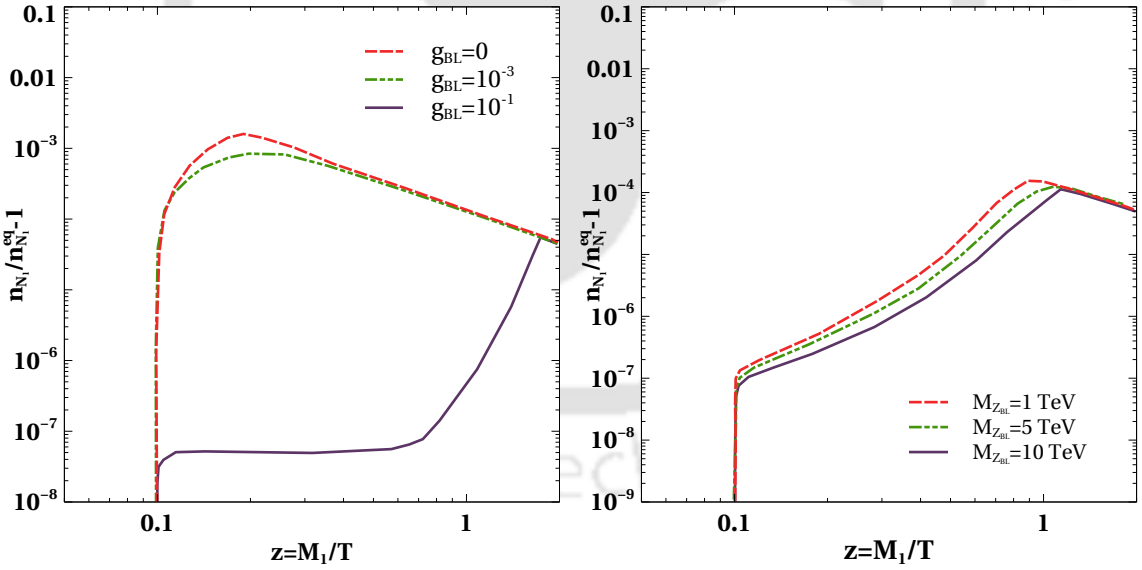

Figure C.2: The deviation of the comoving number density of N_1 (right panel) with $z = \dfrac{M_1}{T}$ from its equilibrium density for different g_{BL} (left panel) and for different $M_{Z_{BL}}$ (right panel). The Yukawa couplings relevant for leptogenesis are taken to be $(Y_\eta)_{\alpha 1} = 10^{-5}(1+i)$ and $(Y_\eta)_{\alpha 2} = 10^{-1}(1.1-i)$. The other important parameters used are $M_1 = 15$ TeV, $M_2 = 150$ TeV, $m_\eta = 5$ TeV. For left (right) panel plot we fix $M_{Z_{BL}} = 5$ TeV ($g_{BL} = 10^{-3}$).

the cross section increases enhancing the washout effects, as pointed out in the discussions above. Also, for very heavy Z_{BL} corresponding to a decoupled scenario, there is no impact of Z_{BL} mass on leptogenesis due to tiny washout effects at the scale of leptogenesis.

In Fig.C.2, we show the effects of $B-L$ gauge sector parameters namely, gauge coupling g_{BL} and gauge boson mass $M_{Z_{BL}}$ on departure in evolution of comoving number density of N_1 from its equilibrium number density. We can clearly notice significant effects due to these parameters as additional gauge interactions lead to N_1 annihilations keeping it in equilibrium for longer duration. With the increase in g_{BL} the rate of N_1 annihilations increases which brings N_1 no density very close to its equilibrium number density, as seen from left panel plot of Fig.C.2. Also, similar behaviour can be seen with the increase in $M_{Z_{BL}}$. Since we are working in the parameter space where $M_{Z_{BL}} \leq 2M_1$, with the increase in $M_{Z_{BL}}$ the cross section for N_1 annihilation increases which again bring the N_1 no density closer to its equilibrium number density.

Finally, we write the expression for $\nu_R\nu_R \longrightarrow f\bar{f}$ cross section mediated by Z_{BL} used in the estimate for ΔN_{eff}. This is given by

$$\sigma_{\nu_R\nu_R\longrightarrow f\bar{f}} = \frac{g_{BL}^4}{48\pi}\frac{1}{(s-M_{Z_{BL}}^2)+\Gamma_{Z_{BL}}^2 M_{Z_{BL}}^2}\sum_f n_f^2 N_f^C \sqrt{1-\frac{4m_f^2}{s}}\left(s+2m_f^2\right). \tag{C.22}$$

C.3 CP asymmetry

The decay width for the decay $N_1 \longrightarrow \eta l$ is given by

$$\Gamma_{N_1\longrightarrow\eta l} = \frac{M_1}{8\pi}(Y_\eta^\dagger Y_\eta)_{11}\left(1-\frac{m_\eta^2}{M_1^2}\right)^2 \tag{C.23}$$

The CP asymmetry parameter for $N_1 \to l_\alpha\eta, \bar{l_\alpha}\bar{\eta}$ is given by

$$\begin{aligned}\epsilon_{1\alpha} = \frac{1}{8\pi(Y_\eta^\dagger Y_\eta)_{11}}\Bigg[& f\left(\frac{M_2^2}{M_1^2},\frac{m_\eta^2}{M_1^2}\right)\text{Im}[(Y_\eta)_{\alpha 1}^*(Y_\eta)_{\alpha 2}(Y_\eta^\dagger Y_\eta)_{12}] \\ & -\frac{M_1^2}{M_2^2-M_1^2}\left(1-\frac{m_\eta^2}{M_1^2}\right)^2\text{Im}[(Y_\eta)_{\alpha 1}^*(Y_\eta)_{\alpha 2}H_{12}]\Bigg]\end{aligned} \tag{C.24}$$

where, the function $f(r_{ji},\eta_i)$ is coming from the interference of the tree-level and one-loop diagrams and has the form

$$f(r_{ji},\eta_i) = \sqrt{r_{ji}}\left[1+\frac{(1-2\eta_i+r_{ji})}{(1-\eta_i^2)^2}\ln\left(\frac{r_{ji}-\eta_i^2}{1-2\eta_i+r_{ji}}\right)\right] \tag{C.25}$$

with $r_{ji} = M_j^2/M_i^2$ and $\eta_i = m_\eta^2/M_i^2$. The self energy contribution H_{ij} is given by

$$H_{ij} = (Y_\eta^\dagger Y_\eta)_{ij}\frac{M_j}{M_i} + (Y_\eta^\dagger Y_\eta)_{ij}^* \tag{C.26}$$

Now, the CP asymmetry parameter, neglecting the flavour effects (summing over final state flavours α) is

$$\epsilon_1 = \frac{1}{8\pi (Y_\eta^\dagger Y_\eta)_{11}} \mathrm{Im}[((Y_\eta^\dagger Y_\eta)_{12})^2] \frac{1}{\sqrt{r_{21}}} F(r_{21}, \eta_1) \tag{C.27}$$

where the function $F(r_{ji}, \eta)$ is defined as

$$F(r_{ji}, \eta_i) = \sqrt{r_{ji}} \left[f(r_{ji}, \eta_i) - \frac{\sqrt{r_{ji}}}{r_{ji} - 1} (1 - \eta_i)^2 \right]. \tag{C.28}$$

Let us denote the Yukawa couplings as

$$(Y_\eta)_{\alpha 1} = a + ia, \tag{C.29}$$

$$(Y_\eta)_{\alpha 2} = b - ic, \tag{C.30}$$

where a, b, c are three real numbers. For this choice of Yukawa, The CP asymmetry parameter for N_1 decay is

$$\begin{aligned} \epsilon_1 &\propto \frac{\mathrm{Im}[(Y_\eta^\dagger Y_\eta)_{12}^2]}{(Y_\eta^\dagger Y_\eta)_{11}} \\ &= \frac{-18a^2(\mathrm{Re}[(b - ic)^2])}{6a^2} \\ &= -3(\mathrm{Re}[(b - ic)^2]) = -3(b^2 - c^2) \end{aligned} \tag{C.31}$$

Here one can also notice that to have a non-vanishing CP asymmetry we must have $b \neq c$.

APPENDIX D

Here we have shown the details of a few calculations related to the WIMPy leptogenesis part discussed in chapter 5.

D.1 Particle Spectrum and Relevant Cross Section

The scalar potential for the model can be identified to be

$$\begin{aligned} V &= -\mu_H^2\left(H^\dagger H\right)+\mu_\eta^2\left(\eta^\dagger\eta\right)+\mu_\Delta^2\mathrm{Tr}[\Delta^\dagger\Delta]+(\mu_{H\Delta}\tilde{H}^\dagger\Delta H+\mu_{\eta\Delta}\eta^\dagger\Delta^\dagger\tilde{\eta}+\mathrm{h.c.}) \\ &\quad \lambda_H(H^\dagger H)^2+\lambda_\eta\left(\eta^\dagger\eta\right)^2+\lambda_\Delta\left(\mathrm{Tr}[\Delta^\dagger\Delta]\right)^2+\lambda_\Delta^{'}\mathrm{Tr}[\Delta^\dagger\Delta\Delta^\dagger\Delta]+\lambda_{H\eta}\mid H^\dagger\eta\mid^2 \\ &\quad +\lambda_{H\eta}^{'}\left(H^\dagger H\right)\left(\eta^\dagger\eta\right)+\lambda_{H\eta}^{''}\left((H^\dagger\eta)^2+\mathrm{h.c.}\right)+\lambda_{H\Delta}\left(H^\dagger H\right)\mathrm{Tr}\left[\Delta^\dagger\Delta\right] \\ &\quad +\lambda_{H\Delta}^{'}\mathrm{Tr}[H^\dagger\Delta\Delta^\dagger H]+\lambda_{\eta\Delta}(\eta^\dagger\eta)\mathrm{Tr}\left[\Delta^\dagger\Delta\right]+\lambda_{\eta\Delta}^{'}\mathrm{Tr}\left[\eta^\dagger\Delta\Delta^\dagger\eta\right], \end{aligned} \tag{D.1}$$

where $\tilde{H}=i\sigma_2H^*$, $\tilde{\eta}=i\sigma_2\eta^*$ and the mass parameters $\mu_H^2>0$ so that the neutral component of H obtains non-vanishing VEV i.e $\langle H^0\rangle=v\simeq 246$ GeV. On the other hand, we consider Particle Spectrum and Relevant Cross Section$\mu_{\eta,\Delta}^2>0$ so that they do not take part in spontaneous symmetry breaking. While η does not acquire a non-zero VEV at any stage keeping the Z_2 symmetry intact, the neutral component of scalar triplet acquires an induced VEV $\langle\Delta^0\rangle=v_\Delta$ after electroweak symmetry breaking.

The physical masses for the neutral and charged scalars can be obtained by the minimization of the scalar potential. Since η is odd under the Z_2 symmetry, it doesn't get any VEV. In this model, we assume the RHNs are heavier than the η scalar such that the lightest neutral component of η plays the role of DM. After the EWSB, the three scalar multiplets can be written in the following form (assuming unitary gauge)

$$H=\begin{pmatrix}0\\ \frac{v+h}{\sqrt{2}}\end{pmatrix},\qquad \eta=\begin{pmatrix}\eta^\pm\\ \frac{\eta_R+i\eta_I}{\sqrt{2}}\end{pmatrix},\qquad \Delta=\begin{pmatrix}\Delta^+/\sqrt{2} & \Delta^{++}\\ \frac{\Delta_R^0+v_\Delta+i\Delta_I^0}{\sqrt{2}} & -\Delta^+/\sqrt{2}\end{pmatrix}. \tag{D.2}$$

Upon minimization of the potential the masses of the charged and neutral scalars can be found out be

$$m_h^2 \simeq \lambda_H v^2, \tag{D.3}$$

$$m^2_{\Delta^0_R} \simeq \frac{\mu_{H\Delta} v^2}{\sqrt{2} v_\Delta}, \tag{D.4}$$

$$m^2_{\Delta^0_I} = \frac{\mu_{H\Delta}}{\sqrt{2} v_\Delta} \left(v^2 + 4 v_\Delta^2\right), \tag{D.5}$$

$$m^2_{\Delta^\pm} = m^2_{\Delta^{\pm\pm}} = \left(\frac{\mu_{H\Delta}}{\sqrt{2} v_\Delta} + \frac{1}{4}\lambda^{'}_{H\Delta}\right)\left(v^2 + 4 v_\Delta^2\right), \tag{D.6}$$

$$m^2_{\eta_{R,I}} = \frac{1}{2}\left(2\mu_\eta^2 + (\lambda_{H\eta} + \lambda^{'}_{H\eta} \pm \lambda^{''}_{H\eta}) v^2 + (\lambda_{\eta\Delta} v_\Delta \mp 2\sqrt{2}|\mu_{\eta\Delta}|) v_\Delta\right), \tag{D.7}$$

$$m^2_{\eta^\pm} = \frac{1}{2}\left(2\mu_\eta^2 + \lambda_{H\eta} v^2 + (\lambda_{\eta\Delta} + \lambda^{'}_{\eta\Delta}) v_\Delta^2\right). \tag{D.8}$$

The masses for the CP even scalars are approximated considering $\mu_{H\Delta} \sim \mathcal{O}(100)$ keV. As mentioned earlier the neutrino masses are generated from both loop-level scotogenic and tree-level type-II seesaw mechanisms in this model and the resultant neutrino mass matrix can be written as

$$m_\nu = \left(Y^N\right)^T \Lambda Y^N + Y^\Delta v_\Delta. \tag{D.9}$$

Here Λ is an effective loop-suppressed RHN mass scale and is given by [112]

$$\Lambda_{ii} = \frac{M_i}{16\pi^2}\left[\frac{m^2_{\eta_R}}{M_i^2 - m^2_{\eta_R}} \ln\left(\frac{M_i^2}{m^2_{\eta_R}}\right) - \frac{m^2_{\eta_I}}{M_i^2 - m^2_{\eta_I}} \ln\left(\frac{M_i^2}{m^2_{\eta_I}}\right)\right]. \tag{D.10}$$

The two types of Yukawa couplings are related to the neutrino oscillation data by the following formulae

$$Y^N_{i\alpha} = F_I^{1/2}\left(\Lambda^{-1/2} \mathcal{O} \hat{m_\nu}^{1/2} U^\dagger_{\rm PMNS}\right), \tag{D.11}$$

$$Y^\Delta_{\alpha\beta} = F_{II} v_\Delta^{-1} (U^*_{\rm PMNS} \hat{m_\nu} U^\dagger_{\rm PMNS}), \tag{D.12}$$

where $\hat{m_\nu} = diag\,(m_{\nu_1}, m_{\nu_2}, m_{\nu_3})$ is the diagonal neutrino mass matrix and U_{PMNS} is the PMNS lepton mixing matrix. Here $\mathcal{O}$ is an any arbitrary orthogonal matrix. We have used the Casas Ibarra (CI) parametrisation [65] to determine the Yukawa couplings. We also assume the two seesaw contributions to be equal namely $F_I \approx F_{II} = 1/2$.

The general expression for the thermally averaged cross sections for the processes are given by [136]

$$\langle\sigma v\rangle_{i_1 i_2 \longrightarrow f_1 f_2} = \frac{1}{2T m^2_{i_1} m^2_{i_2} K_2(m_{i_1}/T) K_2(m_{i_2}/T)} \int_{s_{\rm in}}^\infty \int_{-1}^1 \frac{1}{32\pi} \frac{|\mathcal{M}|^2}{\sqrt{s}} p_{i_1 i_2} p_{f_1 f_2} K_1(\sqrt{s}/T)\, ds\, d(\cos\theta), \tag{D.13}$$

where T is the temperature, K_i are the modified Bessel functions of order i, $\mathcal{M}$ is the amplitude for the process $i_1 i_2 \longrightarrow f_1 f_2$, and

$$p_{ij} = \frac{1}{2}\sqrt{\lambda(s, m_i^2, m_j^2)/s}, \tag{D.14}$$

$$s_{\rm in} = \max[(m_{i_1} + m_{i_2})^2, (m_{f_1} + m_{f_2})^2], \tag{D.15}$$

$$\lambda(x, y, z) = x^2 + y^2 + z^2 - 2xy - 2yz - 2xz. \tag{D.16}$$

The amplitudes relevant for WIMPy leptogenesis are given below [164]

$$\begin{aligned} |\,\mathcal{M}(\eta\eta \longrightarrow LL)\,|^2 &= \frac{\hat{m_\nu^2}}{v_\Delta^2}\frac{F_I^2\mu_{\eta\Delta}^2 s}{(s-m_\Delta^2)^2+m_\Delta^2\Gamma_\Delta^2} + \sum_i F_{II}^2\frac{\hat{m_\nu^2}}{\Lambda_{ii}^2}M_i^2 s\left[\frac{1}{t-M_i^2}+\frac{1}{u-M_i^2}\right]^2 \\ &+\frac{F_I F_{II}\mid\mu_{\eta\Delta}\mid(s-m_\Delta^2)}{(s-m_\Delta)^2+m_\Delta^2\Gamma_\Delta^2}\sum_i\frac{\hat{m_\nu}^2}{\Lambda_{ii}v_\Delta}M_i s\left[\frac{1}{t-M_i^2}+\frac{1}{u-M_i^2}\right] \end{aligned} \tag{D.17}$$

$$\begin{aligned} |\,M(\eta\bar{L} \longrightarrow \eta L)\,|^2 &= \frac{\hat{m_\nu}^2}{v_\Delta^2}\frac{F_I^2\mu^2(m_\eta^2-t)}{(t-m_\eta^2)^2} + \sum_i\frac{\hat{m_\nu^2}}{\Lambda_{ii}^2}\frac{F_{II}^2M_i^2 s}{(s-M_i^2)^2+M_i^2\Gamma_{N_i}^2} \\ &\frac{F_I F_{II}\mid\mu_{\eta\Delta}\mid(m_\eta^2-t)}{(t-m_\Delta^2)^2}\sum_i\frac{\hat{m_\nu^2}}{\Lambda_{ii}v_\Delta}M_i s\left[\frac{s-M_i^2}{(s-M_i^2)^2+M_i^2\Gamma_{N_i}^2}\right] \end{aligned} \tag{D.18}$$

The asymmetry generated from the annihilation, $\eta\eta \longrightarrow \ell\ell$, at the amplitude level, is given by

$$\begin{aligned} \delta &= |\,\mathcal{M}\,|^2 - |\,\bar{\mathcal{M}}\,|^2 \\ &= \sum_i 4{\rm Im}\left[\mu_{\eta\Delta}(Y^N Y^{\Delta *}(Y^N)^T)_{ii}\right] \\ &\times\frac{sM_i m_\Delta\Gamma_\Delta}{(s-m_\Delta^2)^2+m_\Delta^2\Gamma_\Delta^2}\left[\frac{1}{t-M_i^2}+\frac{1}{u-M_i^2}\right], \end{aligned} \tag{D.19}$$

where Γ_Δ is the triplet scalar decay width. The imaginary part appearing in the CP asymmetry parameter can be parametrised as follows

$${\rm Im}\left[\mu_{\eta\Delta}(Y^N Y^{\Delta *}(Y^N)^T)_{ii}\right] = F_I F_{II} v_\Delta^{-1}{\rm Im}\left[\mu_{\eta\Delta}(\Lambda^{-1/2}\mathcal{O}\hat{m_\nu}^2\mathcal{O}^T\Lambda^{-1/2})_{ii}\right]. \tag{D.20}$$

We use the δ or the amplitude squared difference defined above in thermally averaged cross section to evaluate $\langle\sigma v\rangle^\delta_{\eta\eta\to\ell\ell}$ which enter the Boltzmann equations for $B-L$ asymmetry.

D.2 Analytical calculation of asymmetry

The thermally averaged rate for the asymmetric part of the annihilation of η is given by

$$\langle\sigma v\rangle^\delta_{\eta\eta\longrightarrow ll} = \frac{1}{2Tm_\eta^4 K_2^2(m_\eta/T)}\int_{s_{\rm in}}^\infty\int_{-1}^1\frac{1}{32\pi}\frac{\delta}{\sqrt{s}}p_{\eta\eta}p_{ll}K_1(\sqrt{s}/T)\,ds\,d(\cos\theta) \tag{D.21}$$

In the narrow-width approximation, the asymmetry in (D.19) at the resonance point can be simplified to be

$$\delta \simeq 4\sum_i \mathrm{Im}\left[\mu_{\eta\Delta}(Y^N Y^{\Delta^*}(Y^N)^T)\right] sM_i\delta(s-m_\Delta^2)\left[\frac{1}{t-M_i^2}+\frac{1}{u-M_i^2}\right], \tag{D.22}$$

where we have used

$$\frac{\Gamma_\Delta m_\Delta}{(s-m_\Delta^2)^2+m_\Delta^2\Gamma_\Delta^2} \xrightarrow{\Gamma_\Delta/m_\Delta\longrightarrow 0} \pi\delta(s-m_\Delta^2).$$

Replacing (D.22) in (D.21) the $\langle\sigma v\rangle^\delta_{\eta\eta\longrightarrow ll}$ is calculated and is given by

$$\begin{aligned}\langle\sigma v\rangle^\delta_{\eta\eta\longrightarrow ll} &\approx \frac{16\pi}{m_\eta^4}\frac{1}{\tilde{\mu}_{\eta\Delta}^2\sum_{\alpha,\beta}\mid Y^\Delta_{\alpha\beta}\mid^2}\Gamma_{\Delta\longrightarrow\eta\eta}\Gamma_{\Delta\longrightarrow ll}\sum_i\left[\mu_{\eta\Delta}(Y^N Y^{\Delta^*}(Y^N)^T)\right]\\ &\times\frac{f[m_\Delta,m_\eta,M_i]r_{N_i}}{\sqrt{m_\Delta^2-4m_\eta^2}}\frac{zK_1(r_\Delta z)}{K_2^2(z)}\end{aligned} \tag{D.23}$$

where $\tilde{\mu}_{\eta\Delta}=\mu_{\eta\Delta}/m_\Delta$, $r_i=m_i/m_\eta$. We have corrected the above expression by incorporating an additional factor missing in [164]. Here, the function $f[m_\Delta,m_\eta,M_i]$ is given by

$$\begin{aligned}f[m_\Delta,m_\eta,M_i] &= 2\ln\left[\frac{2M_i^2+m_\Delta^2-2m_\eta^2-\sqrt{m_\Delta^2}\sqrt{m_\Delta^2-4m_\eta^2}}{2M_i^2+m_\Delta^2-2m_\eta^2+\sqrt{m_\Delta^2}\sqrt{m_\Delta^2-4m_\eta^2}}\right]\\ &- 2\ln\left[\frac{-M_i^2-m_\Delta^2/2+m_\eta^2-\frac{1}{2}\sqrt{m_\Delta^2}\sqrt{m_\Delta^2-4m_\eta^2}}{-M_i^2-m_\Delta^2/2+m_\eta^2+\sqrt{m_\Delta^2}\sqrt{m_\Delta^2-4m_\eta^2}}\right].\end{aligned} \tag{D.24}$$

In Fig.D.1 we show the comparison of rates of $\langle\sigma v\rangle^\delta_{\eta\eta\longrightarrow ll}$ calculated from the analytical expression in Eq.(D.23) and the exact numerical integration given in Eq.(D.21). It can be seen that there is no significant difference between the two results. Nevertheless, we have used the exact numerical integration result for $\langle\sigma v\rangle_{\eta\eta\longrightarrow ll}$ in our analysis.

D.3 Δ decay contribution to the asymmetry

In this model there can be another source of asymmetry from the decay of the triplet to a pair of leptons. The CP asymmetry parameter associated with this decay is given by [396, 397]

$$\epsilon_\Delta = \sum_i\frac{M_i}{8\pi}\frac{\sum_{\alpha,\beta}\mathrm{Im}[\mu_{\eta\Delta}(Y^N_{i\alpha}Y^N_{i\beta}(Y^\Delta)_{\alpha\beta})]}{\mathrm{Tr}[(Y^\Delta)^\dagger Y_\Delta]m_\Delta^2+\mid\mu_{H\Delta}\mid^2+\mid\mu_{\eta\Delta}\mid^2}\ln[1+\frac{m_\Delta^2}{M_i^2}]. \tag{D.25}$$

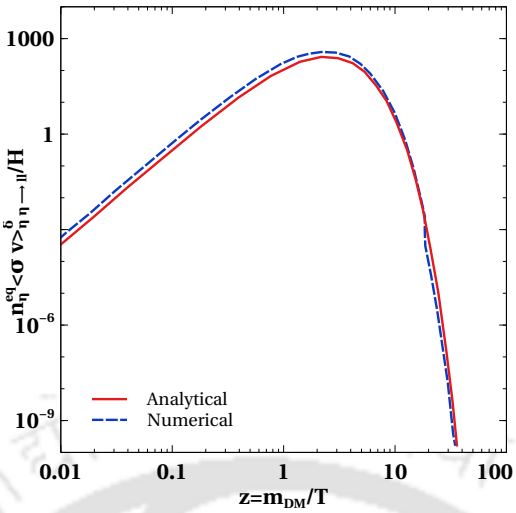

Figure D.1: Comparison plot showing the rates for $\langle\sigma v\rangle^{\delta}_{\eta\eta\longrightarrow ll}$ using the approximate analytical formula in Eq.(D.23) and the exact numerical integration in Eq.(D.21).

The network of Boltzmann equations for scalar triplet leptogenesis irrespective of whether lepton flavor effects are active or not, corresponds to a system of coupled differential equations accounting for the temperature evolution of the triplet density $\sum = \Delta_\Delta + \Delta^\dagger$ the triplet asymmetry $\Delta_\Delta = \Delta - \Delta^\dagger$. These Boltzmann equation for leptogenesis taking the Δ decay and inverse decay into account can be written as [398]

$$\frac{dY_\Sigma}{dz} = -\frac{\gamma_D}{s\mathbf{H}z}\left(\frac{Y_\Sigma}{Y_\Sigma^{\rm eq}} - 1\right), \tag{D.26}$$

$$\frac{dY_{\Delta_\Delta}}{dz} = -\frac{\gamma_D}{s\mathbf{H}z}\left[\frac{Y_{\Delta_\Delta}}{Y_\Sigma^{\rm eq}} - \sum_k \left(B_l C_k^l - B_H C_k^H\right)\frac{Y_{\Delta_k}}{Y_l^{\rm eq}}\right], \tag{D.27}$$

$$\frac{dY_{B-L}}{dz} = -\epsilon_\Delta \frac{\gamma_D}{s\mathbf{H}z}\left(\frac{Y_\Sigma}{Y_\Sigma^{\rm eq}} - 1\right) + 2\left(\frac{Y_{\Delta_\Delta}}{Y_\Sigma^{\rm eq}} - \sum_k C_k^l \frac{Y_{\Delta_k}}{Y_l^{\rm eq}}\right) B_l \frac{\gamma_D}{s\mathbf{H}z}. \tag{D.28}$$

Here Y_{Δ_Δ} is the comoving number density of $\Delta_\Delta = \Delta - \Delta^\dagger$ and Y_Σ is the comoving number density of $\Sigma = \Delta + \Delta^\dagger$. B_l and B_ϕ are triplet decay branching ratios to lepton and scalar final states respectively. The branching ratios are defined as follows

$$B_l = \sum_{i,j} B_{l_{ij}} = \sum_{i,j} \frac{m_\Delta}{8\pi\Gamma_\Delta^{\rm Tot}} \mid (Y^\Delta)^{ij} \mid^2,\ B_H = \frac{\mid \mu_{H\Delta} \mid^2}{8\pi m_\Delta \Gamma_\Delta^{\rm Tot}}, \tag{D.29}$$

where $\Gamma_\Delta^{\rm Tot}$ is the total decay width for the triplet Δ and is given by

$$\begin{aligned}\Gamma_\Delta^{\rm Tot} &= \sum_{ij}\Gamma(\Delta\longrightarrow l_i l_j) + \Gamma(\Delta\longrightarrow HH) + \Gamma(\Delta\longrightarrow\eta\eta),\\ &= \frac{m_\Delta}{8\pi}\left[{\rm Tr}[(Y^\Delta)^\dagger Y_\Delta] + \frac{\mid \mu_{H\Delta}\mid^2 + \mid \mu_{\eta\Delta}\mid^2}{m_\Delta^2}\right].\end{aligned} \tag{D.30}$$

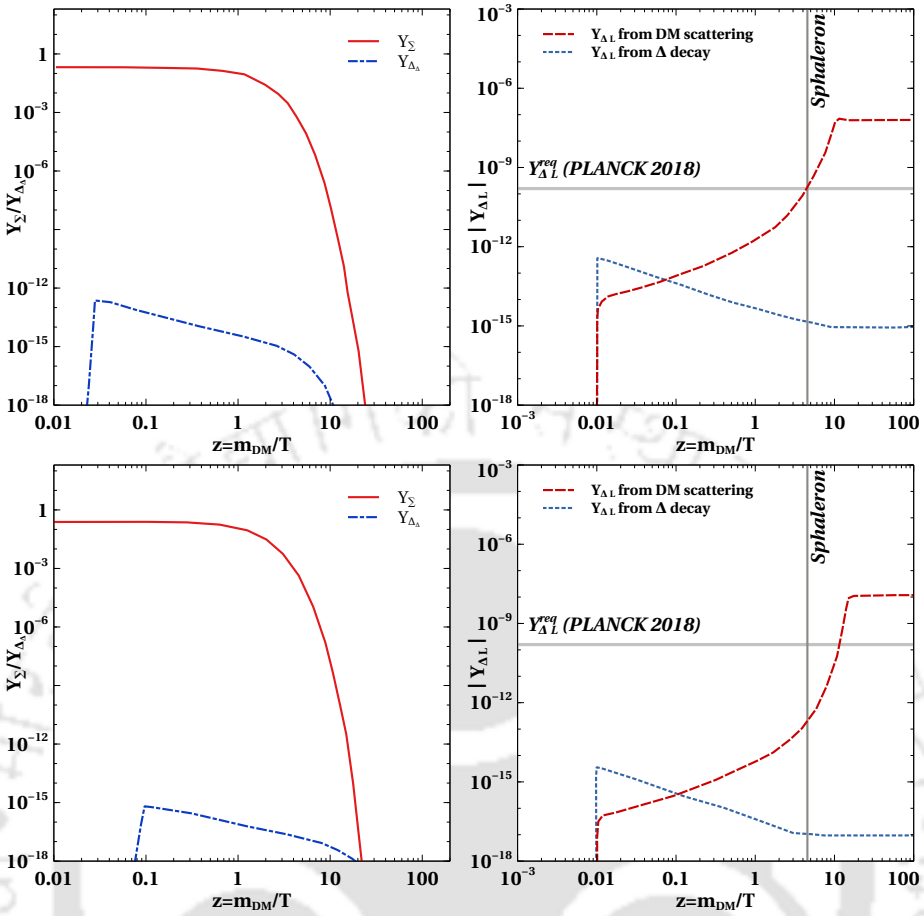

Figure D.2: Plot showing the evolution of the comoving number densities of $\sum$ and Δ (on the left panel) and the generated $B-L$ from the scattering of DM and from the decay of Δ (on the right panel plot). The important parameters are fixed at $m_{\eta_R} = m_{\rm DM} = 600$ GeV, $m_{\Delta^\pm} = m_{\Delta^{\pm\pm}} = m_{\Delta^0} = 1.2$ TeV, $M_1 = 6$ TeV, $M_2 = 6.6$ TeV, $M_3 = 7$ TeV, $\mu_{\eta\Delta} = 10$i, $\lambda''_{H\eta} = 1 \times 10^{-5}$, $v = 1$ keV (for the top panel) and $v = 1$ eV (for the bottom panel).

In the above Boltzmann equations, C_l^k and C_H^k are the conversion factor for the asymmetry in lepton sector as well as in Higgs with the fundamental asymmetries Y_{Δ_Δ} and Y_{B-L}. The conversion matrices relate the asymmetries as follows

$$Y_{\Delta_l} = -\sum_k C_k^l Y_{X_k},\; Y_{\Delta_H} = -\sum_k C_k^H Y_{X_k}, \tag{D.31}$$

where Y_{X_k} are the elements of $Y_X^T = (Y_{\Delta_\Delta}, Y_{B-L})$. The conversion matrices for the unflavored leptogenesis are [398]

$$C^l = \begin{pmatrix} 0 & 1/2 \end{pmatrix},\; C^H = \begin{pmatrix} 3 & 1/2 \end{pmatrix} \tag{D.32}$$

Here we have simplified the situation by considering the chemical potential of the η field to be zero such that C^η and hence the corresponding $B_\phi = \dfrac{|\,\mu_{\eta\Delta}\,|^2}{8\pi m_\Delta \Gamma_\Delta^{\rm Tot}}$ does not appear. For a

detailed analysis of scalar triplet leptogenesis in this model, including flavour effects, please refer to [399].

In Fig.D.2 we have shown the evolution of the comoving number densities of $\sum$, Δ and the $B-L$ asymmetry generated from the annihilation of WIMP DM η and from the decay of Δ. While plotting we have taken both Δ and $\bar{\Delta}$ to be in equilibrium and therefore $Y_{\Delta_\Delta}^{initial} = 0$. From Fig.D.2, it can be seen that the contribution to the $B-L$ asymmetry coming from the decay of Δ is much less compared to that coming from the scattering of DM. Therefore in this work we have neglected the $B-L$ asymmetry coming from the Δ decay. This is expected as the scale of Δ is higher compared to η_R or WIMP DM. Similarly, one can have leptogenesis from decay of Z_2-odd RHNs as well, as discussed in earlier works [113, 123, 139–143, 175, 176, 400]. However, the scale of RHNs is even higher than that of Δ and such high scale generation of asymmetries will be sub-dominant in final asymmetry dominantly generated by lepton number violating WIMP annihilations at lower scales.

D.4 Calculation of the sphaleron factor

Here we show the derivation of the sphaleron conversion factor in our model, following the standard approach outlined in [63]. For a relativistic particle X with spin s and degrees of freedom (dof) g_X, the relation between the asymmetry of particle over antiparticle and the particle's chemical potential is given by

$$Y_{\Delta_X} = \frac{T^2}{6s} g_X \mu_X \quad \text{for fermions,} \tag{D.33}$$

$$Y_{\Delta_X} = \frac{T^2}{6s} 2 g_X \mu_X \quad \text{for boson.} \tag{D.34}$$

In principle, there are as many as chemical potentials (an asymmetry) as the number of particles in the plasma. This number is reduced due to the constraints imposed by a set of chemical equilibrium conditions and some conservation laws in the early universe, as outlined below.

1. Chemical potentials for all the gauge bosons vanishes $\mu_{W^i} = \mu_{\mathcal{B}} = \mu_g = 0$. Therefore the electroweak and colour multiplets have the same chemical potentials.

2. Regardless of the temperature of the universe the electric charge must be conserved and this leads to the following constraint,

$$Q = \sum_i^{N_f} (\mu_{Q_i} + 2\mu_{u_i} - \mu_{d_i} - \mu_{l_i} - \mu_{e_i}) + \sum_i^m 2\mu_\phi + \sum_i^n 6\mu_\Delta = 0. \tag{D.35}$$

   Here μ_{Q_i}, μ_{u_i}, μ_{d_i}, μ_{l_i}, μ_{e_i} are the chemical potential for the left handed quark doublets, right handed up type quarks, right handed down type quarks, left handed lepton doublets and right handed charged leptons respectively. N_f is the number of Fermion generations present in the model. μ_ϕ and μ_Δ are the chemical potentials for the doublets and triplet scalars respectively. m and n are the number of scalar doublet and scalar triplet generations in the model.

3. Non-perturbative electroweak sphaleron and QCD instanton processes, while in thermal equilibrium, imposes the following constraints

$$\begin{aligned} \textstyle\sum_i^{N_f} (3\mu_{Q_i} + \mu_{l_i}) = 0 \Rightarrow 3\mu_Q + \mu_l = 0, \\ \textstyle\sum_i^{N_f} (2\mu_{Q_i} - \mu_{d_i} - \mu_{u_i}) = 0. \end{aligned} \tag{D.36}$$

4. The Yukawa interactions, while in equilibrium, bring the following constraints

$$\mu_{u_i} - \mu_{Q_i} - \mu_\phi = 0, \quad \phi^0 \longleftrightarrow \bar{u_L} + u_R \tag{D.37}$$
$$\mu_{d_i} - \mu_{Q_i} + \mu_\phi = 0, \quad \phi^0 \longleftrightarrow \bar{d_R} + d_L \tag{D.38}$$
$$\mu_{e_i} - \mu_{l_i} + \mu_\phi = 0, \quad \phi^0 \longleftrightarrow e_{iL} + \bar{e_{iR}} \tag{D.39}$$
$$\mu_\Delta - 2\mu_{l_i} = 0, \quad \Delta \longleftrightarrow 2l_{iL} \tag{D.40}$$

Since we are assuming equilibrium among different generations, the generation index i in subscript can be dropped from the above equations. Replacing μ_{u_i}, μ_{d_i}, μ_{e_i} and μ_Δ in Eq.(D.35), μ_ϕ can be expressed in terms of $\mu_{Q_i} \equiv \mu_Q$ as follows

$$\mu_\phi = \frac{36n - 8N_f}{2m + 4N_f}\mu_Q \tag{D.41}$$

Similarly, we can express other chemical potentials in terms of μ_Q.

Now, the baryon number (B) in terms of the chemical potentials is given by

$$B = \sum_i^{N_f} (2\mu_{Q_i} + \mu_{u_i} + \mu_{d_i}) = 4N_f\mu_Q. \tag{D.42}$$

Similarly, the lepton number (L) is given by

$$L = \sum_i^{N_f} (2\mu_{l_i} + \mu_{e_i}) = 3N_f\mu_l - N_f\mu_\phi = -9N_f\mu_Q - \frac{N_f(36n - 8N_f)}{4N_f + 2m}\mu_Q. \tag{D.43}$$

From Eq.(D.42), (D.43), we can now find

$$B = \frac{8N_f + 4m}{22N_f + 13m + 18n}(B - L), \tag{D.44}$$
$$B = -\frac{8N_f + 4m}{14N_f + 9m + 18n}L, \tag{D.45}$$

which for our model with $m = 2, n = 1$ gives $\Delta B = -\frac{16}{39}\Delta L$.

Bibliography

[1] G. Hinshaw et al. Nine-Year Wilkinson Microwave Anisotropy Probe (WMAP) Observations: Cosmological Parameter Results. *Astrophys. J. Suppl.*, 208:19, 2013.

[2] P. A. Zyla et al. Review of Particle Physics. *PTEP*, 2020(8):083C01, 2020.

[3] N. Aghanim et al. Planck 2018 results. VI. Cosmological parameters. *Astron. Astrophys.*, 641:A6, 2020. [Erratum: Astron.Astrophys. 652, C4 (2021)].

[4] V. C. Rubin, N. Thonnard, and W. K. Ford, Jr. Rotational properties of 21 SC galaxies with a large range of luminosities and radii, from NGC 4605 /R = 4kpc/ to UGC 2885 /R = 122 kpc/. *Astrophys. J.*, 238:471, 1980.

[5] F. Zwicky. Die Rotverschiebung von extragalaktischen Nebeln. *Helv. Phys. Acta*, 6:110–127, 1933.

[6] Douglas Clowe, Marusa Bradac, Anthony H. Gonzalez, Maxim Markevitch, Scott W. Randall, Christine Jones, and Dennis Zaritsky. A direct empirical proof of the existence of dark matter. *Astrophys. J. Lett.*, 648:L109–L113, 2006.

[7] Gary Steigman. Primordial nucleosynthesis: successes and challenges. *Int. J. Mod. Phys. E*, 15:1–36, 2006.

[8] Richard H. Cyburt, Brian D. Fields, Keith A. Olive, and Evan Skillman. New BBN limits on physics beyond the standard model from ^4He. *Astropart. Phys.*, 23:313–323, 2005.

[9] Fabio Iocco, Gianpiero Mangano, Gennaro Miele, Ofelia Pisanti, and Pasquale D. Serpico. Primordial Nucleosynthesis: from precision cosmology to fundamental physics. *Phys. Rept.*, 472:1–76, 2009.

[10] S. Riemer-Sørensen, J. K. Webb, N. Crighton, V. Dumont, K. Ali, S. Kotuš, M. Bainbridge, M. T. Murphy, and R. Carswell. A robust deuterium abundance; Re-measurement of the z=3.256 absorption system towards the quasar PKS1937-1009. *Mon. Not. Roy. Astron. Soc.*, 447:2925, 2015.

[11] Wayne Hu and Scott Dodelson. Cosmic Microwave Background Anisotropies. *Ann. Rev. Astron. Astrophys.*, 40:171–216, 2002.

[12] Scott Dodelson. *Modern Cosmology*. Academic Press, Amsterdam, 2003.

[13] Alessandro Strumia. Baryogenesis via leptogenesis. In *Les Houches Summer School on Theoretical Physics: Session 84: Particle Physics Beyond the Standard Model*, pages 655–680, 8 2006.

[14] Edward W. Kolb and Michael S. Turner. *The Early Universe*, volume 69. 1990.

[15] A. D. Sakharov. Violation of CP Invariance, C asymmetry, and baryon asymmetry of the universe. *Pisma Zh. Eksp. Teor. Fiz.*, 5:32–35, 1967.

[16] Gerard 't Hooft. Computation of the Quantum Effects Due to a Four-Dimensional Pseudoparticle. *Phys. Rev. D*, 14:3432–3450, 1976. [Erratum: Phys.Rev.D 18, 2199 (1978)].

[17] V. A. Kuzmin, V. A. Rubakov, and M. E. Shaposhnikov. On the Anomalous Electroweak Baryon Number Nonconservation in the Early Universe. *Phys. Lett. B*, 155:36, 1985.

[18] K. Rummukainen, M. Tsypin, K. Kajantie, M. Laine, and Mikhail E. Shaposhnikov. The Universality class of the electroweak theory. *Nucl. Phys. B*, 532:283–314, 1998.

[19] Christophe Grojean, Geraldine Servant, and James D. Wells. First-order electroweak phase transition in the standard model with a low cutoff. *Phys. Rev. D*, 71:036001, 2005.

[20] Serguei Chatrchyan et al. Observation of a New Boson at a Mass of 125 GeV with the CMS Experiment at the LHC. *Phys. Lett. B*, 716:30–61, 2012.

[21] Georges Aad et al. Observation of a new particle in the search for the Standard Model Higgs boson with the ATLAS detector at the LHC. *Phys. Lett. B*, 716:1–29, 2012.

[22] Makoto Kobayashi and Toshihide Maskawa. CP Violation in the Renormalizable Theory of Weak Interaction. *Prog. Theor. Phys.*, 49:652–657, 1973.

[23] C. Jarlskog. Commutator of the Quark Mass Matrices in the Standard Electroweak Model and a Measure of Maximal CP Nonconservation. *Phys. Rev. Lett.*, 55:1039, 1985.

[24] A. Yu. Ignatiev, N. V. Krasnikov, V. A. Kuzmin, and A. N. Tavkhelidze. Universal CP Noninvariant Superweak Interaction and Baryon Asymmetry of the Universe. *Phys. Lett. B*, 76:436–438, 1978.

[25] Motohiko Yoshimura. Unified Gauge Theories and the Baryon Number of the Universe. *Phys. Rev. Lett.*, 41:281–284, 1978. [Erratum: Phys.Rev.Lett. 42, 746 (1979)].

[26] Savas Dimopoulos and Leonard Susskind. On the Baryon Number of the Universe. *Phys. Rev. D*, 18:4500–4509, 1978.

[27] Steven Weinberg. Cosmological Production of Baryons. *Phys. Rev. Lett.*, 42:850–853, 1979.

[28] John R. Ellis, Mary K. Gaillard, and Dimitri V. Nanopoulos. Baryon Number Generation in Grand Unified Theories. *Phys. Lett. B*, 80:360, 1979. [Erratum: Phys.Lett.B 82, 464 (1979)].

[29] Motohiko Yoshimura. Origin of Cosmological Baryon Asymmetry. *Phys. Lett. B*, 88:294–298, 1979.

[30] Stephen M. Barr, Gino Segre, and H. Arthur Weldon. The Magnitude of the Cosmological Baryon Asymmetry. *Phys. Rev. D*, 20:2494, 1979.

[31] Dimitri V. Nanopoulos and Steven Weinberg. Mechanisms for Cosmological Baryon Production. *Phys. Rev. D*, 20:2484, 1979.

[32] Edward W. Kolb and Stephen Wolfram. Baryon Number Generation in the Early Universe. *Nucl. Phys. B*, 172:224, 1980. [Erratum: Nucl.Phys.B 195, 542 (1982)].

[33] Antonio Riotto and Mark Trodden. Recent progress in baryogenesis. *Ann. Rev. Nucl. Part. Sci.*, 49:35–75, 1999.

[34] James M. Cline. Baryogenesis. In *Les Houches Summer School - Session 86: Particle Physics and Cosmology: The Fabric of Spacetime*, 9 2006.

[35] S. Yu. Khlebnikov and M. E. Shaposhnikov. The Statistical Theory of Anomalous Fermion Number Nonconservation. *Nucl. Phys. B*, 308:885–912, 1988.

[36] K. Kajantie, M. Laine, K. Rummukainen, and Mikhail E. Shaposhnikov. The Electroweak phase transition: A Nonperturbative analysis. *Nucl. Phys. B*, 466:189–258, 1996.

[37] M.B. Gavela, M. Lozano, J. Orloff, and O. Pène. Standard model CP-violation and baryon asymmetry (i). zero temperature. *Nuclear Physics B*, 430(2):345–381, nov 1994.

[38] M.B. Gavela, P. Hernandez, J. Orloff, O. Péne, and C. Quimbay. Standard model CP-violation and baryon asymmetry (II). finite temperature. *Nuclear Physics B*, 430(2):382–426, nov 1994.

[39] Marta Losada. High temperature dimensional reduction of the MSSM and other multiscalar models. *Phys. Rev. D*, 56:2893–2913, 1997.

[40] Marcela Carena, M. Quiros, and C. E. M. Wagner. Opening the window for electroweak baryogenesis. *Phys. Lett. B*, 380:81–91, 1996.

[41] D. Delepine, J. M. Gerard, R. Gonzalez Felipe, and J. Weyers. A Light stop and electroweak baryogenesis. *Phys. Lett. B*, 386:183–188, 1996.

[42] Ian Affleck and Michael Dine. A New Mechanism for Baryogenesis. *Nucl. Phys. B*, 249:361–380, 1985.

[43] Michael Dine, Lisa Randall, and Scott D. Thomas. Baryogenesis from flat directions of the supersymmetric standard model. *Nucl. Phys. B*, 458:291–326, 1996.

[44] M. Fukugita and T. Yanagida. Baryogenesis Without Grand Unification. *Phys. Lett. B*, 174:45–47, 1986.

[45] Peter Minkowski. $\mu \to e\gamma$ at a Rate of One Out of 10^9 Muon Decays? *Phys. Lett. B*, 67:421–428, 1977.

[46] Tsutomu Yanagida. Horizontal gauge symmetry and masses of neutrinos. *Conf. Proc. C*, 7902131:95–99, 1979.

[47] Murray Gell-Mann, Pierre Ramond, and Richard Slansky. Complex Spinors and Unified Theories. *Conf. Proc. C*, 790927:315–321, 1979.

[48] Rabindra N. Mohapatra and Goran Senjanovic. Neutrino Masses and Mixings in Gauge Models with Spontaneous Parity Violation. *Phys. Rev. D*, 23:165, 1981.

[49] S. L. Glashow. The Future of Elementary Particle Physics. *NATO Sci. Ser. B*, 61:687, 1980.

[50] J. Schechter and J. W. F. Valle. Neutrino Masses in SU(2) x U(1) Theories. *Phys. Rev. D*, 22:2227, 1980.

[51] Markus A. Luty. Baryogenesis via leptogenesis. *Phys. Rev. D*, 45:455–465, Jan 1992.

[52] Marion Flanz, Emmanuel A. Paschos, and Utpal Sarkar. Baryogenesis from a lepton asymmetric universe. *Physics Letters B*, 345(3):248–252, 1995.

[53] Laura Covi, Esteban Roulet, and Francesco Vissani. CP violating decays in leptogenesis scenarios. *Phys. Lett. B*, 384:169–174, 1996.

[54] Apostolos Pilaftsis and Thomas E. J. Underwood. Resonant leptogenesis. *Nucl. Phys. B*, 692:303–345, 2004.

[55] Asmaa Abada, Sacha Davidson, Francois-Xavier Josse-Michaux, Marta Losada, and Antonio Riotto. Flavor issues in leptogenesis. *JCAP*, 04:004, 2006.

[56] A. Abada, S. Davidson, A. Ibarra, F. X. Josse-Michaux, M. Losada, and A. Riotto. Flavour Matters in Leptogenesis. *JHEP*, 09:010, 2006.

[57] Enrico Nardi, Yosef Nir, Esteban Roulet, and Juan Racker. The Importance of flavor in leptogenesis. *JHEP*, 01:164, 2006.

[58] Steve Blanchet and Pasquale Di Bari. Flavor effects on leptogenesis predictions. *JCAP*, 03:018, 2007.

[59] Nick Kaiser, R. A. Malaney, and G. D. Starkman. Neutrino lasing in the early universe. *Phys. Rev. Lett.*, 71:1128–1131, 1993.

[60] Michael Plumacher. Baryogenesis and lepton number violation. *Z. Phys. C*, 74:549–559, 1997.

[61] G. F. Giudice, A. Notari, M. Raidal, A. Riotto, and A. Strumia. Towards a complete theory of thermal leptogenesis in the SM and MSSM. *Nucl. Phys. B*, 685:89–149, 2004.

[62] W. Buchmuller, P. Di Bari, and M. Plumacher. Leptogenesis for pedestrians. *Annals Phys.*, 315:305–351, 2005.

[63] Jeffrey A. Harvey and Michael S. Turner. Cosmological baryon and lepton number in the presence of electroweak fermion number violation. *Phys. Rev. D*, 42:3344–3349, 1990.

[64] Sacha Davidson and Alejandro Ibarra. A Lower bound on the right-handed neutrino mass from leptogenesis. *Phys. Lett. B*, 535:25–32, 2002.

[65] J. A. Casas and A. Ibarra. Oscillating neutrinos and $\mu \to e, \gamma$. *Nucl. Phys. B*, 618:171–204, 2001.

[66] M. Magg and C. Wetterich. Neutrino Mass Problem and Gauge Hierarchy. *Phys. Lett. B*, 94:61–64, 1980.

[67] George Lazarides, Q. Shafi, and C. Wetterich. Proton Lifetime and Fermion Masses in an SO(10) Model. *Nucl. Phys. B*, 181:287–300, 1981.

[68] T. P. Cheng and Ling-Fong Li. Neutrino Masses, Mixings and Oscillations in SU(2) x U(1) Models of Electroweak Interactions. *Phys. Rev. D*, 22:2860, 1980.

[69] J. Schechter and J. W. F. Valle. Neutrino Decay and Spontaneous Violation of Lepton Number. *Phys. Rev. D*, 25:774, 1982.

[70] Robert Foot, H. Lew, X. G. He, and Girish C. Joshi. Seesaw Neutrino Masses Induced by a Triplet of Leptons. *Z. Phys. C*, 44:441, 1989.

[71] Apostolos Pilaftsis. Resonant CP violation induced by particle mixing in transition amplitudes. *Nucl. Phys. B*, 504:61–107, 1997.

[72] Massimo Persic, Paolo Salucci, and Fulvio Stel. The Universal rotation curve of spiral galaxies: 1. The Dark matter connection. *Mon. Not. Roy. Astron. Soc.*, 281:27, 1996.

[73] Yoshiaki Sofue and Vera Rubin. Rotation curves of spiral galaxies. *Ann. Rev. Astron. Astrophys.*, 39:137–174, 2001.

[74] A. Bosma. 21-cm line studies of spiral galaxies. 2. The distribution and kinematics of neutral hydrogen in spiral galaxies of various morphological types. *Astron. J.*, 86:1825, 1981.

[75] Markus Weber and Wim de Boer. Determination of the Local Dark Matter Density in our Galaxy. *Astron. Astrophys.*, 509:A25, 2010.

[76] Douglas Clowe, Anthony Gonzalez, and Maxim Markevitch. Weak lensing mass reconstruction of the interacting cluster 1E0657-558: Direct evidence for the existence of dark matter. *Astrophys. J.*, 604:596–603, 2004.

[77] Maxim Markevitch, A. H. Gonzalez, D. Clowe, A. Vikhlinin, L. David, W. Forman, C. Jones, S. Murray, and W. Tucker. Direct constraints on the dark matter self-interaction cross-section from the merging galaxy cluster 1E0657-56. *Astrophys. J.*, 606:819–824, 2004.

[78] Marusa Bradac, Steven W. Allen, Tommaso Treu, Harald Ebeling, Richard Massey, R. Glenn Morris, Anja von der Linden, and Douglas Applegate. Revealing the properties of dark matter in the merging cluster MACSJ0025.4-1222. *Astrophys. J.*, 687:959, 2008.

[79] Liliya LR Williams and Prasenjit Saha. Light/mass offsets in the lensing cluster abell 3827: evidence for collisional dark matter? *Monthly Notices of the Royal Astronomical Society*, 415(1):448–460, 2011.

[80] Photo album :: Frontier fields galaxy clusters :: March 10, 2016.

[81] L. Kantha. A Time-Dependent and Cosmological Model Consistent with Cosmological Constraints. *Adv. Astron.*, 2016:9743970, 2016.

[82] Hong-Yee Chiu. Symmetry between particle and anti-particle populations in the universe. *Phys. Rev. Lett.*, 17:712, 1966.

[83] Benjamin W. Lee and Steven Weinberg. Cosmological Lower Bound on Heavy Neutrino Masses. *Phys. Rev. Lett.*, 39:165–168, 1977.

[84] Giorgio Arcadi, Maíra Dutra, Pradipta Ghosh, Manfred Lindner, Yann Mambrini, Mathias Pierre, Stefano Profumo, and Farinaldo S. Queiroz. The waning of the WIMP? A review of models, searches, and constraints. *Eur. Phys. J. C*, 78(3):203, 2018.

[85] Mark W. Goodman and Edward Witten. Detectability of Certain Dark Matter Candidates. *Phys. Rev. D*, 31:3059, 1985.

[86] Stefano Profumo, Leonardo Giani, and Oliver F. Piattella. An Introduction to Particle Dark Matter. *Universe*, 5(10):213, 2019.

[87] D. S. Akerib et al. Results from a search for dark matter in the complete LUX exposure. *Phys. Rev. Lett.*, 118(2):021303, 2017.

[88] E. Aprile et al. Dark Matter Results from 225 Live Days of XENON100 Data. *Phys. Rev. Lett.*, 109:181301, 2012.

[89] E. Aprile et al. First Dark Matter Search Results from the XENON1T Experiment. *Phys. Rev. Lett.*, 119(18):181301, 2017.

[90] E. Aprile et al. Dark Matter Search Results from a One Ton-Year Exposure of XENON1T. *Phys. Rev. Lett.*, 121(11):111302, 2018.

[91] Andi Tan et al. Dark Matter Results from First 98.7 Days of Data from the PandaX-II Experiment. *Phys. Rev. Lett.*, 117(12):121303, 2016.

[92] Xiangyi Cui et al. Dark Matter Results From 54-Ton-Day Exposure of PandaX-II Experiment. *Phys. Rev. Lett.*, 119(18):181302, 2017.

[93] J. Aalbers et al. First Dark Matter Search Results from the LUX-ZEPLIN (LZ) Experiment. 7 2022.

[94] Oscar Adriani et al. An anomalous positron abundance in cosmic rays with energies 1.5-100 GeV. *Nature*, 458:607–609, 2009.

[95] R. Cowsik, B. Burch, and T. Madziwa-Nussinov. The origin of the spectral intensities of cosmic-ray positrons. *Astrophys. J.*, 786:124, 2014.

[96] R Abbasi, Yasser Abdou, Markus Ackermann, John Adams, Markus Ahlers, K Andeen, Jan Auffenberg, Xinhua Bai, Michael Baker, SW Barwick, et al. Limits on a muon flux from neutralino annihilations in the sun with the icecube 22-string detector. *Physical review letters*, 102(20):201302, 2009.

[97] M. Ageron et al. ANTARES: the first undersea neutrino telescope. *Nucl. Instrum. Meth. A*, 656:11–38, 2011.

[98] F. Aharonian et al. The h.e.s.s. survey of the inner galaxy in very high-energy gamma-rays. *Astrophys. J.*, 636:777–797, 2006.

[99] T. C. Weekes et al. VERITAS: The Very energetic radiation imaging telescope array system. *Astropart. Phys.*, 17:221–243, 2002.

[100] David Green, Tsutomu Nagayoshi, and Francesco dePalma. Gamma-ray Spectral and Morphological study of HESS J1912+101 observed by MAGIC and Fermi-LAT. *PoS*, ICRC2019:564, 2020.

[101] Johan Alwall, Philip Schuster, and Natalia Toro. Simplified Models for a First Characterization of New Physics at the LHC. *Phys. Rev. D*, 79:075020, 2009.

[102] Daniele Alves. Simplified Models for LHC New Physics Searches. *J. Phys. G*, 39:105005, 2012.

[103] Daniel Abercrombie et al. Dark Matter benchmark models for early LHC Run-2 Searches: Report of the ATLAS/CMS Dark Matter Forum. *Phys. Dark Univ.*, 27:100371, 2020.

[104] Anthony Paul Di Franzo. *Simplified Models for Dark Matter Model Building*. PhD thesis, UC, Irvine, 2016.

[105] M. Tanabashi et al. Review of Particle Physics. *Phys. Rev. D*, 98(3):030001, 2018.

[106] Lawrence J. Hall, Karsten Jedamzik, John March-Russell, and Stephen M. West. Freeze-In Production of FIMP Dark Matter. *JHEP*, 03:080, 2010.

[107] Nicolás Bernal, Matti Heikinheimo, Tommi Tenkanen, Kimmo Tuominen, and Ville Vaskonen. The Dawn of FIMP Dark Matter: A Review of Models and Constraints. *Int. J. Mod. Phys. A*, 32(27):1730023, 2017.

[108] Anirban Biswas and Aritra Gupta. Calculation of Momentum Distribution Function of a Non-thermal Fermionic Dark Matter. *JCAP*, 03:033, 2017. [Addendum: JCAP 05, A02 (2017)].

[109] Thomas Hambye, Michel H. G. Tytgat, Jérôme Vandecasteele, and Laurent Vanderheyden. Dark matter direct detection is testing freeze-in. *Phys. Rev. D*, 98(7):075017, 2018.

[110] Raymond T. Co, Francesco D'Eramo, Lawrence J. Hall, and Duccio Pappadopulo. Freeze-In Dark Matter with Displaced Signatures at Colliders. *JCAP*, 12:024, 2015.

[111] Amin Aboubrahim, Wan-Zhe Feng, and Pran Nath. A long-lived stop with freeze-in and freeze-out dark matter in the hidden sector. *JHEP*, 02:118, 2020.

[112] Ernest Ma. Verifiable radiative seesaw mechanism of neutrino mass and dark matter. *Phys. Rev. D*, 73:077301, 2006.

[113] Thomas Hugle, Moritz Platscher, and Kai Schmitz. Low-Scale Leptogenesis in the Scotogenic Neutrino Mass Model. *Phys. Rev. D*, 98(2):023020, 2018.

[114] Takashi Toma and Avelino Vicente. Lepton Flavor Violation in the Scotogenic Model. *JHEP*, 01:160, 2014.

[115] Arnab Dasgupta and Debasish Borah. Scalar Dark Matter with Type II Seesaw. *Nucl. Phys. B*, 889:637–649, 2014.

[116] Arindam Das, Takaaki Nomura, Hiroshi Okada, and Sourov Roy. Generation of a radiative neutrino mass in the linear seesaw framework, charged lepton flavor violation, and dark matter. *Phys. Rev. D*, 96(7):075001, 2017.

[117] Rabindra N. Mohapatra and Goran Senjanovic. Neutrino Mass and Spontaneous Parity Nonconservation. *Phys. Rev. Lett.*, 44:912, 1980.

[118] Nilendra G. Deshpande and Ernest Ma. Pattern of Symmetry Breaking with Two Higgs Doublets. *Phys. Rev. D*, 18:2574, 1978.

[119] Marco Cirelli, Nicolao Fornengo, and Alessandro Strumia. Minimal dark matter. *Nucl. Phys. B*, 753:178–194, 2006.

[120] Riccardo Barbieri, Lawrence J. Hall, and Vyacheslav S. Rychkov. Improved naturalness with a heavy Higgs: An Alternative road to LHC physics. *Phys. Rev. D*, 74:015007, 2006.

[121] Ernest Ma. Common origin of neutrino mass, dark matter, and baryogenesis. *Mod. Phys. Lett. A*, 21:1777–1782, 2006.

[122] Laura Lopez Honorez, Emmanuel Nezri, Josep F. Oliver, and Michel H. G. Tytgat. The Inert Doublet Model: An Archetype for Dark Matter. *JCAP*, 02:028, 2007.

[123] T. Hambye, F. S. Ling, L. Lopez Honorez, and J. Rocher. Scalar Multiplet Dark Matter. *JHEP*, 07:090, 2009. [Erratum: JHEP 05, 066 (2010)].

[124] Ethan M. Dolle and Shufang Su. The Inert Dark Matter. *Phys. Rev. D*, 80:055012, 2009.

[125] Laura Lopez Honorez and Carlos E. Yaguna. The inert doublet model of dark matter revisited. *JHEP*, 09:046, 2010.

[126] Laura Lopez Honorez and Carlos E. Yaguna. A new viable region of the inert doublet model. *JCAP*, 01:002, 2011.

[127] Michael Gustafsson, Sara Rydbeck, Laura Lopez-Honorez, and Erik Lundstrom. Status of the Inert Doublet Model and the Role of multileptons at the LHC. *Phys. Rev. D*, 86:075019, 2012.

[128] A. Goudelis, B. Herrmann, and O. Stål. Dark matter in the Inert Doublet Model after the discovery of a Higgs-like boson at the LHC. *JHEP*, 09:106, 2013.

[129] Abdesslam Arhrib, Yue-Lin Sming Tsai, Qiang Yuan, and Tzu-Chiang Yuan. An Updated Analysis of Inert Higgs Doublet Model in light of the Recent Results from LUX, PLANCK, AMS-02 and LHC. *JCAP*, 06:030, 2014.

[130] Marco Aurelio Díaz, Benjamin Koch, and Sebastián Urrutia-Quiroga. Constraints to Dark Matter from Inert Higgs Doublet Model. *Adv. High Energy Phys.*, 2016:8278375, 2016.

[131] Amine Ahriche, Adil Jueid, and Salah Nasri. Radiative neutrino mass and Majorana dark matter within an inert Higgs doublet model. *Phys. Rev. D*, 97(9):095012, 2018.

[132] Alexander Merle and Moritz Platscher. Running of radiative neutrino masses: the scotogenic model — revisited. *JHEP*, 11:148, 2015.

[133] Gerard 't Hooft. Naturalness, chiral symmetry, and spontaneous chiral symmetry breaking. *NATO Sci. Ser. B*, 59:135–157, 1980.

[134] P. F. de Salas, D. V. Forero, C. A. Ternes, M. Tortola, and J. W. F. Valle. Status of neutrino oscillations 2018: 3σ hint for normal mass ordering and improved CP sensitivity. *Phys. Lett. B*, 782:633–640, 2018.

[135] Ivan Esteban, M. C. Gonzalez-Garcia, Alvaro Hernandez-Cabezudo, Michele Maltoni, and Thomas Schwetz. Global analysis of three-flavour neutrino oscillations: synergies and tensions in the determination of θ_{23}, δ_{CP}, and the mass ordering. *JHEP*, 01:106, 2019.

[136] Paolo Gondolo and Graciela Gelmini. Cosmic abundances of stable particles: Improved analysis. *Nucl. Phys. B*, 360:145–179, 1991.

[137] Kim Griest and David Seckel. Three exceptions in the calculation of relic abundances. *Phys. Rev. D*, 43:3191–3203, 1991.

[138] Debasish Borah, Dibyendu Nanda, Nimmala Narendra, and Narendra Sahu. Right-handed neutrino dark matter with radiative neutrino mass in gauged B − L model. *Nucl. Phys. B*, 950:114841, 2020.

[139] Shoichi Kashiwase and Daijiro Suematsu. Baryon number asymmetry and dark matter in the neutrino mass model with an inert doublet. *Phys. Rev. D*, 86:053001, 2012.

[140] Shoichi Kashiwase and Daijiro Suematsu. Leptogenesis and dark matter detection in a TeV scale neutrino mass model with inverted mass hierarchy. *Eur. Phys. J. C*, 73:2484, 2013.

[141] J. Racker. Mass bounds for baryogenesis from particle decays and the inert doublet model. *JCAP*, 03:025, 2014.

[142] Jackson D. Clarke, Robert Foot, and Raymond R. Volkas. Natural leptogenesis and neutrino masses with two Higgs doublets. *Phys. Rev. D*, 92(3):033006, 2015.

[143] Debasish Borah, P. S. Bhupal Dev, and Abhass Kumar. TeV scale leptogenesis, inflaton dark matter and neutrino mass in a scotogenic model. *Phys. Rev. D*, 99(5):055012, 2019.

[144] Bhupal Dev, Mathias Garny, Juraj Klaric, Peter Millington, and Daniele Teresi. Resonant enhancement in leptogenesis. *Int. J. Mod. Phys. A*, 33:1842003, 2018.

[145] Pasquale Di Bari. Seesaw geometry and leptogenesis. *Nucl. Phys. B*, 727:318–354, 2005.

[146] O. Vives. Flavor dependence of CP asymmetries and thermal leptogenesis with strong right-handed neutrino mass hierarchy. *Phys. Rev. D*, 73:073006, 2006.

[147] Steve Blanchet and Pasquale Di Bari. New aspects of leptogenesis bounds. *Nucl. Phys. B*, 807:155–187, 2009.

[148] Xiao-Gang He, Sandy S. C. Law, and Raymond R. Volkas. Determining the heavy seesaw neutrino mass matrix from low-energy parameters. *Phys. Rev. D*, 78:113001, 2008.

[149] Stefan Antusch, Pasquale Di Bari, David A. Jones, and Steve F. King. A fuller flavour treatment of N_2-dominated leptogenesis. *Nucl. Phys. B*, 856:180–209, 2012.

[150] Steve Blanchet, Pasquale Di Bari, David A. Jones, and Luca Marzola. Leptogenesis with heavy neutrino flavours: from density matrix to Boltzmann equations. *JCAP*, 01:041, 2013.

[151] Pasquale Di Bari, Sophie King, and Michele Re Fiorentin. Strong thermal leptogenesis and the absolute neutrino mass scale. *JCAP*, 03:050, 2014.

[152] Pasquale Di Bari and Michele Re Fiorentin. Supersymmetric $SO(10)$-inspired leptogenesis and a new N_2-dominated scenario. *JCAP*, 03:039, 2016.

[153] Pasquale Di Bari and Stephen F. King. Successful N_2 leptogenesis with flavour coupling effects in realistic unified models. *JCAP*, 10:008, 2015.

[154] Pasquale Di Bari, Luca Marzola, and Michele Re Fiorentin. Decrypting $SO(10)$-inspired leptogenesis. *Nucl. Phys. B*, 893:122–157, 2015.

[155] Pasquale Di Bari and Antonio Riotto. Testing SO(10)-inspired leptogenesis with low energy neutrino experiments. *JCAP*, 04:037, 2011.

[156] Jue Zhang. Confronting four zero neutrino Yukawa textures with N_2-dominated leptogenesis. *Phys. Rev. D*, 91(7):073012, 2015.

[157] Pasquale Di Bari and Antonio Riotto. Successful type I Leptogenesis with SO(10)-inspired mass relations. *Phys. Lett. B*, 671:462–469, 2009.

[158] G. Belanger, F. Boudjema, A. Pukhov, and A. Semenov. micrOMEGAs_3: A program for calculating dark matter observables. *Comput. Phys. Commun.*, 185:960–985, 2014.

[159] P. S. Bhupal Dev, Pasquale Di Bari, Bjorn Garbrecht, Stéphane Lavignac, Peter Millington, and Daniele Teresi. Flavor effects in leptogenesis. *Int. J. Mod. Phys. A*, 33:1842001, 2018.

[160] Antonio Masiero and Antonio Riotto. Cosmic Delta B from lepton violating interactions at the electroweak phase transition. *Phys. Lett. B*, 289:73–80, 1992.

[161] Rathin Adhikari and Utpal Sarkar. Baryogenesis in a supersymmetric model without R-parity. *Phys. Lett. B*, 427:59–64, 1998.

[162] Utpal Sarkar and Rathin Adhikari. Baryogenesis through R-parity violation. *Phys. Rev. D*, 55:3836–3843, 1997.

[163] Thomas Hambye. Leptogenesis at the TeV scale. *Nucl. Phys. B*, 633:171–192, 2002.

[164] Arnab Dasgupta, P. S. Bhupal Dev, Sin Kyu Kang, and Yongchao Zhang. New mechanism for matter-antimatter asymmetry and connection with dark matter. *Phys. Rev. D*, 102(5):055009, 2020.

[165] Waleed Abdallah, Abhass Kumar, and Abhijit Kumar Saha. Soft leptogenesis in the NMSSM with a singlet right-handed neutrino superfield. *JHEP*, 04:065, 2020.

[166] Yuval Grossman, Tamar Kashti, Yosef Nir, and Esteban Roulet. Leptogenesis from supersymmetry breaking. *Phys. Rev. Lett.*, 91:251801, 2003.

[167] Giancarlo D'Ambrosio, Gian F. Giudice, and Martti Raidal. Soft leptogenesis. *Phys. Lett. B*, 575:75–84, 2003.

[168] Chee Sheng Fong, M. C. Gonzalez-Garcia, and Enrico Nardi. Leptogenesis from Soft Supersymmetry Breaking (Soft Leptogenesis). *Int. J. Mod. Phys. A*, 26:3491–3604, 2011.

[169] Debasish Borah and Rathin Adhikari. Abelian Gauge Extension of Standard Model: Dark Matter and Radiative Neutrino Mass. *Phys. Rev. D*, 85:095002, 2012.

[170] Rathin Adhikari, Debasish Borah, and Ernest Ma. New U(1) Gauge Model of Radiative Lepton Masses with Sterile Neutrino and Dark Matter. *Phys. Lett. B*, 755:414–417, 2016.

[171] Dibyendu Nanda and Debasish Borah. Common origin of neutrino mass and dark matter from anomaly cancellation requirements of a $U(1)_{B-L}$ model. *Phys. Rev. D*, 96(11):115014, 2017.

[172] Basabendu Barman, Debasish Borah, Purusottam Ghosh, and Abhijit Kumar Saha. Flavoured gauge extension of singlet-doublet fermionic dark matter: neutrino mass, high scale validity and collider signatures. *JHEP*, 10:275, 2019.

[173] Anirban Biswas, Debasish Borah, and Dibyendu Nanda. Type III seesaw for neutrino masses in $\mathrm{U}(1)_{BL}$ model with multi-component dark matter. *JHEP*, 12:109, 2019.

[174] Dibyendu Nanda and Debasish Borah. Connecting Light Dirac Neutrinos to a Multi-component Dark Matter Scenario in Gauged $B - L$ Model. *Eur. Phys. J. C*, 80(6):557, 2020.

[175] Devabrat Mahanta and Debasish Borah. Fermion dark matter with N_2 leptogenesis in minimal scotogenic model. *JCAP*, 11:021, 2019.

[176] Devabrat Mahanta and Debasish Borah. TeV Scale Leptogenesis with Dark Matter in Non-standard Cosmology. *JCAP*, 04(04):032, 2020.

[177] Lavina Sarma, Pritam Das, and Mrinal Kumar Das. Scalar dark matter and leptogenesis in the minimal scotogenic model. *Nucl. Phys. B*, 963:115300, 2021.

[178] A. Ibarra and Graham G. Ross. Neutrino phenomenology: The Case of two right-handed neutrinos. *Phys. Lett. B*, 591:285–296, 2004.

[179] Erik Lundstrom, Michael Gustafsson, and Joakim Edsjo. The Inert Doublet Model and LEP II Limits. *Phys. Rev. D*, 79:035013, 2009.

[180] Morad Aaboud et al. Combination of searches for invisible Higgs boson decays with the ATLAS experiment. *Phys. Rev. Lett.*, 122(23):231801, 2019.

[181] Georges Aad et al. Search for invisible Higgs-boson decays in events with vector-boson fusion signatures using 139 fb^{-1} of proton-proton data recorded by the ATLAS experiment. *JHEP*, 08:104, 2022.

[182] Debasish Borah and Arnab Dasgupta. Left–right symmetric models with a mixture of keV–TeV dark matter. *J. Phys. G*, 46(10):105004, 2019.

[183] Xinyu Miao, Shufang Su, and Brooks Thomas. Trilepton Signals in the Inert Doublet Model. *Phys. Rev. D*, 82:035009, 2010.

[184] Amitava Datta, Nabanita Ganguly, Najimuddin Khan, and Subhendu Rakshit. Exploring collider signatures of the inert Higgs doublet model. *Phys. Rev. D*, 95(1):015017, 2017.

[185] P. Poulose, Shibananda Sahoo, and K. Sridhar. Exploring the Inert Doublet Model through the dijet plus missing transverse energy channel at the LHC. *Phys. Lett. B*, 765:300–306, 2017.

[186] Majid Hashemi and Saereh Najjari. Observability of Inert Scalars at the LHC. *Eur. Phys. J. C*, 77(9):592, 2017.

[187] Alexander Belyaev, Giacomo Cacciapaglia, Igor P. Ivanov, Felipe Rojas-Abatte, and Marc Thomas. Anatomy of the Inert Two Higgs Doublet Model in the light of the LHC and non-LHC Dark Matter Searches. *Phys. Rev. D*, 97(3):035011, 2018.

[188] A. Belyaev, T. R. Fernandez Perez Tomei, P. G. Mercadante, C. S. Moon, S. Moretti, S. F. Novaes, L. Panizzi, F. Rojas, and M. Thomas. Advancing LHC probes of dark matter from the inert two-Higgs-doublet model with the monojet signal. *Phys. Rev. D*, 99(1):015011, 2019.

[189] Debasish Borah, Soumya Sadhukhan, and Shibananda Sahoo. Lepton Portal Limit of Inert Higgs Doublet Dark Matter with Radiative Neutrino Mass. *Phys. Lett. B*, 771:624–632, 2017.

[190] Marc Sher. Electroweak Higgs Potentials and Vacuum Stability. *Phys. Rept.*, 179:273–418, 1989.

[191] Kristjan Kannike. Vacuum Stability Conditions From Copositivity Criteria. *Eur. Phys. J. C*, 72:2093, 2012.

[192] Joydeep Chakrabortty, Partha Konar, and Tanmoy Mondal. Copositive Criteria and Boundedness of the Scalar Potential. *Phys. Rev. D*, 89(9):095008, 2014.

[193] Debasish Borah, Arnab Dasgupta, and Sin Kyu Kang. TeV Scale Leptogenesis via Dark Sector Scatterings. *Eur. Phys. J. C*, 80(6):498, 2020.

[194] Debasish Borah, Arnab Dasgupta, and Sin Kyu Kang. Two-component dark matter with cogenesis of the baryon asymmetry of the Universe. *Phys. Rev. D*, 100(10):103502, 2019.

[195] Wei-Chih Huang, Heinrich Päs, and Sinan Zeißner. Scalar Dark Matter, GUT baryogenesis and Radiative neutrino mass. *Phys. Rev. D*, 98(7):075024, 2018.

[196] Subhaditya Bhattacharya, Purusottam Ghosh, Abhijit Kumar Saha, and Arunansu Sil. Two component dark matter with inert Higgs doublet: neutrino mass, high scale validity and collider searches. *JHEP*, 03:090, 2020.

[197] Qing-Hong Cao, Ernest Ma, Jose Wudka, and C. P. Yuan. Multipartite dark matter. 11 2007.

[198] Kathryn M. Zurek. Multi-Component Dark Matter. *Phys. Rev. D*, 79:115002, 2009.

[199] Diego Chialva, P. S. Bhupal Dev, and Anupam Mazumdar. Multiple dark matter scenarios from ubiquitous stringy throats. *Phys. Rev. D*, 87(6):063522, 2013.

[200] Julian Heeck and He Zhang. Exotic Charges, Multicomponent Dark Matter and Light Sterile Neutrinos. *JHEP*, 05:164, 2013.

[201] Anirban Biswas, Debasish Majumdar, Arunansu Sil, and Pijushpani Bhattacharjee. Two Component Dark Matter : A Possible Explanation of 130 GeV $\gamma-$ Ray Line from the Galactic Centre. *JCAP*, 12:049, 2013.

[202] Subhaditya Bhattacharya, Aleksandra Drozd, Bohdan Grzadkowski, and Jose Wudka. Two-Component Dark Matter. *JHEP*, 10:158, 2013.

[203] Ligong Bian, Ran Ding, and Bin Zhu. Two Component Higgs-Portal Dark Matter. *Phys. Lett. B*, 728:105–113, 2014.

[204] Ligong Bian, Tianjun Li, Jing Shu, and Xiao-Chuan Wang. Two component dark matter with multi-Higgs portals. *JHEP*, 03:126, 2015.

[205] Sonja Esch, Michael Klasen, and Carlos E. Yaguna. A minimal model for two-component dark matter. *JHEP*, 09:108, 2014.

[206] Alexandros Karam and Kyriakos Tamvakis. Dark matter and neutrino masses from a scale-invariant multi-Higgs portal. *Phys. Rev. D*, 92(7):075010, 2015.

[207] Alexandros Karam and Kyriakos Tamvakis. Dark Matter from a Classically Scale-Invariant $SU(3)_X$. *Phys. Rev. D*, 94(5):055004, 2016.

[208] Anthony DiFranzo and Gopolang Mohlabeng. Multi-component Dark Matter through a Radiative Higgs Portal. *JHEP*, 01:080, 2017.

[209] Subhaditya Bhattacharya, Poulose Poulose, and Purusottam Ghosh. Multipartite Interacting Scalar Dark Matter in the light of updated LUX data. *JCAP*, 04:043, 2017.

[210] Amit Dutta Banik, Madhurima Pandey, Debasish Majumdar, and Anirban Biswas. Two component WIMP–FImP dark matter model with singlet fermion, scalar and pseudo scalar. *Eur. Phys. J. C*, 77(10):657, 2017.

[211] Michael Klasen, Florian Lyonnet, and Farinaldo S. Queiroz. NLO+NLL collider bounds, Dirac fermion and scalar dark matter in the B–L model. *Eur. Phys. J. C*, 77(5):348, 2017.

[212] Purusottam Ghosh, Abhijit Kumar Saha, and Arunansu Sil. Study of Electroweak Vacuum Stability from Extended Higgs Portal of Dark Matter and Neutrinos. *Phys. Rev. D*, 97(7):075034, 2018.

[213] Aqeel Ahmed, Mateusz Duch, Bohdan Grzadkowski, and Michal Iglicki. Multi-Component Dark Matter: the vector and fermion case. *Eur. Phys. J. C*, 78(11):905, 2018.

[214] Subhaditya Bhattacharya, Purusottam Ghosh, Tarak Nath Maity, and Tirtha Sankar Ray. Mitigating Direct Detection Bounds in Non-minimal Higgs Portal Scalar Dark Matter Models. *JHEP*, 10:088, 2017.

[215] Subhaditya Bhattacharya, Abhijit Kumar Saha, Arunansu Sil, and Jose Wudka. Dark Matter as a remnant of SQCD Inflation. *JHEP*, 10:124, 2018.

[216] Subhaditya Bhattacharya, Purusottam Ghosh, and Narendra Sahu. Multipartite Dark Matter with Scalars, Fermions and signatures at LHC. *JHEP*, 02:059, 2019.

[217] Mayumi Aoki and Takashi Toma. Boosted Self-interacting Dark Matter in a Multi-component Dark Matter Model. *JCAP*, 10:020, 2018.

[218] Amit Dutta Banik, Abhijit Kumar Saha, and Arunansu Sil. Scalar assisted singlet doublet fermion dark matter model and electroweak vacuum stability. *Phys. Rev. D*, 98(7):075013, 2018.

[219] Basabendu Barman, Subhaditya Bhattacharya, and Mohammadreza Zakeri. Multipartite Dark Matter in $SU(2)_N$ extension of Standard Model and signatures at the LHC. *JCAP*, 09:023, 2018.

[220] Seyed Yaser Ayazi and Ahmad Mohamadnejad. Scale-Invariant Two Component Dark Matter. *Eur. Phys. J. C*, 79(2):140, 2019.

[221] Alexandre Poulin and Stephen Godfrey. Multicomponent dark matter from a hidden gauged SU(3). *Phys. Rev. D*, 99(7):076008, 2019.

[222] Sreemanti Chakraborti and Poulose Poulose. Interplay of Scalar and Fermionic Components in a Multi-component Dark Matter Scenario. *Eur. Phys. J. C*, 79(5):420, 2019.

[223] Sreemanti Chakraborti, Amit Dutta Banik, and Rashidul Islam. Probing Multi-component Extension of Inert Doublet Model with a Vector Dark Matter. *Eur. Phys. J. C*, 79(8):662, 2019.

[224] Nicolás Bernal, Diego Restrepo, Carlos Yaguna, and Óscar Zapata. Two-component dark matter and a massless neutrino in a new $B - L$ model. *Phys. Rev. D*, 99(1):015038, 2019.

[225] Fatemeh Elahi and Sara Khatibi. Multi-Component Dark Matter in a Non-Abelian Dark Sector. *Phys. Rev. D*, 100(1):015019, 2019.

[226] Debasish Borah, Rishav Roshan, and Arunansu Sil. Minimal two-component scalar doublet dark matter with radiative neutrino mass. *Phys. Rev. D*, 100(5):055027, 2019.

[227] Subhaditya Bhattacharya, Nabarun Chakrabarty, Rishav Roshan, and Arunansu Sil. Multicomponent dark matter in extended $U(1)_{B-L}$: neutrino mass and high scale validity. *JCAP*, 04:013, 2020.

[228] Debasish Borah, Satyabrata Mahapatra, Dibyendu Nanda, and Narendra Sahu. Inelastic fermion dark matter origin of XENON1T excess with muon ($g2$) and light neutrino mass. *Phys. Lett. B*, 811:135933, 2020.

[229] Debasish Borah and Aritra Gupta. New viable region of an inert Higgs doublet dark matter model with scotogenic extension. *Phys. Rev. D*, 96(11):115012, 2017.

[230] Vanda Silveira and A. Zee. SCALAR PHANTOMS. *Phys. Lett. B*, 161:136–140, 1985.

[231] John McDonald. Gauge singlet scalars as cold dark matter. *Phys. Rev. D*, 50:3637–3649, 1994.

[232] C. P. Burgess, Maxim Pospelov, and Tonnis ter Veldhuis. The Minimal model of nonbaryonic dark matter: A Singlet scalar. *Nucl. Phys. B*, 619:709–728, 2001.

[233] Peter Athron et al. Status of the scalar singlet dark matter model. *Eur. Phys. J. C*, 77(8):568, 2017.

[234] Debasish Borah, Rishav Roshan, and Arunansu Sil. Sub-TeV singlet scalar dark matter and electroweak vacuum stability with vectorlike fermions. *Phys. Rev. D*, 102(7):075034, 2020.

[235] G. Bélanger, F. Boudjema, A. Pukhov, and A. Semenov. micrOMEGAs4.1: two dark matter candidates. *Comput. Phys. Commun.*, 192:322–329, 2015.

[236] Adam Alloul, Neil D. Christensen, Céline Degrande, Claude Duhr, and Benjamin Fuks. FeynRules 2.0 - A complete toolbox for tree-level phenomenology. *Comput. Phys. Commun.*, 185:2250–2300, 2014.

[237] Alexander Belyaev, Neil D. Christensen, and Alexander Pukhov. CalcHEP 3.4 for collider physics within and beyond the Standard Model. *Comput. Phys. Commun.*, 184:1729–1769, 2013.

[238] Juan Herrero-Garcia, Andre Scaffidi, Martin White, and Anthony G. Williams. On the direct detection of multi-component dark matter: sensitivity studies and parameter estimation. *JCAP*, 11:021, 2017.

[239] Juan Herrero-Garcia, Andre Scaffidi, Martin White, and Anthony G. Williams. Time-dependent rate of multicomponent dark matter: Reproducing the DAMA/LIBRA phase-2 results. *Phys. Rev. D*, 98(12):123007, 2018.

[240] Werner Rodejohann. Neutrino-less Double Beta Decay and Particle Physics. *Int. J. Mod. Phys. E*, 20:1833–1930, 2011.

[241] K. S. Babu and X. G. He. DIRAC NEUTRINO MASSES AS TWO LOOP RADIATIVE CORRECTIONS. *Mod. Phys. Lett. A*, 4:61, 1989.

[242] J. T. Peltoniemi, D. Tommasini, and J. W. F. Valle. Reconciling dark matter and solar neutrinos. *Phys. Lett. B*, 298:383–390, 1993.

[243] Salvador Centelles Chuliá, Ernest Ma, Rahul Srivastava, and José W. F. Valle. Dirac Neutrinos and Dark Matter Stability from Lepton Quarticity. *Phys. Lett. B*, 767:209–213, 2017.

[244] Alfredo Aranda, Cesar Bonilla, S. Morisi, E. Peinado, and J. W. F. Valle. Dirac neutrinos from flavor symmetry. *Phys. Rev. D*, 89(3):033001, 2014.

[245] Peng Chen, Gui-Jun Ding, Alma. D. Rojas, C. A. Vaquera-Araujo, and J. W. F. Valle. Warped flavor symmetry predictions for neutrino physics. *JHEP*, 01:007, 2016.

[246] Ernest Ma, Nicholas Pollard, Rahul Srivastava, and Mohammadreza Zakeri. Gauge $B - L$ Model with Residual Z_3 Symmetry. *Phys. Lett. B*, 750:135–138, 2015.

[247] Mario Reig, Jose W. F. Valle, and C. A. Vaquera-Araujo. Realistic $\mathrm{SU(3)_c \otimes SU(3)_L \otimes U(1)_X}$ model with a type II Dirac neutrino seesaw mechanism. *Phys. Rev. D*, 94(3):033012, 2016.

[248] Weijian Wang and Zhi-Long Han. Naturally Small Dirac Neutrino Mass with Intermediate $SU(2)_L$ Multiplet Fields. *JHEP*, 04:166, 2017.

[249] Weijian Wang, Ronghui Wang, Zhi-Long Han, and Jin-Zhong Han. The $B - L$ Scotogenic Models for Dirac Neutrino Masses. *Eur. Phys. J. C*, 77(12):889, 2017.

[250] Fei Wang, Wenyu Wang, and Jin Min Yang. Split two-Higgs-doublet model and neutrino condensation. *EPL*, 76:388–394, 2006.

[251] S. Gabriel and S. Nandi. A New two Higgs doublet model. *Phys. Lett. B*, 655:141–147, 2007.

[252] Shainen M. Davidson and Heather E. Logan. Dirac neutrinos from a second Higgs doublet. *Phys. Rev. D*, 80:095008, 2009.

[253] Shainen M. Davidson and Heather E. Logan. LHC phenomenology of a two-Higgs-doublet neutrino mass model. *Phys. Rev. D*, 82:115031, 2010.

[254] Cesar Bonilla and Jose W. F. Valle. Naturally light neutrinos in *Diracon* model. *Phys. Lett. B*, 762:162–165, 2016.

[255] Yasaman Farzan and Ernest Ma. Dirac neutrino mass generation from dark matter. *Phys. Rev. D*, 86:033007, 2012.

[256] Cesar Bonilla, Ernest Ma, Eduardo Peinado, and Jose W. F. Valle. Two-loop Dirac neutrino mass and WIMP dark matter. *Phys. Lett. B*, 762:214–218, 2016.

[257] Ernest Ma and Oleg Popov. Pathways to Naturally Small Dirac Neutrino Masses. *Phys. Lett. B*, 764:142–144, 2017.

[258] Ernest Ma and Utpal Sarkar. Radiative Left-Right Dirac Neutrino Mass. *Phys. Lett. B*, 776:54–57, 2018.

[259] Debasish Borah. Light sterile neutrino and dark matter in left-right symmetric models without a Higgs bidoublet. *Phys. Rev. D*, 94(7):075024, 2016.

[260] Debasish Borah and Arnab Dasgupta. Common Origin of Neutrino Mass, Dark Matter and Dirac Leptogenesis. *JCAP*, 12:034, 2016.

[261] Debasish Borah and Arnab Dasgupta. Observable Lepton Number Violation with Predominantly Dirac Nature of Active Neutrinos. *JHEP*, 01:072, 2017.

[262] Debasish Borah and Arnab Dasgupta. Naturally Light Dirac Neutrino in Left-Right Symmetric Model. *JCAP*, 06:003, 2017.

[263] Salvador Centelles Chuliá, Rahul Srivastava, and José W. F. Valle. Generalized Bottom-Tau unification, neutrino oscillations and dark matter: predictions from a lepton quarticity flavor approach. *Phys. Lett. B*, 773:26–33, 2017.

[264] Cesar Bonilla, J. M. Lamprea, Eduardo Peinado, and Jose W. F. Valle. Flavour-symmetric type-II Dirac neutrino seesaw mechanism. *Phys. Lett. B*, 779:257–261, 2018.

[265] Nina Memenga, Werner Rodejohann, and He Zhang. A_4 flavor symmetry model for Dirac neutrinos and sizable U_{e3}. *Phys. Rev. D*, 87(5):053021, 2013.

[266] Debasish Borah and Biswajit Karmakar. A_4 flavour model for Dirac neutrinos: Type I and inverse seesaw. *Phys. Lett. B*, 780:461–470, 2018.

[267] Salvador Centelles Chuliá, Rahul Srivastava, and José W. F. Valle. Seesaw roadmap to neutrino mass and dark matter. *Phys. Lett. B*, 781:122–128, 2018.

[268] Salvador Centelles Chuliá, Rahul Srivastava, and José W. F. Valle. Seesaw Dirac neutrino mass through dimension-six operators. *Phys. Rev. D*, 98(3):035009, 2018.

[269] Zhi-Long Han and Weijian Wang. Z' Portal Dark Matter in $B - L$ Scotogenic Dirac Model. *Eur. Phys. J. C*, 78(10):839, 2018.

[270] Debasish Borah, Biswajit Karmakar, and Dibyendu Nanda. Common Origin of Dirac Neutrino Mass and Freeze-in Massive Particle Dark Matter. *JCAP*, 07:039, 2018.

[271] Debasish Borah and Biswajit Karmakar. Linear seesaw for Dirac neutrinos with A_4 flavour symmetry. *Phys. Lett. B*, 789:59–70, 2019.

[272] Salvador Centelles Chuliá, Ricardo Cepedello, Eduardo Peinado, and Rahul Srivastava. Systematic classification of two loop $d = 4$ Dirac neutrino mass models and the Diracness-dark matter stability connection. *JHEP*, 10:093, 2019.

[273] Sudip Jana, P. K. Vishnu, and Shaikh Saad. Minimal realizations of Dirac neutrino mass from generic one-loop and two-loop topologies at $d = 5$. *JCAP*, 04:018, 2020.

[274] Debasish Borah, Dibyendu Nanda, and Abhijit Kumar Saha. Common origin of modified chaotic inflation, nonthermal dark matter, and Dirac neutrino mass. *Phys. Rev. D*, 101(7):075006, 2020.

[275] Arnab Dasgupta, Sin Kyu Kang, and Oleg Popov. Radiative Dirac neutrino mass, neutrinoless quadruple beta decay, and dark matter in B-L extension of the standard model. *Phys. Rev. D*, 100(7):075030, 2019.

[276] S. S. Correia, R. G. Felipe, and F. R. Joaquim. Dirac neutrinos in the 2HDM with restrictive Abelian symmetries. *Phys. Rev. D*, 100(11):115008, 2019.

[277] Ernest Ma. Two-loop Z_4 Dirac neutrino masses and mixing, with self-interacting dark matter. *Nucl. Phys. B*, 946:114725, 2019.

[278] Ernest Ma. Scotogenic cobimaximal Dirac neutrino mixing from $\Delta(27)$ and $U(1)_\chi$. *Eur. Phys. J. C*, 79(11):903, 2019.

[279] Seungwon Baek. Dirac neutrino from the breaking of Peccei-Quinn symmetry. *Phys. Lett. B*, 805:135415, 2020.

[280] Shaikh Saad. Simplest Radiative Dirac Neutrino Mass Models. *Nucl. Phys. B*, 943:114636, 2019.

[281] Sudip Jana, P. K. Vishnu, and Shaikh Saad. Minimal dirac neutrino mass models from $\mathrm{U(1)_R}$ gauge symmetry and left–right asymmetry at colliders. *Eur. Phys. J. C*, 79(11):916, 2019.

[282] Karin Dick, Manfred Lindner, Michael Ratz, and David Wright. Leptogenesis with Dirac neutrinos. *Phys. Rev. Lett.*, 84:4039–4042, 2000.

[283] Hitoshi Murayama and Aaron Pierce. Realistic Dirac leptogenesis. *Phys. Rev. Lett.*, 89:271601, 2002.

[284] Muge Boz and Namik K. Pak. Dirac Leptogenesis and anomalous U(1). *Eur. Phys. J. C*, 37:507–510, 2004.

[285] Brooks Thomas and Manuel Toharia. Phenomenology of Dirac neutrinogenesis in split supersymmetry. *Phys. Rev. D*, 73:063512, 2006.

[286] Brooks Thomas and Manuel Toharia. Lepton flavor violation and supersymmetric Dirac leptogenesis. *Phys. Rev. D*, 75:013013, 2007.

[287] D. G. Cerdeno, A. Dedes, and T. E. J. Underwood. The Minimal Phantom Sector of the Standard Model: Higgs Phenomenology and Dirac Leptogenesis. *JHEP*, 09:067, 2006.

[288] Pei-Hong Gu and Hong-Jian He. Neutrino Mass and Baryon Asymmetry from Dirac Seesaw. *JCAP*, 12:010, 2006.

[289] Pei-Hong Gu, Hong-Jian He, and Utpal Sarkar. Realistic neutrinogenesis with radiative vertex correction. *Phys. Lett. B*, 659:634–639, 2008.

[290] Eung Jin Chun and Probir Roy. Dirac Leptogenesis in extended nMSSM. *JHEP*, 06:089, 2008.

[291] Andreas Bechinger and Gerhart Seidl. Resonant Dirac leptogenesis on throats. *Phys. Rev. D*, 81:065015, 2010.

[292] Mu-Chun Chen, Jinrui Huang, and William Shepherd. Dirac Leptogenesis with a Non-anomalous $U(1)'$ Family Symmetry. *JHEP*, 11:059, 2012.

[293] Ki-Young Choi, Eung Jin Chun, and Chang Sub Shin. Dark matter asymmetry in supersymmetric Dirac leptogenesis. *Phys. Lett. B*, 723:90–94, 2013.

[294] Pei-Hong Gu. Peccei-Quinn symmetry for Dirac seesaw and leptogenesis. *JCAP*, 07:004, 2016.

[295] Nimmala Narendra, Nirakar Sahoo, and Narendra Sahu. Dark matter assisted Dirac leptogenesis and neutrino mass. *Nucl. Phys. B*, 936:76–90, 2018.

[296] Julian Heeck. Leptogenesis with Lepton-Number-Violating Dirac Neutrinos. *Phys. Rev. D*, 88:076004, 2013.

[297] Pei-Hong Gu. Leptogenesis with testable Dirac neutrino mass generation. *Phys. Lett. B*, 805:135411, 2020.

[298] Aharon Davidson. BL as the fourth color within an $\mathrm{SU}(2)_L \times \mathrm{U}(1)_R \times \mathrm{U}(1)$ model. *Phys. Rev. D*, 20:776, 1979.

[299] Rabindra N. Mohapatra and R. E. Marshak. Local B-L Symmetry of Electroweak Interactions, Majorana Neutrinos and Neutron Oscillations. *Phys. Rev. Lett.*, 44:1316–1319, 1980. [Erratum: Phys.Rev.Lett. 44, 1643 (1980)].

[300] R. E. Marshak and Rabindra N. Mohapatra. Quark - Lepton Symmetry and B-L as the U(1) Generator of the Electroweak Symmetry Group. *Phys. Lett. B*, 91:222–224, 1980.

[301] A. Masiero, J. F. Nieves, and T. Yanagida. B-L violating proton decay and late cosmological baryon production. *Physics Letters B*, 116(1):11–15, September 1982.

[302] Rabindra N. Mohapatra and Goran Senjanovic. Spontaneous Breaking of Global B^-l Symmetry and Matter - Antimatter Oscillations in Grand Unified Theories. *Phys. Rev. D*, 27:254, 1983.

[303] W. Buchmuller, C. Greub, and P. Minkowski. Neutrino masses, neutral vector bosons and the scale of B-L breaking. *Phys. Lett. B*, 267:395–399, 1991.

[304] J. T. Peltoniemi and J. W. F. Valle. Reconciling dark matter, solar and atmospheric neutrinos. *Nucl. Phys. B*, 406:409–422, 1993.

[305] Yann Mambrini. The ZZ' kinetic mixing in the light of the recent direct and indirect dark matter searches. *JCAP*, 07:009, 2011.

[306] Satoshi Iso, Nobuchika Okada, and Yuta Orikasa. Resonant Leptogenesis in the Minimal B-L Extended Standard Model at TeV. *Phys. Rev. D*, 83:093011, 2011.

[307] Nobuchika Okada, Yuta Orikasa, and Toshifumi Yamada. Minimal Flavor Violation in the Minimal $U(1)_{B-L}$ Model and Resonant Leptogenesis. *Phys. Rev. D*, 86:076003, 2012.

[308] Julian Heeck and Daniele Teresi. Leptogenesis and neutral gauge bosons. *Phys. Rev. D*, 94(9):095024, 2016.

[309] P. S. Bhupal Dev, Rabindra N. Mohapatra, and Yongchao Zhang. Leptogenesis constraints on BL breaking Higgs boson in TeV scale seesaw models. *JHEP*, 03:122, 2018.

[310] Gianpiero Mangano, Gennaro Miele, Sergio Pastor, Teguayco Pinto, Ofelia Pisanti, and Pasquale D. Serpico. Relic neutrino decoupling including flavor oscillations. *Nucl. Phys. B*, 729:221–234, 2005.

[311] E. Grohs, G. M. Fuller, C. T. Kishimoto, M. W. Paris, and A. Vlasenko. Neutrino energy transport in weak decoupling and big bang nucleosynthesis. *Phys. Rev. D*, 93(8):083522, 2016.

[312] Pablo F. de Salas and Sergio Pastor. Relic neutrino decoupling with flavour oscillations revisited. *JCAP*, 07:051, 2016.

[313] Kevork Abazajian et al. CMB-S4 Science Case, Reference Design, and Project Plan. 7 2019.

[314] Kevork N. Abazajian and Julian Heeck. Observing Dirac neutrinos in the cosmic microwave background. *Phys. Rev. D*, 100:075027, 2019.

[315] Pavel Fileviez Pérez, Clara Murgui, and Alexis D. Plascencia. Neutrino-Dark Matter Connections in Gauge Theories. *Phys. Rev. D*, 100(3):035041, 2019.

[316] Chengcheng Han, M. L. López-Ibáñez, Bo Peng, and Jin Min Yang. Dirac dark matter in $U(1)_{B-L}$ with the Stueckelberg mechanism. *Nucl. Phys. B*, 959:115154, 2020.

[317] Xuheng Luo, Werner Rodejohann, and Xun-Jie Xu. Dirac neutrinos and $N_{\rm eff}$. *JCAP*, 06:058, 2020.

[318] Debasish Borah, Arnab Dasgupta, Chayan Majumdar, and Dibyendu Nanda. Observing left-right symmetry in the cosmic microwave background. *Phys. Rev. D*, 102(3):035025, 2020.

[319] Peter Adshead, Yanou Cui, Andrew J. Long, and Michael Shamma. Unraveling the Dirac neutrino with cosmological and terrestrial detectors. *Phys. Lett. B*, 823:136736, 2021.

[320] Xuheng Luo, Werner Rodejohann, and Xun-Jie Xu. Dirac neutrinos and $\rm N_{eff}$. Part II. The freeze-in case. *JCAP*, 03:082, 2021.

[321] Marcela Carena, Alejandro Daleo, Bogdan A. Dobrescu, and Timothy M. P. Tait. Z' gauge bosons at the Tevatron. *Phys. Rev. D*, 70:093009, 2004.

[322] G. Cacciapaglia, C. Csaki, G. Marandella, and A. Strumia. The Minimal Set of Electroweak Precision Parameters. *Phys. Rev. D*, 74:033011, 2006.

[323] Morad Aaboud et al. Search for new high-mass phenomena in the dilepton final state using 36 $\rm fb^1$ of proton-proton collision data at $\sqrt{s}$ = 13 TeV with the ATLAS detector. *JHEP*, 10:182, 2017.

[324] Georges Aad et al. Search for high-mass dilepton resonances using 139 $\rm fb^{-1}$ of pp collision data collected at $\sqrt{s}$ =13 TeV with the ATLAS detector. *Phys. Lett. B*, 796:68–87, 2019.

[325] Albert M Sirunyan et al. Search for high-mass resonances in dilepton final states in proton-proton collisions at $\sqrt{s} = 13$ TeV. *JHEP*, 06:120, 2018.

[326] Kevork N. Abazajian et al. CMB-S4 Science Book, First Edition. 10 2016.

[327] B. A. Benson et al. SPT-3G: A Next-Generation Cosmic Microwave Background Polarization Experiment on the South Pole Telescope. *Proc. SPIE Int. Soc. Opt. Eng.*, 9153:91531P, 2014.

[328] Nobuchika Okada and Osamu Seto. Higgs portal dark matter in the minimal gauged $U(1)_{B-L}$ model. *Phys. Rev. D*, 82:023507, 2010.

[329] Tanushree Basak and Tanmoy Mondal. Constraining Minimal $U(1)_{B-L}$ model from Dark Matter Observations. *Phys. Rev. D*, 89:063527, 2014.

[330] Nobuchika Okada and Satomi Okada. Z'_{BL} portal dark matter and LHC Run-2 results. *Phys. Rev. D*, 93(7):075003, 2016.

[331] Satomi Okada. Z' Portal Dark Matter in the Minimal $B - L$ Model. *Adv. High Energy Phys.*, 2018:5340935, 2018.

[332] Miguel Escudero, Samuel J. Witte, and Nuria Rius. The dispirited case of gauged $\rm U(1)_{B-L}$ dark matter. *JHEP*, 08:190, 2018.

[333] Debasish Borah, Suruj Jyoti Das, and Abhijit Kumar Saha. Cosmic inflation in minimal $U(1)_{B-L}$ model: implications for (non) thermal dark matter and leptogenesis. *Eur. Phys. J. C*, 81(2):169, 2021.

[334] Chiara Arina and Nicolao Fornengo. Sneutrino cold dark matter, a new analysis: Relic abundance and detection rates. *JHEP*, 11:029, 2007.

[335] J. McDonald. WIMP Densities in Decaying Particle Dominated Cosmology. *Phys. Rev. D*, 43:1063–1068, 1991.

[336] Marc Kamionkowski and Michael S. Turner. THERMAL RELICS: DO WE KNOW THEIR ABUNDANCES? *Phys. Rev. D*, 42:3310–3320, 1990.

[337] Daniel J. H. Chung, Edward W. Kolb, and Antonio Riotto. Production of massive particles during reheating. *Phys. Rev. D*, 60:063504, 1999.

[338] Takeo Moroi and Lisa Randall. Wino cold dark matter from anomaly mediated SUSY breaking. *Nucl. Phys. B*, 570:455–472, 2000.

[339] Gian Francesco Giudice, Edward W. Kolb, and Antonio Riotto. Largest temperature of the radiation era and its cosmological implications. *Phys. Rev. D*, 64:023508, 2001.

[340] Rouzbeh Allahverdi and Manuel Drees. Production of massive stable particles in inflaton decay. *Phys. Rev. Lett.*, 89:091302, 2002.

[341] Rouzbeh Allahverdi and Manuel Drees. Thermalization after inflation and production of massive stable particles. *Phys. Rev. D*, 66:063513, 2002.

[342] Bobby Samir Acharya, Gordon Kane, Scott Watson, and Piyush Kumar. A Non-thermal WIMP Miracle. *Phys. Rev. D*, 80:083529, 2009.

[343] Hooman Davoudiasl, Dan Hooper, and Samuel D. McDermott. Inflatable Dark Matter. *Phys. Rev. Lett.*, 116(3):031303, 2016.

[344] Manuel Drees and Fazlollah Hajkarim. Neutralino Dark Matter in Scenarios with Early Matter Domination. *JHEP*, 12:042, 2018.

[345] Nicolás Bernal, Catarina Cosme, and Tommi Tenkanen. Phenomenology of Self-Interacting Dark Matter in a Matter-Dominated Universe. *Eur. Phys. J. C*, 79(2):99, 2019.

[346] Nicolás Bernal, Catarina Cosme, Tommi Tenkanen, and Ville Vaskonen. Scalar singlet dark matter in non-standard cosmologies. *Eur. Phys. J. C*, 79(1):30, 2019.

[347] Paola Arias, Nicolás Bernal, Alan Herrera, and Carlos Maldonado. Reconstructing Non-standard Cosmologies with Dark Matter. *JCAP*, 10:047, 2019.

[348] M. Sten Delos, Tim Linden, and Adrienne L. Erickcek. Breaking a dark degeneracy: The gamma-ray signature of early matter domination. *Phys. Rev. D*, 100(12):123546, 2019.

[349] Nicolás Bernal, Fatemeh Elahi, Carlos Maldonado, and James Unwin. Ultraviolet Freeze-in and Non-Standard Cosmologies. *JCAP*, 11:026, 2019.

[350] Alexandre Poulin. Dark matter freeze-out in modified cosmological scenarios. *Phys. Rev. D*, 100(4):043022, 2019.

[351] Carlos Maldonado and James Unwin. Establishing the Dark Matter Relic Density in an Era of Particle Decays. *JCAP*, 06:037, 2019.

[352] Amalia Betancur and Óscar Zapata. Phenomenology of doublet-triplet fermionic dark matter in nonstandard cosmology and multicomponent dark sectors. *Phys. Rev. D*, 98(9):095003, 2018.

[353] Francesco D'Eramo, Nicolas Fernandez, and Stefano Profumo. When the Universe Expands Too Fast: Relentless Dark Matter. *JCAP*, 05:012, 2017.

[354] Francesco D'Eramo, Nicolas Fernandez, and Stefano Profumo. Dark Matter Freeze-in Production in Fast-Expanding Universes. *JCAP*, 02:046, 2018.

[355] Anirban Biswas, Debasish Borah, and Dibyendu Nanda. keV Neutrino Dark Matter in a Fast Expanding Universe. *Phys. Lett. B*, 786:364–372, 2018.

[356] Luca Visinelli and Paolo Gondolo. Kinetic decoupling of WIMPs: analytic expressions. *Phys. Rev. D*, 91(8):083526, 2015.

[357] Luca Visinelli. (Non-)thermal production of WIMPs during kination. *Symmetry*, 10(11):546, 2018.

[358] Shao-Long Chen, Amit Dutta Banik, and Ze-Kun Liu. Leptogenesis in fast expanding Universe. *JCAP*, 03:009, 2020.

[359] W. Abdallah, D. Delepine, and S. Khalil. TeV Scale Leptogenesis in B-L Model with Alternative Cosmologies. *Phys. Lett. B*, 725:361–367, 2013.

[360] Bhaskar Dutta, Chee Sheng Fong, Esteban Jimenez, and Enrico Nardi. A cosmological pathway to testable leptogenesis. *JCAP*, 10:025, 2018.

[361] Riccardo Catena, N. Fornengo, A. Masiero, Massimo Pietroni, and Francesca Rosati. Dark matter relic abundance and scalar - tensor dark energy. *Phys. Rev. D*, 70:063519, 2004.

[362] R. Catena, N. Fornengo, M. Pato, L. Pieri, and A. Masiero. Thermal Relics in Modified Cosmologies: Bounds on Evolution Histories of the Early Universe and Cosmological Boosts for PAMELA. *Phys. Rev. D*, 81:123522, 2010.

[363] Michael T. Meehan and Ian B. Whittingham. Dark matter relic density in scalar-tensor gravity revisited. *JCAP*, 12:011, 2015.

[364] Bhaskar Dutta, Esteban Jimenez, and Ivonne Zavala. Dark Matter Relics and the Expansion Rate in Scalar-Tensor Theories. *JCAP*, 06:032, 2017.

[365] Bhaskar Dutta, Esteban Jimenez, and Ivonne Zavala. D-brane Disformal Coupling and Thermal Dark Matter. *Phys. Rev. D*, 96(10):103506, 2017.

[366] M. Kawasaki, Kazunori Kohri, and Naoshi Sugiyama. MeV scale reheating temperature and thermalization of neutrino background. *Phys. Rev. D*, 62:023506, 2000.

[367] Steen Hannestad. What is the lowest possible reheating temperature? *Phys. Rev. D*, 70:043506, 2004.

[368] Kazuhide Ichikawa, Masahiro Kawasaki, and Fuminobu Takahashi. The Oscillation effects on thermalization of the neutrinos in the Universe with low reheating temperature. *Phys. Rev. D*, 72:043522, 2005.

[369] S. M. Boucenna and S. Morisi. Theories relating baryon asymmetry and dark matter: A mini review. *Front. in Phys.*, 1:33, 2014.

[370] S. Nussinov. TECHNOCOSMOLOGY: COULD A TECHNIBARYON EXCESS PROVIDE A 'NATURAL' MISSING MASS CANDIDATE? *Phys. Lett. B*, 165:55–58, 1985.

[371] Hooman Davoudiasl and Rabindra N. Mohapatra. On Relating the Genesis of Cosmic Baryons and Dark Matter. *New J. Phys.*, 14:095011, 2012.

[372] Kalliopi Petraki and Raymond R. Volkas. Review of asymmetric dark matter. *Int. J. Mod. Phys. A*, 28:1330028, 2013.

[373] Kathryn M. Zurek. Asymmetric Dark Matter: Theories, Signatures, and Constraints. *Phys. Rept.*, 537:91–121, 2014.

[374] Basabendu Barman, Debasish Borah, Suruj Jyoti Das, and Rishav Roshan. Non-thermal origin of asymmetric dark matter from inflaton and primordial black holes. *JCAP*, 03(03):031, 2022.

[375] Yanou Cui and Michael Shamma. WIMP Cogenesis for Asymmetric Dark Matter and the Baryon Asymmetry. *JHEP*, 12:046, 2020.

[376] Edward W. Kolb and Michael S. Turner. Grand Unified Theories and the Origin of the Baryon Asymmetry. *Ann. Rev. Nucl. Part. Sci.*, 33:645–696, 1983.

[377] Iason Baldes, Nicole F. Bell, Kalliopi Petraki, and Raymond R. Volkas. Particle-antiparticle asymmetries from annihilations. *Phys. Rev. Lett.*, 113(18):181601, 2014.

[378] Xiaoyong Chu, Yanou Cui, Josef Pradler, and Michael Shamma. Dark freeze-out cogenesis. *JHEP*, 03:031, 2022.

[379] Yanou Cui, Lisa Randall, and Brian Shuve. A WIMPy Baryogenesis Miracle. *JHEP*, 04:075, 2012.

[380] Nicolas Bernal, Francois-Xavier Josse-Michaux, and Lorenzo Ubaldi. Phenomenology of WIMPy baryogenesis models. *JCAP*, 01:034, 2013.

[381] Nicolás Bernal, Stefano Colucci, François-Xavier Josse-Michaux, J. Racker, and Lorenzo Ubaldi. On baryogenesis from dark matter annihilation. *JCAP*, 10:035, 2013.

[382] Jason Kumar and Patrick Stengel. WIMPy Leptogenesis With Absorptive Final State Interactions. *Phys. Rev. D*, 89(5):055016, 2014.

[383] J. Racker and N. Rius. Helicitogenesis: WIMPy baryogenesis with sterile neutrinos and other realizations. *JHEP*, 11:163, 2014.

[384] Arnab Dasgupta, Chandan Hati, Sudhanwa Patra, and Utpal Sarkar. A minimal model of TeV scale WIMPy leptogenesis. 5 2016.

[385] Debasish Borah, Arnab Dasgupta, and Devabrat Mahanta. Dark sector assisted low scale leptogenesis from three body decay. *Phys. Rev. D*, 105(1):015015, 2022.

[386] Michela D'Onofrio, Kari Rummukainen, and Anders Tranberg. Sphaleron Rate in the Minimal Standard Model. *Phys. Rev. Lett.*, 113(14):141602, 2014.

[387] M. Fierz. On the physical interpretation of P.Jordan's extended theory of gravitation. *Helv. Phys. Acta*, 29:128–134, 1956.

[388] C. Brans and R. H. Dicke. Mach's principle and a relativistic theory of gravitation. *Phys. Rev.*, 124:925–935, 1961.

[389] Avelino Vicente and Carlos E. Yaguna. Probing the scotogenic model with lepton flavor violating processes. *JHEP*, 02:144, 2015.

[390] Debasish Borah, Arnab Dasgupta, Kohei Fujikura, Sin Kyu Kang, and Devabrat Mahanta. Observable Gravitational Waves in Minimal Scotogenic Model. *JCAP*, 08:046, 2020.

[391] Yanou Cui, Marek Lewicki, David E. Morrissey, and James D. Wells. Probing the pre-BBN universe with gravitational waves from cosmic strings. *JHEP*, 01:081, 2019.

[392] Nicolás Bernal and Fazlollah Hajkarim. Primordial Gravitational Waves in Nonstandard Cosmologies. *Phys. Rev. D*, 100(6):063502, 2019.

[393] Massimo Giovannini. Gravitational waves constraints on postinflationary phases stiffer than radiation. *Phys. Rev. D*, 58:083504, 1998.

[394] Ken'ichi Saikawa and Satoshi Shirai. Primordial gravitational waves, precisely: The role of thermodynamics in the Standard Model. *JCAP*, 05:035, 2018.

[395] Herbi K. Dreiner, Howard E. Haber, and Stephen P. Martin. Two-component spinor techniques and Feynman rules for quantum field theory and supersymmetry. *Phys. Rept.*, 494:1–196, 2010.

[396] Thomas Hambye and Goran Senjanovic. Consequences of triplet seesaw for leptogenesis. *Phys. Lett. B*, 582:73–81, 2004.

[397] Thomas Hambye, Martti Raidal, and Alessandro Strumia. Efficiency and maximal CP-asymmetry of scalar triplet leptogenesis. *Phys. Lett. B*, 632:667–674, 2006.

[398] D. Aristizabal Sierra, Mikaël Dhen, and Thomas Hambye. Scalar triplet flavored leptogenesis: a systematic approach. *JCAP*, 08:003, 2014.

[399] Arghyajit Datta, Rishav Roshan, and Arunansu Sil. Scalar triplet flavor leptogenesis with dark matter. *Phys. Rev. D*, 105(9):095032, 2022.

[400] Suruj Jyoti Das, Devabrat Mahanta, and Debasish Borah. Low scale leptogenesis and dark matter in the presence of primordial black holes. *JCAP*, 11:019, 2021.